

The ventilation of a chick transport vehicle

by Andrew Quinn, BSc

Thesis submitted to the University of Nottingham
for the degree of Doctor of Philosophy, October 1996

Supervisor

Dr C J Baker - Department of Civil Engineering

Associate Supervisors

Dr R P Hoxey - Bio-engineering Division, Silsoe Research Institute
Mr P J Kettlewell - Bio-engineering Division, Silsoe Research Institute

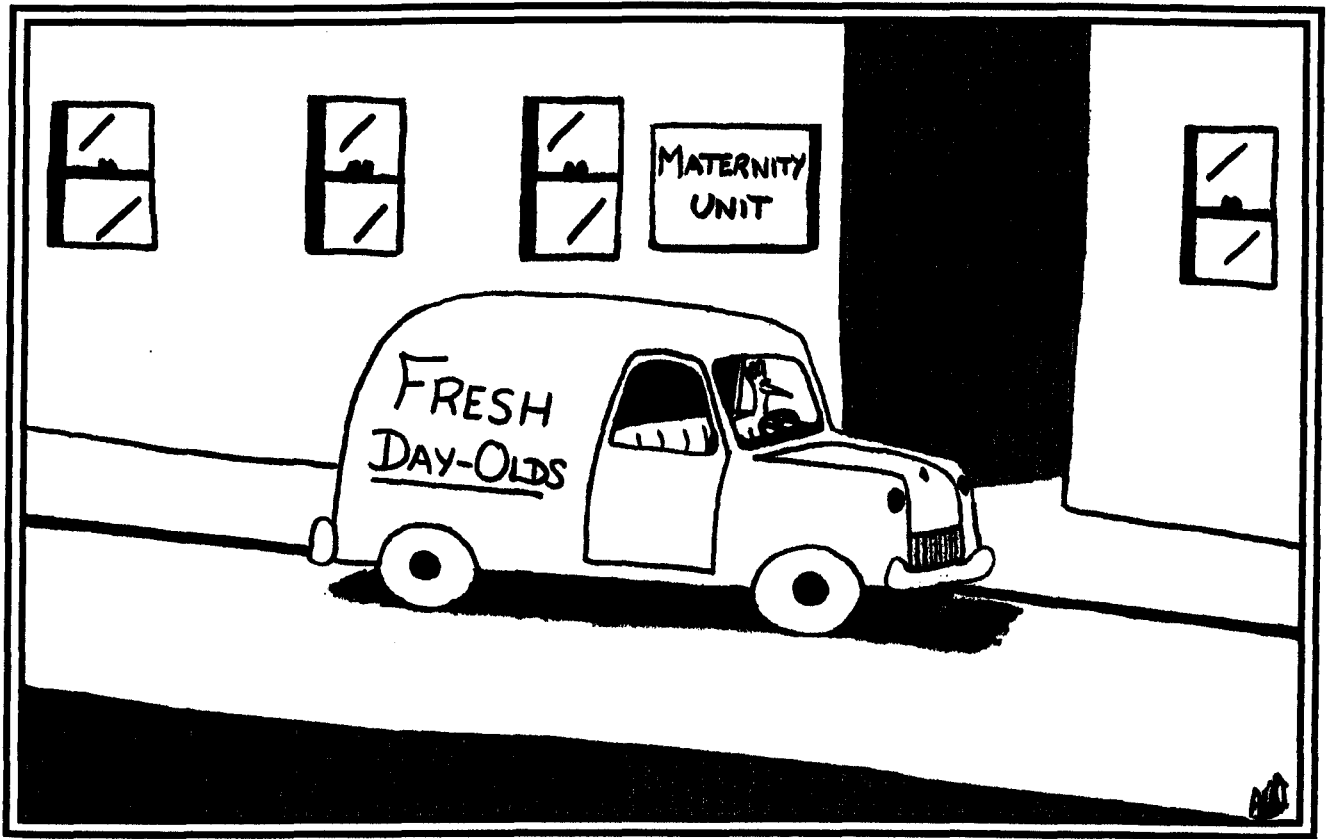


Table of contents

| | |
|--|----------|
| Abstract | - iv - |
| List of figures | - v - |
| List of tables | - xiii - |
| 1. Introduction | |
| 1.1 The industry | - 1 - |
| 1.2 Problems of chick transportation | - 11 - |
| 1.3 The structure of the investigation | |
| 1.3.1 Overall objectives | - 28 - |
| 1.3.2 Experimental objective | - 28 - |
| 1.3.3 Numerical simulation objectives | - 28 - |
| 1.4 Outline of the thesis | - 29 - |
| 2 The experiments | |
| 2.1 The parameters to be measured | |
| 2.1.1 Introduction | - 31 - |
| 2.1.2 Definition of parameters | - 34 - |
| 2.2 Experimental techniques | |
| 2.2.1 Experimental model construction | - 40 - |
| 2.2.2 Fan calibration | - 52 - |
| 2.2.3 Ceiling jet measurements | - 58 - |
| 2.2.4 Ultrasonic anemometer details | - 61 - |
| 2.2.5 Experimental run length | - 65 - |
| 2.2.6 Main experimental procedure | - 67 - |
| 2.3 Experimental cases | |
| 2.3.1 Loading arrangements | - 69 - |
| 2.3.2 Measurement locations | - 72 - |
| 2.4 Data analysis | - 74 - |
| 3 The numerical simulation | |
| 3.1 Introduction | - 79 - |
| 3.2 Software implementation | - 84 - |
| 3.3 Numerical model development | |
| 3.3.1 Preliminary models | - 86 - |
| 3.3.2 Load space models | - 90 - |
| 3.3.3 Loading models | - 97 - |
| 3.3.4 Numerical model summary | - 100 - |
| 3.4 Computational cases | - 104 - |
| 3.5 Interpretation of CFD results | - 106 - |

| | | |
|----------|--|---------|
| 4 | Results | |
| 4.1 | Introduction | - 107 - |
| 4.2 | Time averaged velocity, Reynolds stress and temperature results | |
| 4.2.1 | Empty load space case | - 111 - |
| 4.2.2 | Front half loaded case | - 132 - |
| 4.2.3 | Side half loaded case | - 141 - |
| 4.2.4 | Fully loaded case | - 148 - |
| 4.2.5 | Non-isothermal numerical results | - 155 - |
| 4.2.6 | Ventilation rate results | - 164 - |
| 4.3 | Correlation and Spectral analysis results | |
| 4.3.1 | Autocorrelation results | - 172 - |
| 4.3.2 | Spectral analysis results | - 180 - |
| 4.3.3 | Cross-correlation and cross-spectral results | - 190 - |
| 4.4 | Discussion of experimental and numerical results | - 196 - |
| 5 | Quantitative comparison of experimental and numerical results | |
| 5.1 | Comparison methodology | - 202 - |
| 5.2 | Comparison of cases | |
| 5.2.1 | Empty load space case | - 210 - |
| 5.2.2 | Front half loaded case | - 216 - |
| 5.2.3 | Side half loaded case | - 220 - |
| 5.2.4 | Fully loaded case | - 223 - |
| 5.3 | Discussion of comparison methodology and results | - 226 - |
| 6 | Implications | |
| 6.1 | Implications for CFD studies | - 230 - |
| 6.2 | Interpretation of the predicted temperature results | - 233 - |
| 6.3 | Implications for transporter design and ventilation rate | - 238 - |
| 7 | Conclusions and recommendations for further work | |
| 7.1 | Conclusions | - 241 - |
| 7.2 | Recommendations for further work | - 247 - |
| 7.3 | General conclusions for CFD modelling | - 249 - |
| | References | - 250 - |

Appendices

| | | |
|------------|--|---------|
| appendix 1 | Experimental model construction | - 256 - |
| appendix 2 | Experimental data | - 265 - |
| appendix 3 | CFD methodology | - 279 - |
| appendix 4 | CFD model instruction summary | - 286 - |
| appendix 5 | Ventilation rate calculation results | - 295 - |
| appendix 6 | Experimental - Numerical comparison results | - 306 - |

Abstract

The increasing size and complexity of road vehicles used for the transport of day-old chicks has raised concerns about the thermal environment achieved within the load space of such transporters. Current designs have not been based on scientific information or evaluation, making new development difficult for the industry. To address this lack of information, given the high cost of these vehicles, modelling of this situation would seem a viable option.

The work presented in this thesis illustrates the effectiveness of experimental and numerical modelling. Results collected using an ultrasonic anemometer from a full-scale isothermal model of a particular load space and ventilation system are presented for different load configurations of empty chick boxes. These cases were also simulated using commercially available computational fluid dynamics software [PHOENICS with high-Re $k-\epsilon$ turbulence model and hybrid convective differencing]. These numerical model results were then validated against the experimental data using a novel statistical method based on the repeatability of the experimental data. In further numerical simulations a heat load model, representing the presence of the chicks, was also incorporated and the likely thermal environment assessed. These numerical results were used to assess the ventilation delivered to each chick box based on the predicted mean air velocities.

These results indicated that experimental modelling was a time consuming process with difficulties of accessibility for instrumentation within a loaded vehicle. Numerical simulation gave a good approximation of the experimental data but required a number of significant assumptions and simplifications to be made. The main area of disagreement with the experimental data was in the predicted turbulence levels. Ventilation rates and thermal conditions within the load space studied suggested an adequate environment is achieved for normal journeys but that the potential for heat stress exists. Further field work to validate these findings is suggested.

List of figures

| | | |
|-----------|--|--------|
| Figure 1 | Total annual chick placings in the EU 1987 - 1995. | - 1 - |
| Figure 2 | A diagrammatic representation of the traditional design of chick transport vehicle. | - 5 - |
| Figure 3 | A diagrammatic representation of the false floor type of chick transport vehicle. | - 6 - |
| Figure 4 | A diagrammatic representation of the false ceiling type of chick transport vehicle. | - 7 - |
| Figure 5 | A photograph of typical chick boxes. | - 8 - |
| Figure 6 | A diagrammatic representation of relationships between heat production, evaporative and non-evaporative (sensible) heat loss and deep body temperature in a homeothermic animal. | - 12 - |
| Figure 7 | A diagrammatic representation of relationships between heat production, evaporative and non-evaporative (sensible) heat loss and deep body temperature for a day-old chick. | - 14 - |
| Figure 8 | The heat and CO ₂ production and air requirement of a day-old chick with changing ambient temperature. | - 18 - |
| Figure 9 | The variation of heat production of day-old chicks with environmental temperature. | - 19 - |
| Figure 10 | A photograph of the chick transport vehicle chosen for this project. | - 41 - |
| Figure 11 | A photograph of the internal arrangement of the chick transport vehicle chosen for this project. | - 42 - |
| Figure 12 | A photograph of the air conditioning equipment seen inside the chick transport vehicle. | - 43 - |
| Figure 13 | A photograph of the trollies used in this chick transport vehicle. | - 45 - |
| Figure 14 | A photograph of the full scale model vehicle load space under construction. | - 46 - |
| Figure 15 | A photograph of the model vehicle load space plenum chamber and false ceiling. | - 47 - |
| Figure 16 | A photograph of the outside of the model vehicle load space before the installation of the fan rig. | - 48 - |
| Figure 17 | Locations of the fixed ultrasonic anemometer positions on the side wall of the model load space, measured from the base of the front wall. | - 51 - |
| Figure 18 | A diagrammatic representation of the experimental arrangement for calibration of the fan rig. | - 52 - |
| Figure 19 | A reproduction of the turbine-meter calibration curve. | - 53 - |
| Figure 20 | The circuit diagram of the pressure signal accumulator. | - 56 - |
| Figure 21 | The results of the calibration of the fan rig. | - 57 - |

| | | |
|-----------|---|---------|
| Figure 22 | The distribution of jet speed across the false ceiling holes in the full scale model chick transport vehicle load space. | - 59 - |
| Figure 23 | A diagrammatic representation of the ultrasonic anemometer viewed from end on, showing the internal co-ordinate system. (After Gill 1992) | - 61 - |
| Figure 24 | The results of the variance of means to determine experimental run length. | - 65 - |
| Figure 25 | A photograph of empty chick boxes loaded onto trollies inside the model load space. | - 69 - |
| Figure 26 | A diagrammatic representation of the load configuration for the front half loaded case. | - 70 - |
| Figure 27 | A diagrammatic representation of the load configuration for the side half loaded case. | - 71 - |
| Figure 28 | A diagrammatic representation of the load configuration for the fully loaded case. | - 72 - |
| Figure 29 | A diagrammatic representation of the flow of data through the analysis routines written for this project. | - 75 - |
| Figure 30 | A diagrammatic representation of the chick transport vehicle, highlighting the areas of concern in the numerical modelling. | - 86 - |
| Figure 31 | A cross section of the grid used in these numerical studies. The viewpoint is along the length of the load space, with the black outline showing the front wall and plenum chamber vents. | - 93 - |
| Figure 32 | A cross section along the length of the load space of the grid used in these numerical studies for the empty, front half and fully loaded cases (EFF grid). | - 94 - |
| Figure 33 | A cross section along the length of the load space of the grid used in these numerical studies for the empty and side half loaded cases (ES grid). | - 94 - |
| Figure 34 | The overall co-ordinate system employed throughout these experiments and numerical simulations. | - 109 - |
| Figure 35 | A vector diagram of experimental results from a lengthwise cross section of the empty model load space, 0.7 m from the side wall, with streamlines. | - 111 - |
| Figure 36 | A vector diagram of experimental results from a widthwise cross section of the empty model load space, 4.2 m from the front wall. | - 113 - |
| Figure 37 | A vector diagram of experimental results from a plan view cross section of the empty model load space, 0.3 m from the floor. | - 114 - |
| Figure 38 | A vector diagram of experimental results from a lengthwise cross section of the empty model load | |

| | |
|-----------|--|
| | space, 0.7 m from the side wall, with turbulence data presented as local percentage turbulence intensity. - 115 - |
| Figure 39 | A vector diagram of numerical simulation results from a lengthwise cross-section of the empty model load space, 0.7 m from the side wall, using EFF grid and 100% inlet jet speed. - 115 - |
| Figure 40 | A vector diagram of numerical simulation results from a widthwise cross-section of the empty model load space, 4.2 m from the front wall, using EFF grid and 100% inlet jet speed. - 116 - |
| Figure 41 | A vector diagram of numerical simulation results from a lengthwise cross-section of the empty model load space, 0.7 m from the side wall, using EFF grid and 50% inlet jet speed. - 117 - |
| Figure 42 | A vector diagram of numerical simulation results from a widthwise cross-section of the empty model load space, 4.2 m from the front wall, using EFF grid and 50% inlet jet speed. - 118 - |
| Figure 43 | A vector diagram of numerical simulation results from a lengthwise cross-section of the empty model load space, 0.7 m from the side wall, using ES grid and 100% inlet jet speed. - 119 - |
| Figure 44 | A vector diagram of numerical simulation results from a widthwise cross-section of the empty model load space, 4.2 m from the front wall, using ES grid and 100% inlet jet speed. - 120 - |
| Figure 45 | A vector diagram of numerical simulation results from a lengthwise cross-section of the empty model load space, 0.7 m from the side wall, using ES grid and 50% inlet jet speed. - 121 - |
| Figure 46 | A vector diagram of numerical simulation results from a widthwise cross-section of the empty model load space, 4.2 m from the front wall, using ES grid and 50% inlet jet speed. - 121 - |
| Figure 47 | A vector diagram of numerical simulation results from a widthwise cross-section of the empty model load space, 4.2 m from the front wall, using an X doubled EFF grid and 50% inlet jet speed. - 122 - |
| Figure 48 | A vector diagram of numerical simulation results from a lengthwise cross-section of the empty model load space, 0.7 m from the side wall, using an Z doubled EFF grid and 50% inlet jet speed. - 123 - |
| Figure 49 | A vector diagram of numerical simulation results from a lengthwise cross-section of the empty model load space, 0.7 m from the side wall, using an Y doubled EFF grid and 50% inlet jet speed. - 124 - |

| | | |
|-----------|--|-------|
| Figure 50 | A vector diagram of numerical simulation results from a widthwise cross-section of the empty model load space, 4.2 m from the front wall, using an Y doubled EFF grid and 50% inlet jet speed. | 125 - |
| Figure 51 | Graph of the mean shear stress along a horizontal traverse of the width of the empty experimental model load space, 4.2 m from the front wall and 1.7 m above the floor. | 126 - |
| Figure 52 | Graph of the mean shear stress along a horizontal traverse of the width of the empty numerical model load space, 4.2 m from the front wall and 1.7 m above the floor, using EFF grid and 50% inlet jet speed. | 128 - |
| Figure 53 | Graph of the mean shear stress along a vertical traverse of the empty experimental model load space, 4.2 m from the front wall and 0.95 m from the side wall. | 129 - |
| Figure 54 | Graph of the mean shear stress along a vertical traverse of the empty numerical model load space, 4.2 m from the front wall and 0.95 m from the side wall, using EFF grid and 50% inlet jet speed. | 130 - |
| Figure 55 | Graph of the mean shear stress along a horizontal traverse of the length of the empty experimental load space, 0.7 m from the side wall and 2.1 m above the floor. | 131 - |
| Figure 56 | A vector diagram of experimental results from a lengthwise cross section of the front half loaded model load space, 0.7 m from the side wall, with streamlines. | 132 - |
| Figure 57 | A vector diagram of numerical simulation results from a lengthwise cross-section of the front half loaded model load space, 0.7 m from the side wall, using EFF grid, 50% inlet jet speed and standard load model. | 133 - |
| Figure 58 | A vector diagram of numerical results from a lengthwise cross-section of the front half loaded model load space, 0.7 m from the side wall, using EFF grid, 50% inlet jet speed and reduced porosity load model. | 134 - |
| Figure 59 | A vector diagram of experimental results from a widthwise cross section of the front half loaded model load space, 4.6 m from the front wall. | 136 - |
| Figure 60 | A vector diagram of numerical simulation results from a widthwise cross-section of the front half loaded model load space, 4.2 m from the front wall, | |

| | | |
|-----------|--|---------|
| | using EFF grid, 50% inlet jet speed and standard load model. | - 137 - |
| Figure 61 | A vector diagram of numerical results from a widthwise cross-section of the front half loaded model load space, 4.2 m from the front wall, using EFF grid, 50% inlet jet speed and reduced porosity load model. | - 138 - |
| Figure 62 | A vector diagram of experimental results from a widthwise cross section of the front half loaded model load space, 4.2 m from the front wall. | - 139 - |
| Figure 63 | Graph of the mean shear stress along a horizontal traverse of the length of the front half loaded experimental model load space, 0.7 m from the side wall and 2.1 m above the floor. | - 140 - |
| Figure 64 | A vector diagram of experimental results from a lengthwise cross section of the side half loaded model load space, 0.7 m from the side wall. | - 141 - |
| Figure 65 | A vector diagram of numerical simulation results from a lengthwise cross-section of the side half loaded model load space, 0.7 m from the side wall, using ES grid, 50% inlet jet speed and standard load model. | - 142 - |
| Figure 66 | A vector diagram of numerical results from a lengthwise cross-section of the side half loaded model load space, 0.7 m from the side wall, using ES grid, 50% inlet jet speed and reduced porosity load model. | - 143 - |
| Figure 67 | A vector diagram of experimental results from a widthwise cross-section of the side half loaded model load space, 4.2 m from the front wall. | - 144 - |
| Figure 68 | A vector diagram of numerical results from a widthwise cross-section of the side half loaded model load space, 4.2 m from the front wall, using ES grid, 50% inlet jet speed and standard porosity load model. | - 145 - |
| Figure 69 | A vector diagram of numerical results from a widthwise cross-section of the side half loaded model load space, 4.2 m from the front wall, using ES grid, 50% inlet jet speed and reduced porosity load model. | - 146 - |
| Figure 70 | Graph of the mean shear stress along a horizontal traverse of the length of the side half loaded experimental model load space, 0.7 m from the side wall and 2.1 m above the floor. | - 147 - |

| | | |
|-----------|--|---------|
| Figure 71 | A vector diagram of experimental results from a lengthwise cross-section of the fully loaded model load space, 0.7 m from the side wall. | - 148 - |
| Figure 72 | A vector diagram of experimental results from a widthwise cross-section of the fully loaded model load space, 4.2 m from the front wall. | - 149 - |
| Figure 73 | A vector diagram of numerical simulation results from a lengthwise cross-section of the fully loaded model load space, 0.7 m from the side wall, using EFF grid, 50% inlet jet speed and standard load model. | - 150 - |
| Figure 74 | A vector diagram of numerical simulation results from a widthwise cross-section of the fully loaded model load space, 4.2 m from the front wall, using EFF grid, 50% inlet jet speed and standard load model. | - 150 - |
| Figure 75 | A vector diagram of numerical results from a lengthwise cross-section of the fully loaded model load space, 0.7 m from the side wall, using EFF grid, 50% inlet jet speed and reduced porosity load model. | - 151 - |
| Figure 76 | A vector diagram of numerical results from a widthwise cross-section of the fully loaded model load space, 4.2 m from the front wall, using EFF grid, 50% inlet jet speed and reduced porosity load model. | - 151 - |
| Figure 77 | Graph of the mean shear stress along a horizontal traverse of the length of the fully loaded experimental model load space, 0.7 m from the side wall and 2.1 m above the floor. | - 154 - |
| Figure 78 | A vector diagram of numerical results from a lengthwise cross-section of the front half loaded model load space, 0.7 m from the side wall, using EFF grid, 77% inlet jet speed and standard, heated, load model. | - 156 - |
| Figure 79 | A diagram of temperature results from a lengthwise cross-section of the front half loaded model load space, 0.7 m from the side wall, using EFF grid, 77% inlet jet speed and standard, heated, load model. | - 157 - |
| Figure 80 | A vector diagram of numerical results from a widthwise cross-section of the front half loaded model load space, 4.2 m from the front wall, using EFF grid, 77% inlet jet speed and standard, heated, load model. | - 158 - |
| Figure 81 | A vector diagram of numerical results from a lengthwise cross-section of the fully loaded model | |

| | | |
|-----------|---|---------|
| | load space, 0.7 m from the side wall, using EFF grid, 77% inlet jet speed and reduced porosity, heated, load model. | - 159 - |
| Figure 82 | A diagram of temperature results from a lengthwise cross-section of the fully loaded model load space, 0.7 m from the side wall, using EFF grid, 77% inlet jet speed and reduced porosity, heated, load model. | - 160 - |
| Figure 83 | A diagram of numerical results from a widthwise cross-section of the fully loaded model load space, 0.7 m from the front wall, using EFF grid, 77% inlet jet speed and reduced porosity, heated, load model. | - 161 - |
| Figure 84 | A diagram of numerical results from a widthwise cross-section of the fully loaded model load space, 4.2 m from the front wall, using EFF grid, 77% inlet jet speed and reduced porosity, heated, load model. | - 162 - |
| Figure 85 | A vector diagram of numerical results from a widthwise cross-section of the fully loaded model load space, 4.2 m from the front wall, using EFF grid, 77% inlet jet speed and reduced porosity, heated, load model. | - 163 - |
| Figure 86 | A photograph of the arrangement of chick boxes within the model load space. | - 164 - |
| Figure 87 | A plot of the autocorrelation function from data collected in the vehicle load space. | - 173 - |
| Figure 88 | A plot of the autocorrelation function from data collected at position 1 in the empty model load space. | - 174 - |
| Figure 89 | A plot of the autocorrelation function from data collected at position 1 in the front half loaded model load space. | - 177 - |
| Figure 90 | A plot of the autocorrelation function from data collected at position 1 in the side half loaded model load space. | - 178 - |
| Figure 91 | A plot of the autocorrelation function from data collected at position 1 in the fully loaded model load space. | - 179 - |
| Figure 92 | A plot of the spectrum from data collected in the vehicle load space. | - 181 - |
| Figure 93 | A plot of the spectrum from data collected at position 1 in the empty model load space. | - 182 - |
| Figure 94 | A plot of the non-dimensional spectrum from data collected at position 1 in the empty model load space. | - 183 - |
| Figure 95 | A plot of the spectrum from data collected at position 1 in the front half loaded model load space. | - 184 - |

| | | |
|------------|---|---------|
| Figure 96 | A plot of the spectrum from data collected at position 11 in the front half loaded model load space. | - 185 - |
| Figure 97 | A plot of the spectrum from data collected at position 1 in the side half loaded model load space. | - 186 - |
| Figure 98 | A plot of the spectrum from data collected at position 11 in the side half loaded model load space. | - 187 - |
| Figure 99 | A plot of the spectrum from data collected at position 1 in the fully loaded model load space. | - 188 - |
| Figure 100 | A plot of the spectrum from data collected at position 4 in the fully loaded model load space. | - 189 - |
| Figure 101 | A plot of the spectrum from data collected at position 11 in the fully loaded model load space. | - 190 - |
| Figure 102 | A plot of the cross-correlation function from data collected at positions 1 and 4 in the empty model load space. | - 191 - |
| Figure 103 | A plot of the cross-correlation function from data collected at positions 1 and 2 in the empty model load space. | - 192 - |
| Figure 104 | A plot of the co-spectrum from data collected at positions 1 and 4 in the empty model load space. | - 193 - |
| Figure 105 | A plot of the spectrum from data collected at position 1 in the empty model load space, plotted on a linear vertical axis. | - 194 - |
| Figure 106 | A plot of the cross-correlation function from data collected at positions 1 and 4 in the side half loaded model load space. | - 195 - |
| Figure 107 | A graph of the frequency of occurrence of values of turbulence intensity for all loading cases. | - 196 - |
| Figure 108 | A graph of the variation of turbulence intensity along the length of the front half loaded model load space. | - 197 - |
| Figure 109 | A graph of the variation of turbulence intensity with position across the width of the side half loaded model load space. | - 198 - |
| Figure 110 | Illustration of the comparison technique for determining numerical prediction errors. | - 205 - |
| Figure 111 | Distribution of error in terms of SDs for the empty load space simulation using standard EFF grid and 50% inlet jet speed (simulation 3). | - 213 - |

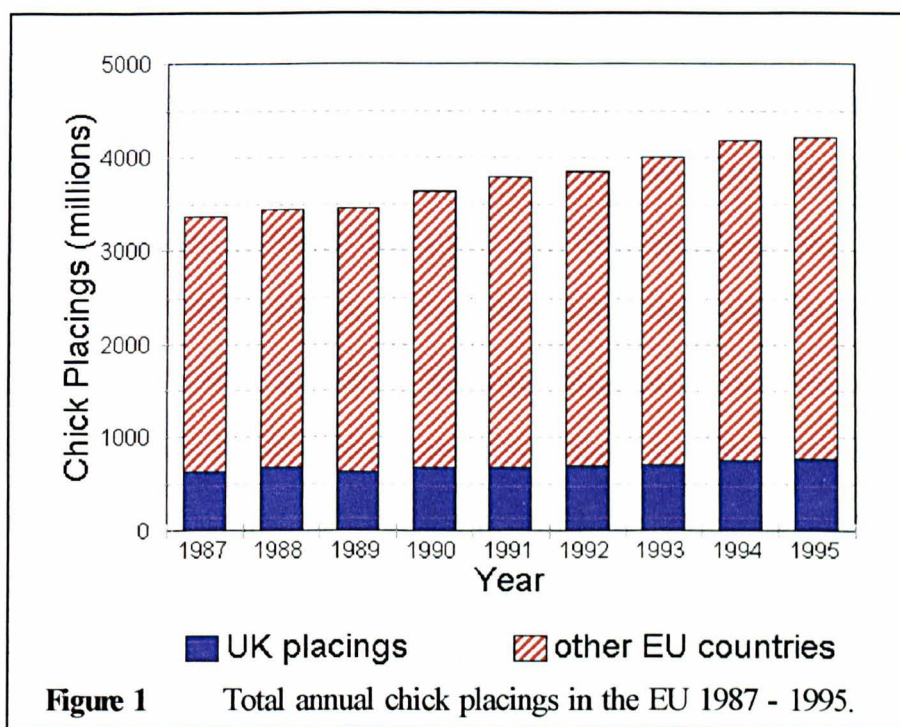
List of tables

| | | |
|-------------|--|---------|
| Table I | Lethal temperatures for day-old chicks. | - 16 - |
| Table II | Oxygen requirements of the day-old chick. | - 25 - |
| Table III | Suggested ventilation rates for day-old chicks. | - 25 - |
| Table IV | Variation of numerical results to inlet turbulence level. | - 92 - |
| Table V | A summary of the predicted ventilation rates for the empty load space case. | - 166 - |
| Table VI | A summary of the predicted ventilation rates for the front half loaded model case. | - 168 - |
| Table VII | A summary of the predicted ventilation rates for the side half loaded model case. | - 169 - |
| Table VIII | A summary of the predicted ventilation rates for the fully loaded model case. | - 170 - |
| Table IX | Integral length scale summary | - 176 - |
| Table X | Summary of the experimental data collected in the empty model load space case. | - 210 - |
| Table XI | Overall total absolute errors as a fraction of total absolute measured values for simulations of the empty load space. | - 214 - |
| Table XII | Fraction of points within 3 SDs of measured values for simulations of the empty load space. | - 215 - |
| Table XIII | Summary of the experimental data collected in the front half loaded model load space case. | - 216 - |
| Table XIV | Overall total absolute errors as a fraction of total absolute measured values for simulations of the front half loaded load space. | - 218 - |
| Table XV | Fraction of points within 3 SDs of measured values for simulations of the front half loaded load space. | - 219 - |
| Table XVI | Summary of the experimental data collected in the side half loaded model load space case. | - 220 - |
| Table XVII | Overall total absolute errors as a fraction of total absolute measured values for simulations of the side half loaded load space. | - 222 - |
| Table XVIII | Fraction of points within 3 SDs of measured values for simulations of the side half loaded load space. | - 223 - |
| Table XIX | Summary of the experimental data collected in the fully loaded model load space case. | - 223 - |
| Table XX | Overall total absolute errors as a fraction of total absolute measured values for simulations of the fully loaded load space. | - 225 - |
| Table XXI | Fraction of points within 3 SDs of measured values for simulations of the fully loaded load space. | - 226 - |

1. Introduction

1.1 The industry

The transportation of day-old chicks is a vitally important step in the production of both layer and broiler chickens. The steady expansion of the poultry meat industry, reflected in the growth of the numbers of chicks being reared (figure 1), has meant that the UK is now among the leading



producer nations in the EU, with a daily output of over three million chicks [MAFF 1993, MAFF 1995, Randall 1993, Randall 1995]. In order to achieve these numbers the industry has moved toward larger, purpose built

hatcheries. These are able to supply chicks to many growing unit farms, both national and international in the case of breeding stock. This procedure centralises the capital intensive hatchery equipment and reduces the risk of cross-generation pathogen contamination but requires an efficient transportation system for day-old chicks.

Long-haul transport is normally achieved by air freight but its high cost means that national and shorter international transport, such as that within the EU, is normally done by purpose built road vehicles. The only reported study of the variety of road transporters used was conducted by the US Department of Agriculture [Hinds 1958]. This found a wide variety of vehicles in use and many different techniques for maintaining adequate on board conditions. In Britain, the purpose built chick transporters first seen in the early 1960s have now become the standard road vehicles for the industry and a small number of different designs have been developed. However, with the increasing volume of chicks, lengthening delivery journeys and demand for vehicles able to carry fertile egg loads back to the hatchery, the size and complexity of vehicles in recent years has grown rapidly. The high cost of systematically developing new designs, and the time required, has led to a tendency to simply "stretch" an existing design to suit a larger vehicle, installing extra environmental control equipment to compensate for design problems. Vehicles with a normal capacity of up to 80 000 chicks are now in service throughout the EU. These vehicles now

commonly have automatically controlled air conditioning units, consisting of heaters and chillers, with separate power supplies, to maintain air conditions within the load.

The design of any new purpose built chick transporter in the UK must satisfy certain requirements. These can be summarised as follows:

i) The legislation and practical restrictions on motor vehicles. This mainly consists of maximum overall dimensions, axle weights and restrictions on driving times for workers. This final point leads to the requirement that environmental conditions are maintained for the chicks whilst the vehicle is stationary.

ii) Legislation and published guidelines for animal transport conditions. In the UK these are covered by the MAFF Codes of Recommendations for the Welfare of Livestock: Domestic Fowls (1987) and The Welfare of Poultry Transport Order (1988). These specify that "poultry are sheltered from the action of the weather", "protected from exposure to *undue* fluctuations in temperature, humidity or air pressure.", "have available to them an *adequate* supply of fresh air", "are *not overcrowded*" and that "any receptacle (containing poultry) is stowed in such a way as to allow *adequate* ventilation to the poultry". Also it is recommended that the best indicator of the adequacy of conditions is the chicks behaviour (*i.e.* panting, huddling

etc.). Transportation time and delays should also be *minimised*. (Authors italics)

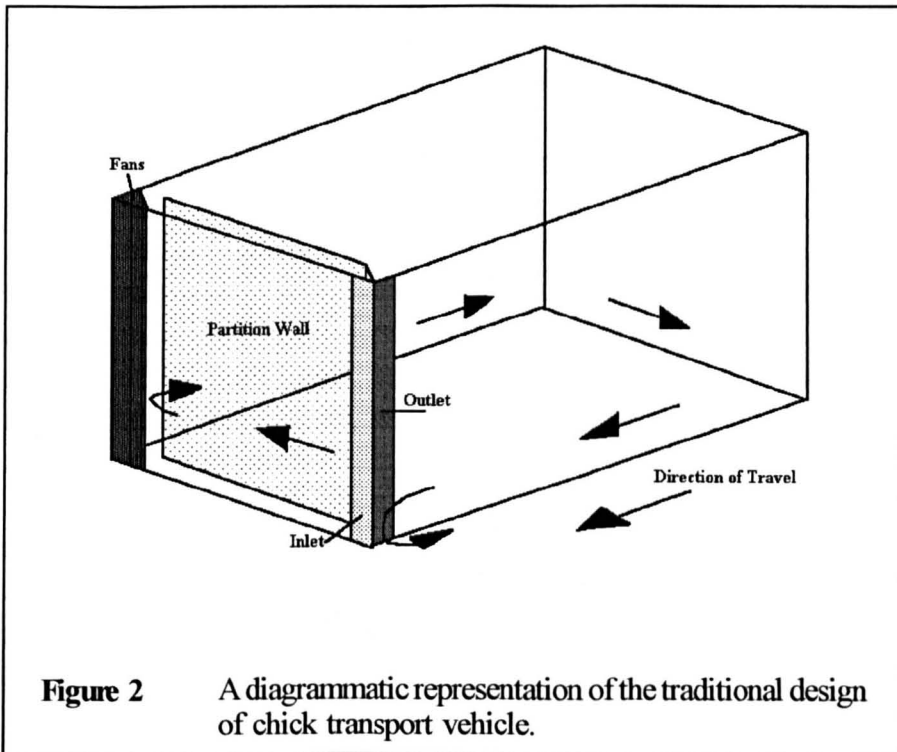
These guidelines however do not contain any practical definitions of the words such as 'adequate' or 'undue'.

The EU (1991) and Canada [Agriculture Canada 1989] have adopted similar guidelines, again without definitions, except for the provision of a time limit for transportation; 48 hours (Canada) and 24 hours (without food) within 72 hours of hatching (EU).

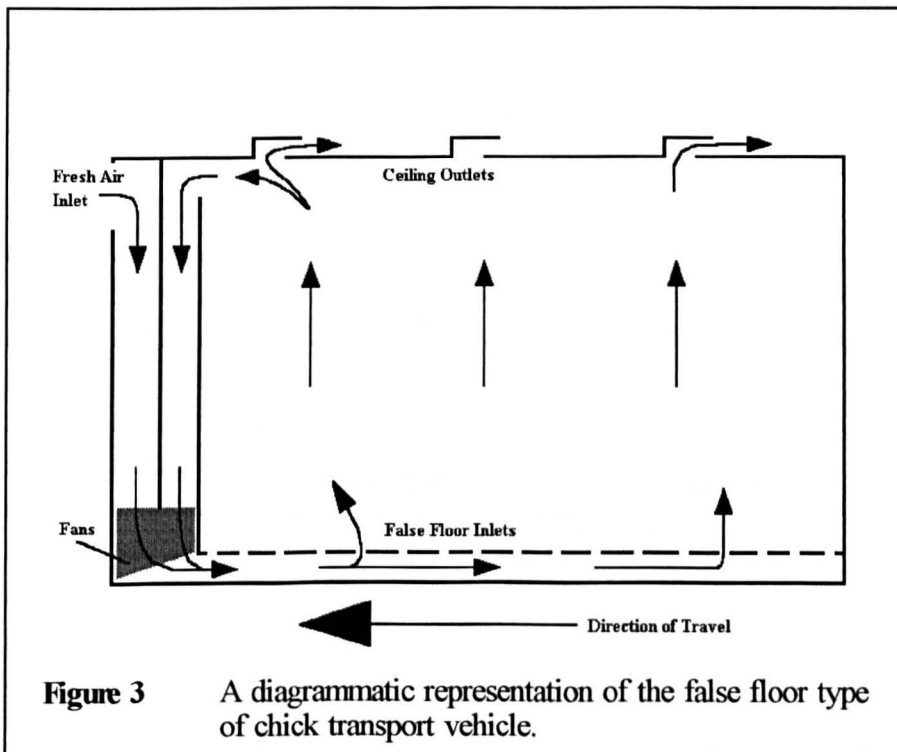
iii) The practical requirements of disinfection and cleaning which must be carried out after every journey to minimise cross infection.

iv) The business requirements for maximising load size and simplicity of construction for maintenance.

The first design, widely used even today, is illustrated in figure 2 [Banks 1983, Anon 1988]. This design uses a horizontal flow pattern (*i.e.* flow is approximately two dimensional in a horizontal plane) to pass fresh, cooled air around the vehicle in a circular route. Its advantages stem from the lack of any false floor, ceiling or walls (except the front chamber which is required by all systems for the air conditioning equipment). Thus load

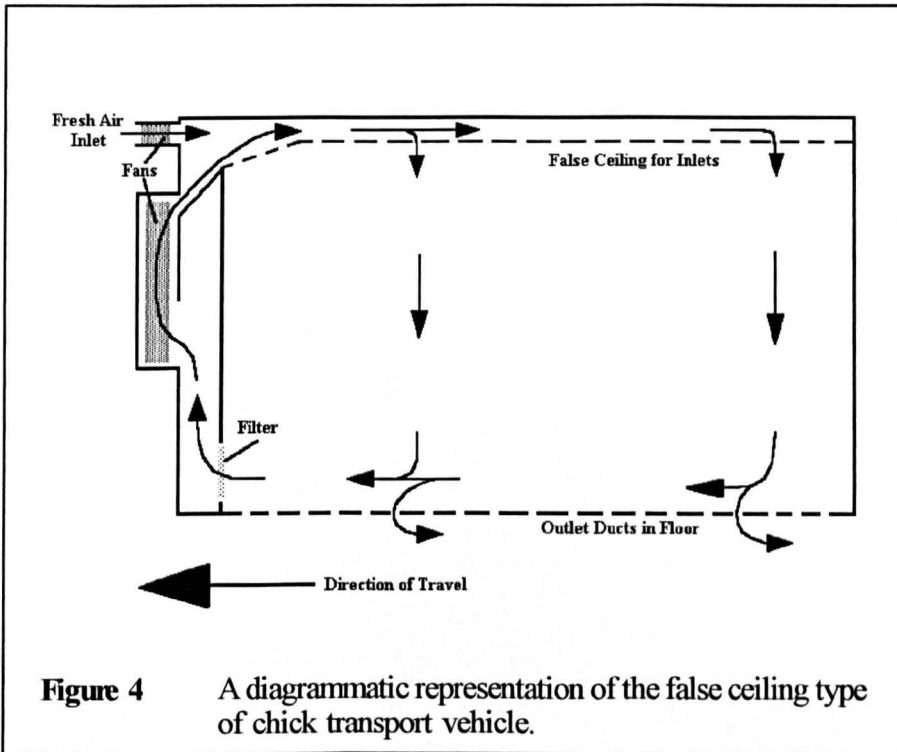


space is maximised and it is easy to use and maintain. However "hot-spots" are known by operators to exist because of the circulation pattern through the load, and thus the distribution of fresh air is not uniform. This has become particularly noticeable as vehicle lengths have increased (the only practical method of increasing load size). One other criticism of this design is that it does not take account of the buoyancy effects due to the heat production of the load. This has led to designs such as in figure 3. These circulate air from bottom to top through the load and thereby supply fresh air more evenly to the birds. However this requires either false flooring or the raising of the load off the floor, both of which reduce load size and can complicate construction, maintenance and cleaning of the vehicles.



Another desirable feature of any design would be that the ventilation system reduces the quantity of loose feathers and dirt being blown through the vehicle, as these can clog or damage ventilation equipment. Thus filtering the recirculated air is desirable but requires that the filters be easily accessible for cleaning. This has led to designs such as figure 4 which circulate air top to bottom through the load. This requires a false ceiling and outlets in the floor, which is a structurally simpler design than that in figure 3, but does mean that the air flow is again opposed to the natural buoyancy.

Early designs in the US [Hinds 1958] often had inlets for fresh air high above the cab and outlet grills over many areas of the sides and rear of the load space. These designs are reported to have worked well but do



not appear to have taken into account the external pressure field of the vehicle in motion which may cause an inflow of polluted air at the rear of the vehicle [Hoxey *et al* 1992, Hoxey *et al* 1996, Baker *et al* 1996, Dalley *et al* 1996].

Construction of chick transporter bodies is a very specialised business due to the requirements of air conditioning, insulation and hygiene that must be fulfilled [Banks 1983, Anon. 1988]. The bodywork design is normally modified to fit each individual truck since chassis and cab designs are not standard. However there are no guidelines or monitoring of the designs used.

Within the load space, whichever design is used, chicks are normally held in purpose made cardboard or plastic boxes. A typical chick-box (figure 5) is approximately 0.5 m x 0.5 m x 0.15 m deep with a lid and

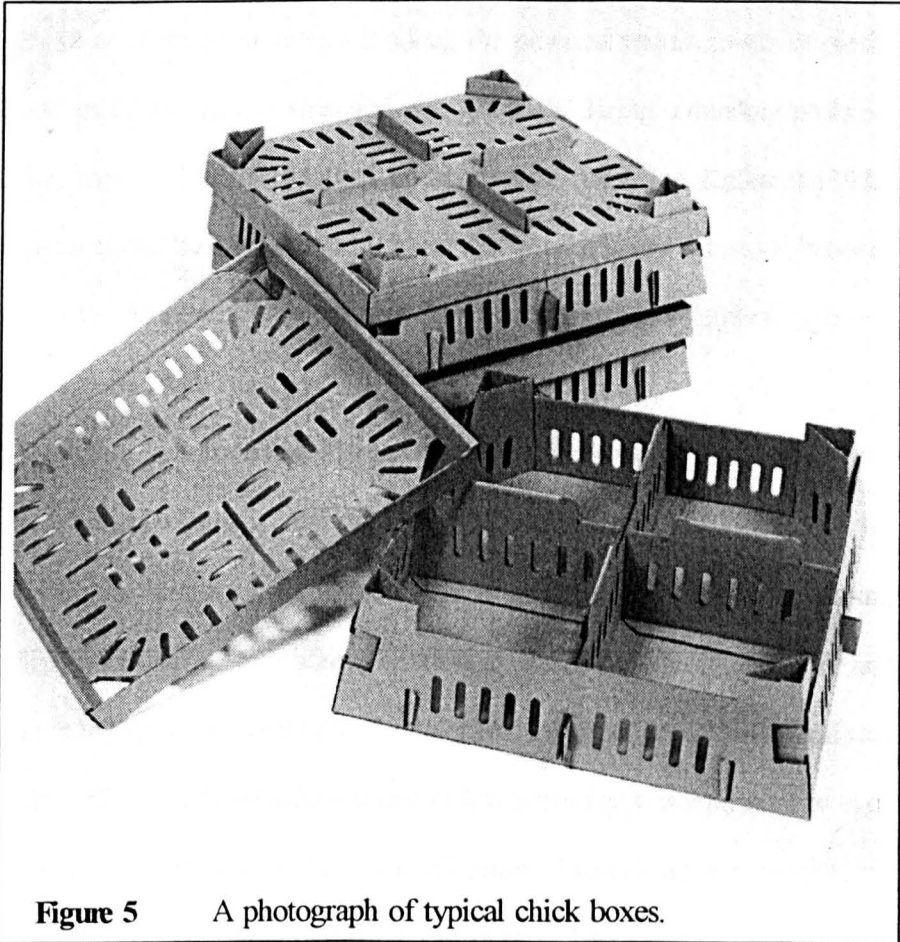


Figure 5 A photograph of typical chick boxes.

ventilation holes. This type of box holds 80-150 chicks (normally 100) in four internal compartments (25 chicks in each). These boxes can be stacked on one another and on metal frame 'trolleys' which give greater ease of (un)loading. Various trolley sizes and types are used, sometimes even varying amongst the vehicles of an individual haulier. The simplest type is

a wheeled base plate on to which boxes are stacked 10-12 high and secured within the vehicle. More complicated designs, such as shown in figure 13 (section 2.2.1), hold a number of smaller stacks on separate shelves. The arrangement of boxes and trolleys within a vehicle is usually determined by the driver or attendant during loading, the practical requirements of partial loads, multiple delivery sites and ease of access during unloading probably being most influential on final arrangements. Joshi and Kulkarni (1986) suggest stacks be limited to 3 high and that good spacing is needed between stacks to ensure sufficient air movement during transport and storage.

The environment during road transport has had very little investigation. Tamlyn and Starr (1987) monitored the conditions of temperature and relative humidity (RH) inside a UK transporter during deliveries of up to two hours duration in moderate conditions (May and August). This study found that the temperature variation within a load was up to 8 °C and that dehydration due to low humidity was a possibility even on wet days. These conditions and duration of travel are not uncommon, indeed trans-european journeys can last over 24 hours and extreme weather is not usually a reason for delaying delivery because hatcheries cannot hold chicks for more than 24 hours after hatch.

As previously stated, recommendations are that the assessment of suitability of conditions in a transporter be based largely upon chick

behaviour. This is practical given some knowledge and experience of chicks. However it must be remembered that chicks' reactions vary and these danger signals may only occur after conditions have reached a critical level [Wilson and Plaister 1951, Misson 1976]. Also modern transporters, unlike early designs [Hinds 1958], have no contact between driver/attendant and chicks during the journey. So although observation is a practical method of determining the general settings of a vehicle's air conditioning system when at the hatchery, it is no substitute for a more detailed knowledge of the actual conditions prevailing in the transporter at all times. Toward this end many transporters have temperature sensors in the load space which give the driver a continuous read out. These must of course be carefully positioned and calibrated if they are to give a true picture of the state of the load (that is the microclimate of the birds). It must also be considered that temperature alone may not be representative of the environmental state within the load, RH for example may be equally important.

1.2 Problems of chick transportation

An understanding of the environmental conditions that arise in any situation involving animals must be achieved with respect to the animals concerned. Thus before an evaluation of conditions on board a transporter can be undertaken a knowledge of chick requirements is necessary. The importance of the correct conditions for transportation also needs to be understood. It is thus necessary to decide what criteria are to be used in the assessment of the environment and the weighting of each factor. Welfare considerations would minimise stress on the chicks whereas industry considers minimum mortality and maximum subsequent growth rate. These factors may of course be linked but such links are specific to the species concerned. It is also important to remember that the environmental factors one can normally measure (global ventilation rate, ambient temperature and relative humidity (RH) etc) are not necessarily those factors experienced by the animal (microclimate) or most important to the animal (*e.g.* oxygen requirement). However one must assume that there exists a practical relationship between these variables.

For its survival a day-old chick must have sufficient oxygen to breath and be able to maintain its body temperature. The function of the transporter air conditioning system must therefore be to maintain an environment in which the chick can survive most readily.

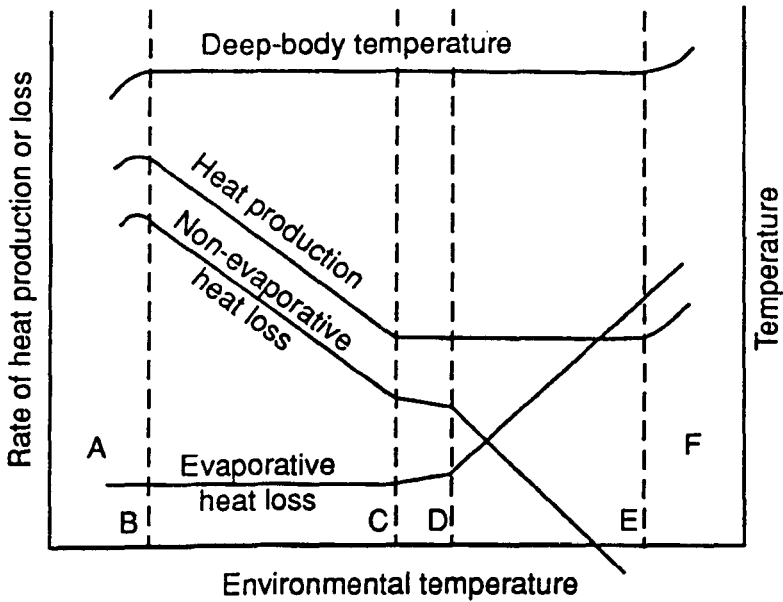


Figure 6 A diagrammatic representation of relationships between heat production, evaporative and non-evaporative (sensible) heat loss and deep body temperature in a homeothermic animal.

- Key**
- A: zone of hypothermia;
 - B: temperature of summit metabolism and incipient hypothermia;
 - C: critical temperature;
 - D: temperature of marked increase in evaporative heat loss;
 - E: temperature of incipient hyperthermal rise;
 - F: zone of hyperthermia;
 - CD: zone of least thermoregulatory effort;
 - CE: zone of minimal metabolism;
 - BE: thermoregulatory range.
- [after Mount (1974)].

One method of determining the most appropriate environment is to correlate the effort required for survival against the environmental variable(s) available - normally environmental temperature. This gives rise to a diagram such as figure 6 [after Mount 1974] which shows the energy balance of a perfectly homeothermic animal (that is one able to maintain a constant deep body temperature) over a range of environmental temperature. In the areas A and F the animal is unable to maintain its body temperature and will die. Between B and C the animal is maintaining its body temperature by internal heat production and is therefore depleting its internal energy reserves which it requires to survive. Between D and E it is losing heat by evaporation of moisture (from the skin and/or respiratory tract) and is therefore depleting its internal water supply which may lead to dehydration. Thus it can be seen that the most appropriate temperature is between C and D - the zone of least thermoregulatory effort.

For chicks this idealised picture is not entirely applicable since they are able to survive changes in deep body temperature which are lethal to older birds [Moreng and Shaffner 1951]. This is required because chicks are unable to maintain deep body temperature (homiothermy) outside a narrow range of environmental temperatures. However the general boundaries of the regions are consistent and have been investigated [Mount 1979, Poczopko 1981].

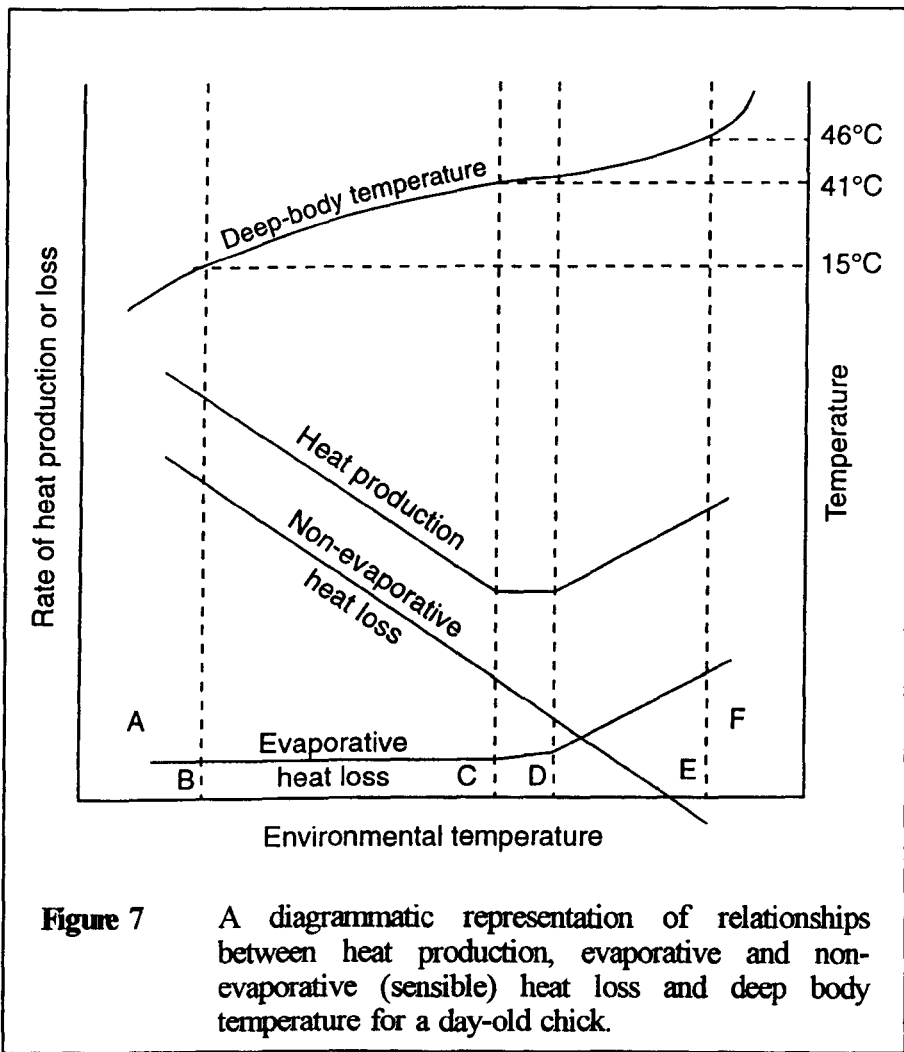


Figure 7 A diagrammatic representation of relationships between heat production, evaporative and non-evaporative (sensible) heat loss and deep body temperature for a day-old chick.

- Key**
- A: zone of hypothermia;
 - B: temperature of summit metabolism and incipient hypothermia;
 - C: critical temperature;
 - D: temperature of marked increase in evaporative heat loss;
 - E: temperature of incipient hyperthermal rise;
 - F: zone of hyperthermia;
 - CD: zone of least thermoregulatory effort and zone of minimal metabolism;
 - BE: survival zone.

Moreng and Shaffner (1951) studied the boundaries B and E in terms of the lethal internal (deep body) temperature of chickens between hatch and maturity. They found that newly hatched chicks could survive for about one half of an hour at $-23\text{ }^{\circ}\text{C}$ ($-10\text{ }^{\circ}\text{F}$) and that the lowest body temperature reached was $15\text{ }^{\circ}\text{C}$ ($60\text{ }^{\circ}\text{F}$). At the other extreme chicks survived only 10 - 13 minutes at $71\text{ }^{\circ}\text{C}$, with deep body temperature reaching $46.6\text{ }^{\circ}\text{C}$ ($116\text{ }^{\circ}\text{F}$). These studies suggest a modified form of figure 6 for day-old chicks (figure 7) and that heat stress is a more important problem for chicks than dry, cold conditions. It should be noted at this point that work to determine the effects of temperature on poultry has been done since the early twentieth century. As poultry production has become more intensive, selective breeding has meant that broilers can now reach slaughter weight in less than half the time it took 50 years ago. Although these changes in the birds have been primarily to increase productivity it must be borne in mind that other factors may also have changed. However Freeman (1984) has shown that some more recent results are in agreement with these previous experiments.

More valuable to the problem of transporter environment however is a knowledge of what ambient conditions, combined with insulation, heat production and confinement of the chicks, can lead to mortality, either by overheating or suffocation due to huddling for warmth. Some published results for overheating are presented in table I.

Table I Lethal temperatures for day-old chicks.

| Reference | Ambient Temp °C | Exposure Time | Result |
|-----------------------------|-----------------|---------------|-------------------------------|
| Moreng & Shaffner (1951) | 71 | 13 mins | 50% mortality [*] |
| Henken <i>et al</i> (1987) | >38.2 | 24+ hrs | some mortality |
| Wilson & Plaister (1951) | 43 | >2.5 hrs | 33% mortality ^{**} |
| Booty (1982) | >35 | <30 mins | some mortality ^{***} |
| Henken & Van der Hel (1990) | 38.8 | 48 hrs | 14.5% mortality |
| Henken & Van der Hel (1990) | 40.0 | 48 hrs | 53.5% mortality |
| Henken & Van der Hel (1990) | 41.2 | 14 hrs | 73.2% mortality |
| Henken & Van der Hel (1990) | 42.0 | 14 hrs | 84.6% mortality |

Notes:

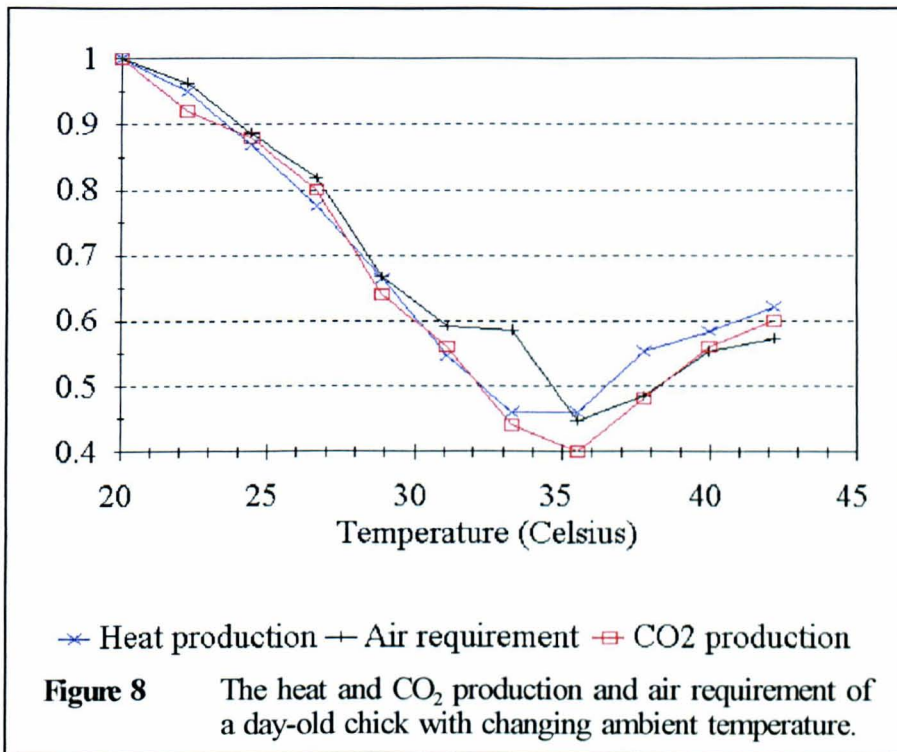
- * Deep body temperature at death 46.6°C.
- ** Mean mortality rate for 2 breeds of chick housed in cardboard boxes during experiment.
- *** Chicks housed in cardboard boxes.

These results show two distinct groups and illustrate the two different causes of death amongst heat-stressed birds. The birds subjected to higher temperatures [Moreng and Shaffner 1951, Wilson and Plaister 1951, Booty 1982, Henken and Van der Hel 1990] are unable to thermoregulate sufficiently by panting (evaporation) and thus die of hyperthermia. Birds subjected to lower temperatures [Henken *et al* 1987,

Henken and Van der Hel 1990] however are able to thermoregulate by panting. This can continue until the water supply of the bird is exhausted and it passes out from dehydration and dies. This illustrates the zone DE of figures 6/7.

Chicks are composed of 85% water and are very vulnerable to dehydration during transport [Qureshi 1991] due to their reliance on evaporative cooling. The chick does have a reserve of food and water, held in the body after hatching, in the yolk sac. This consists of about 2 g fat and about 2.5 ml water [Freeman 1984] - enough to last up to 72 hours in good conditions [Booty 1982, Macleod 1982, Freeman 1984, Joshi and Kulkarni 1986]. However not only can the supply of water be exhausted in 8-10 hours due to evaporation at high temperatures (around 40 °C) but also the natural variation in hatching time (up to 2 days) means that otherwise identical 'day-old' chicks can have very different survival capabilities [Macleod 1982].

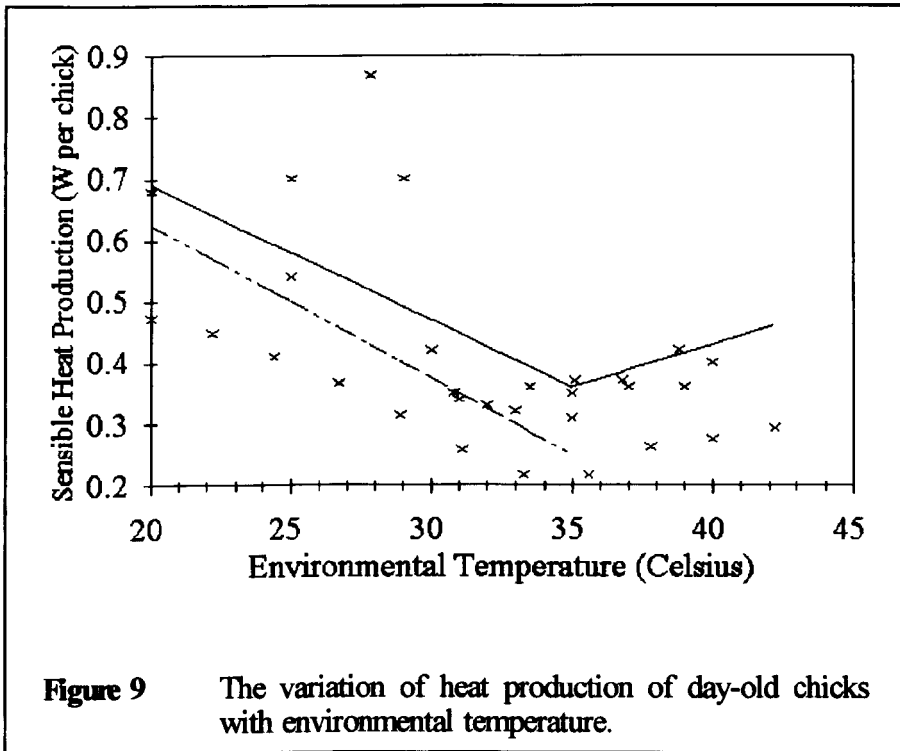
As mentioned previously figure 6 does not give an entirely true picture of the responses of neonatal chick to environmental temperature. A more realistic view of the appropriateness of a given temperature is gained by study of the heat production, oxygen consumption or carbon dioxide production of chicks at various temperatures. This gives rise to a graph such as figure 8 which shows that the minimum metabolic rate is achieved at



Data from Hinds (1958).

Scaled in the y axis as a fraction of the value at 20°C.

between 33 °C - 36 °C. Other authors have also measured the heat production of neonatal chicks [Misson 1976, Charles 1981, Henken *et al* 1991a, Van der Hel *et al* 1991, Turner *et al* 1992] and determined trends of dependence on temperature [Misson 1976, Macleod 1982, Freeman 1984]. These are summarised in figure 9. Not all these studies have taken into account the variation of heat production with ambient temperature or the relative contributions of the sensible and latent components of heat loss. For a more detailed discussion of the latter see Turner *et al* (1992).



Data from Charles (1981), Van der Hel *et al* (1991), Turner *et al* (1992), Henken *et al* (1991a), Macleod (1982), Mission (1976), Hinds (1958) and Freeman (1984). The dotted and solid lines represent the trends of heat production with temperature suggested by MacLeod (1982) and Freeman (1984) respectively.

Although there is a variation in absolute value of heat production at minimum metabolism, it can be seen that this minimum lies in the temperature range 32 °C - 37 °C. This agrees with the range of thermal neutrality reported by Poczojko (1981) for a neonatal chick as 34 °C - 36 °C. However the upper limit of 37 °C may be unreasonable, due to lack of data, considering the upper critical temperatures of 35 °C - 38 °C reported by Misson (1976), Henken *et al* 1987 and Van der Hel *et al* 1991.

The variation in value at the minimum may be due to experimental technique (direct or indirect calorimetry), genetic factors, breed or age differences in the chicks used as well as the natural variation which is to be expected.

This range is then the zone CD of figures 6/7 - the zone of least thermoregulatory effort for the chicks. This zone is very narrow for a chick compared with many other animals and is therefore often considered as a point rather than a range. It is the temperature of the microclimate most suitable for the chick bearing in mind the possibility of dehydration discussed above.

Various authors have suggested optimal temperatures for neonatal poultry transportation or initial brooding [Hinds 1958, Mount 1979, Charles 1981, Sainsbury 1981, Deaton 1983, Qureshi 1991, Herbut *et al* 1992], others have tested the thermal preferences of day-old chicks [Alsam and Wathes 1991b, Charles 1986] or the temperatures for optimum initial growth [Mount 1979, Charles 1986]. All except Charles (1981) (27 °C) covered the range 31 °C - 35 °C which agrees well with the previous analysis of heat production.

Mention has already been made of the latent or insensible component of heat loss by chicks. This occurs in three ways; panting to lose

heat by evaporation over the respiratory tract, evaporation of the skin moisture and heat loss in faecal moisture. The last of these does not significantly reduce body temperature because of the water (*i.e.* weight) loss which accompanies it. It is however a serious cause of dehydration in heat stressed poultry especially during transport. It also causes another major problem for confined birds which is that of increased relative humidity (RH). Qureshi (1991) suggests that RH should be as important a concern as temperature when transporting or housing chicks. Low RH obviously leads to dehydration, especially when accompanied by high temperature. This situation is likely to occur not only in desert climates but in cool climates where the air temperature is maintained by dry heating alone. For example air at 10 °C 70% RH heated to 35 °C with no change in its moisture content will have only 15% RH. Qureshi 1991 suggests RH in the range 60% - 80% is suitable for chicks.

High RH, when coupled with high temperature is also dangerous because of the likelihood of overheating. The high moisture content of the air makes evaporation (especially panting) for heat loss a very inefficient process. Thus the limited sensible heat loss of the birds due to the high temperature is coupled with limited latent heat loss and increasing heat production (due to the effort of panting) making hyperthermia likely.

These problems of dehydration and overheating led Henken and Van der Hel 1990 to suggest that an effective environmental temperature of

$$T_{eff} = 0.81T_d + 0.19T_w \quad \text{where } T_d = \text{dry bulb temperature} \\ \text{and } T_w = \text{wet bulb temperature}$$

should be used for maintaining the conditions in which chicks are held and that this measure should be kept below 35 °C at all times. This measure is a weighted temperature derived from their experiments concerning weight (water) loss and heat production of day-old chicks in different conditions of temperature and RH. They also suggested that water loss or body weight loss is a better measure of the appropriateness of conditions than mortality during transport. This view is supported by a number of studies which have noted that temperature stress and/or dehydration can lead to increased susceptibility to disease [Prabakaren 1990], suppression of the immune system [World Meteorological Organization 1989] and damage to the respiratory tract [Qureshi 1991]. These effects are combined with a reduction of food intake and growth and with increased mortality in the subsequent weeks of life [Williams *et al* 1951, Deaton 1983, Ernst *et al* 1984, Charles 1986, Henken *et al* 1987, World Meteorological Organization 1989, Prabakaren 1990, Henken *et al* 1991b].

This inclusion of humidity and dry temperature in one indicator of environmental conditions is similar to the "apparent equivalent temperature" (AET) proposed by Mitchell and Kettlewell (1993) for mature broiler chickens during transport. However, where the former has been derived

from body temperature and weight (water) loss, the latter can be calibrated in terms of many physiological parameters including changes in blood chemistry. The latter also incorporates the humidity of the environment in terms of the vapour density which has been found to be more clearly related to indicators of thermal stress than RH. Mitchell (1996) has extended this idea of AET to day-old chicks by assessment of the changes in deep body temperature, weight loss, heat production and blood chemistry due to various thermal environments. This led to the suggestion that the optimum microclimate conditions during transport are 24.5 °C - 25 °C with corresponding RH of 63% - 60%. This clearly differs from the previously stated values of 32 °C - 37 °C for the range of minimum metabolism. However, these differences may be explicable in terms of: the uncontrolled humidity of earlier experiments, low humidity giving the chicks improved thermoregulatory capacity at higher temperatures; the effects of grouping and boxing chicks as per normal commercial practice in the latter study; or the effect of evaluating the environment in terms of multiple physiological parameters rather than heat production alone.

Methods have been suggested to increase the survivability of poultry (mostly mature birds) to heat stress [Daghir 1988, Singh 1988, Burger 1989, Prabakaren 1990]. However these are of limited applicability to chicks in transport. Other methods including additives in drinking water, tranquillisers and injections with water before transport have been found to be mostly

inapplicable or impractical [Freeman 1984, Kettlewell 1989]. However it has been noted by Freeman (1984), in older broilers, that the calming effect of cool ventilation to the head alone reduces significantly the effects of high ambient temperature by suppressing excessive panting and thereby minimising heat production. This then enhances the survivability and condition of birds in addition to the benefits of ventilation increasing the conductance [Bakken 1991] and convective heat loss [World Meteorological Organization 1989] of the birds. These effects are exploited, if space allows, by behavioural as well as physiological responses [Alsam and Wathes 1991a].

Ventilation is also required to supply fresh air to the chicks and remove carbon dioxide and other pollutants such as ammonia produced by the birds. These pollutants, in sufficient concentration, can also cause mortality or increased susceptibility to diseases [Mount 1979, World Meteorological Organization 1989, Wathes 1992]. The quantity of fresh air required by a day-old chick has been measured [Misson 1976, Poczopko 1981] as at least 1.6×10^{-2} ml oxygen per second (see table II), from this the required air supply can be estimated.

However the removal of waste gases and heat will require a much higher ventilation rate, and will depend on the air flow distribution more than the volume flow rate of the ventilation. This has been studied in

Table II Oxygen requirements of the day-old chick.

| Reference | Requirement per chick |
|-----------------|--|
| Poczopko (1981) | 1.7x10 ⁻² ml oxygen s ⁻¹ (minimum) 4.0x10 ⁻² ml oxygen s ⁻¹ (maximum) |
| Mission (1976) | 4.1x10 ⁻² ml oxygen s ⁻¹ (at 20°C) 1.6x10 ⁻² ml oxygen s ⁻¹ (at 35°C) 2.0x10 ⁻² ml oxygen s ⁻¹ (at 40°C) |
| Hinds (1958) | 5.6x10 ⁻² ml air s ⁻¹ (minimum) 12.5x10 ⁻² ml air s ⁻¹ (maximum) |

considerable depth for the case of livestock buildings - see Carpenter (1981) for more details. Consideration of air flow distribution as well as factors of climate may explain the wide range of figures quoted for ventilation rate in table III.

Table III Suggested ventilation rates for day-old chicks.

| Reference | Ventilation Rate (ml s ⁻¹ per bird) | Notes |
|----------------|--|--------------|
| MacLeod (1982) | 0.5 | minimum rate |
| Hinds (1958) | 4.7 | minimum rate |
| Hinds (1958) | 9.4 | |
| Charles (1981) | 13 | minimum rate |
| Charles (1981) | 16 | |
| Muller (1985) | 26 | |
| Mount (1979) | 28 | |
| Randall (1977) | 32 | |

A study of the flow pattern, as well as an estimation of the required flow volume, is therefore necessary in the design of animal transporters, for reasons of ventilation efficiency in the removal of both waste heat and gases.

The differences of ventilation system design outlined previously (figures 2-4 section 1.1) are similar in some respects to those found in aircraft hold ventilation during the transport of day-old chicks. Aircraft holds generally have little if any ventilation and are often used as the exhaust areas for the passenger compartment air. Studies into chick survival during air transport [Hoogerbrugge and Ormel 1982, Henken *et al* 1987, Roberts 1987] have shown that high temperatures and RH are the main causes of death, due to the enclosed nature of the hold space and consequent lack of ventilation. These problems occur at 'ambient' hold temperatures 8 °C - 14 °C below the upper critical temperature for chicks. This is due to the difference between ambient and microclimate conditions because of the heat and moisture trapped by the chick-box. This build up of lethal conditions can occur within 10 - 15 minutes if the load space is not ventilated and the mortality rate can be close to 100% in less than 1 hour. It was found however that the stacking arrangement of the boxes in the hold could be used to offset this problem, by making use of the natural buoyancy-driven ventilation due to the heat production of the chicks. This led to suggestions that:

i) Vertical spacing around each column of boxes is essential. ~10 cm between stacks on at least two sides, with some missing stacks to give 'chimneys'.

ii) space above the top box of ~30 cm to remove hot air.

iii) space below the lowest box of ~10 cm to allow fresh air in.

Booty (1982) also suggests that these measures alone cannot replace the need for individual evaluation of each situation by a competent person. Hence some airlines and hatchery suppliers have collaborated to give training to personnel in how to accommodate the needs of chicks in the various situations found on board different aircraft.

1.3 The structure of the investigation

1.3.1 Overall objectives

The overall objectives of this study are twofold: to gain an understanding of the air flow inside a commercial chick transport vehicle and to assess the appropriateness of computer modelling to this situation. The former objective will be achieved by experimental work to collect details of the air movement inside a vehicle, whilst the latter is done by comparison of predicted statistics with the data collected.

1.3.2 Experimental objective

The experimental objective of this study is to collect a detailed set of measurements representative of the isothermal air flow pattern inside a chick transport vehicle under various loading configurations.

1.3.3 Numerical simulation objectives

The numerical simulation objectives are to produce a computational fluid dynamics (CFD) model, of the replica transporter employed in the experiments, using a standard commercial software package in order to evaluate its appropriateness to this situation. This assessment will be done

by comparison of the predicted results with those from the experimental data.

1.4 Outline of the thesis

The experimental details of this project will be presented in chapter 2, starting with a discussion of the measurements required and the analysis of these measurements. The details of experimental methodology for each part of the project are presented as sub-sections of chapter 2 concluding with a description of the loading configurations used in this project and details of the data analysis routines used.

Chapter 3 covers the numerical simulation methodology with a description of the resources used and the development of the models used in the final simulations. The computational cases studied are presented and the analysis techniques for the results discussed.

Results for both the experimental and numerical models are presented in chapter 4, which is divided into two sections. The first of these deals with those experimental results which can be directly compared to the numerical predictions, that is the time averaged results. The second covers spectral and correlation results which cannot be compared directly with the steady state numerical predictions.

Quantitative comparison of the experimental and numerical results is covered in chapter 5, where the background, methodology and results are presented. The implications, both for chick transport in terms of the predicted conditions during transport and for general CFD studies, are discussed in chapter 6 with a summary of the overall project conclusions in chapter 7. Detailed background information and lengthy detailed results are presented as appendices where necessary.

2 The experiments

2.1 The parameters to be measured

2.1.1 Introduction

Ideally, given a turbulent three dimensional internal flow situation, it would be desirable to measure the air-flow at all points throughout the space, yielding mean speed, direction and variability. As this is not possible experimentally it is required to derive a representative sample of these statistics from individual point measurements made sequentially. This requires a knowledge of the stability of the system, that is the repeatability of such sequential measurements over time. This knowledge is also required in order to derive statistics about variability from such time series measurements, the means having to be constant if the variance about such a mean is to be a useful turbulence measure. Assuming that the system is steady over some sufficiently long time period one can derive meaningful average flow statistics from time series of this length. Turbulence however is a continuous process with a broad spectral content. In order to capture a representative idea of turbulent structure one must sample the flow over periods representative of all the structures present. This means that in addition to a minimum sample length required to be representative of the large structures, which is equivalent to the requirement for a steady mean,

there is also a high frequency constraint to be considered. This is embodied within the frequency response of the measuring system employed, which may be limited by the physical size of the instrument, the sensitivity of the instrument or the techniques of frequency analysis used on the data. The adequacy of whatever method used can be analyzed by calculating the energy content of the time series in the frequency domain, which should be closed at both high and low frequencies if an adequate range has been sampled.

Further information about the turbulent length scales present can also be extracted in the time domain by considering the autocorrelation function derived from the original time series. In addition to these turbulence statistics it is also possible to determine the shear stresses by combining the time series of the separate components, if these have been measured simultaneously at a single location. These can then be expressed either as time averaged values or in the frequency domain.

It is also possible to determine some general statistics about the air flow between measuring points if simultaneous measurements can be made at two or more spatially separate locations. The time series from pairs of points can then be combined to give cross-correlation or cross-spectral functions which can yield transit times for the flow between the points and the coherence of the structures at the separate locations.

One further important parameter which must also be measured is the volume (or mass) flow of air passing through the system per unit time. This is important not only for accurate simulation work but also to ensure the replication of conditions for series measurements. This can be achieved for example by measuring the pressure loss across a section of the flow through which all or a known fraction of the air must pass, if a suitable calibration method can be achieved.

2.1.2 Definition of parameters

Given that most experimental results are in digital or digitized analogue form, these definitions are given in terms of finite discrete time series. The exact continuous (infinite) results are derived in Bendat and Piersol (1980). It is however important to note that the statistics calculated from any finite discrete time series can only ever be an estimate of the exact mathematical functions. For this reason the normal ideas of repeated experiments and errors in values must be considered for these type of statistics.

Mean

Consider a finite discrete time series $\langle x_i \rangle : 1 \leq i \leq N$, recorded at a frequency $\frac{1}{t_s}$, where t_s is the (constant) time between measurements.

Assuming $\langle x_i \rangle$ is a well behaved sequence with constant mean (*i.e.* the measurements are of a stationary, ergodic process), then this mean can be

written as $\bar{x} = \frac{1}{N} \sum_{i=1}^N x_i$.

Variance

The spread of values taken by $\langle x_i \rangle$ about \bar{x} can then be expressed in terms of the sample variance of $\langle x_i \rangle$ namely,

$\sigma_x^2 \doteq \frac{1}{N-1} \sum_{i=1}^N (x_i - \bar{x})^2$. Note that if (and only if) $\langle x_i \rangle$ is a sequence of

speed measurements then σ_x^2 has the units of specific energy (energy per unit mass) so the kinetic energy content of the airflow due to turbulent fluctuations (the so called Turbulent Kinetic Energy [TKE]) can be defined as $k \doteq \frac{1}{2}(\sigma_x^2 + \sigma_y^2 + \sigma_z^2)$ where x,y,z represent an orthogonal coordinate

system on which simultaneous measurements $\langle x_i \rangle$, $\langle y_i \rangle$, $\langle z_i \rangle$ have been made. This measure is sometimes expressed as a turbulence intensity $I \doteq \frac{k}{U^2}$

where U is some representative speed such as $U^2 = \bar{x}^2 + \bar{y}^2 + \bar{z}^2$ or some other characteristic value for the system. The variance of means $\sigma_{\bar{x}}^2$,

where repeated measurements $\langle x_i \rangle_j : 1 \leq j \leq M$ exist, is also used to express the repeatability of experimental runs. This is defined

$\sigma_{\bar{x}}^2 \doteq \frac{1}{M-1} \sum_{j=1}^M (\bar{x}_j - \bar{\bar{x}})^2$ where $\bar{\bar{x}} = \frac{1}{M} \sum_{j=1}^M \bar{x}_j$ is the mean mean or true mean of the repeated data.

Lagged Variance and Autocorrelation Function

The lagged variance $\sigma_{xx}(r) \doteq \frac{1}{N-r-1} \sum_{i=1}^{N-r} (x_i - \bar{x})(x_{i+r} - \bar{x})$

where $1 \leq r \leq N-1$ is the lag in terms of number of measurements, usually expressed as a lag time $\tau \doteq r t_s$. This lagged variance can be expressed in a non-dimensional form, the autocorrelation function

$R_{xx}(\tau) \doteq \frac{\sigma_{xx}(\tau)}{\sigma_x^2} : -1 \leq R_{xx} \leq 1$. This function reflects the structures of the

turbulence in terms of the time lag between similar peaks/troughs in the measured values. For example if

$$\begin{aligned} x_{i+k} &= x_i \quad \forall i \rightarrow R_{xx}(k) = 1 \\ x_{i+k} &= -x_i \quad \forall i \rightarrow R_{xx}(k) = -1 \end{aligned}$$

Note that the former of these cases is always satisfied by a lag time k of zero and that by definition the autocorrelation function must be symmetric because of the symmetry of the lagged covariance. From this autocorrelation function it is possible to determine whether any structure exists within the turbulent flow measured, which is so if the autocorrelation function is significantly non-zero for any non-zero time lag.

Length Scale of Turbulence

The size of the largest such structures (the length scale) can be gauged by multiplying a representative lag time from the autocorrelation function by a representative speed of the mean flow. Two possible practical interpretations of this are:

1. the positive length scale where the representative lag time is defined as $\max \tau [R_{xx}(r) > 0 \quad \forall 0 \leq r \leq \tau]$ and the speed as the magnitude of the mean velocity; [$\forall 0 \leq r \leq \tau$ means for all values of r between zero and τ inclusive.]

2. the integral length scale where the autocorrelation coefficient is used as a weighting function in determining the representative lag time equal to $\int_0^\tau R_{xx}(r) dr$, where τ is sufficiently large as to include all significant non-zero contributions to the autocorrelation function, the magnitude of the mean flow again being the representative speed.

Spectral Density Functions

The turbulent structure of the flow can also be expressed in the frequency domain by means of the one (or two) sided autospectral density function (spectrum).

$$\begin{aligned} G_{xx}(f) &\doteq \mathcal{F}(R_{xx}) \\ &= \mathcal{F}^*(x_i) \mathcal{F}(x_i) \\ &\rightarrow G_{xx} \in \mathbb{R} \end{aligned}$$

where \mathcal{F} is the Fourier transform of a real series, \mathcal{F}^* is its complex conjugate and f is the frequency [$G_{xx} \in \mathbb{R}$ means G_{xx} is an element of the set of real numbers.]. A finite discrete sequence $\langle x_i \rangle$ of length N would

generally yield an spectrum value at frequencies $\left[0, \frac{1}{Nt_s}, \frac{2}{Nt_s}, \dots, \frac{N}{2Nt_s} \right]$.

The spectrum has the units of σ_x^2 per unit frequency and shows the frequency distribution of the contributions to σ_x^2 . It is sometimes normalised by σ_x^2 in order to give an integral of unity or by a characteristic speed squared (say \bar{x}^2) to give a frequency distribution of turbulence intensity I . The contribution of each frequency range Δf to the

total σ_x^2 is clearly the area $\int_f^{f+\Delta f} G_{xx}(n) dn$. The importance of this

contribution in terms of the power contained within this range Δf is then

$\int_f^{f+\Delta f} n G_{xx}(n) dn$. This function $f G_{xx}(f)$ is called the non-dimensional spectrum and is used to identify the frequencies which make significant contributions to the TKE.

Covariance and Cross-correlation Function

The variance, lagged variance, autocorrelation function and spectrum can be generalised to include two simultaneous time series from different spatial locations, say $\langle x_i \rangle$, $\langle y_i \rangle$. This gives rise to:

$$\text{the covariance } \sigma_{xy} \doteq \frac{1}{N-1} \sum_{i=1}^N (x_i - \bar{x})(y_i - \bar{y}) ,$$

$$\text{the lagged covariance } \sigma_{xy}(r) \doteq \frac{1}{N-r-1} \sum_{i=1}^{N-r} (x_i - \bar{x})(y_{i+r} - \bar{y}) ,$$

$$\text{the cross-correlation function } R_{xy}(\tau) \doteq \frac{\sigma_{xy}(\tau)}{\sigma_x \sigma_y} : -1 \leq R_{xy} \leq 1 \quad \text{where}$$

$\sigma_x = +\sqrt{\sigma_x^2}$ is the sample standard deviation. This reflects the transit time and similarity of structures moving between and through the spatially separate points.

Cross-Spectral Density Functions

Finally the one (or two) sided cross spectral density function (cross-spectrum)

$$\begin{aligned} G_{xy}(f) &\doteq \mathcal{F}(R_{xy}) \\ &= \mathcal{F}^*(x_i) \mathcal{F}(y_i) \rightarrow G_{xy} \in \mathbb{C} \\ &= C_{xy}(f) + iQ_{xy}(f) \\ &= M_{xy}(f) e^{i\Theta_{xy}(f)} \end{aligned}$$

where $C_{xy}(f)$ is called the co-spectrum, $Q_{xy}(f)$ the quad-spectrum,

$M_{xy}(f)$ the magnitude and $\Theta_{xy}(f)$ the phase angle. $G_{xy}(f)$ can be normalised by the covariance σ_{xy} or by some representative speeds (e.g.

$\bar{x}\bar{y}$). Non-dimensional spectra can also be formed in the same way as for the spectrum. By combining the cross-spectrum and the two related

autospectra one can also construct the squared coherence function

$$H_{xy}(f) \doteq \frac{|G_{xy}(f)|}{\sqrt{G_{xx}G_{yy}}} \in \mathbb{R}$$

which is a frequency domain equivalent of the cross-correlation function in that it is non-dimensional and represents the relationship between structures in the airflow at separate locations. It is effectively a normalised magnitude accounting for the frequency domain variations in the component signals, and as such is normally considered with an associate phase angle in the same way as the magnitude.

Shear Stress

If $\langle x_i \rangle$ and $\langle y_i \rangle$ represent simultaneous measurements of orthogonal components of velocity at the same location then the mean shear stress (off diagonal Reynolds stress) can be calculated as

$$\tau_{xy} \doteq -\rho \frac{1}{N} \sum_{i=1}^N (x_i - \bar{x})(y_i - \bar{y})$$

. Note that $\tau_{xy} \neq -\rho \sigma_{xy}$ since the former is a

mean and the latter a sample variance. This shear stress can be expressed

as a frequency distribution, the shear stress spectrum, $G_{\tau_{xy}} \doteq \Re[\mathcal{F}^*(x_i)\mathcal{F}(y_i)]$ taking the co-spectrum only because of the realizability constraint. This can be normalised and non-dimensional spectra

formed in the same way as for the co-spectrum.

2.2 Experimental techniques

2.2.1 Experimental model construction

The particular design of transporter chosen for this study is of the false ceiling type illustrated in figure 4. The specific design chosen was a newly built model not seen before in this country. The reasons for this choice were:

- i) that this design was newly available to the industry and of a type likely to be important in the future;
- ii) that this vehicle had a new type of air conditioning system substantially different to previous transporters;
- iii) that this vehicle would be in service for at least the next five years and therefore of current relevance.

Figure 10 shows the transporter chosen for this project. This vehicle is based on a 16 tonne (maximum gross laden weight) chassis with a specially constructed body capable of holding 57 600 chicks. This body includes a separate air conditioning system (with power supply) which is located just behind the cab. Access to this is via the first side door behind the cab [A]. The other side doors [B,C] (two on either side of the body), of which one is hidden in this picture by the open rear door, are used for the unloading of chick boxes in an effort to maintain conditions inside the load



Figure 10 A photograph of the chick transport vehicle chosen for this project.

space during unloading. The fresh air inlets are located behind the cab mounted air deflector [D]. The floor outlets are open to the underside of the vehicle except for a plate which protects against the ingress of water.

Figure 11 shows the load space of the vehicle in which the boxes of chicks are stacked. This figure also shows the floor outlet ducts [A,B,C] (the middle cover plate has been lifted), the rear side door [D] for unloading and the ceiling air inlet holes [E]. The empty trolleys can be seen in normal

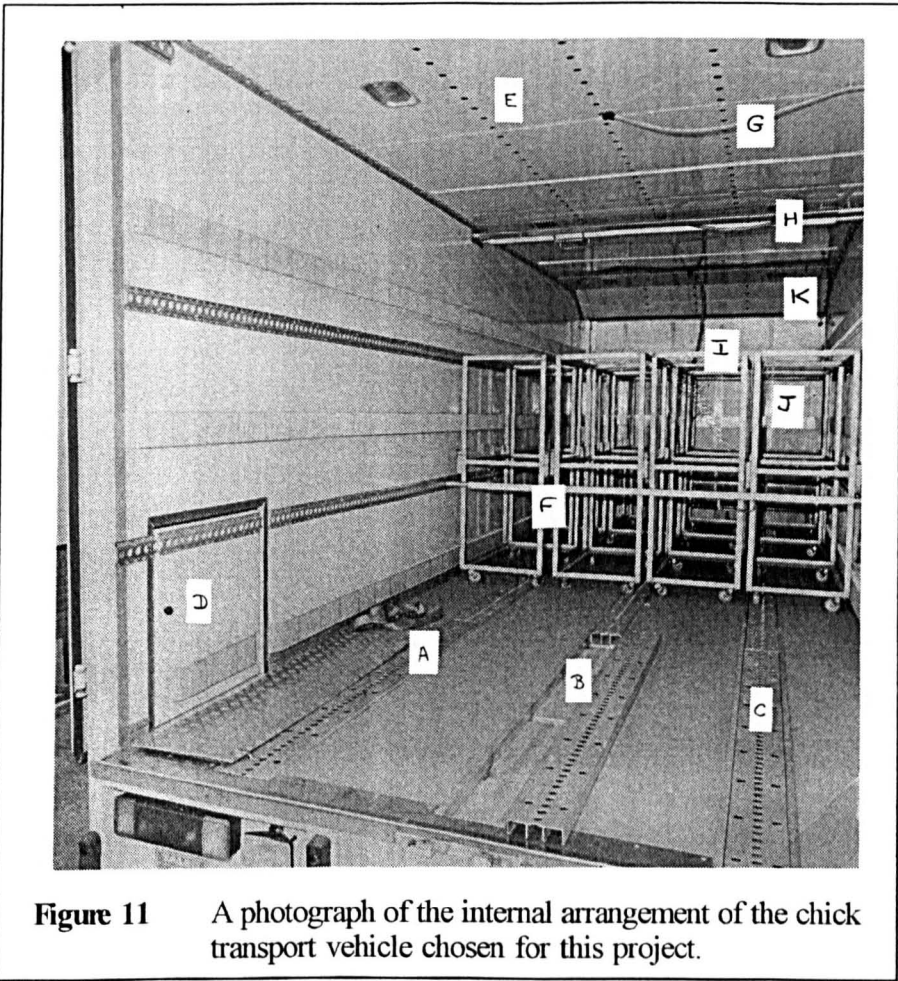


Figure 11 A photograph of the internal arrangement of the chick transport vehicle chosen for this project.

loaded arrangement for a partial load [F]. Also visible, hanging from the ceiling, are the three temperature sensors [G,H,I] which relay the temperature to the driver/attendant. The air conditioning system is located behind the front wall [J] seen in this picture. Note the angled ceiling plate [K] just above this front wall, which acts as part of the ducting to move air into the false ceiling.

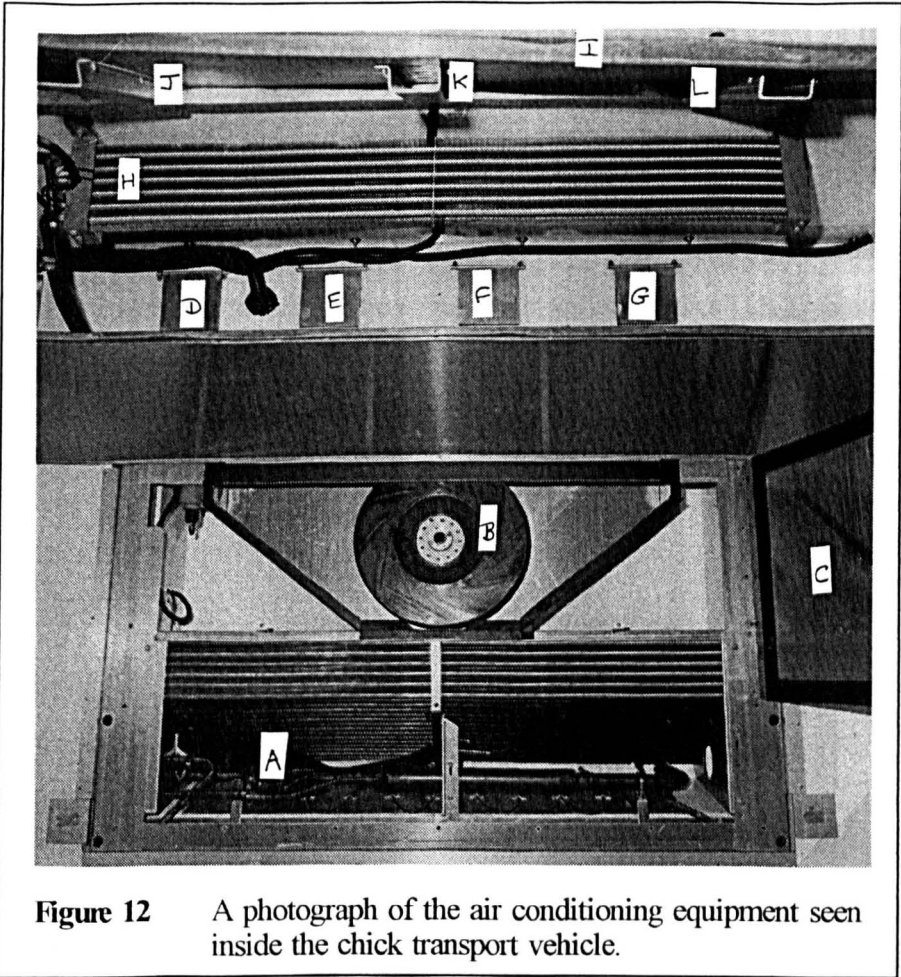


Figure 12 A photograph of the air conditioning equipment seen inside the chick transport vehicle.

Figure 12 reveals the air conditioning system which is located behind the front wall of the load space. The other features in this figure are the heater/chiller unit [A], the recirculating fan [B], and the covering door [C] which is closed during operation, the four fresh air inlet flap valves [D,E,F,G] above the central metal plate and a secondary heating coil [H] which is connected to the engine cooling system. The method of operation (see figure 4) is that air is drawn through the heater/chiller unit, into ducting which leads to the rear of the recirculation fan. This blows the air upwards

where it is deflected out above the metal plate seen across the centre of the picture. Fresh air is added through the flap valves automatically by temperature controlled fans, before the air passes up into the false ceiling. At the very top of the picture the angled ceiling plate [I] can be seen (folded toward the camera). The covers over the inlet holes [J,K,L] are to prevent excessive amounts of air being blown through the front of the load.

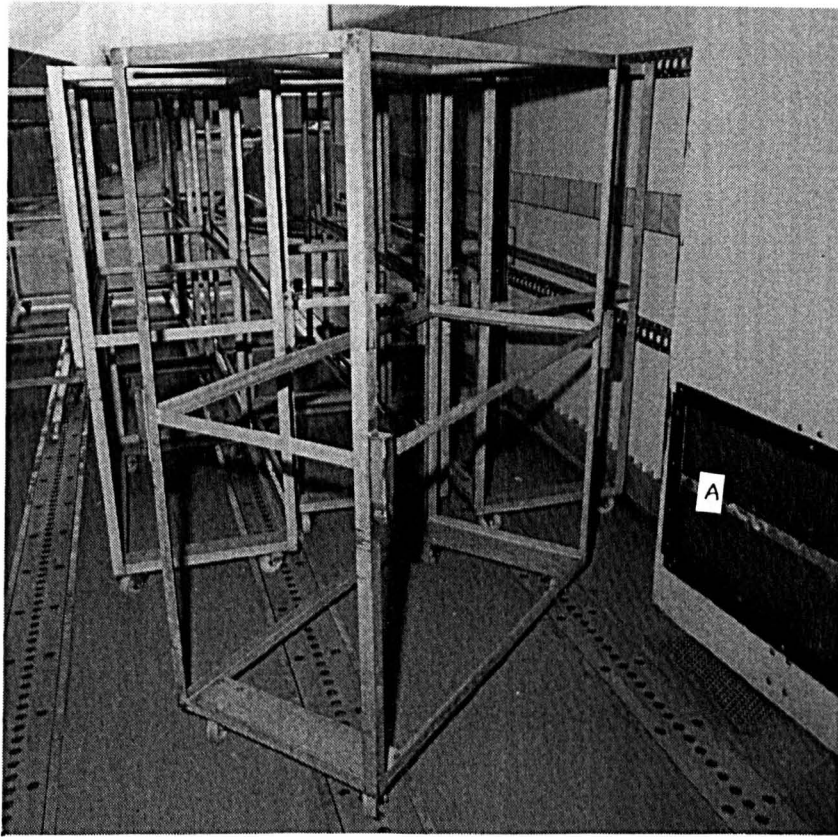
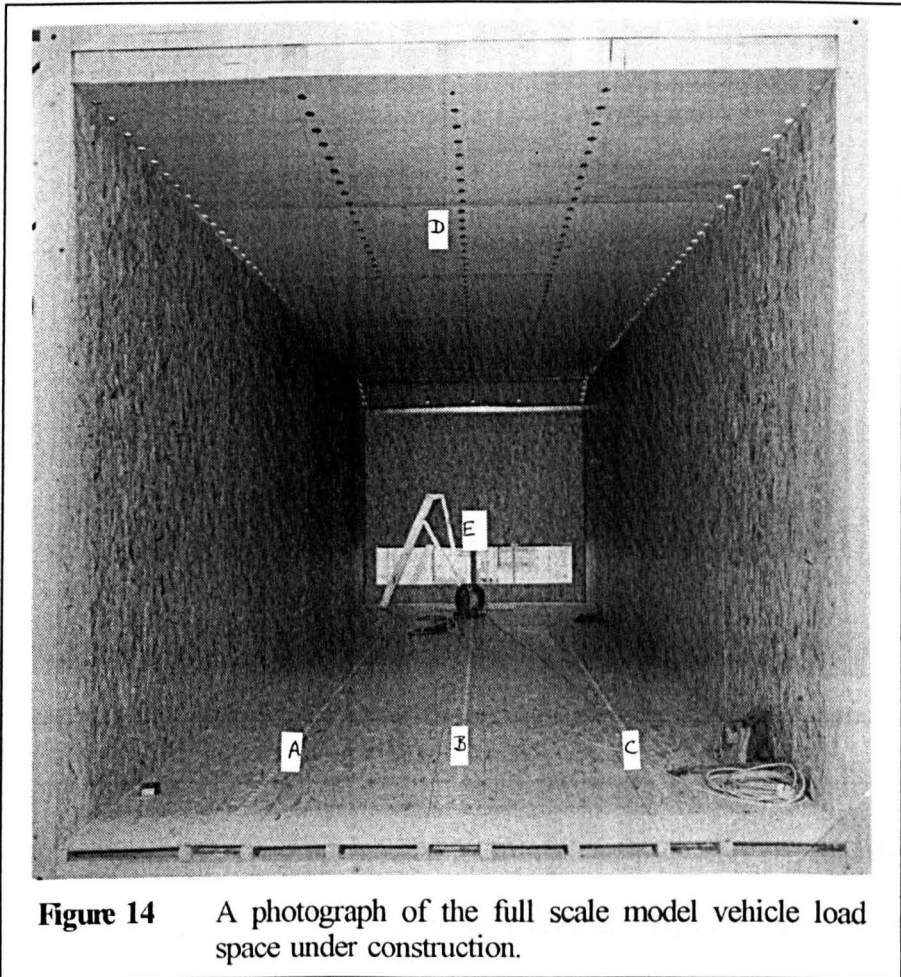


Figure 13 A photograph of the trollies used in this chick transport vehicle.

The type of trolley shown in figure 13 holds up to 24 boxes (normally 18). These are stacked up to four high (normally three) and two abreast on the three levels of the trolley. This vehicle can carry 24 such trollies, normally arranged in 6 rows 4 abreast if fully loaded, giving a maximum capacity of 576 boxes. Also visible, on the right, is the filter pad [A] through which the air is drawn before reaching the air conditioning system.

Measurements of the interior detail were made of the vehicle from which a full scale model was constructed. This model (whilst under



construction) is pictured in figure 14. The outlet ducts in the floor [A,B,C] are visible, as are the inlet ceiling holes [D] and the filter pad vents [E] in the front wall. The effects of the open doors during unloading are not being studied and therefore these are not included.

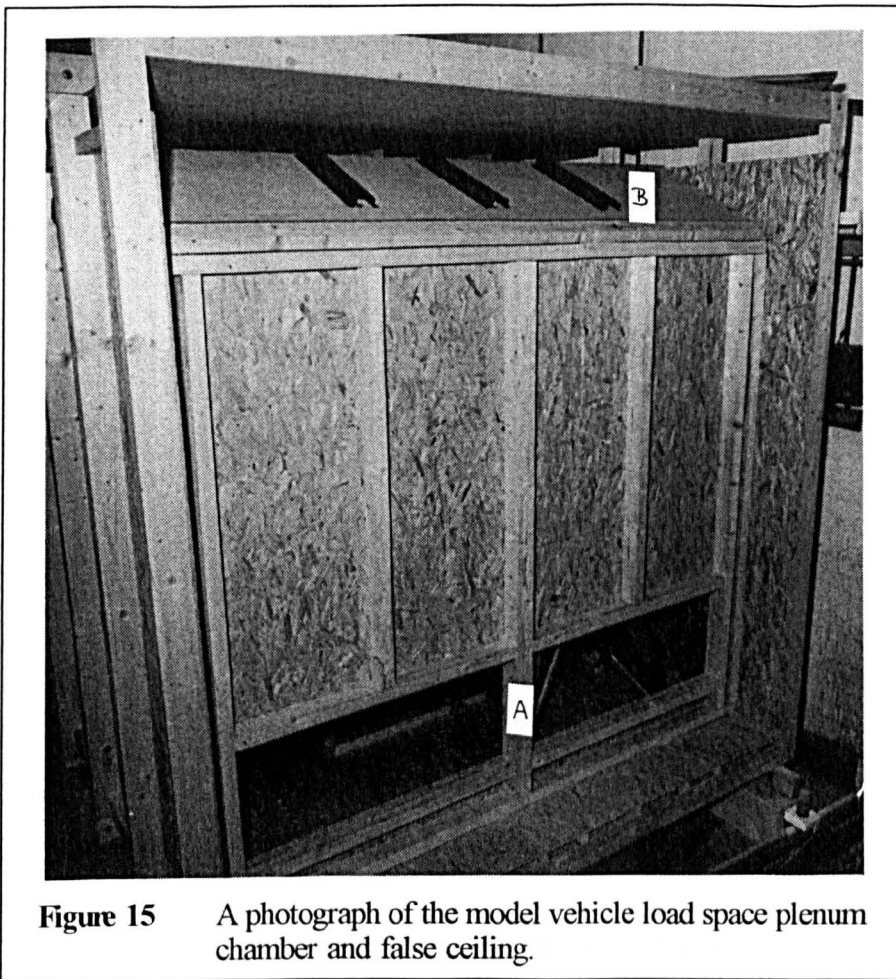


Figure 15 A photograph of the model vehicle load space plenum chamber and false ceiling.

Figure 15 shows the other side of the filter pad vents [A] and the angled ceiling panel [B] leading to the false ceiling. The plate seen in figure 12 has not been installed in this picture.

Figure 16 views the front end of the model vehicle (as figure 15) after completion but before the installation of the fan rig. In the lower part of the picture, between the first and second cross pieces, the recirculation vent [A] where the heater/chiller unit would be located can be seen. Above

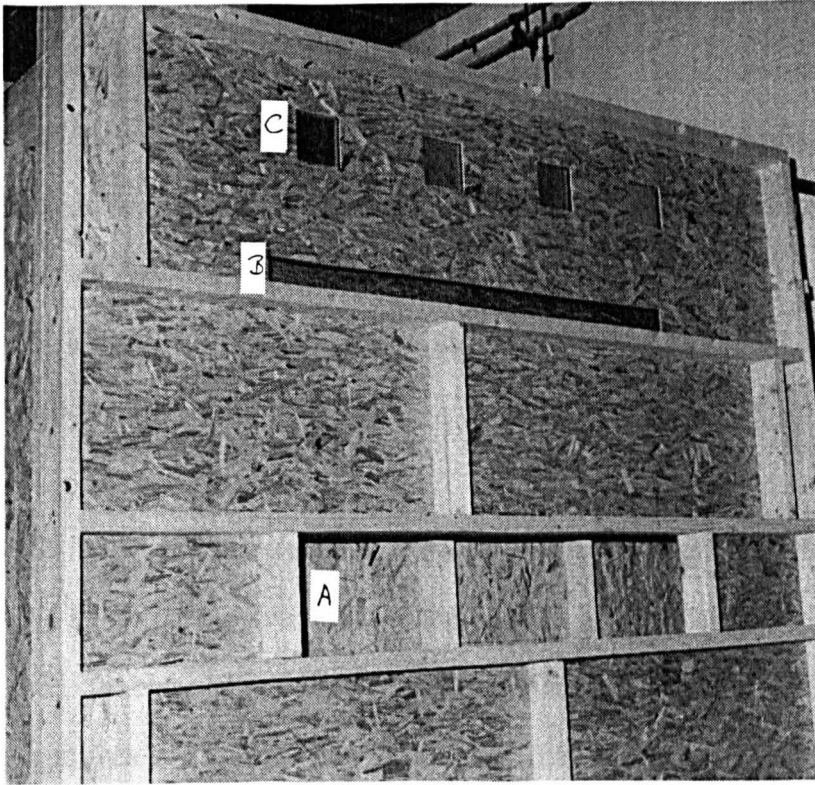


Figure 16 A photograph of the outside of the model vehicle load space before the installation of the fan rig.

this is the slot [B] through which the conditioned air is blown into the ceiling space and at the top of the picture the four fresh air inlet flap valves [C].

This model, although not in the original materials, provides a readily accessible basis for the experimental and computational work. It was constructed of a 100 x 50 mm softwood framework clad on the inside faces with 9 mm Sterling board and 5 mm plywood. This timber construction

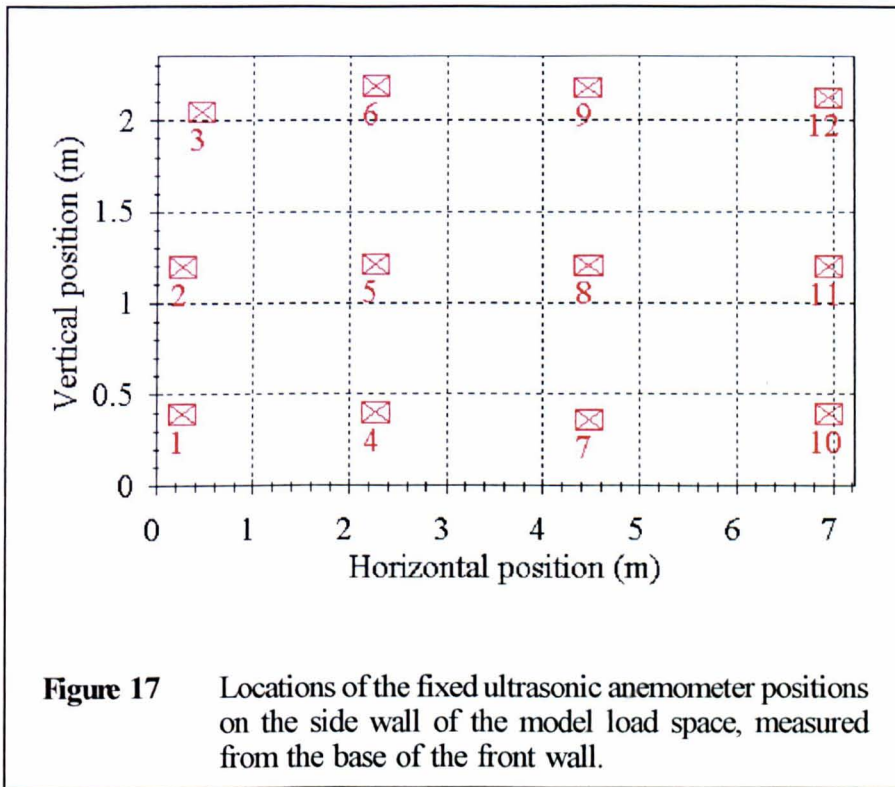
alone is not sufficient to model the thermal properties of the vehicle, the thermal conductance of the model cladding being $\sim 30 \text{ Wm}^{-2}\text{K}^{-1}$ compared to that of the vehicle $\sim 0.4 \text{ Wm}^{-2}\text{K}^{-1}$ [Wathes 1981]. However it is sufficient to obtain air flow measurements when temperature effects are not involved. These effects can be incorporated separately into the computational model without necessarily being experimentally obtained. Details of the construction are given in appendix 1.

In the original vehicle the air flow is driven by two sets of fans (see figure 4). Firstly the main recirculation fan which is of the centrifugal type, mounted in the plane of the front wall (figure 12) and secondly four smaller centrifugal fans which drive fresh air through flap valves into the false ceiling. It was found to be extremely difficult to purchase similar fans for the model, therefore it was decided to mount available centrifugal fans to create a similar effect. These were mounted in a fan rig (see appendix 1 figures A1.5 and A1.6) in such a way as to extract air from the box through the lower slot and blow it vertically upwards. This jet is then deflected back into the false ceiling, through the upper slot, by means of a metal "hood" over the fans (see appendix 1 figure A1.7). This arrangement is then similar to the recirculation fan which exists in the original vehicle (see figure 4). These fans are controlled by variable resistance speed controls which give a variable voltage output. No equivalent of the "fresh air" fans has been installed. This approach was adopted because of the reluctance of the

vehicle's manufacturer to release the specification of the vehicle or any of its components.

The boxes containing chicks in the vehicle are stacked on metal frame trollies as seen in figure 13. It was therefore decided to use a similar trolley to mount the instrumentation for use inside the model vehicle. Such a trolley was constructed from "Dexion" as shown in appendix 1 figure A1.8. This construction allows the trolley to be modified as necessary to allow any vertical positioning of the instruments, and the minimising of interference by the structure of the trolley on the air flow measured. The instrumentation chosen for the major part of this study is an ultrasonic anemometer (see section 2.2.4), which can be mounted on this trolley so as to take measurements at any (3D) location. In addition to this, twelve mounting points were positioned, in four columns of three, along the side wall of the model (that is on the left wall of figure 14), these positions allowed measurements to be made at exactly reproducible locations. The position of these locations is shown in figure 17. Note that due to the length of the anemometer the actual measurement locations were ~0.7 m from the wall.

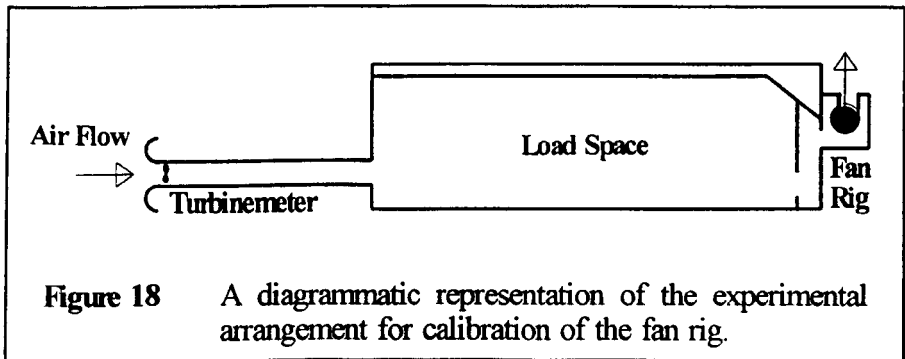
Four pressure tapping points were also been installed in the model allowing relative or absolute pressure measurements to be taken. These can give an indication of the reproducibility of conditions and were used in the



calibration of the experimental model (see section 2.2.2). The tapping points were located on the rear wall of the fan rig (that is the outside wall parallel to the front of the model shown in figure 16); on the base of the fan rig; above the inlet slot on the end wall of the model (figure 16) and on the side wall of the main load space (that is on the left wall of figure 14). These locations were chosen to give pressure readings above and below the fans as well as in the main body of the model. These positions were not chosen to give a representation of the actual pressure drop across the fans, merely an indication of the repeatability of conditions and a calibration measure for reference during the main experiments.

2.2.2 Fan calibration

The calibration of the fans mounted in the fan rig was done *in situ* as far as possible. It was not found to be possible to calibrate them whilst maintaining a recirculating flow through the model, so a straight-through arrangement involving a volume flow meter and the removal of the metal hood from over the fan rig was used (figure 18).

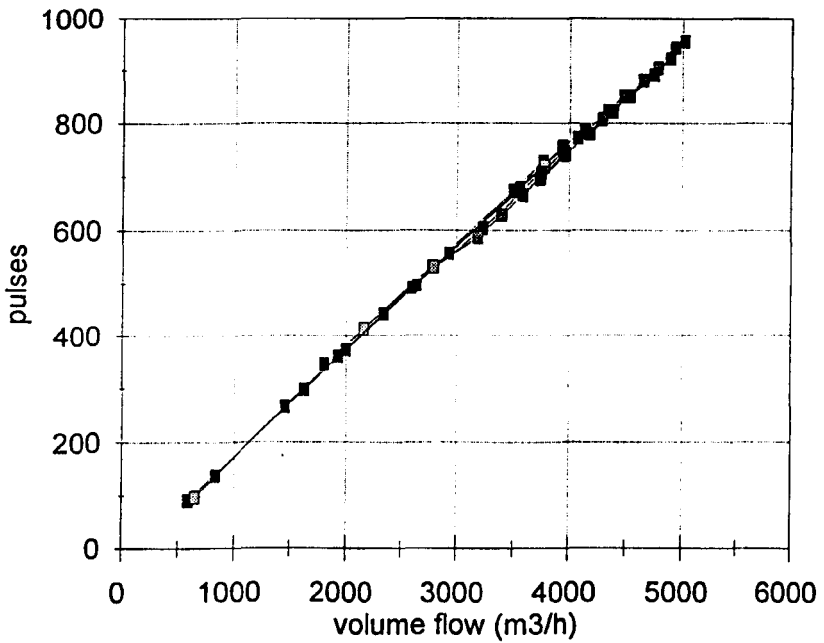


The volume flow meter, or turbine-meter, was housed in a bell-mouthed pipe [3.6 m (12 feet) long and 0.36 m (14 inches) in diameter], attached to the centre-line of the model, and consisted of a two bladed rotor with a rotation counter. This equipment had previously been calibrated (figure 19) on the Silsoe Research Institute fan test facility and was based on the description of equipment given by Berckmans *et al* (1986). The volume flow readings given by this equipment, for various power (voltage) settings on the fan rig, were correlated against the differential pressure measurements taken between two of the pressure tapping points fitted to the model. The taps chosen, for reasons of stability and appropriateness, were

calibration curve

1 long tube left fan nr.0393

$$Q_v = 5.189 * \text{puls}/10\text{s} + 73.8$$



■ -60 Pa ■ -45 Pa ■ -30 Pa □ -15 Pa ■ 0 Pa
■ 15 Pa ■ 30 Pa ■ 45 Pa ■ 60 Pa

Figure 19 A reproduction of the turbine-meter calibration curve.

those located on the base of the fan rig and the side wall of the load space. The differential pressure was measured using a micro-manometer [Furness Controls Ltd model MDC FC 001] whose output [a 0-1 V signal] was stored on a reel to reel [Store4] tape recorder. This signal was then digitized [at 50 Hz with a low pass 25 Hz analogue filter] and processed, using the DATS [Prosig Computer Consultants Ltd] software package on a MicroVAX II [running VMS 5.5-2H4], to give a mean pressure over each experimental period. The micro-manometer and tape recorded signal were calibrated using a water manometer and rubber bulb system to give constant reference pressures and a multimeter to monitor the output signal.

During the calibration experiments the following experimental procedure was adopted.

1. Before the first experiment of the day allow the fans to run for 20 minutes in order for an equilibrium to be established.
2. Zero output of micro-manometer using water manometer, rubber bulb and multimeter.
3. Connect the micro-manometer output to the tape recorder and note the zero error from the tape recorder signal. Record this signal for ten tape counts as a reference for digitising.
4. Input a known pressure, measured on the water manometer, from the rubber bulbs to the micro-manometer. Note the pressure, micro-manometer

and tape recorder output voltages. Record this signal for a further ten tape counts as a calibration signal.

5. Check the zero output of the micro-manometer and repeat steps 1 - 4 if necessary.

6. Connect the pressure tapping points to the micro-manometer and record output for over ten minutes. During this time note the 10 second count values given by the rotation counter of the volume flow meter. [Due to a built in time delay for display of this value there were 48 such values per 10 minute experimental period].

7. Check the zero output of the micro-manometer.

Steps 2-7 were repeated for each calibration run. It was found to be unnecessary to recheck the calibration of the micro-manometer after each run, only the zero error was found to vary significantly. The fans were left running between calibration runs and it was found that steps 2-5 gave sufficient time for equilibrium to be achieved after altering the fan power setting.

The digitised pressure data were analyzed to give the mean of the 10 minute experimental period corrected for the zero error and calibration recorded at each run. It was found that the peak pressure signal varied by up to $\pm 25\%$ of the mean value because of the unsteady nature of the airflow around the tapping points. Therefore the monitoring of the volume flow

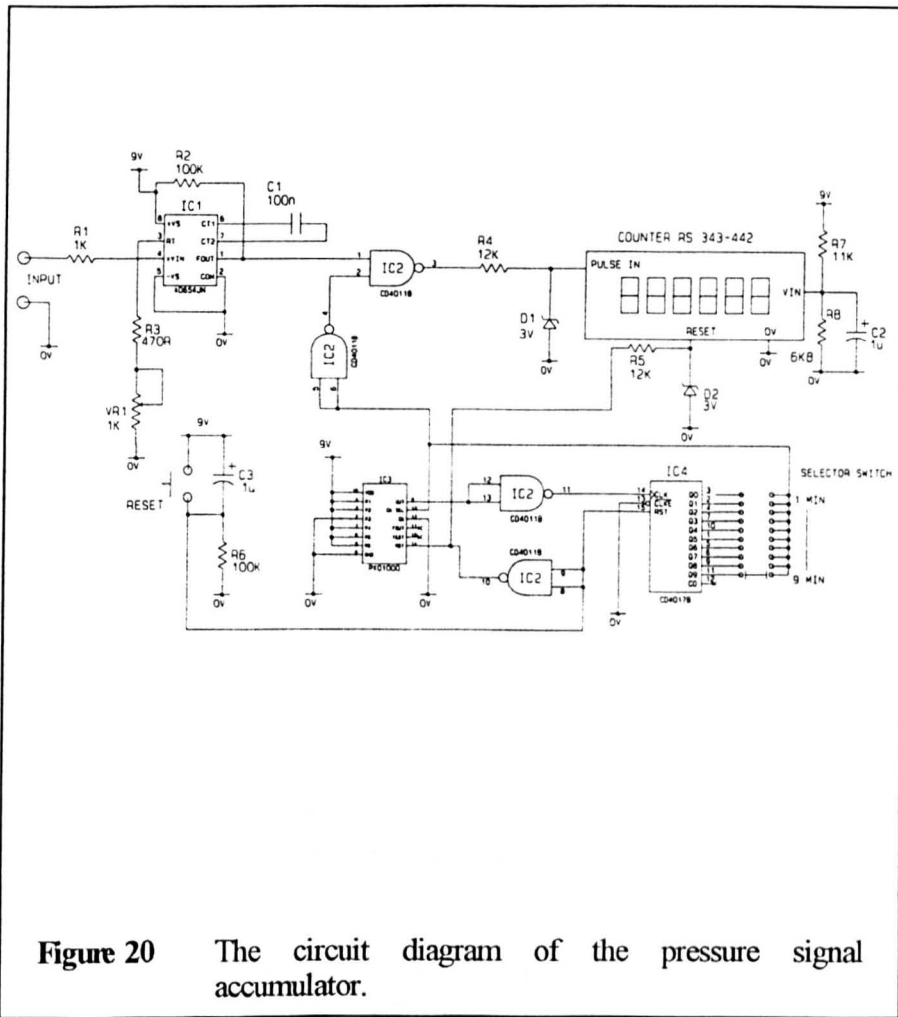
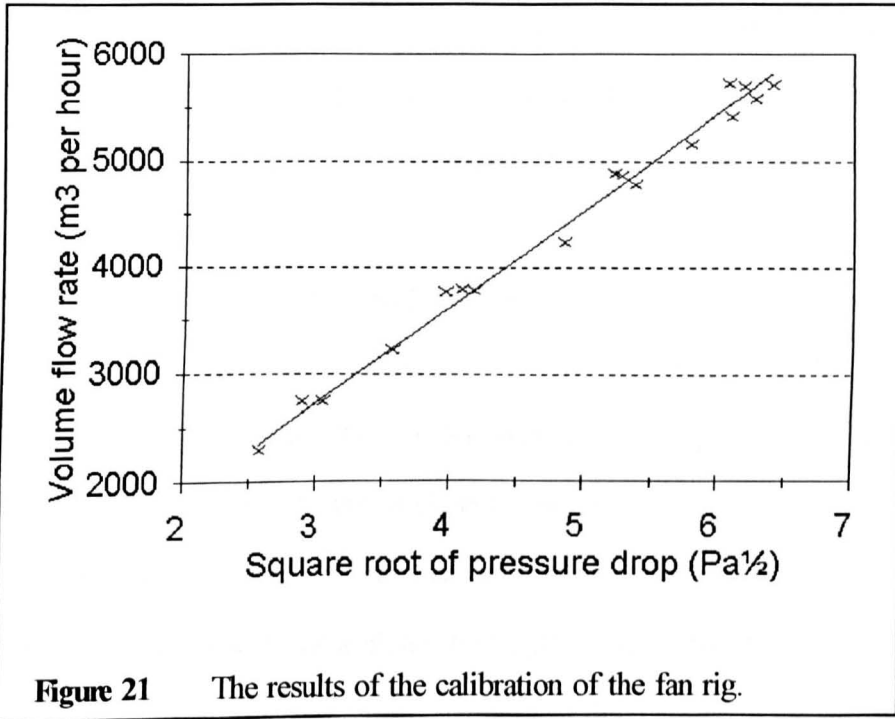


Figure 20 The circuit diagram of the pressure signal accumulator.

during the main experiments was done using an instrument which would effectively average the micro-manometer output over a known period. This instrument, known as a pressure signal accumulator, was constructed at the Silsoe Research Institute and a circuit diagram is given in figure 20. It replaced the reel to reel tape recorder in the main experimental methodology thus removing the need to digitise large quantities of pressure data in order to monitor the volume flow rate over short periods.

Seventeen calibration runs were taken at power levels between 50% and 95% of nominal. These showed that there exists a simple linear relationship between the volume throughput of the fans and the square root



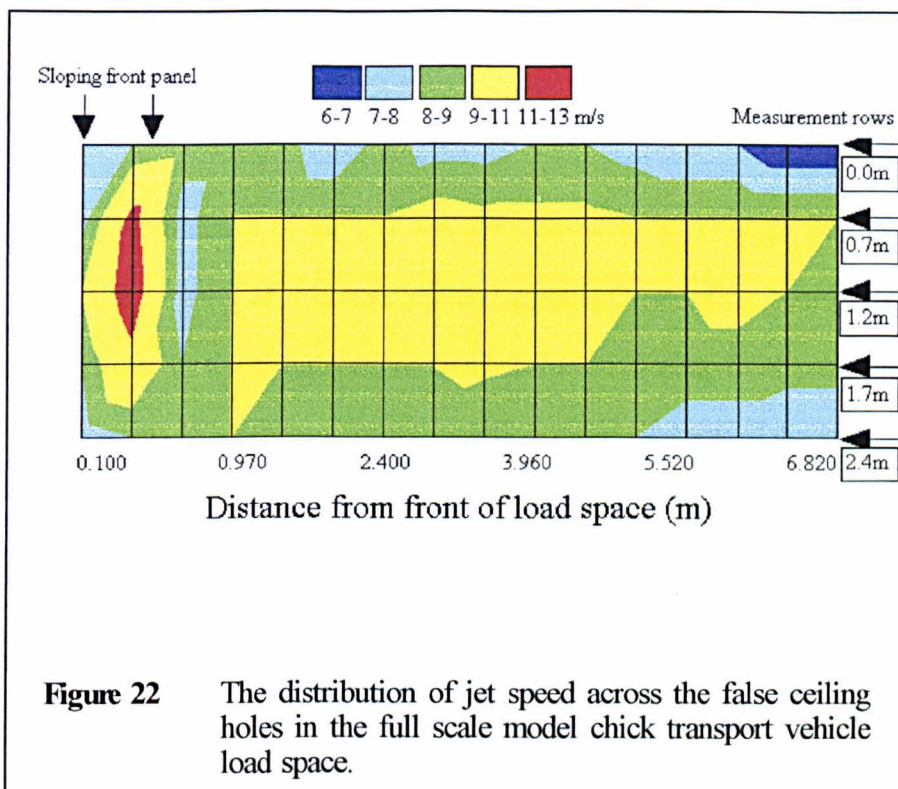
of the differential pressure measured (figure 21).

During the subsequent experiments the micro-manometer and signal averaging instrument were used to monitor the volume flow rate, which was set to the maximum which could be achieved in the recirculating mode of operation ($3800 \text{ m}^3\text{hr}^{-1} \pm 200 \text{ m}^3\text{hr}^{-1}$). This equates to a global ventilation rate of 93 air changes per hour (ach) $\pm 5\%$.

2.2.3 Ceiling jet measurements

The ceiling inlet ducts are designed to promote an even distribution of air along the length of the vehicle load space and it was therefore decided to investigate the effectiveness of this design. It was also necessary to detail the velocity distribution from the inlet holes as this was to be used as a boundary condition in the computational modelling (see section 3.4).

For this experiment a hand held vane anemometer [Envit Flomaster 2 cm head diameter], mounted on a ~1 m long pole with a flexible end piece, was used to measure the peak jet speed from a sample of the ceiling holes. These holes are 29 mm in diameter and arranged in 5 rows of 54 along the entire ceiling of the load space. Measurements were made approximately every 5 holes along the length of the vehicle, with extra measurements being made at the sloping front section because of the special detailing (holes covers *etc.*) which occur there. At each measurement location the anemometer, mounted on the pole and angled so as to give a maximum reading, was placed across the hole face and given time to reach a settled value which was noted. The reading at each location was repeated a number of times in order to confirm these values. The volume flow rate during this experiment was $3800 \text{ m}^3\text{hr}^{-1} \pm 5\%$ and the load space was empty throughout except for the experimenter's presence.



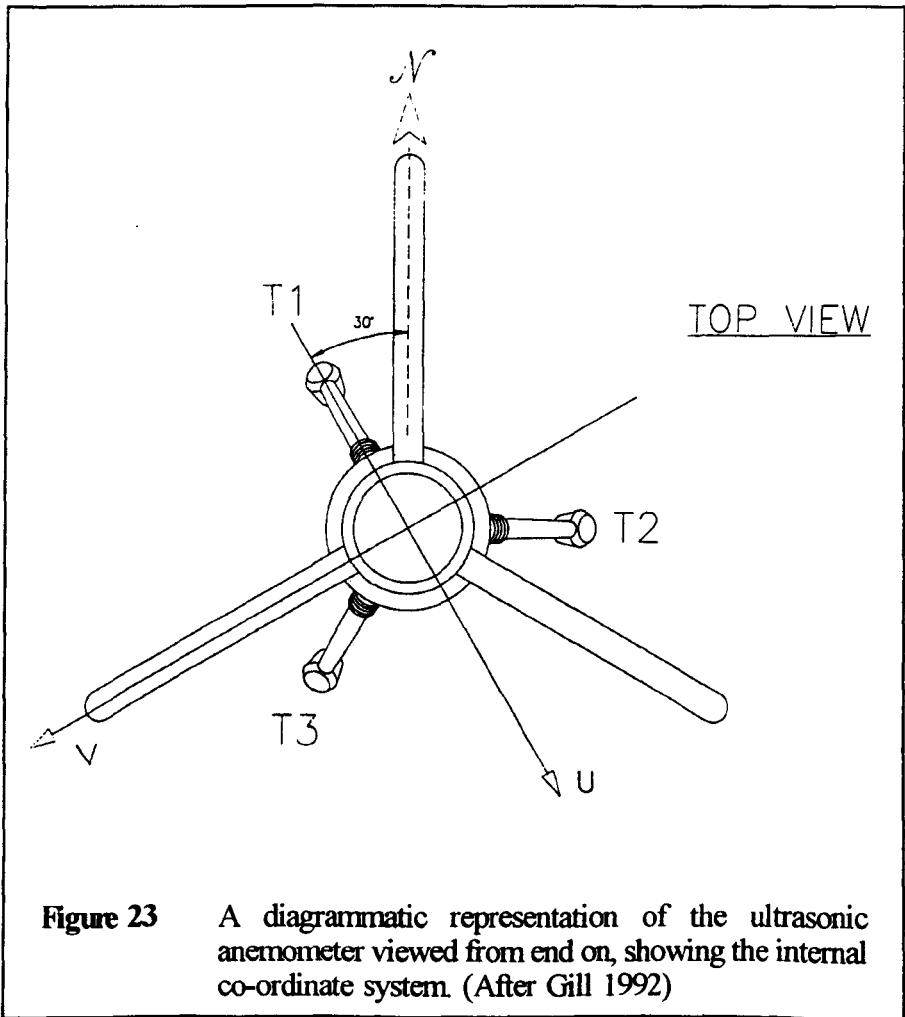
The measured distribution of ceiling jet speeds is given in figure 22, experimental locations being indicated by the intersections of the overlaid grid. These results show a wide range of jet speeds ($6.5 - 12.5 \text{ ms}^{-1}$) occurring, with particular extremes around the sloping front plate. There is, however, a clear maintenance of jet speed along the length of the load space, with 75% of jet speeds in the $8-10 \text{ ms}^{-1}$ range. The slight asymmetry of the overall pattern is thought to be due to the necessary asymmetry of the fan mounting positions, which would not occur in the vehicle with its single recirculation fan mounted centrally. In order to remove this asymmetry in the numerical modelling, where only one half of the load space width is considered, the average value from the two corresponding positions on

either side of the centre line was used in the description of boundary conditions (see section 3.4).

The direction of the jets was also measured, as an angle from the vertical, by means of a cotton tuft and graduated mounting board. This showed that in the main section, away from the sloping front panel, jet direction was 15° - 30° away from the vertical toward the rear of the vehicle. This is due to the momentum of the ducted air within the false ceiling. On the sloping front plate the side (wall) jets were found to be vertical, whereas the jets of the central three rows were at an angle of 60° to the vertical, toward the rear of the load space. This variation is due to the presence of covers over these central rows on the sloping plate (see section 2.2.1, figure 12 [J,K,L], figure 15 [B] and appendix 1 figure A1.4). These variations in jet angle were also incorporated into the numerical model (section 3.4).

2.2.4 Ultrasonic anemometer details

The instrument used for the collection of data during the main experiments was a Solent research ultrasonic anemometer manufactured by Gill instruments similar to the type used in meteorological observations.



This instrument (pictured in figure 23) consists of three pairs of opposing ultrasonic transceivers, each separated by 15 cm from its partner, arranged

around a measuring volume so as to give simultaneous measurements along three separate axes. The principle of operation is that the first member of each pair, say A, transmits an ultrasonic pulse which propagates through the air to its partner, B say. The time delay, measured by the electronics within the mounting, say t_{AB} , is then proportional to the separation distance of the transceivers (L) and inversely proportional to the speed of sound propagation between the sensors. This final element is made up of the speed of sound in air (S_s) plus the air speed in the axis of the sensors (U). So

$$t_{AB} = \frac{L}{S_s + U} \quad . \quad \text{This process is then reversed to give } t_{BA} = \frac{L}{S_s - U} \quad . \quad \text{These two}$$

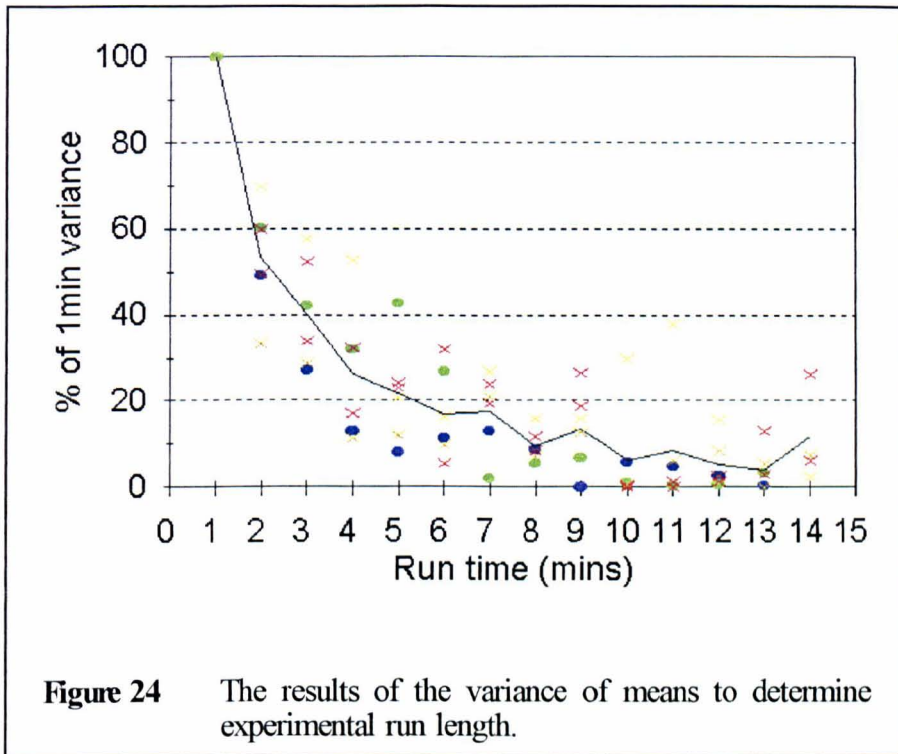
equations can then be solved, eliminating S_s for $U = \frac{L}{2} \left(\frac{1}{t_{AB}} - \frac{1}{t_{BA}} \right)$. This can be repeated for each pair of transceivers giving a simultaneous measure of the air speed in 3 components, which can be combined to give the cartesian components of the air velocity. The cartesian co-ordinate system thus produced, and supplied as the instrument's output, is fixed with respect to its sensor head. Thus it is necessary whilst using the instrument to know the orientation of the sensor head within a larger reference co-ordinate system, otherwise these measurements will lose their directional information. The instrument used in these experiments also automatically accounts for variation in the speed of sound due to air temperature and the distortion of the air flow due to the presence of the sensor head.

The instrument used for the main experiments of this study sampled air velocity in this way every 48 ms for a specified number of samples (see section 2.2.5), outputting the results directly to an IBM compatible PC, where they were stored in binary format files. These files were then converted, by a software utility supplied with the anemometer, into DOS text files which were processed (see section 2.2.6) to give the various flow statistics discussed in section 2.1.2.

This type of instrument is increasingly being used both for internal and external flow situations because of its robust nature and simplicity. Yost and Spear (1992) successfully used an ultrasonic anemometer to map the airflow pattern in a test building and Hope and Milholland (1993) describe its use in the evaluation of a ventilation system for a clean room environment. Boon (1978), Heber and Boon (1993) and Boon *et al* (1994) have mapped the airflow inside a full scale section of an livestock building with thermal effects and pollutant transport. These studies have shown that the ultrasonic anemometer is a practical instrument for internal flow measurements, able to capture the important details of low speed, turbulent air flow without undue disturbance. This method of data collection does however have a possible problem concerning the sampling volume of the instrument. Since the instantaneous measurements are effectively average values for the volume of the measuring head ($\sim 0.014 \text{ m}^3$) and for the sample time (48 ms) the ability of the instrument to resolve the gradients

in the flow is limited by the sampling frequency and the spacing between transceiver heads, the latter being considered the more fundamental restriction in this case. These limitations may lead to an inaccurate estimate of the instantaneous velocity at a given point within the measuring volume and thus to an under- or over-estimate of the Reynolds stresses in flows with large gradients over small areas, or where the measuring volume contains a wide velocity distribution, as with a small jet issuing into the volume. These possible problems are however clearly avoidable in the main by careful siting of the measurement locations away from such problem areas and the success this instrument has shown in many applications means that these possible shortcomings must be considered in proportion.

2.2.5 Experimental run length



The coloured points represent individual data set results, crosses for velocity data and solid circles for pressure data, and the solid line shows the mean of the points plotted.

This preliminary experiment was undertaken to determine the necessary length of recording time for each main experimental measurement. In order to determine this period a number of approximately 30 minute records of both pressure (as in the calibration runs, section 2.2.2) and velocity (using ultrasonic anemometry) were made in the empty model load space. These time series were then analyzed using a statistics software package [Genstat 5 Release 3/3.1 running on a VAX 4000-100 or VAX

4000-400 under VMS 5.5-2H4] to give the variance of means about the true mean, of the total 30 minute run, when subdivided into intervals of 1,2,3,...,15 minutes.

The result of this analysis can be seen in figure 24, where the variance of means is plotted, as a percentage of the value for 1 minute intervals, against interval length in minutes, for a number of data sets of both pressure and velocity measurements. The solid line shows the mean of the scattered points. This indicates that the mean of a data set of less than 5 minutes duration is prone to distortion due to large scale fluctuations within the system. It was therefore decided that when making measurements of the system a run time of ~10 minutes was sufficient, and would allow, if necessary, the division of data sets into two halves, both of which could be considered equally valid.

2.2.6 Main experimental procedure

The main experiments, to measure the airflow inside a full scale model of a commercial chick transport vehicle, were undertaken using the ultrasonic anemometer (section 2.2.4), mounted on a trolley similar to that used for the loading of chick boxes (section 2.2.1), and the volume (mass) flow monitoring system used during the calibration experiments (section 2.2.2).

For these experiments the general procedure below, adapted from that used during the calibration experiments, was adopted.

1. Before the first experiment of the day allow the fans to run for 20 minutes in order for an equilibrium to be established.
2. Zero output of micro-manometer using water manometer, rubber bulb and multimeter.
3. Calibrate the micro-manometer using water manometer, rubber bulb and pressure signal accumulator, noting the calibration values of pressure and the reading given by the accumulator.
4. Check the zero output of the micro-manometer.
5. Position the ultrasonic anemometer (and the empty chick box load if necessary, see section 2.3) in the load space of the model, noting its position (measured by tape measure from the walls of the model) and orientation.

6. Check the zero output of the micro-manometer.
7. Record the ultrasonic anemometer output for 12000 samples (9.6 minutes). During this time note the 8 minute total value given by the accumulator.

Steps 5-7 were repeated for each subsequent run. The fans were left running between runs and it was found that step 6 gave sufficient time for equilibrium to be achieved after altering the anemometer position. If larger changes were made, say in load configuration, then 10 minutes was given for equilibrium to be re-established.

The analysis of the time series produced by the ultrasonic anemometer will be covered in section 2.4. The daily calibration and volume flow results confirmed that the micro-manometer was very consistent in calibration and that volume flow was stable.

2.3 Experimental cases

2.3.1 Loading arrangements

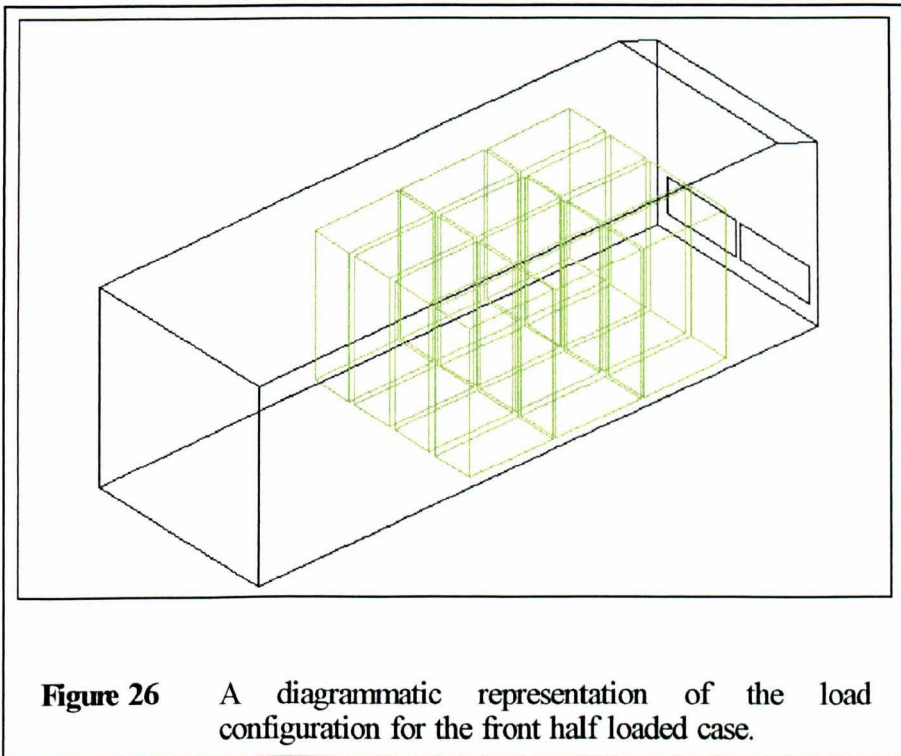
The cardboard chick boxes and metal frame trollies, normally used in the vehicle being studied, have been described in sections 1.1 and 2.2.1. These trollies are normally stacked with 18 chick boxes, in six stacks of



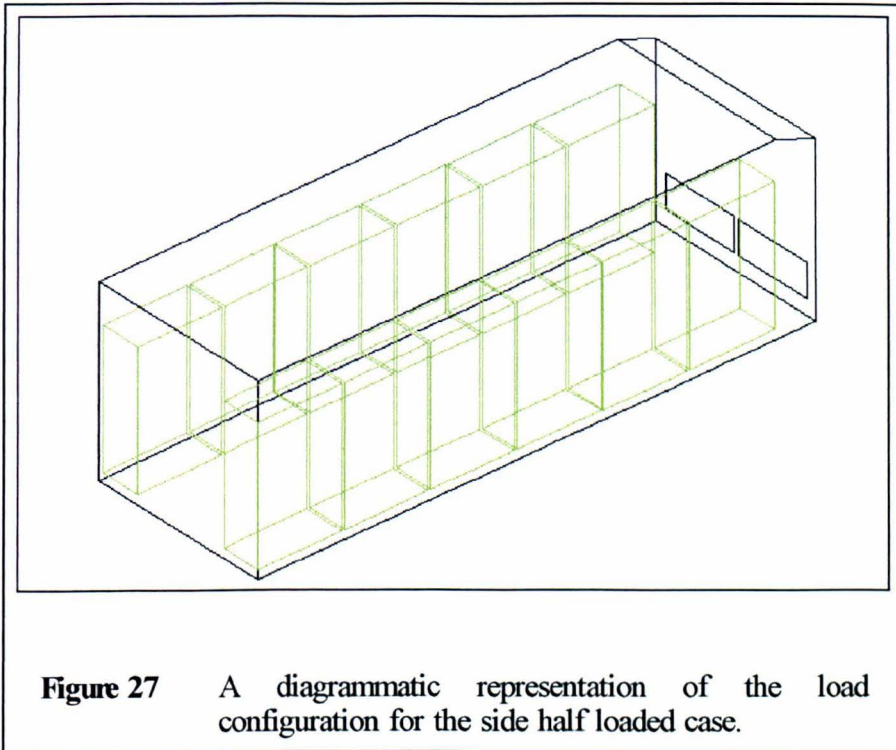
Figure 25 A photograph of empty chick boxes loaded onto trollies inside the model load space.

three on three levels (figure 25). This arrangement being standard practice on the vehicle studied, it was adopted for all of the loading configurations investigated. It has also been mentioned that the loading arrangement of trollies within the load space is not subject to any standard conditions. Therefore for the main experiments it was decided to use three loading configurations of trollies, chosen to represent a variety of airflow problems, and the unloaded empty case as a baseline for comparison.

The loading cases chosen were:



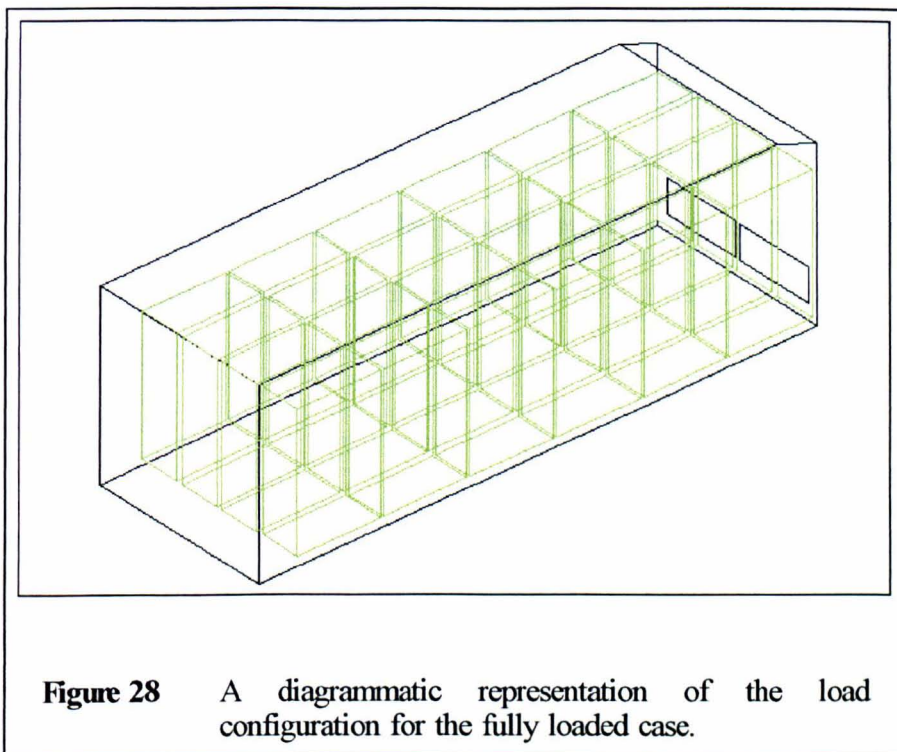
1. A front half load, 12 trollies arranged in 3 rows of 4 at the front of the vehicle model (figure 26).



2. A side half load, 12 trolleys arranged in 2 rows of 6 along either side wall of the vehicle model (figure 27).

3. A full load, 24 trolleys arranged in 6 rows of 4 (figure 28).

As the ultrasonic anemometer was 0.75 m in length, it was sometimes necessary to disturb the load in order to achieve the desired measurement position. Where this could not be avoided, by reorienting the anemometer for example, the chick boxes causing the obstruction were replaced by others which had been modified so as to allow positioning of the instrument whilst preserving as much as possible the load integrity.



2.3.2 Measurement locations

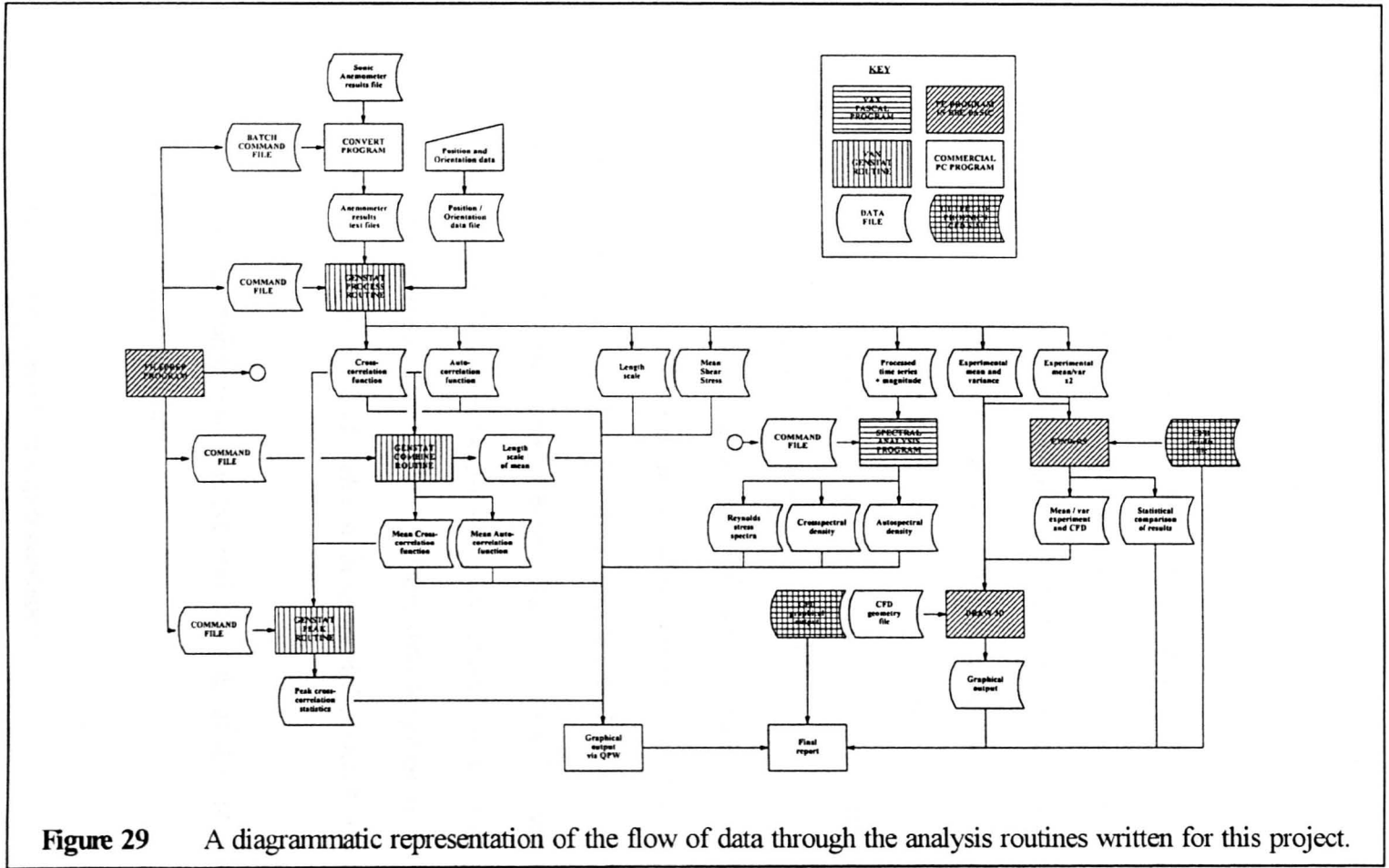
The positions chosen for experimental measurements were not pre-defined, but were taken approximately evenly, over the entire volume of the load space, extra measurements being made at locations of particular interest. The only fixed locations for measurement in all four cases were the twelve ultrasonic anemometer mounting points along the side wall of the model (figure 17), one of which can be seen in use in figure 25. These locations were used for the cross-correlation/cross-spectral studies in which the location closest to the front vents, position 1 in figure 17, was taken as a reference location in all but two cases.

A small number of experimental data sets were also obtained from one location, close to the front vents, on the original vehicle whilst empty and stationary. These have been analyzed in the same way as the model data (see section 2.4) and used for comparison of the experimental model with the vehicle on which it is based.

2.4 Data analysis

The analysis of the data collected by the ultrasonic anemometer was conducted using a variety of techniques which gave flexibility, consistency and inherent error checks. The outline of the processes used is given in figure 29 which illustrates the flow of data through the various stages.

Binary ultrasonic anemometer output files were first processed on the PC, using software supplied with the anemometer, to give DOS text files. These contained a header plus 12000 lines of data in the form u,v,w components of velocity and a speed of sound measurement. Copies of these files were archived before processing and details can be found in appendix 2. The three components of velocity are given at this stage in terms of the anemometer's own internal co-ordinate system. This conversion process was controlled by a DOS batch file created by a BASIC program on the PC. This program was written to provide command files for each of the data analysis routines in order that multiple data files could be processed in batch. The measured position and orientation of the ultrasonic anemometer were also entered into a DOS text file.



These DOS text files were then transferred to the mainframe and processed using a statistics software package [Genstat 5 Release 3/3.1 running on a VAX 4000-100 or VAX 4000-400 under VMS 5.5-2H4] which could run a specially written routine [called "PROCESS"] according to the instructions contained within the command file. The mainframe was used for all the primary processing because of the large number of files and their size. The output from this routine was a number of text files, some containing information about every data file processed and others which contained detailed information about an individual file. In the former group were files containing the following information.

1. The position, mean and variance of each 9.6 minute run. Here the components of velocity had been sorted into the overall reference coordinate system in use. This file then provided the basis for plotting the experimental data as vector diagrams using a BASIC program called "DRAW3D" and for the comparison of the experimental results and the numerical predictions (see section 5). These data are given in appendix 2.
2. The mean shear stress of each run, in terms of the overall reference coordinate system.
3. The length scales, both positive and integral, of the autocorrelation function of individual runs.

In the latter group were files which contained:

1. The autocorrelation function of an individual run.

2. The cross-correlation function of two individual runs.
3. The 12000 u,v,w velocity component samples, in terms of the overall reference co-ordinate system, and the instantaneous magnitude at each sample. This file is then further processed by the spectral analysis software which is described below.

Further analysis of these files was then performed by a series of software routines. The individual autocorrelation and cross-correlation files, which related to repeated runs at the same position(s), were first combined to give mean functions, using a GENSTAT "COMBINE" routine. This routine also provided, in the case of autocorrelations, the associated mean positive and integral length scales derived from this new function. Cross-correlation functions, both individual and mean functions, were also processed by a GENSTAT "PEAK" routine which gave the peak correlation coefficient and the associated lag time.

Spectral analysis of pre-processed data files was achieved using a PASCAL program on the VAX mainframe cluster which accessed a Fast Fourier Transform (FFT) routine from the NAG library. This program calculated the FFT of the individual velocity component time series, including the series of magnitudes, and from these constructed the spectrum, cross-spectrum and shear stress spectra. If a series of repeated measurements had been made these could be analyzed as one set thus giving mean spectra

directly. Cosine windowing and area smoothing were also employed to give a smooth spectrum, and checksum routines calculated the appropriate variance statistic both from the spectra and the direct time series. The spectra produced could then be normalised by any appropriate statistic.

These final result data files of correlation functions and spectra were then transferred back to the PC and plotted using a standard spreadsheet and graphics package [Borland Quattro Pro for Windows Version 5].

3 The numerical simulation

3.1 Introduction

The numerical simulation undertaken in this project used a standard, general purpose, commercially available, computational fluid dynamics (CFD) software package [PHOENICS¹] to model the airflow inside the replica vehicle used for the experiments.

CFD is an increasingly widely used system for solving the equations of fluid dynamics in specific situations. Its advantages are that it is relatively quick and easy compared to extensive experimental work, especially with the increasing availability of powerful computing systems. Its major disadvantage is, however, that like any computed solution to a set of equations, there is no guarantee that this solution is either unique or physically realisable.

The solution method used in PHOENICS is known as a finite volume method, which is one of several techniques currently used for solving the equations of fluid dynamics. The basis for all these methods are the conservation laws for mass, momentum and energy as well as for any

¹ Parabolic Hyperbolic Or Elliptic Numerical Integration Code Series produced by CHAM (Concentration Heat and Momentum Limited), Bakery House, 40 High Street, Wimbledon, London, SW19 5AU.

other properties specified, such as chemical species. The methods differ in how a specific situation is described and solved. In a finite volume code system the first step is to define the space which contains the fluid, called the domain, throughout which a solution is to be sought. This domain is then sub-divided into many small volumes, called cells, each of which will be treated as a fundamental unit of space throughout which the fluid properties are constant. Normally these cells are topographically cubic and form a topographically cartesian grid throughout the domain. It is on this grid that the solution will be determined, giving a value for each fluid property, such as pressure, velocity etc, for each cell. In order to do this the equations which govern fluid motion, the Navier-Stokes equations, and others controlling the other conserved properties, must be determined in a form suitable for such application. These transport equations, so called because they govern the transport of the various fluid properties in space and time, are usually derived in terms of a continuum of fluid media from the conservation laws. This gives, for example, the Navier-Stokes equations, which govern the transport of fluid mass and momentum:

$$\frac{\partial \rho}{\partial t} + \frac{\partial(\rho U_i)}{\partial x_i} = 0$$

$$\frac{\partial(\rho U_i)}{\partial t} + \frac{\partial(\rho U_i U_j)}{\partial x_j} = -\frac{\partial P}{\partial x_i} - \frac{\partial}{\partial x_j} \left(\mu \left(\frac{\partial U_i}{\partial x_j} + \frac{\partial U_j}{\partial x_i} \right) \right) + \rho g_i$$

For more information about these continuum equations see Acheson (1990).

In order to render these equations into a form suitable for solution by a computer in a specific problem, they must be simplified into algebraic equations which can be applied to each individual cell in turn, yielding a solution over the entire domain. This simplification process is known as discretisation (see appendix 3) and is necessary because the continuum equations cannot be solved directly except in simplified forms. These discretised equations can then be solved by a computer algorithm which iteratively modifies the fluid property values of pressure, velocity etc, in each cell until a stable solution, satisfying the fluid equations and any user-specified boundary conditions, is achieved. The algorithm used in PHOENICS is derived from the work of Patankar and Spalding (1972) [see also Chow (1979), Patankar (1980) and Kakaç *et al* (1987)]. This iterative procedure clearly raises an issue of convergence of the solution to a stable state. This is quantified by the calculation of continuity errors at every iteration which are called residuals. These residuals will tend to zero as a solution satisfying the continuity equations is reached. However, many numerical problems can cause a lack of convergence. These can be due to problems with grid specification, insufficient number or inappropriate spacing of cells, un-physical boundary conditions or unsuitable numerical methodology. The degree of convergence achievable or required to give an adequate solution is not clearly defined. Various criteria can be used, the relative size of residuals to some constant derived from average cell values and number of cells, the absolute residual size, the change in cell values

becoming small or the rate of change of the residuals becoming small. For this study a combination of these factors was considered, see section 3.4.

As well as the uniqueness and realizability problems inherent in CFD, it is also necessary to remember that, as with any simulation, the solution is to some degree dependent on the assumptions and simplifications made in its development. In the case of CFD, one of the most often cited shortcomings is with the modelling of turbulence. Turbulence is treated as a number of separate parameters in most CFD codes because simulations which are truly time and space dependent, on all length scales, are beyond current computer technology except in very simplified cases. This approach, called direct numerical simulation because it solves the transport equations directly, is therefore currently limited to theoretical studies of turbulence. Numerical models such as PHOENICS therefore predict the mean values of flow parameters, such as velocity, and some statistic(s) such as turbulent kinetic energy (TKE) to account for the fluctuating components. How these components should be handled within the simulation, however, is not clearly defined, and therefore various models have been proposed. These each have their own strengths and weaknesses and are often used in a given situation purely because they work. One of the most often used, because of its relative simplicity and wide range of previous successful usage, is called the k - ϵ model. This model proposes two parameters, with associated transport equations, to specify the turbulence; namely k , the TKE and ϵ the

rate of dissipation of k . This model is implemented in PHOENICS and was used throughout this study. For further information about turbulence and its modelling see Tennekes and Lumley (1972) and UMIST (1995).

There are also various other sources of possible numerical error with these CFD code systems, for example the discretisation method can lead to problems with diffusion, and these errors cannot easily be quantified [Mehta 1991]. The exact way in which a problem is specified can also lead to either wide variations in solutions to supposedly identical situations [Freitas 1995] or even trouble in obtaining any solution.

Since for a general fluid flow problem most of these possible sources of error cannot be quantified it is vital that some prior knowledge of the correct solution be obtained and used to verify that the numerical results are realistic. This process is called validation and is the only way of determining the likely error in numerical simulation results. These possible problems, however, have not stopped many successful applications of CFD in diverse situations from aeronautics to artificial heart valves.

3.2 Software implementation

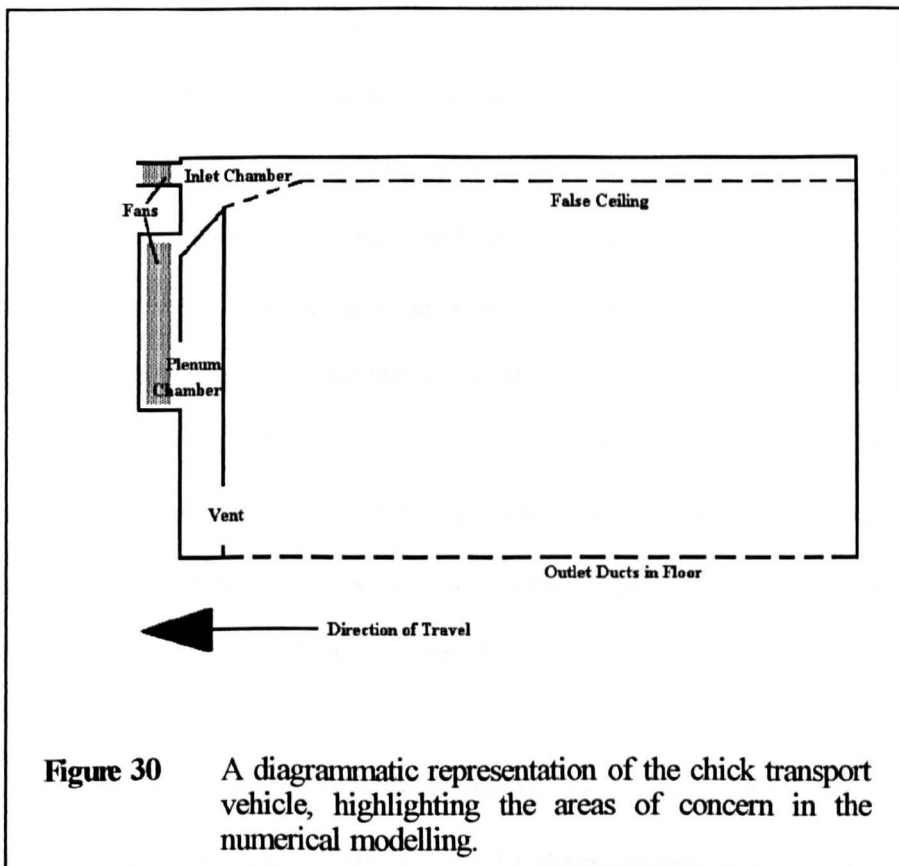
The implementation of PHOENICS used for this project was version 1.6.6 with 3D body fitted co-ordinate support, which allows a topographically cartesian grid to be fitted within a solution domain of almost any shape. This installation was mounted on a VAX 4000-100 and VAX 4000-400 cluster running VMS 5.5-2H4. As with most CFD packages, PHOENICS adopts a three stage approach to problem solution. The first stage is user specification of the problem in terms of the input language of the software. This is done using a pre-processor, called SATELLITE in PHOENICS, which interprets commands from the user specifying the grid, fluid properties such as density, viscosity etc, boundary conditions such as inlets and outlets for fluid from the grid, heat sources etc, and details of the solution methodology to be adopted by the second stage. Having created an instruction file using the pre-processor, this is presented to the second stage, the solver, called EARTH in PHOENICS, which calculates the solution using the details specified by the user. Results produced by this routine are then stored in files for post-processing by graphics programs, called PHOTON and AUTO PLOT in PHOENICS, which create graphs and diagrams displaying these results.

In all these stages it is important to stress that the emphasis is always upon the user to check that the results are of a suitable quality. At any stage incorrect input or assumptions can distort a model but give apparently reasonable results. This is a constant problem for CFD users.

3.3 Numerical model development

3.3.1 Preliminary models

This investigation took the form of a number of partial models of the chick transporter ventilation system in order to note any obvious simplifications or necessary inclusions in the final model. It effectively sought to answer the question, how much of the ventilation system should



be included in order to give a realistic load space model? This in practice raises two main questions (see figure 30).

1. Does the ventilation plenum chamber at the front of the load space need to be included or can a suitable boundary condition be imposed at the vent from the load space?
2. Do the inlet chamber and false ceiling need to be included or can a suitable boundary condition be imposed across the ceiling holes to the load space.

Two PHOENICS models were constructed to answer these questions. The first of these consisted of a simplified 2 m section of the front of the load space, with plenum chamber and open connecting vent. The boundary conditions imposed were, zero pressure at the open load space, a nominal negative pressure at the fan rig exit from the plenum chamber and solid, free slip, boundaries at all other surfaces. The simplification of the ceiling inlets to a zero pressure load space boundary was not found to affect the results, and neither did the imposition of no-slip solid boundaries. The negative pressure condition at the exit from the domain acts as the volume flow regulator without imposing any velocity distribution at the outlet, which might otherwise distort the results.

The results of this model were that the velocity distribution through the filter vents was not uniform and that the plenum chamber flow is highly

three dimensional with complex recirculation zones. The velocity distribution result showed a variation in magnitude of a factor of two across the filter vents. This was confirmed by spot measurements taken in the experimental model using a hand held vane anemometer (see section 2.2.3). This variation was considered to be uneven too allow a simple boundary condition to be substituted at the filter vents, especially in the light of the complex recirculating flows predicted inside the plenum chamber. Therefore it was decided to include the plenum chamber in the final models, with a constant negative pressure boundary condition at the fan rig exit.

The second model was constructed to consider the false ceiling and the necessity of its inclusion in any final model. The domain for this model was the ceiling inlet chamber and 3 m length of the false ceiling, which did not include any ducting. The boundary conditions imposed were again simplified, a constant velocity boundary condition at the chamber inlet, zero pressure at the opposite end of the domain and solid no-slip boundary conditions elsewhere. This simplification of the outlet boundary condition was considered reasonable because this model was to test the CFD models ability to generate a spatially variable pressure field corresponding to the variable velocity field seen at the ceiling holes (section 2.2.3 figure 22).

The results of this model clearly showed a significant, non uniform, pressure distribution across the domain boundary corresponding to the

ceiling hole vents. This was caused by the sharp edged geometry of the false ceiling and chamber and would imply a wide variation in jet velocities issuing from such holes, as was indeed found (section 2.2.3). This would suggest that the false ceiling should be included in any model, in order to reduce the influence of any simplifications at the boundaries over the flow in the load space. It is, however, possible that a boundary condition of velocity distribution, based on the experimental data of jet velocity at the ceiling of the load space, might be more accurate than the predicted jet velocities from a model including the false ceiling. This is because of the complex fine geometry of the false ceiling holes, which cannot be modelled numerically due to the restrictions of computer resources on the size and complexity of the domain. It was therefore decided to include both the plenum chamber and false ceiling in the first version of the CFD load space model and to assess the effect of the geometry problem.

3.3.2 Load space models

The first load space model was based around a body fitted grid 18 cells wide, 19 cells high and 29 cells in length. This domain covered one half of the load space, plenum chamber and false ceiling of the empty chick transport vehicle, making use of the symmetry line along its length. The load space itself was divided into a grid $18 \times 17 \times 25$ cells which allowed the geometric features of the plenum chamber vents and ceiling sources to be fixed correctly. Cells not fixed by the geometry of physical features were distributed uniformly throughout the grid.

The plenum chamber and false ceiling were modelled in the same way as in the preliminary tests except that the false ceiling holes were now modelled by a series of lines of porous media along the length of the vehicle. These lines had the correct width, 29 mm, but were continuous along the length of the load space model and effectively modelled the series of discrete holes as a diffuser line source. The porosity of these strips (P)

was fixed at $P = \frac{C_D N \pi r^2}{A}$ where C_D is a discharge coefficient, N the number of holes in a row, r the radius of a hole and A the area of the porous strip used to represent the line of holes. Using a nominal discharge coefficient of 0.65, which is usual for sharp edged openings, this can be

evaluated as $P = \frac{0.65 \times 54 \times \pi \times \left(\frac{1}{2}(0.029)\right)^2}{0.029 \times 7.21} = 0.11$. This model also included

the ducts within the false ceiling, created by blocking some appropriately shaped cells between each porous line. Constant velocity and pressure boundary conditions were used for the ceiling inlet and plenum chamber outlet as in the preliminary tests. Solid boundary walls were given a no-slip boundary condition.

This model failed to produce usable results of air movement because of convergence problems, which were traced to the modelling to the false ceiling. Specifically the algorithm could not resolve sufficiently the complex three dimensional flows within the false ceiling, especially where air was forced to move through the porous media into the load space. This was due to the small number of grid cells available to cover this region and the sharp changes in cell size caused by the physical geometry. Simply increasing the number would therefore not improve the results unless a similar increase could be made in the cell numbers within the load space, which was judged to be unrealistic in terms of computer resources. This being the case, a simplification to the ceiling boundary condition was sought in the form of a pressure and air velocity distribution at the ceiling holes themselves, based on the experimental results for volume flow (section 2.2.2) and jet velocity (section 2.2.3).

The second series of models was thus a representation of the load space and plenum chamber only, based on the version one grid with the

Table IV Variation of numerical results to inlet turbulence level.

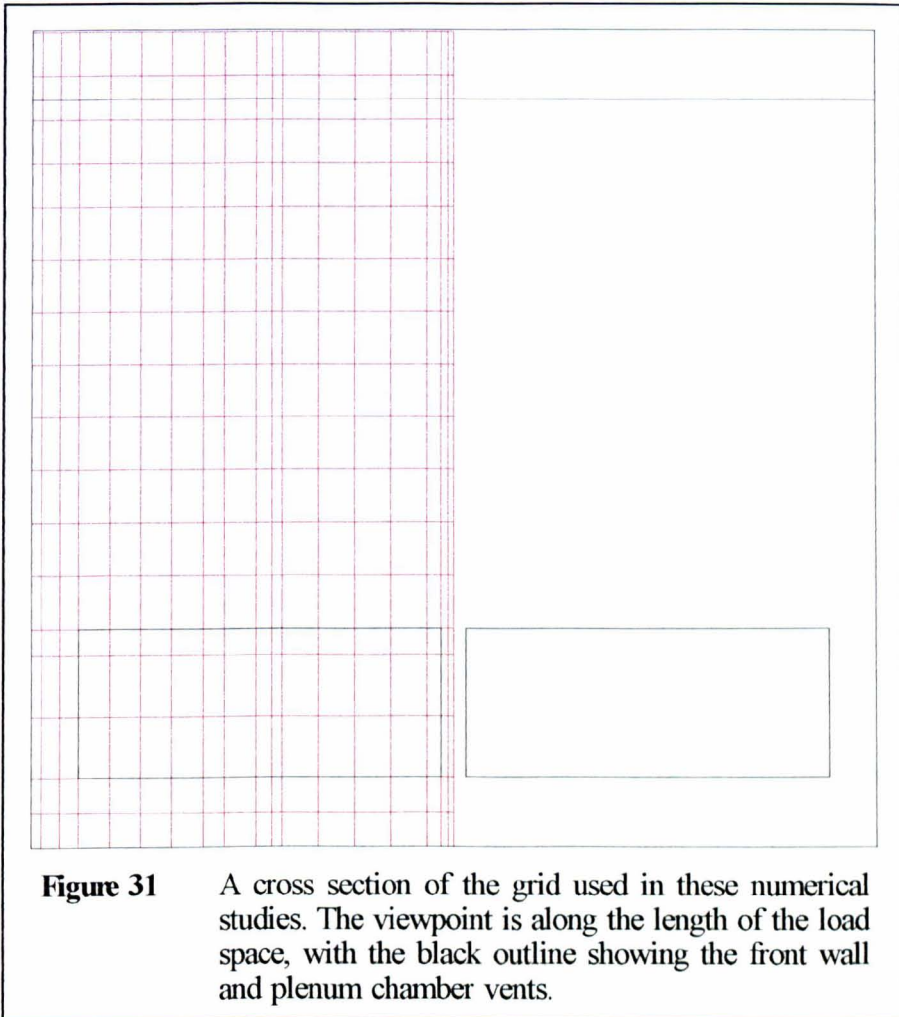
| Inlet Conditions | | TKE (k) result Jkg^{-1} | |
|---------------------------|--------------------------|----------------------------------|---------|
| TKE (k) Jkg^{-1} | Disp. rate(ϵ) | mean | maximum |
| 0.01 | 0.03 | 0.15 | 1.04 |
| 0.01 | 0.10 | 0.15 | 1.04 |
| 0.01 | 1.00 | 0.12 | 1.09 |
| 0.01* | 1.00* | 0.06 | 0.39 |
| 0.067 | 0.01 | 0.16 | 1.04 |
| 0.10 | 0.01 | 0.16 | 1.04 |

* jet velocity decreased by 50% from previous test.

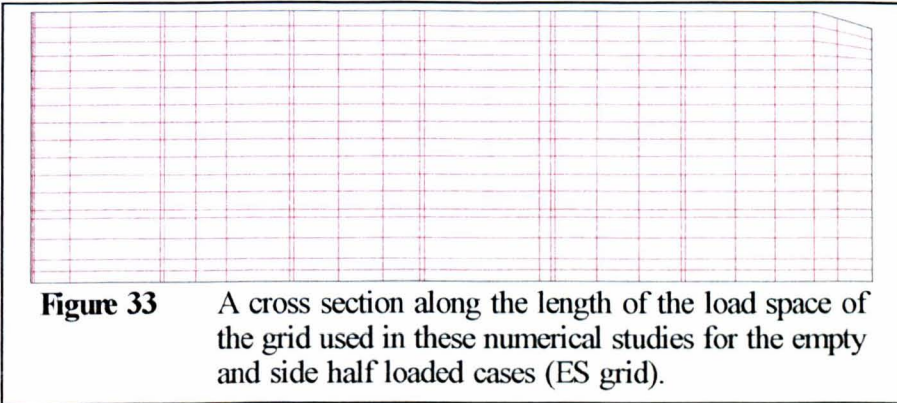
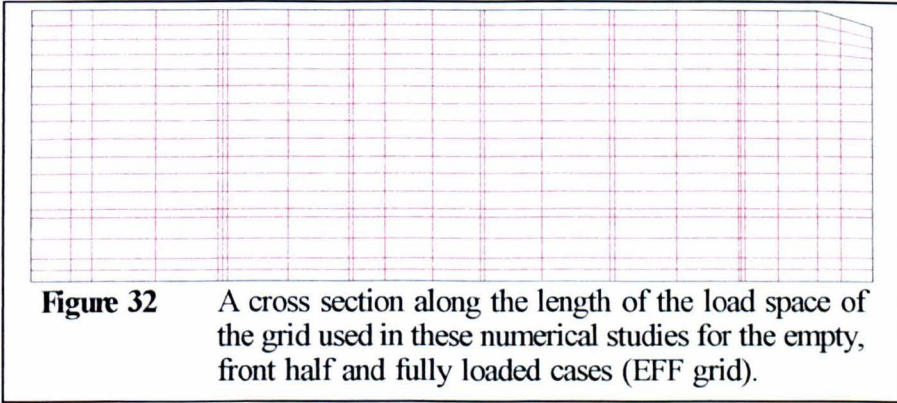
The mean and maximum are calculated from those cells for which experimental data was available for comparison (see section 5).

false ceiling section removed. This was thus an $18 \times 17 \times 29$ cell grid with fixed pressure boundary condition at the plenum chamber outlet and fixed velocity and pressure boundaries along the ceiling line sources. These pressures and velocities were derived from the experimental results to give an overall volume flow of $3800 \text{ m}^3\text{hr}^{-1}$ and a velocity distribution similar to that seen in section 2.2.3, with the asymmetry removed by averaging the results from corresponding positions either side of the centre line. The turbulence values, k and ϵ , given to the incoming air were investigated by varying the values within the model. The analysis of these runs, given in table IV, showed that the final results for both velocity and turbulence were highly insensitive to inlet values of k and ϵ . This is because the strength of the inlet jets causes very high levels of k and ϵ to be generated around the

inlet and these make the incoming values insignificant. This being the case, the values $k=0.01$ and $\epsilon=1.00$ were adopted.



This model gave good preliminary results when compared to the data collected in the empty experimental case, and was therefore further modified to allow for the full range of loading cases. The grid modifications required, in order to incorporate the locations of potential load positions, necessitated the development of two separate grid structures, because of the large differences in loading configuration between the front half / fully



loaded cases and the side loaded case (figures 26 - 28). These two grids were therefore known as the EFF (Empty/Front/Full) grid and the ES (Empty/Side) grid. These grids shared the same structure in planes perpendicular to the symmetry plane (figure 31), but had a different arrangement of cells along its length to account for the different positions of trollies (figures 32 - 33). Both grid structures were used with an empty load space case in order to test that there was no difference in the results due to these grid variations. This type of test, a grid independence test, is very important when considering the results from a CFD model because the results should not depend on the structure of the grid used to create them.

In order to verify this, one grid structure, that covering the front half and full loads, was programmed so that the number of grid cells could be doubled in each individual direction without altering the overall structure. This grid was then used to check that the results were equivalent to those produced on the standard grid. One final modification was also made, to incorporate the positions of the underfloor outlet ducts in both grid models. These ducts, although sealed during all experimental cases and therefore not used during most runs of the CFD model, were used in the final CFD model runs which incorporated heat production and the underfloor ducts. The modelling of the load itself, including the heat production model, is covered in section 3.3.3 and results for all these cases are given in section 4.

The incorporation of heat into the model also required some other features to be used in order that the effects of the heat distribution would be reflected in the air flow, namely buoyancy effects. These effects are modelled in PHOENICS using the Boussinesq approximation. This formulation allows the density to be held constant, thus saving computational work, and provides a term in the momentum equations proportional to the mass in each cell times the relative cell temperature.

The body force term ρg_i of the momentum equations is modelled as $\rho_{ref}(1+\beta(T-T_{ref}))g_i$ which implies a momentum source proportional to the

fluctuating density (temperature) times the gravitational acceleration. This creates a buoyancy force which is appropriate for small variations in temperature, where the coefficients can be taken as constants. For this model the properties of air were fixed at those values for 27 °C and 1 atmosphere, this being approximately the middle of the expected temperature range. The values taken for this model were therefore $T_{ref} = 27$ °C, $\rho_{ref} = 1.161$ kg m⁻³ and $\beta = 3.33 \times 10^{-3}$ K⁻¹.

3.3.3 Loading models

The CFD modelling covered the same cases of loading arrangement as the experimental work, a front half load, a side half load and a fully loaded case (figures 26 - 28 section 2.3.1). The modelling of the chick boxes within the load, whichever configuration was used, was a simple two step approach.

The first part of this model was to restrict the flow of air through the cell faces corresponding to the walls, floor, lid and internal partitions of the chick boxes. As with the initial attempts with the ceiling holes, this was done by partially blocking these faces according to the effective free area left by the ventilation holes in a chick box (see section 3.3.2). The potential blockage caused by the presence of the chicks within the boxes was neglected at this stage because it was not included in the experimental model.

The second step was to introduce a momentum sink to model the energy loss of the air, due to friction, moving through such a confined space. This momentum sink was modelled as proportional to the square of the velocity present within each cell, the constant of proportionality being chosen to be between zero, if the cell is open, and unity, if the cell is completely blocked. The value used in this model was one minus the

porosity factor used in the first part of the box model. So the source term for the momentum equations was $-\rho AU^2 + p\rho AU^2$. Where A is the geometric cell face area, ρ the air density, p the face porosity and U the air speed through the cell face. This effectively reduces the momentum of the air moving through each cell to that momentum which is associated with the reduced air flow through the partially blocked cell face. This momentum sink model was applied separately to each component of the velocity, with a different constant of proportionality in each direction, according to the different porosity factors, therefore modelling the different resistances to motion through and between chick boxes.

In the final CFD runs, heat production by the load was also included. This was modelled using a simple volume heat source corresponding to each stack of six chick boxes, which is one shelf load. The amount of heat to be introduced was expressed as a constant power input to the model of 0.4 W per chick. This corresponds to a total heat source of 40 W per box or 720 W per trolley. This value is taken from the literature as a representative sensible heat production figure for a resting chick in good conditions, although it has been noted that heat production does vary with temperature and that evaporative heat loss is important for chicks (section 1.2). However, since these variations are not clearly understood, it was considered more appropriate to include a simple representative figure. It should also be noted that this figure is probably a minimum value and

therefore represents a possible underestimate of the total heat production within the load. The results from this model are given in section 4, with a discussion of the interpretation in section 6.

3.3.4 Numerical model summary

To summarise the preceding sections, the details of the final CFD models used are given here, with edited PHOENICS instruction files in appendix 4.

Grids

Two grid structures were used in the final model: one for the empty, front half and fully loaded cases (the EFF grid) and the second for the empty and side half loaded cases (the ES grid). These grids are pictured in figures 31 - 33 and were based around the physical locations of features of the load space and loading configurations. These grids of $18 \times 17 \times 25$ cells were used in most of the CFD runs except for grid independence tests, where the number of cells was doubled in each individual direction.

Inlets

The ceiling inlet jets were modelled as porous strips, regulating the volume flow using a calculated over pressure boundary condition. The velocity of the incoming air was also specified according to a distribution derived from the experimental results (section 2.2.3). Since these measurements were peak velocities, it was also investigated whether some fixed proportion of the measured velocity would be a more appropriate boundary condition. The proportions tested were 66% and 50% since the

latter would give the average velocity, assuming a parabolic velocity distribution, and the former would allow for some smoothing by the vane anemometer itself during the measurements. The turbulence parameters, k and ϵ , of the incoming air were also set to values of 0.01 and 1 respectively; however, it has already been noted (section 3.3.2) that the results were highly insensitive to these values. Where heat production was included in the model, the incoming air was specified as having a temperature of 22 °C, this being the normal set-point temperature of the air conditioning installed in the actual vehicle. For these non-isothermal cases the global volume flow through the load space was also increased (see section 3.4) and therefore the inlet jet speed was increased proportionally from the measured values.

Outlets

The plenum chamber outlet was specified as a constant pressure boundary condition, as were the underfloor ducts when these were used. The values chosen were -2.5 Pa (relative pressure) for the plenum chamber, derived from the volume flow requirement, and zero (relative) pressure for the underfloor ducts. This latter figure was chosen because there is no published value for such underbody pressures in commercial vehicles, and although it is clear that any such figure would be highly dependent on local flow features, there seems no reason to assume any overall under or over pressure across the entire vehicle underside. Where the volume flow rate

was increased, in the non-isothermal cases, the relative pressure of the plenum chamber boundary was altered accordingly.

Walls

Solid surfaces within the load space and plenum chamber were treated as no-slip boundary conditions with a log-law friction applied and a roughness length of 5×10^{-4} m. This figure was taken as representative of the wooden surfaces in the experimental model (Abbot and Basco 1989), however, it was not found to affect any overall results significantly. Heat flow through the walls was modelled using a constant temperature boundary condition of 22 °C.

Load

The blockage caused by the load itself was modelled by restricting the free areas of cells corresponding to the chick box lid, sides, internal partitions and floor. The porosity of these was 0.082, 0.147, 0.110 and 0.007 respectively if all openings were considered (called the standard load model), although if ventilation holes only were considered these values are 0.082, 0.147, 0.110 and 0.000 (called the reduced porosity load model). Both of these sets of figures were used in the model in order to compare the results. No inclusion was made at any time for the blockage caused by the birds themselves as it was unclear how this should be included.

The momentum loss due to the presence of the boxes was represented by a form drag model, that is proportional to the square of the velocity. The constant of proportionality was taken as one minus the appropriate porosity factor for each cartesian component of velocity. Finally, heat sources were modelled as volume space heaters with a power output of 1067 Wm^{-3} , which equates to 0.4 W per bird, which as previously mentioned may constitute an under estimate of heat load.

3.4 Computational cases

The following computational cases were undertaken.

1. With the empty load space, isothermal, floor ducts closed and volume flow of $\sim 3800 \text{ m}^3\text{hr}^{-1}$. Tests of the ceiling jet velocity distribution using 100%, 66% and 50% of the measured values, tests of the two grid structures, EFF and ES, and grid independence tests using the EFF grid structure with the number of cells in each individual cartesian direction doubled.

2. With the front half loaded space, isothermal, floor ducts closed and volume flow of $\sim 3800 \text{ m}^3\text{hr}^{-1}$. Tests of the ceiling jet velocity distribution using 100% and 50% of the measured values and tests of the two loading models. A further test included heat production and the underfloor ducts with a volume flow rate of $\sim 5800 \text{ m}^3\text{hr}^{-1}$ (142 ach), this higher flow rate being equivalent to the recirculation plus two fresh air fans found in the actual vehicle.

3. With the side half loaded space, isothermal, floor ducts closed, ceiling jet velocity at 50% of measured values and volume flow rate of $\sim 3800 \text{ m}^3\text{hr}^{-1}$. Tests of the two loading models.

4. With the fully loaded space, isothermal, floor ducts closed and volume flow rate of $\sim 3800 \text{ m}^3\text{hr}^{-1}$. Tests of the ceiling jet velocity distribution using 100% and 50% of the measured values and, with the latter, tests of the two loading models. A further test included heat

production and the underfloor ducts with a volume flow rate of $\sim 5800 \text{ m}^3\text{hr}^{-1}$ (142 ach).

The convergence of all these test cases was monitored using a number of measures. Firstly the overall volume flow rate through the domain was required to be stable, with equal inflow and outflow. For the second convergence measure the in-cell values of all the solved-for variables was monitored in a test cell, grid position (5,6,20), and convergence was accepted only when these values had stabilised. The third convergence measure was the absolute value and behaviour of the residuals during convergence. The criteria for convergence were that the absolute values of the non-dimensional residuals for pressure and velocity components was of order 1 ($\alpha(1)$), and for k, ϵ and enthalpy (which is proportional to temperature) were of order 10 ($\alpha(10)$). This involved the residuals being reduced by several orders of magnitude from their initial values and therefore involved several tens of thousands of iterations (called sweeps) of the solution domain, requiring up to 50 hours CPU time on a VAX 4000-100. Typical runs required 15 000 - 20 000 sweeps and 25 - 30 hours CPU time. Behaviour of the residuals was also considered and convergence was not accepted if the residuals were cyclic or in any way unstable, since this could mean that the result was intermediate between two stable solutions.

3.5 Interpretation of CFD results

As previously mentioned, the results of a CFD simulation are stored in two types of file. The first is a text file containing selected cell values of user-specified variables and other summary information. The second is a compressed format file containing information for the graphical post-processors. The information in both of these files is stored on a cell by cell value basis and is interpreted as such, so the value of any given variable at any given point in space can be determined by converting that position into a cell address and obtaining that cell value. Combinations of cell values obtained in this way can therefore give mean values over larger volumes. In particular the local ventilation rate associated with an individual chick box can be calculated from the mean flow field, by combining the velocity from each cell corresponding to a box boundary, with a normal to the box face and the face area. This gives the ventilation rate through each face, with the sign denoting inflow or outflow, the absolute sum of either the positive or the negative values is then box ventilation rate. Note also that the conservation of mass implies that the sum of all these flow rates should be zero and this gives another indirect measure of convergence.

4 Results

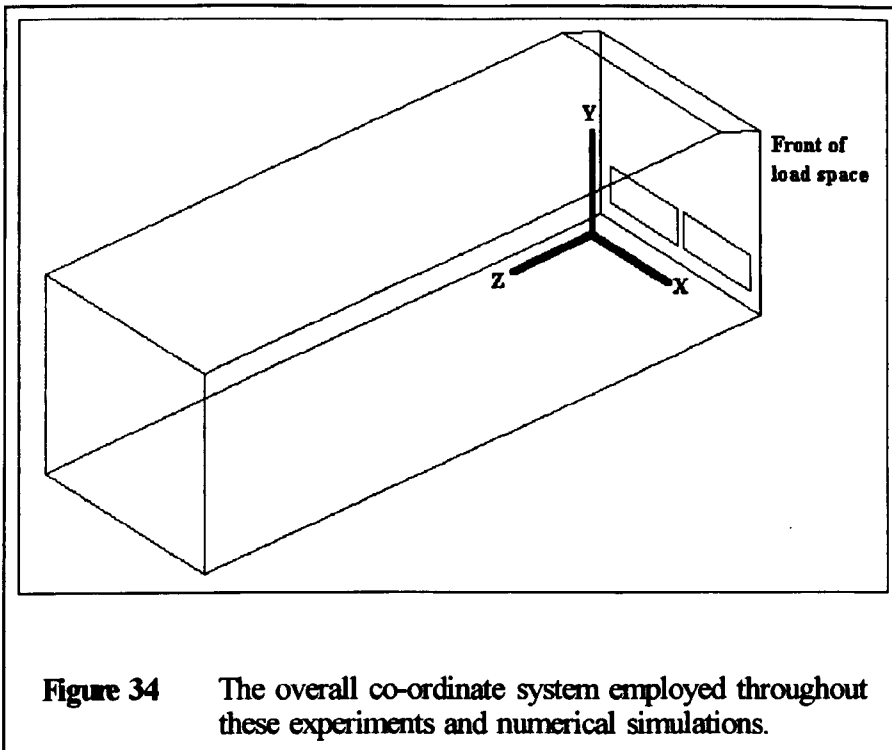
4.1 Introduction

In this chapter the results of both the experimental and numerical work will be presented. The detailed results given are those considered to give the clearest representation of the findings without undue repetition. This chapter is divided into two main sections; the first covers time averaged values obtained by experiment and those equivalent results obtained by numerical simulation. The second covers the correlation and spectral analysis results for which there are no equivalent simulation results. Within each section the results are further grouped according to loading configuration.

In the section dealing with time averaged results, velocity data is presented as vector plots representing cross sections through the load space. Two cross sections have been used throughout for consistency, these are: along the length of the load space under the row of ceiling jet holes 0.7 m from the side wall, and across the width of the load space 4.5 m from the front wall. These were chosen because they contain most of the interesting features of the flow and were therefore well represented in the experimental results, allowing visual comparison with the equivalent simulation predictions. The statistical comparison of the simulation results with

experimental data is covered in chapter 5. Further cross sections have been used where necessary throughout these results to give more detail on particular features. These will be explained as they are introduced.

In all these vector plots the size and direction of the arrows indicate the magnitude and direction of the mean air flow at the measurement point, given by the base of the arrow, with the scale indicated on each plot, the colour of the arrows in this case being for clarity only. Also included on each plot is an outline of the load space, from whichever viewpoint, including the positions of the plenum chamber vents and appropriate load, if it impinges on the cross section in question. In the plots relating to experimental data multiple arrows at one location show repeated runs, giving a visual measure of the repeatability. Also in the plots the turbulent kinetic energy (TKE) at each measurement position is indicated by a figure at the measurement location, this is the mean (specific) TKE in J kg^{-1} . In the plots relating to numerical simulations the same data is presented as colour contours with the scale shown at the side of each plot. These contours are normally drawn at intervals of 0.1 J kg^{-1} . Plots of the numerical results relating to temperature are also presented in the form of colour coded contours with associated scales given on each plot, contours relating to temperature are normally drawn every 1°C .



The shear stress measurements presented have been standardised to an overall frame of reference within the load space. This allows direct comparisons of the individual components at different spatial locations to be made. The co-ordinate frame employed is shown in figure 34, the +Z axis being along the length of the load space from front to rear, +Y being the vertical axis, from floor to ceiling, and +X being across the load space so as to give a right handed co-ordinate frame, in which all points of the load space have positive position values. These values of shear stress can be converted into a local co-ordinate system, giving principle and secondary shear stress values with the third value of zero, by tensor transformation, using the mean local velocity vector as the first axis and calculating the other axes by rotation about this.

The spectral analysis results presented in this chapter have been normalised by the mean magnitude of velocity, squared, for the time series analyzed. In the case of cross-spectral results this has been taken as the product of the mean magnitudes of the two time series involved. This means that the levels of the individual component spectra, and the spectra of the instantaneous magnitude, can be compared both within and between plots. The individual components of velocity in these plots are standardised to the same overall frame of reference as the shear stresses.

4.2 Time averaged velocity, Reynolds stress and temperature results

4.2.1 Empty load space case

Mean velocity and Turbulent Kinetic Energy

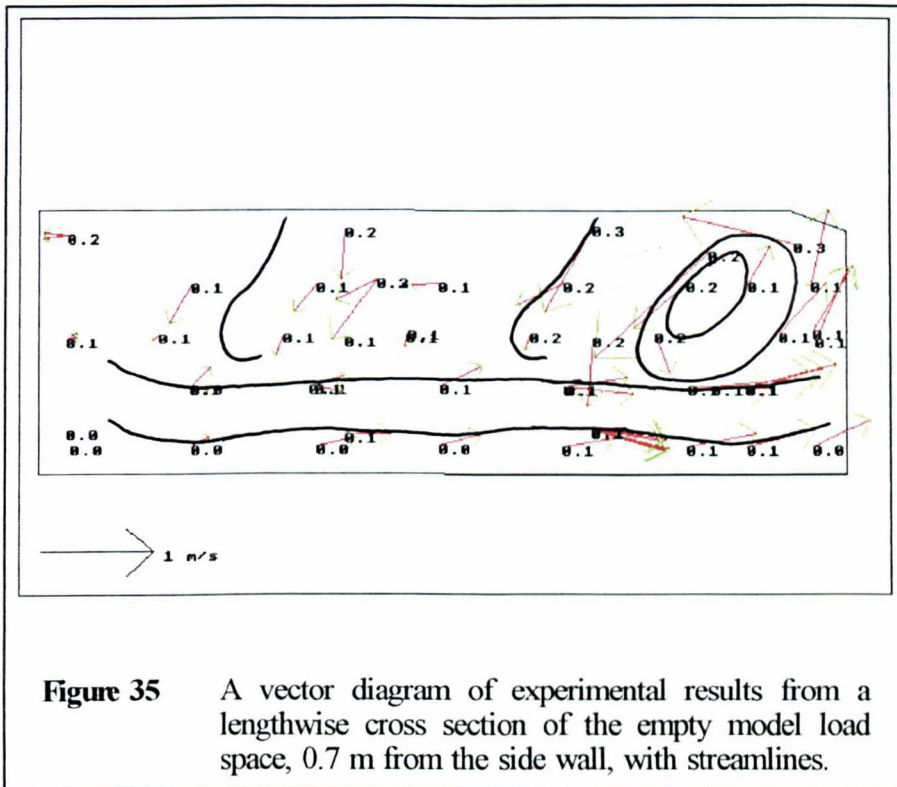
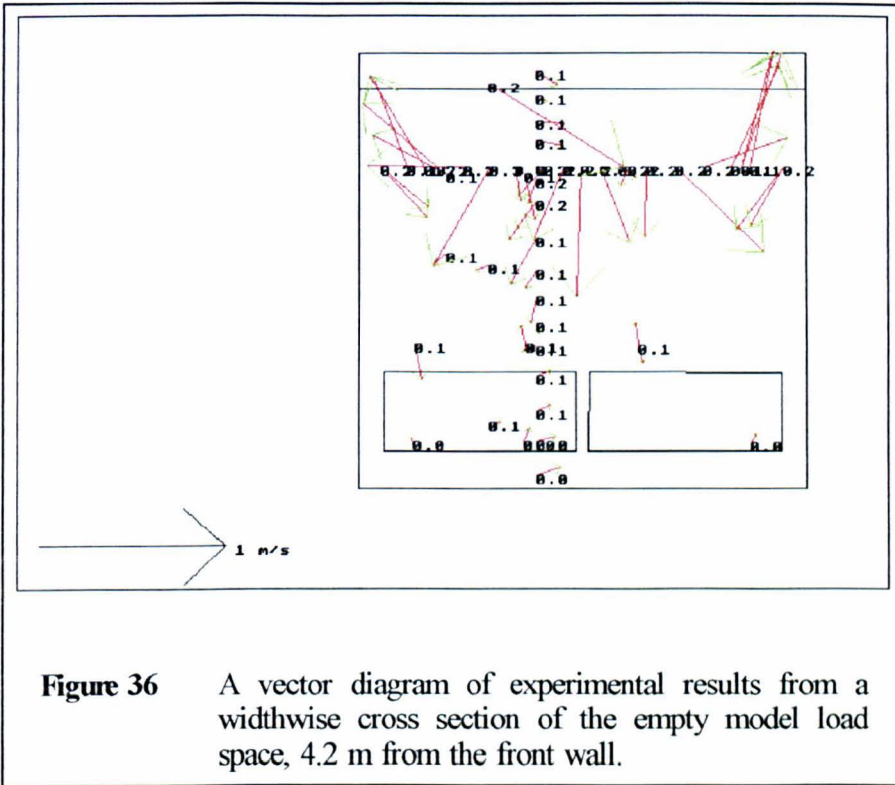


Figure 35 shows the mean velocity and TKE for the experimental measurements on the standard lengthwise cross section (see section 4.1) though the unloaded vehicle model. The flow pattern indicates four main areas within this cross section:

Firstly there is a strong flow along the floor of the model toward the plenum chamber vents. This flow shows a low turbulence level and

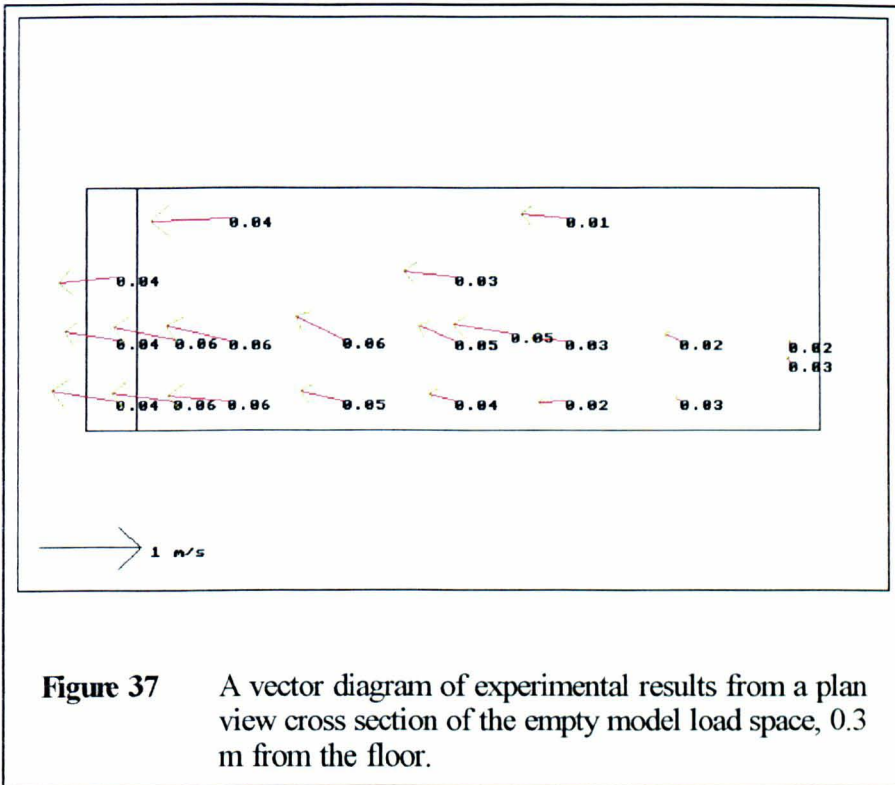
dominates the lower portion of the load space. The second important feature is the large recirculation region at the front of the load space, above the plenum chamber vents. This motion is partially driven by the strong flow toward the vents and partially by the incoming air jets, which have a strong horizontal component because of the sloping front plate arrangement of the false ceiling. The upper portion of the load space, to the rear of this recirculation zone, is dominated by the jet flow from the ceiling holes. This is characterised by the strong down-flow in this region and the relatively high turbulence levels. Between these upper and lower regions there is a mixing region which extends from the recirculation zone to the stagnation area at the rear of the load space. This mixing region is part of the three dimensional nature of the flow circulating about this point (figure 36).

In this latter figure, which is a cross section of the width of the load space 4.2 m from the front wall, the results of two transects can be seen. The vertical transect clearly shows the cross-flow in the lower region of the load space and the slight asymmetry, thought to be due to the asymmetric arrangement of the fans and the resulting asymmetry of the ceiling jet velocities (figure 22). This slight asymmetry seen in the vertical transect of figure 36 is clearly visible in figure 37, which is a plan view cross section of the empty load space at a vertical height of ~0.3 m. The horizontal transect (of figure 36) shows the complex recirculation which occurs within the upper jet dominated region. Here the five rows of jets across the width



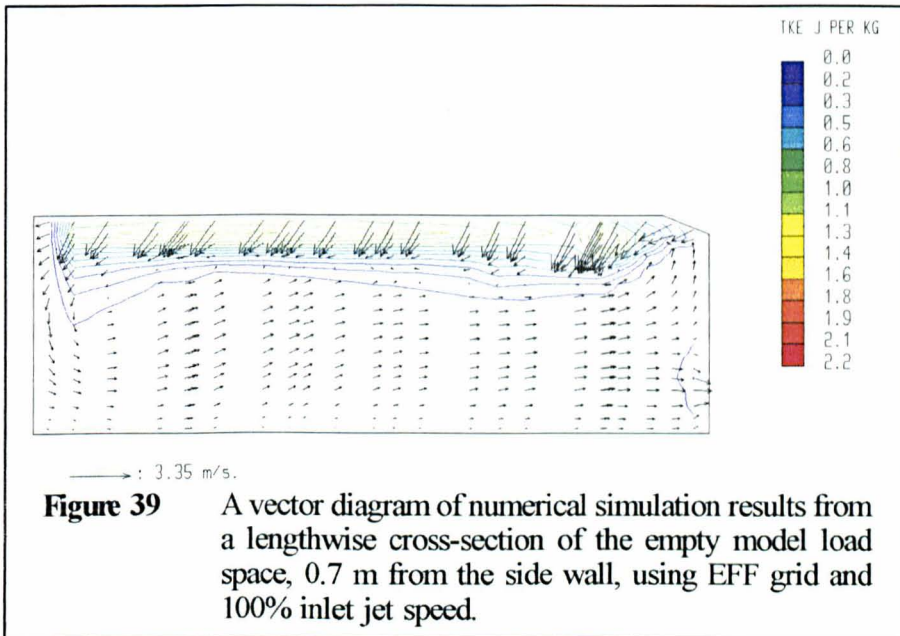
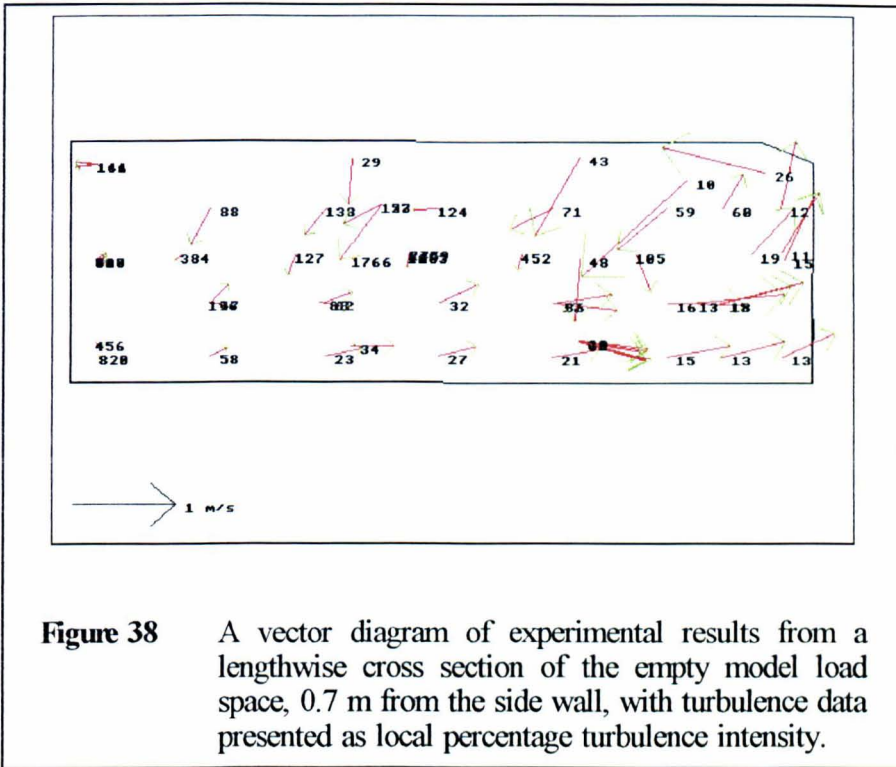
of the load space give rise to recirculating cells between the ceiling and the level at which the jets merge. These cells were observed using a smoke tracer and could be seen within the top ~1 m of the load space. The up-flow between the wall jets and the first row, at 0.7 m from the wall, can be seen in these results although the central cells are less clear, probably due to the cross-flow shown in the top of the vertical transect.

Figure 38 shows the same results as figure 35 but with the turbulence data expressed as local percentage turbulence intensity (TI). This measure normalises the turbulent kinetic energy (TKE) with respect to the local magnitude of velocity (see section 2.1.2) and is expressed as a

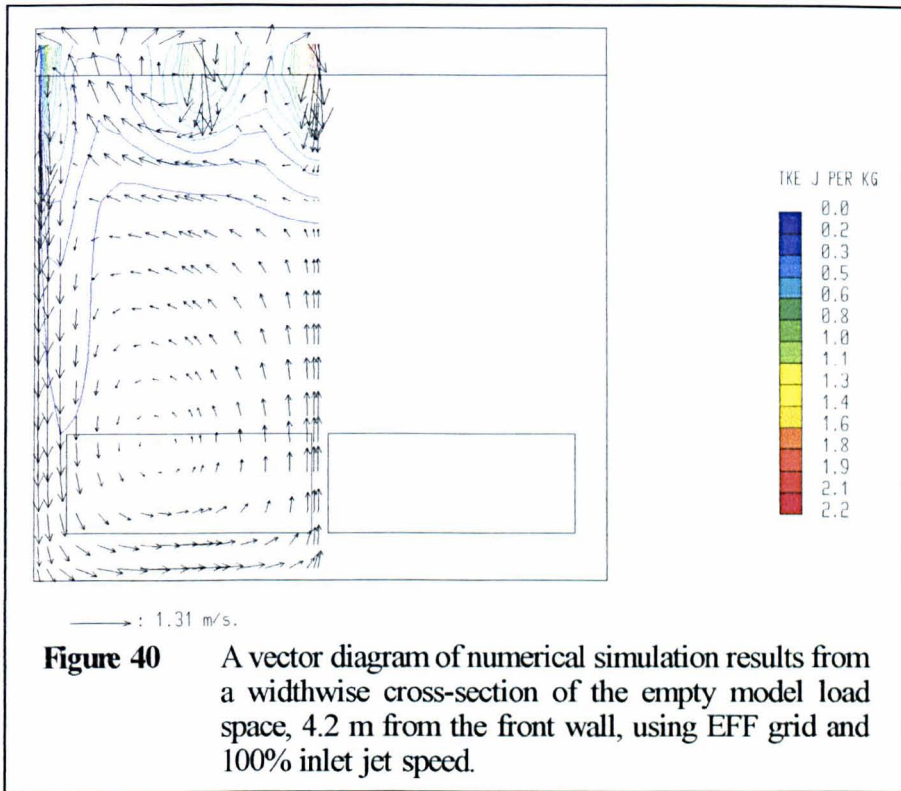


percentage in this case. Values greater than 100% are clearly possible, usually where the velocity is small, and these are visible in this figure. The majority of points, over 70% in this case, have values <50% TI however. This distribution of TI is discussed in section 4.4.

Figure 39 gives the first numerical simulation equivalent to figure 35. This simulation used the Empty/Front/Full (EFF) grid and jet inlet velocities of 100% of the measured values. This flow pattern predicts many of the same type of features seen in the experimental results: the strong flow toward the vents, the recirculation region and the jet dominated upper region. There are however obvious differences in the size and location of

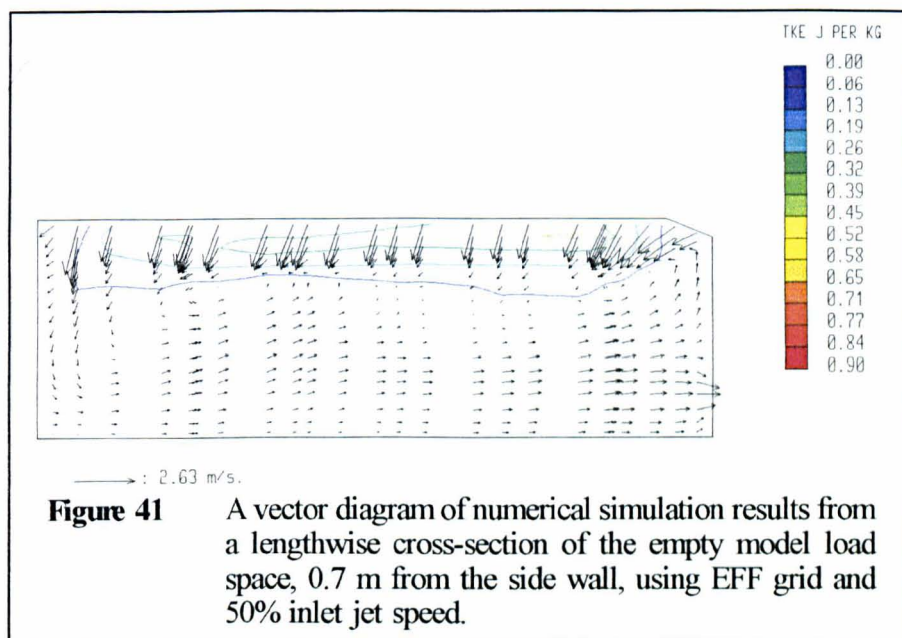


the recirculation zone, the magnitude of the flow through the rear of the load space and the levels and distribution of the turbulent kinetic energy

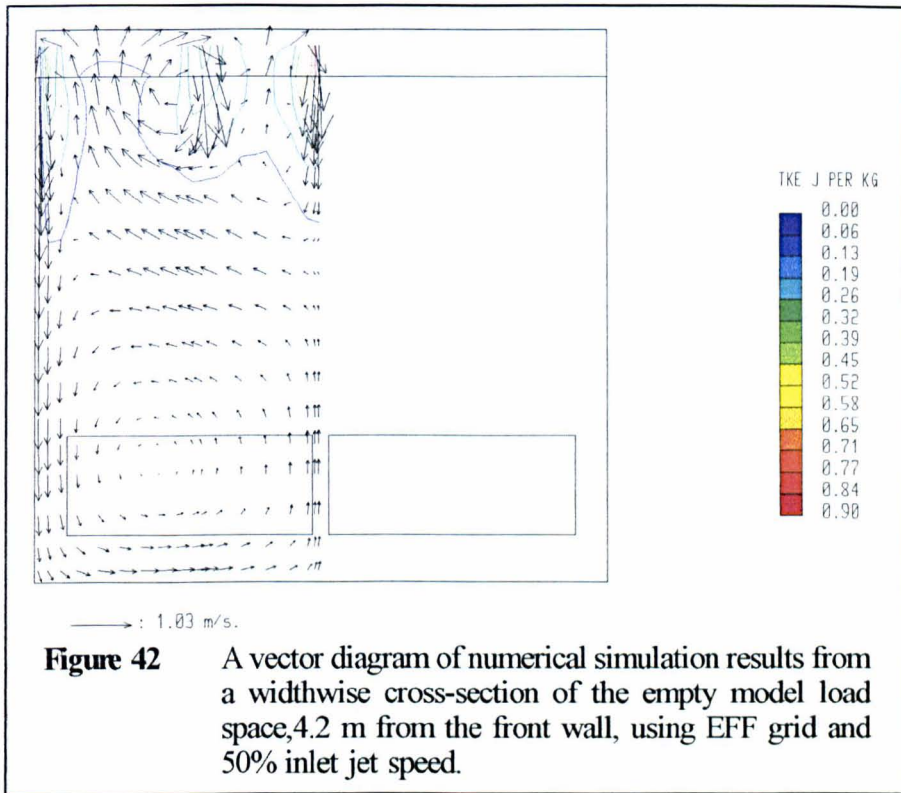


(TKE). Figure 40 also presents results from this first simulation in a cross section equivalent to figure 36. These figures again show some similarities, the updraught between the wall jets and first row of central ceiling jets for example, but with notable differences such as the strength of the central updraught in the lower recirculation region, the penetration distance of the central jets and the distribution of TKE. This final point is particularly striking, the experimental results show levels of $0.0 - 0.3 \text{ J kg}^{-1}$ with no large gradients in the values, whereas the numerical results have a range of $0.0 - 2.2 \text{ J kg}^{-1}$ and show very large gradients around the inlet jets with very low values throughout the rest of the load space. These discrepancies suggest that the momentum of the incoming air in the numerical model is

too great, causing high levels of TKE to be generated in the jet region and excessive recirculation speeds in the lower region. This would be consistent with the view that the measurements of inlet jet speed (section 2.2.3) should be considered as peak values, and therefore the numerical boundary condition based on them, which is a mean value, should reflect this by a suitable reduction (section 3.3.4).



Figures 41 and 42 show the results obtained by one such modification of the inlet jet speed to 50% of the measured values. This has reduced the peak levels of TKE in the load space by 60% and thereby brought the range of predicted values, 0.0 - 0.9 J kg⁻¹, closer to the experimental results. The remaining high predictions occur around the central jet and this would appear to be caused by the large velocity gradient which is poorly resolved in this region due to lack of grid cells. The TKE

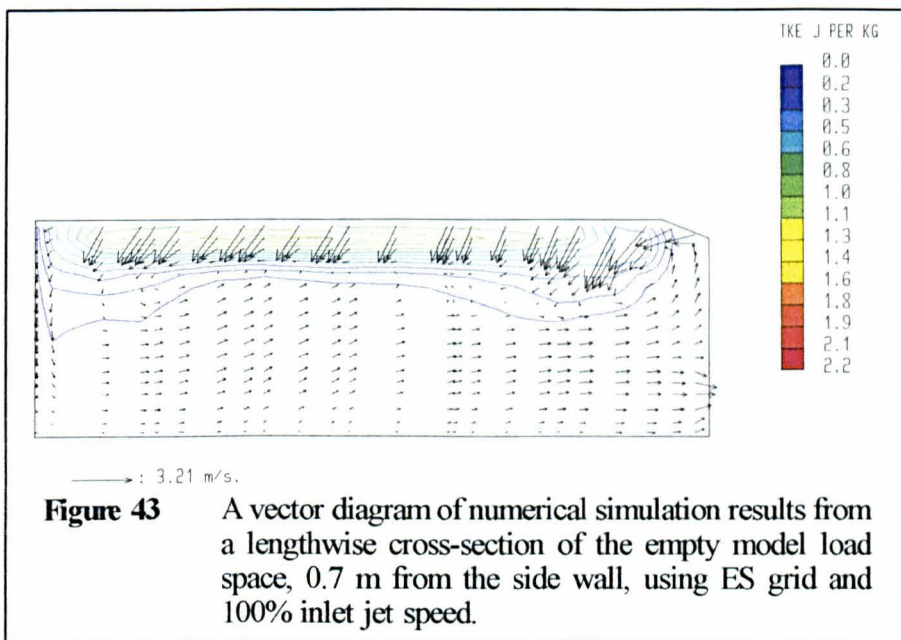


in the lower areas of the load space however is still under predicted.

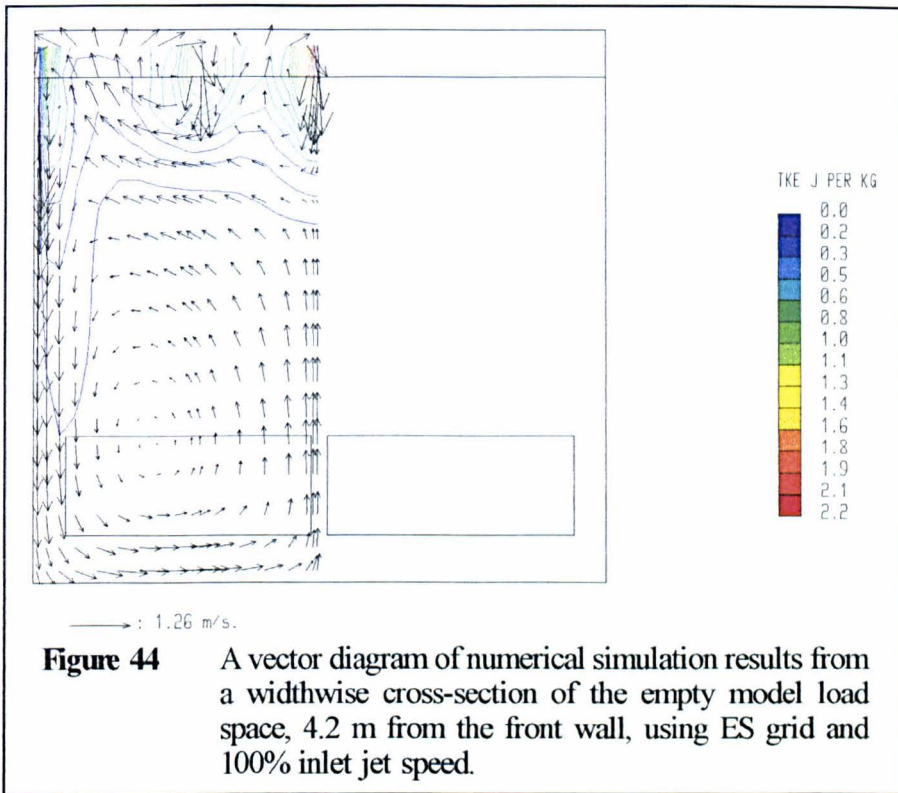
The velocity distribution of these results would appear to be similar to the previous predictions, with a general reduction in speeds due to the reduction of inflow momentum. This reduction has improved somewhat the definition of the upper jet dominated region from the lower forward flow region and the location of the front recirculation zone, but velocities in the rear section are still over predicted. The reduction in overall air speeds has also improved the central ceiling jet penetration slightly but not sufficiently to bring it into line with the experimental results shown in figure 36. The discrepancy in velocities in the rear of the load space may be due to the

simplifications in the inlet jet angle and volume flow rate made in the numerical simulations. These do not account for any features associated with the tapered false ceiling ducts in the experimental model, which may affect the jet angle and volume flow rate from the holes in the rear section.

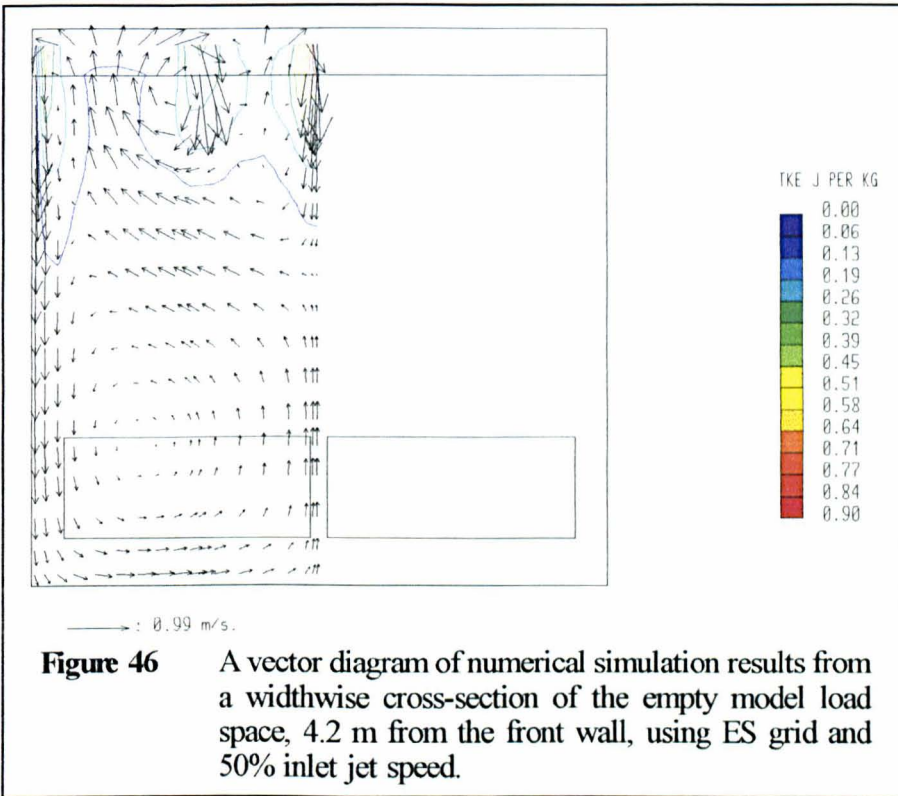
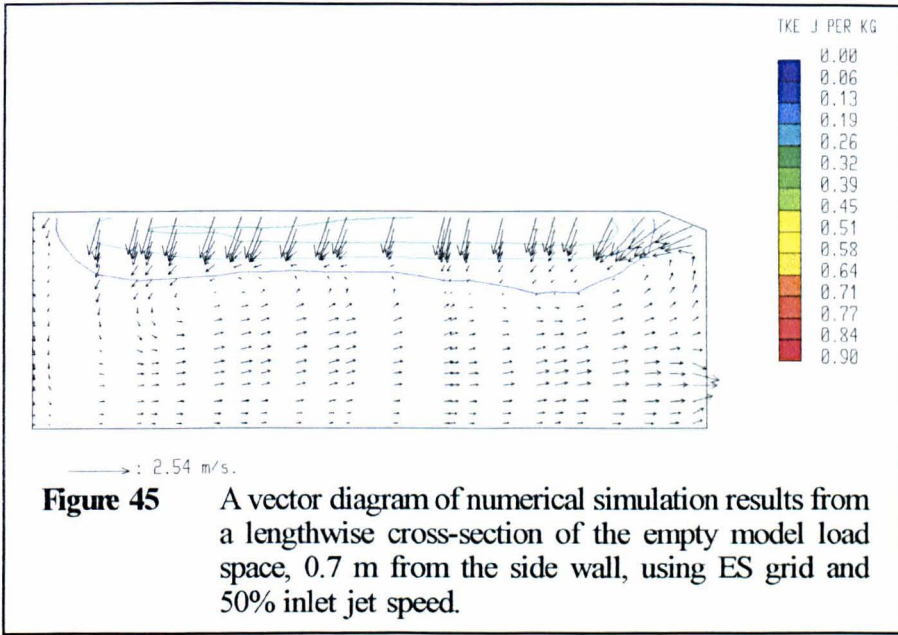
The numerical results using an inlet jet speed of 66% of the measured values gave intermediate results between the two cases presented above. Those results are not presented here but are included in the discussion of statistical comparison (section 5) and ventilation rate (section 4.2.6).



Figures 43 and 44 show the results of the numerical simulation using the alternate grid structure developed for the side half loaded model and an inlet jet speed of 100% of the measured values. These results are therefore



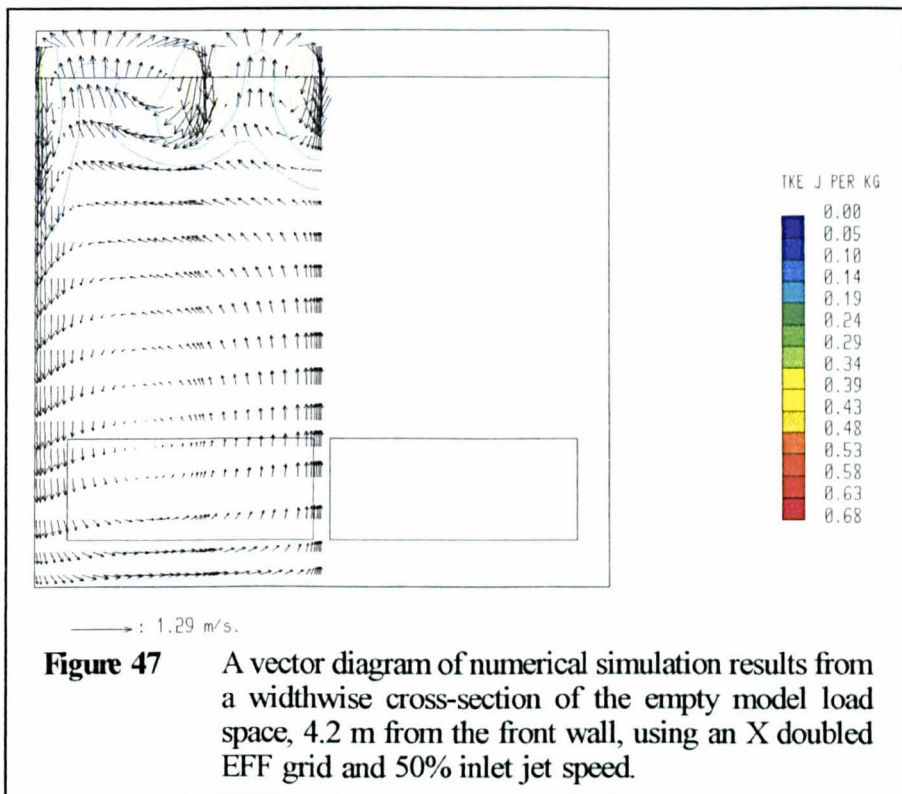
comparable to figures 39 and 40, which use the EFF grid, and show that the solution appears independent of the lengthwise grid structure. The noticeable difference in these plots is the absence of the peak in the TKE at the front of the load space in figure 43 which occurs in figure 39. This is due to the difference in the number of cells at that point, because the high velocity gradient caused by the inlet jets gives rise to a high TKE value which does not occur when the grid has fewer cells and the gradient is not resolved. This point aside the same criticisms of the over prediction of TKE in figures 39 and 40 equally apply to figures 43 and 44.



Similarly figures 45 and 46 are comparable to figures 41 and 42 and again show a general independence of grid structure. The discrepancies in

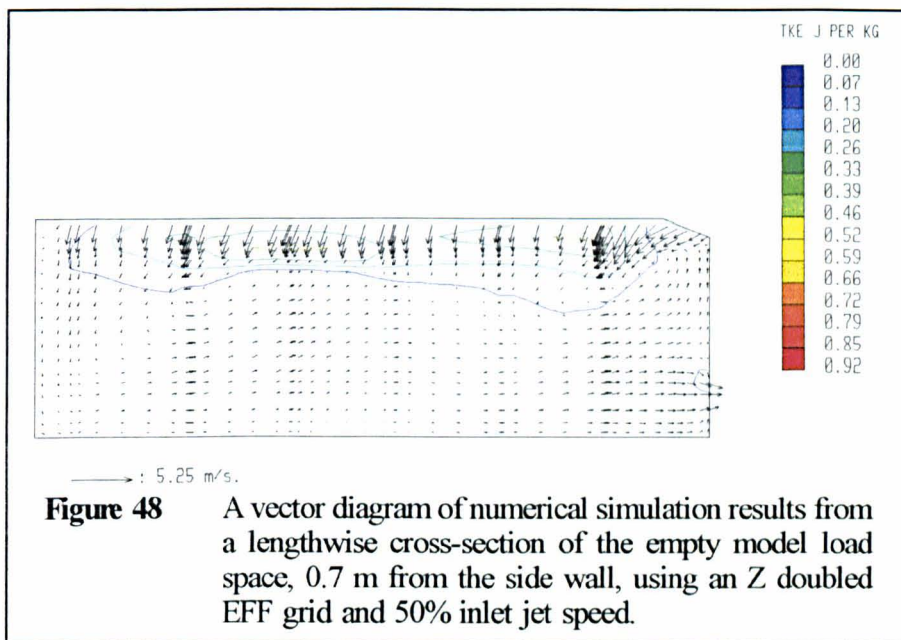
these figures are less noticeable and centre on the location and extent of the stagnation line between the upper and lower flow regions in figures 41 and 45. These differences are not as easily explained but must be due to the change of grid structure and are probably determined by the changes in cell volumes over which the velocities are integrated, thus making the mean velocities in the solution appear different.

The final elements of this numerical simulation case were three further grid independence tests involving the doubling of the number of

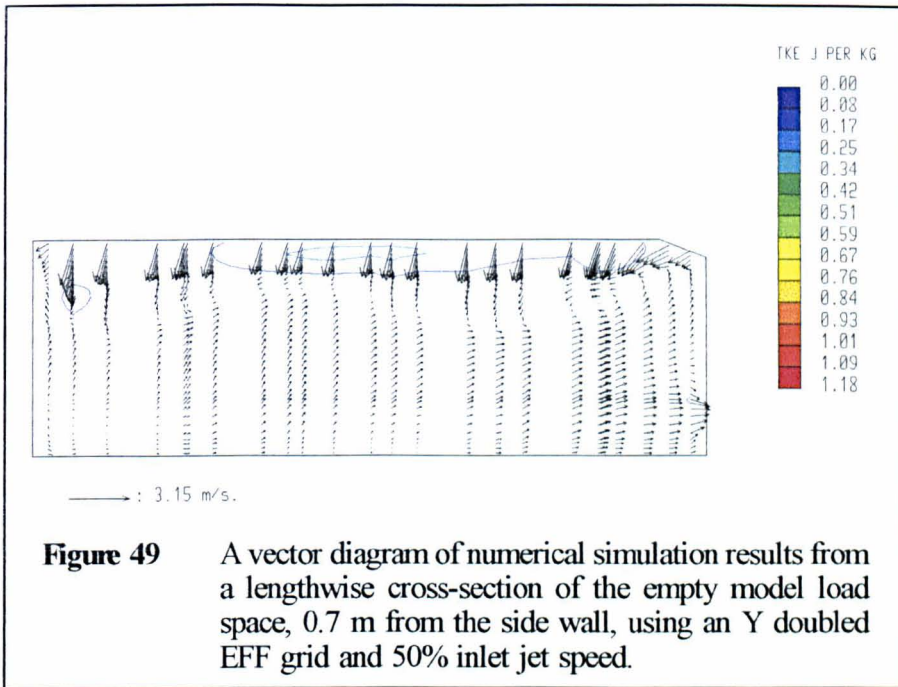


cells in each cartesian direction. The results of these simulations are given

in figures 47 - 50. The first of these shows the result of doubling the number of cells in the X direction, that is across the width of the load space. The only noticeable effect of this change is the reduction in peak TKE generated at the jet in the centre of the load space. Notice however that the shape of the contours remains consistent with the previous comparable simulations, figures 42 and 46. This change in value is due to the improved resolution of the gradients in the jet and subsequent lessening of TKE generation.

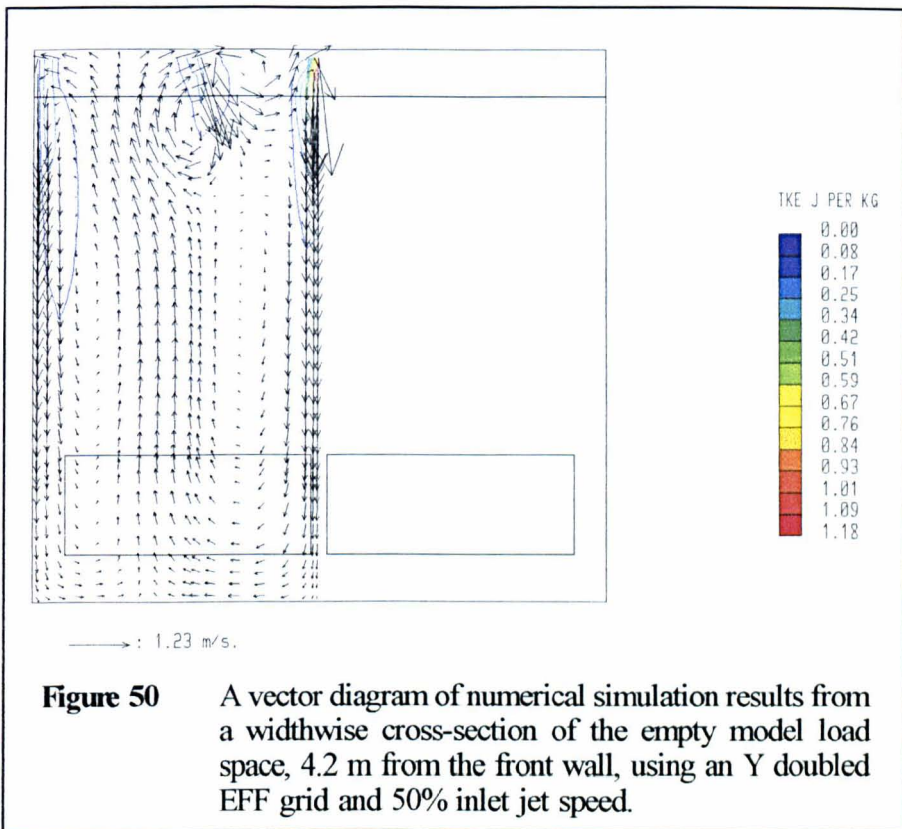


The next result, figure 48, shows the effects of doubling the grid in the Z direction, that is along the length of the load space. Once again the mean flow pattern and general levels of TKE are unchanged from the basic grid results, figures 41 and 45. The source of the slight increase in overall TKE is unclear, but is probably due to the relative decrease in size of the

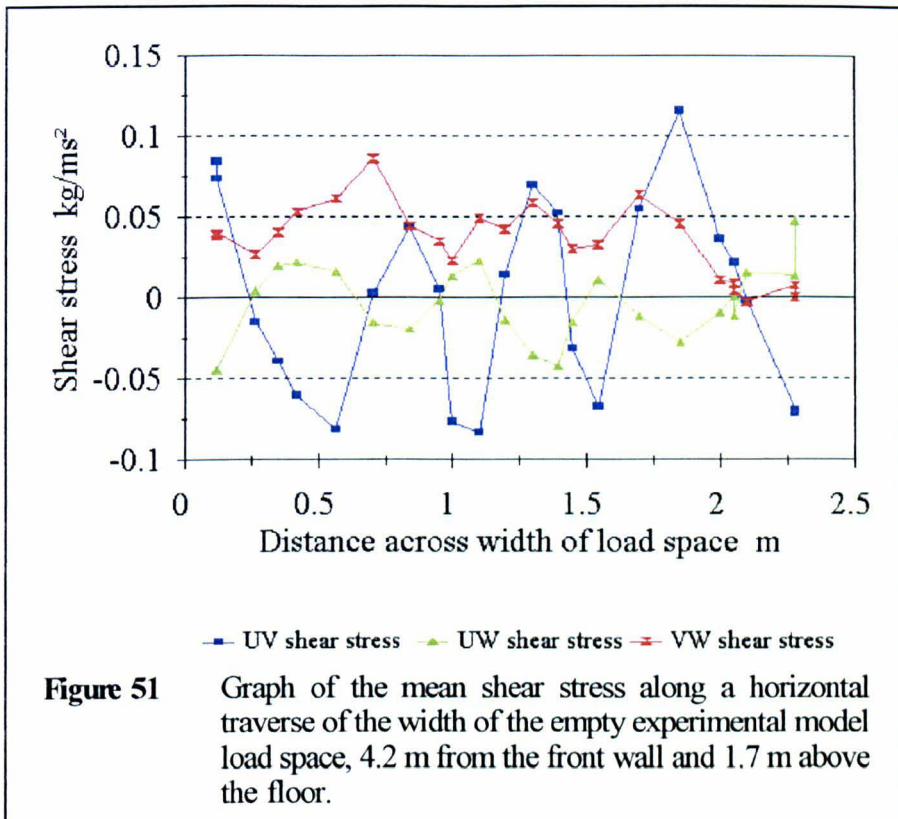


cells in the lengthwise direction compared to that in the remaining directions.

The effect that this change in relative sizes can have is most clearly shown by the final grid test, with the number of cells doubled in the vertical axis (figures 49 and 50). Here the mean flow field has become very unstable and the TKE predictions have again increased. These results are drastically different both in mean flow and TKE from the previous cases. This is considered to be due to the interaction between the decreased cell size in the vertical direction and the high gradients in the jet regions, especially the central jet. The comparative lack of resolution in the gradients compared to that in the streamwise direction gives a decreased momentum sink for the jet and thus leads to excessive jet penetration, in this case to



mirror the wall jet on the opposite side. These results are clearly not in accordance with the experimental evidence and so it must be concluded that this type of grid independence test must be treated with some care in order to avoid the grid induced problems seen here. This also illustrates that a certain level of user expertise, experience and simulation validation is required in any situation to avoid spurious results. This point accepted, the first two tests seem to indicate a reasonable level of agreement with the basic grid results of both grid structures.

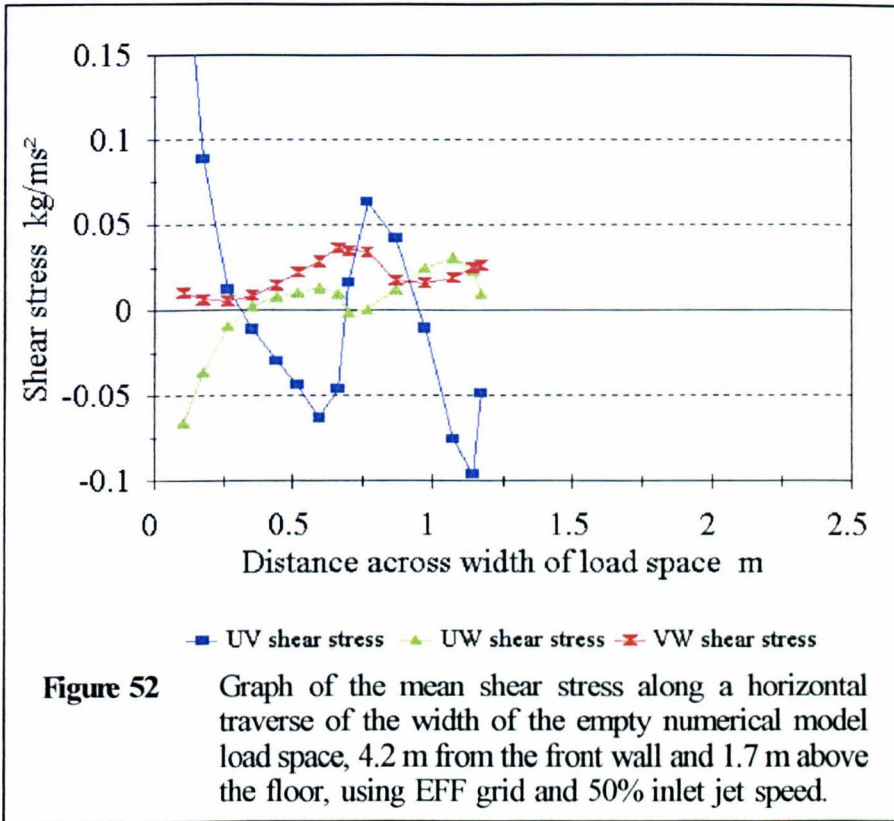


Mean Shear Stress

The mean shear stress measurements made in the empty experimental model along various traverses are presented in figures 51, 53 and 55. These measurements combine the information about two velocity components measured simultaneously at one point by one ultrasonic anemometer. The first of these figures shows the variation in measured shear stress along a traverse across the width of the load space at a height of 1.73 m (74% of the vertical height) and a distance of 4.18 m (58% of the load space length) from the front vents. This traverse therefore crosses the five ceiling jets which are at 0, 0.7, 1.2, 1.7 and 2.4 m. The shear stresses reflect these jet positions very well, shown by the zeros of the jet dominated

UV and UW components at 0.7, 1.2 and 1.7 m. This indicates that the ultrasonic anemometer is adequately measuring the velocity fluctuations in this region to resolve the variation of the shear stress. The dominant vertical component of the jets is indicated by the large UV shear stress peaks and troughs on either side of the jet positions, the sign indicating the direction of the shear. The secondary W velocity component of the jets is also visible in the UW shear stress which follows the same changes of sign as the UV component across the traverse but is of smaller magnitude. The final VW component is clearly not defined by jet position, but is due to the overall flow along the length of the load space which creates a shear layer into which the jets penetrate and provide a momentum source for the mean flow.

In the previous comparison of experimental and numerical mean velocity results the apparent lack of penetration of the central jets was noted as a discrepancy in the numerical predictions and this problem can also be seen in the comparison of figures 51 and 52. Figure 52 shows the mean shear stress predictions calculated from the numerical results for mean velocity using the values in neighbouring cells and their separation to give an approximation of the velocity gradient between points. The shear stress is then calculated by $\tau_{ij} = (\mu + \mu_t) \left(\frac{\partial U_i}{\partial X_j} + \frac{\partial U_j}{\partial X_i} \right)$ where μ is the fluid viscosity ($\approx 1.8 \times 10^{-5} \text{ kg m}^{-1} \text{ s}^{-1}$ for air at room temperature) and μ_t is the turbulent viscosity. This latter value has for these plots been calculated using the predicted values of TKE and the Prandtl-Kolmogorov energy model where



$\mu_t = \rho C_\mu l \sqrt{k}$ and the prescribed length scale l takes the value 0.7 m which is the average wall distance of the traverses. Subsequent analysis also shows that this value of the length scale agrees well with the experimentally determined values (table IX section 4.3.1). The result shows that predicted UV stress has a realistic behaviour conforming to the jet positions. However the UW and VW components are less well behaved. The UW component does not change sign appropriately away from the wall and both the UW and VW component magnitudes are underestimated with respect to the UV component magnitude which is reasonably reproduced.

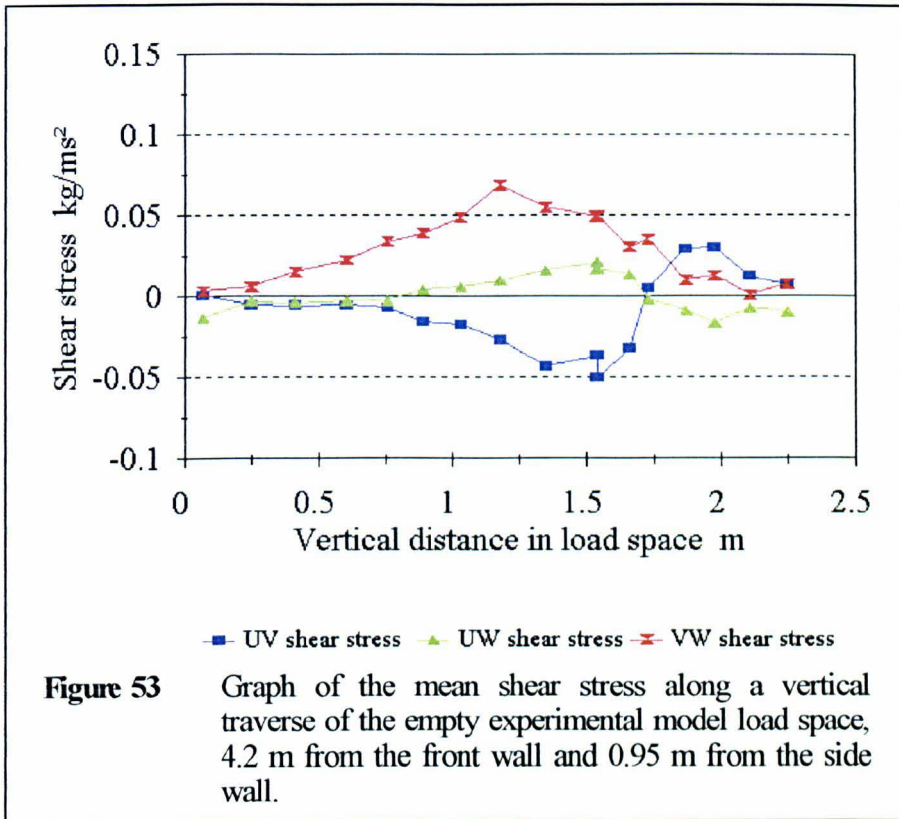
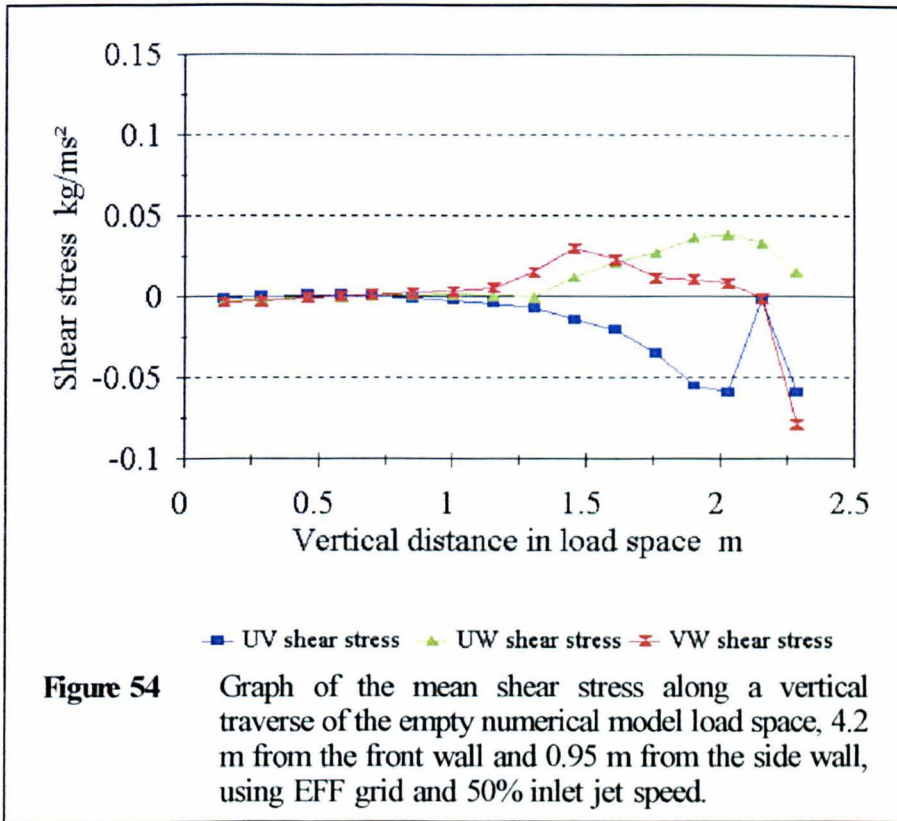
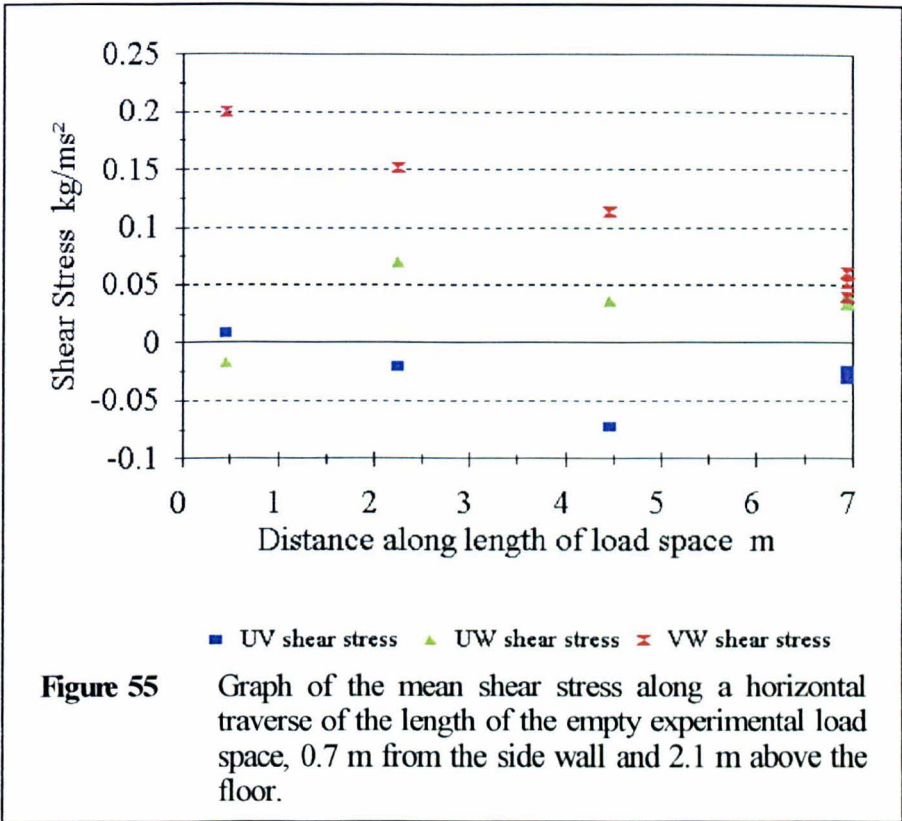


Figure 53 shows the mean shear stress measured on a vertical traverse of the empty load space at 0.95 m from the side wall (directly between two central jets) and 4.18 m from the front vents (as for the horizontal traverse). Figure 54 shows the numerical predictions for the same positions. The differences in form of these graphs are probably due to the asymmetry of the experimental results, that is the significant cross flow in the upper jet region, see figure 36, compared to the symmetric prediction, figure 42. This asymmetry gives rise to the positive UV shear seen in the experimental results which does not occur in the predictions. Also the peak in VW shear, due to the interface between the upper jet region and the lower forward flow region, occurs at a lower position in the experiment



than in the predictions. This is again due to the under-prediction of jet penetration, as is the under-predicted negative UV shear stress in this same region.

Finally figure 55 shows the changing experimental shear stress results for a series of points ~2.1 m above the load space floor (90% of the vertical height) and 0.7 m from the side wall (directly beneath a ceiling jet). These are four of the fixed anemometer positions (numbers 3, 6, 9 and 12) shown in figure 17 and show the variation of shear stress along the length of the load space. In this loading case the UV shear component changes little over the length of the load space, reflecting the proximity of the



measuring position to an inlet jet. This is also reflected in the UW component which changes only near the front angled plate, at which the jet angle is significantly different, introducing a much higher W velocity component whilst reducing the V component. Finally the VW component shows a clear downward trend along the length of the load space.

4.2.2 Front half loaded case

Mean velocity and Turbulent Kinetic Energy

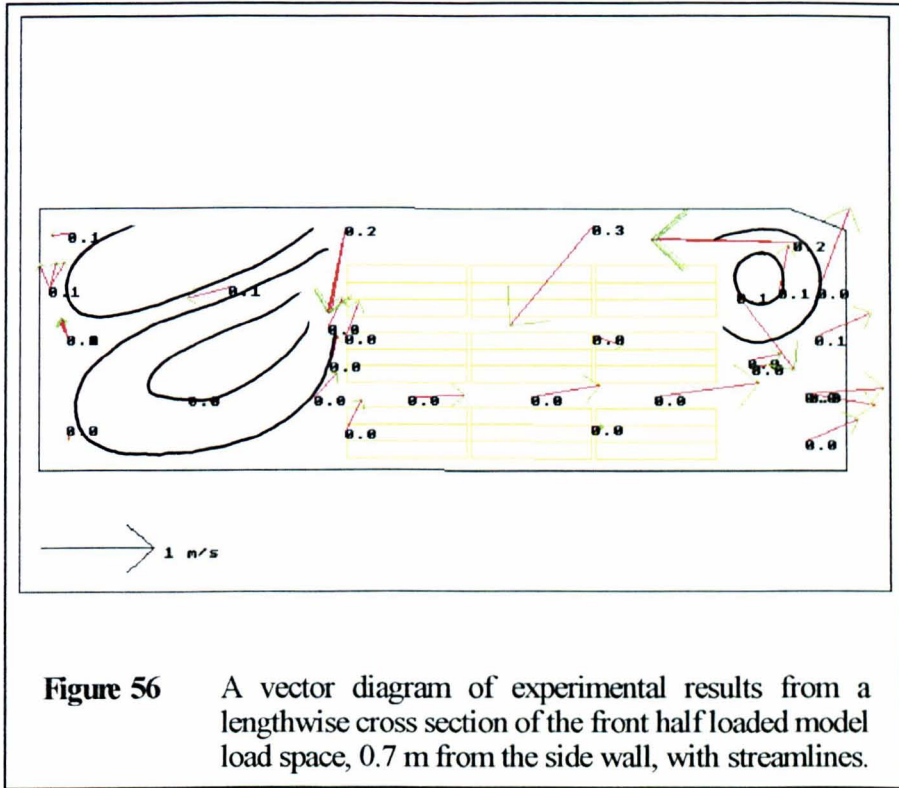
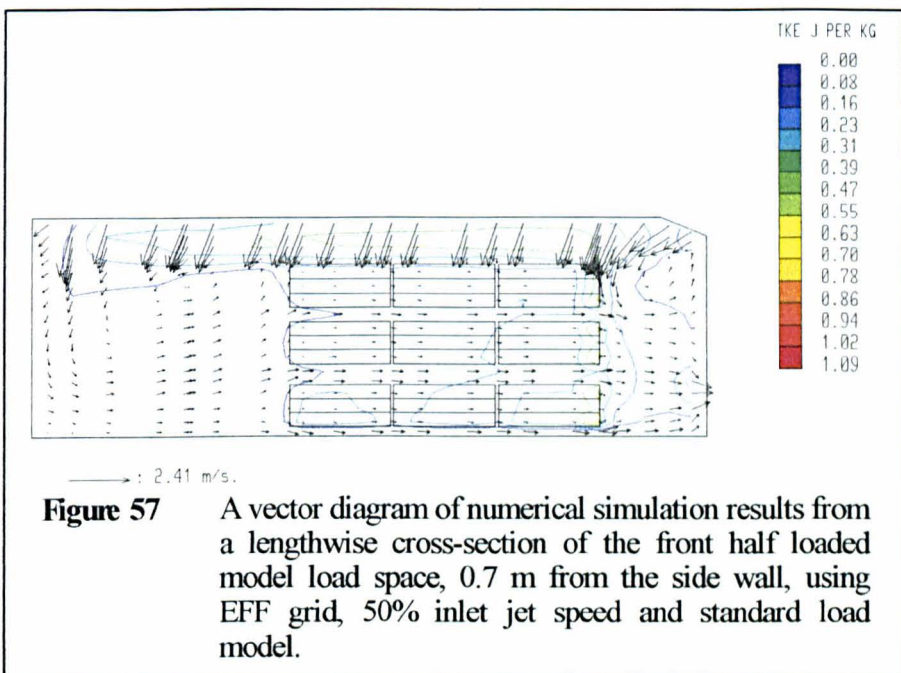


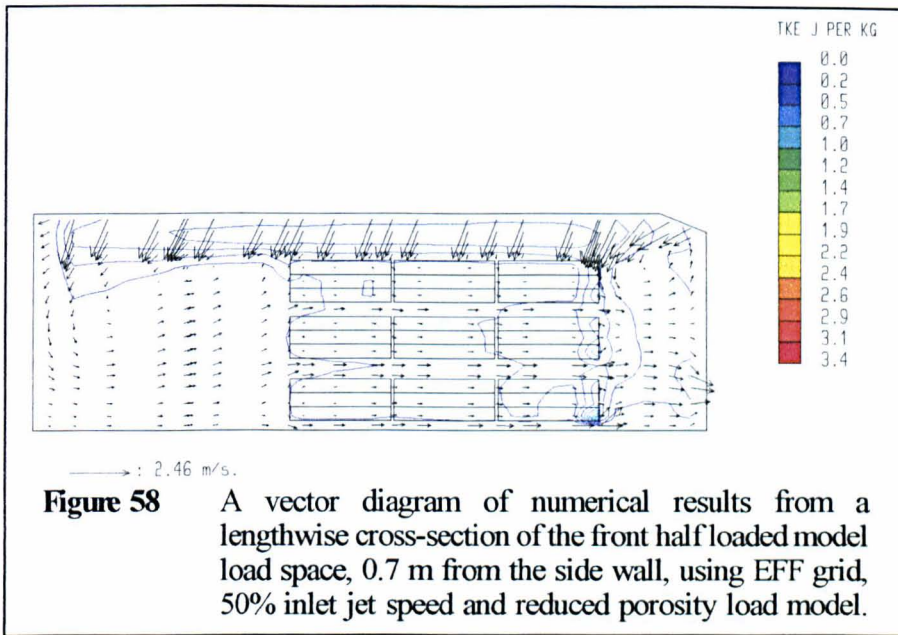
Figure 56 shows the mean velocity and TKE for the experimental measurements on the standard lengthwise cross section (see section 4.1) through the front half loaded model vehicle. The flow pattern again indicates four main areas:

Firstly there is a highly turbulent, jet dominated region above the load with a general movement toward the rear of the load space. This balances the forward flow of air through the load itself, drawn one again by the plenum chamber vents at the front of the load space. Turbulence levels within the

load are very low, as would be expected, because of the affect of the load as a momentum sink. Ahead of the load and above the vents there is a small but significant recirculation zone with moderately high turbulence levels which is driven by the opposite flows into the vents and out of the angled ceiling section. Finally there is a second recirculation zone behind the load. This may in fact be two recirculating cells, as indicated in the figure, or one zone as predicted by the CFD (figures 57 and 58).



The difference between these recirculation patterns is likely to be the treatment of the ceiling jets in the rear section of the load space. The simplified model used in these CFD simulations may overestimate the inlet jet strength in this region and thereby drive the circulation seen in the predictions where a reduced ceiling jet strength would allow a secondary flow to form. However, since both the 100% and 50% inlet jet speed



models predicted similar recirculation zones (only the 50% result is shown), this implies that an even greater reduction in jet velocity would be required which is not experimentally justified. Therefore it may be that other experimental details of the ceiling holes are important in generating this feature of the flow. For example, the decreasing ceiling duct width above the holes in the rear of the load space may be reducing the effective hole area, increasing the measured jet velocity and causing an over-estimate in the CFD boundary momentum source.

Further comparison of the experimental and CFD results shows that the recirculation zone in front of the load is also incorrectly represented, the centre being closer to the load than prediction suggests and the updraught of recirculated air from the load being stronger. The reduced porosity load

model in this case gives a better prediction than the standard model, suggesting that the load resistance is an important factor. The velocity of the air between the shelves is also more accurately predicted by the reduced porosity load model, suggesting that this increased channelling of air is the important consideration in determining the position of the front recirculation zone.

Turbulence levels within the majority of the load space are similarly predicted by the two simulations. The difference, and the major problem with these load models, occurs at the front of the loaded section where TKE levels are greatly over-predicted at the top and bottom of each stack, especially at the lowest point. This is caused by the mixing of air which has been slowed by passage through the loaded region and air which has passed through the open channels. This large velocity differential, particularly in the case of the reduced porosity model, causes very high generation rates of TKE which are clearly un-physical and can become an impediment to convergence. This problem might be overcome by increasing grid density in this region, but a considerable number of extra nodes may be necessary. A comparison with the experimental levels of TKE shows that agreement is reasonable in the open spaces in front of and behind the load. Within the load however, TKE levels are elevated by the CFD simulation because of the velocity differentials discussed above. This is not found in the

experimental data where turbulence levels are limited by the restrictions on eddy size amongst the load.

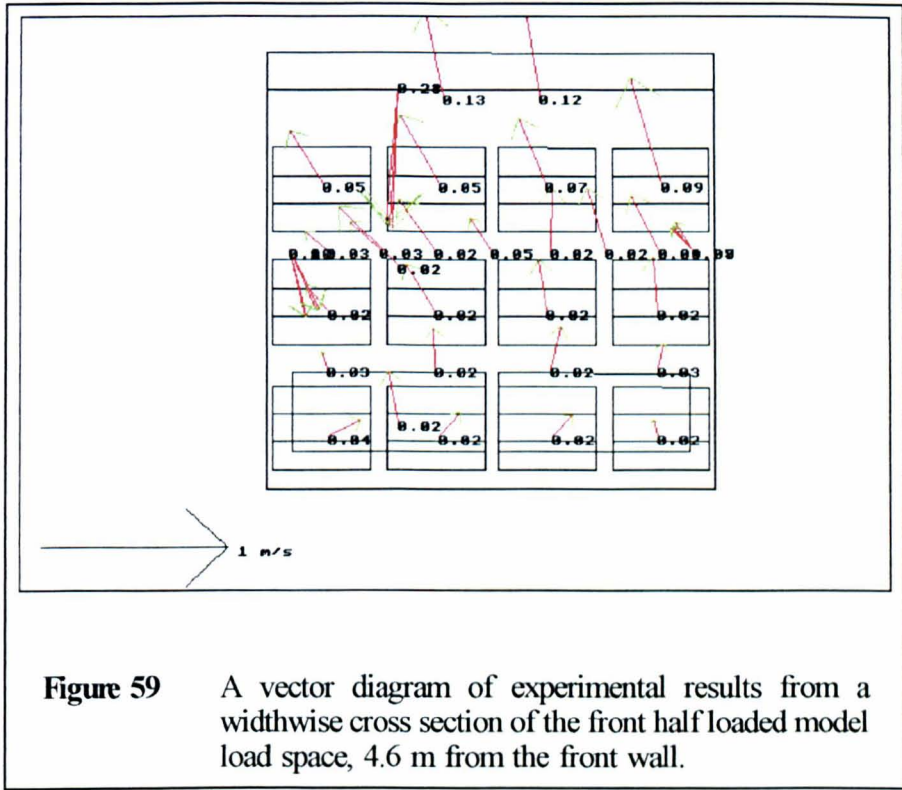
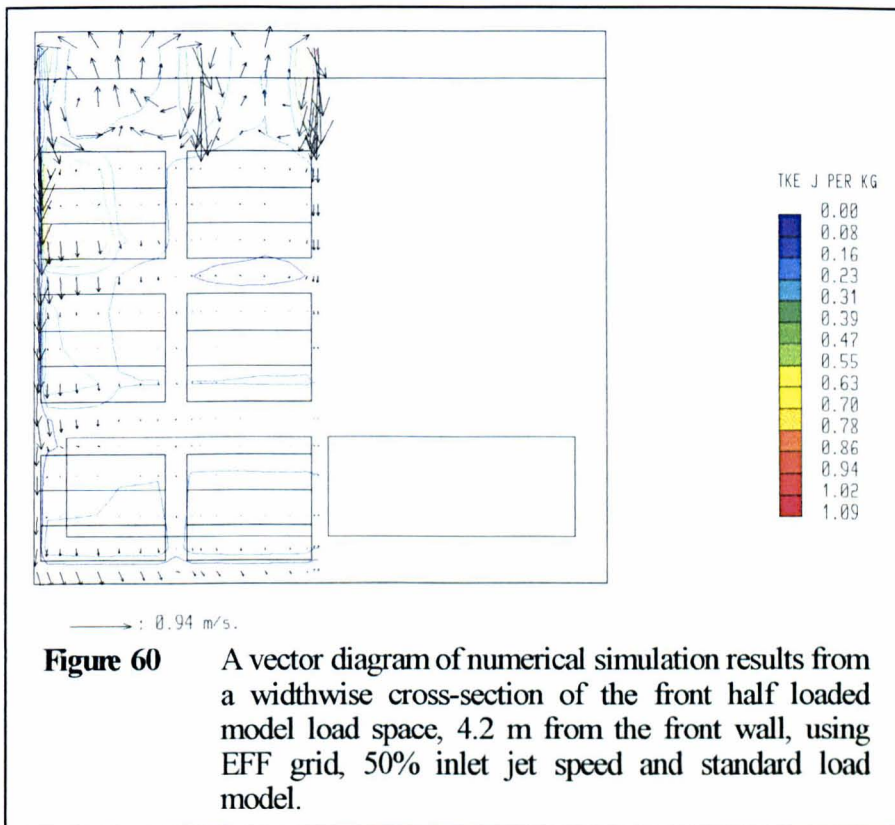
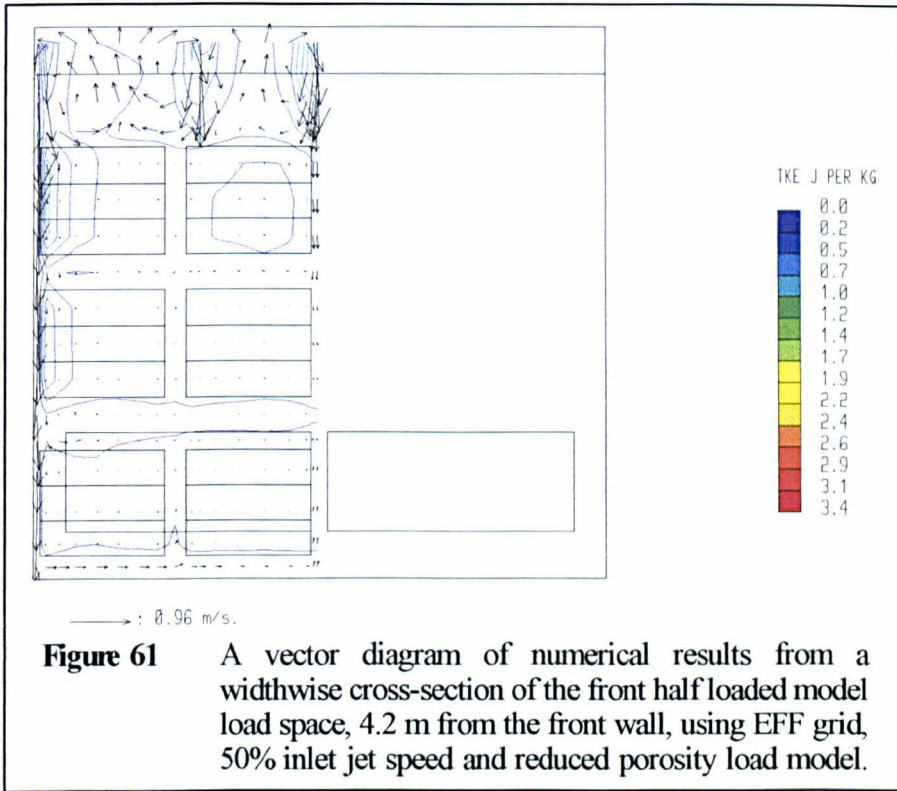


Figure 59 shows the experimental velocity data for a widthwise cross-section which falls just behind the loaded portion of the load space. The general pattern of these results shows the strength of the recirculation in the rear portion of the load space, with a noticeable asymmetry presumably caused by unequal wall jet effects on either side of the load space. Experimental results for the standard widthwise cross-section are given in figure 62 with comparable numerical results for the two loading models in figures 60 and 61. Considering first the numerical results, the difference between the two load models is clearly visible as flow through



the lowest floor of each box stack on the wall side in figure 60, the standard load model case. This contrasts with the increased cross flow in the reduced porosity model which has air from the wall jet moving beneath both lines of boxes and up the central gap. The central down-draught also penetrates further in the latter case, with increased cross flow between the upper shelves. Flow through the boxes themselves, except for the flow through the stack bases noted above, seem minimal in this plane compared to that seen in the lengthwise cross-section (figures 57 and 58). This implies that the ventilation rate will be dominated by the flow along the length of the load space with the inherent problem of air bypassing the boxes through the channels of lower resistance. The high turbulence levels within the load



are once again reflected in these figures, with particularly high levels where the wall jet interacts with the topmost box giving the same problematic velocity gradients as seen previously in figures 57 and 58.

The experimental data for this cross section (figure 62) shows a variable but small cross flow component between shelves with a very low turbulence level. The cross flow within the box spaces, recalling that alterations to the boxes surrounding such locations means that these are not true in-box measurements, is also small. One feature which is clearly not predicted well is the penetration of the central jet, which is present at the lowest stack level. Also poorly predicted is the ceiling jet strength seen in

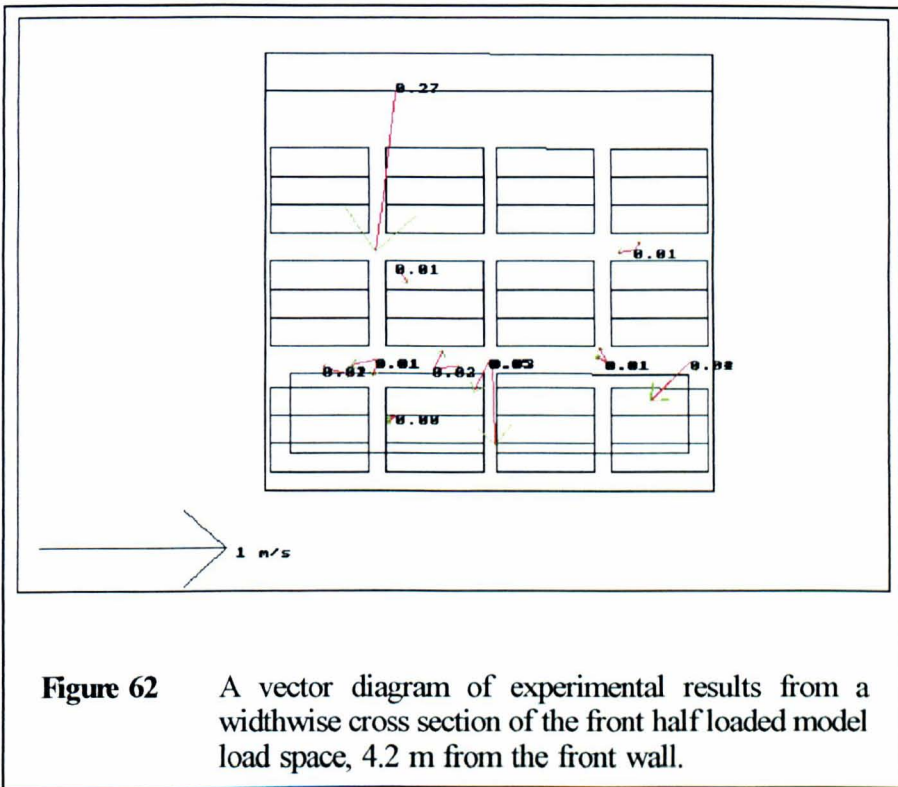
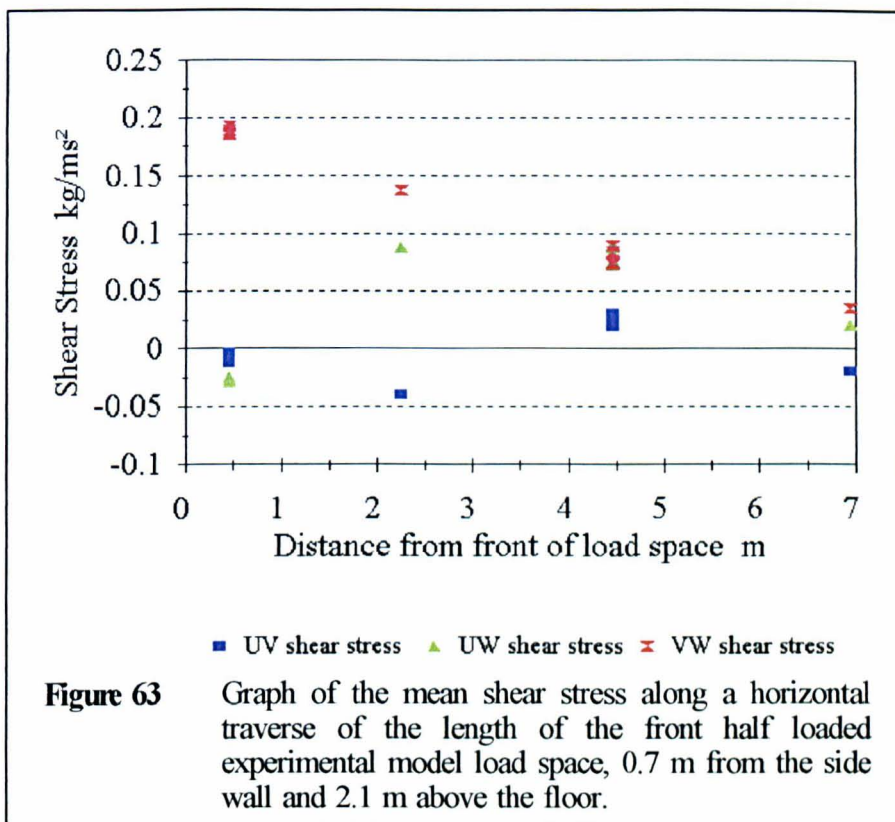


Figure 62 A vector diagram of experimental results from a wide cross section of the front half loaded model load space, 4.2 m from the front wall.

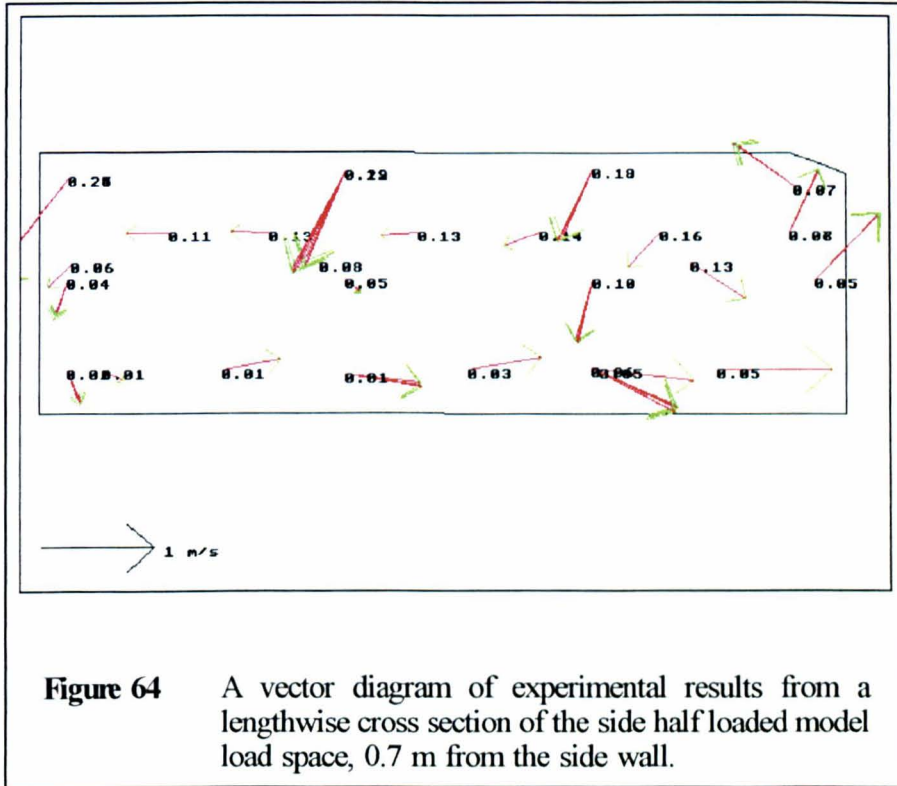
figure 62, where this experimental result is approximately half the corresponding prediction. This suggests that in the experimental situation the decay of the jet velocity is much faster than predicted. This is possibly due to the difference in the set-up of the sources, that is the multiple point sources, holes, in the experiments, simulated by a line source. Measurements from within the load, such as under the trollies, would also be useful in this situation, however practical difficulties because of the size of the sensor head preclude the use of the standard ultrasonic anemometer.



Finally figure 63 shows the changing experimental shear stress results for a series of the fixed anemometer positions (numbers 3, 6, 9 and 12 shown in figure 17) along the length of the load space. In this case, as with the empty load space case, the UV shear component changes little over the length of the load space, reflecting the proximity of the measuring position to an inlet jet. The UW component, which changes near the front angled plate where the jet angle is significantly different, also increases over the load because of the recirculation in the top section. Finally the VW component again shows a clear downward trend along the length of the load space.

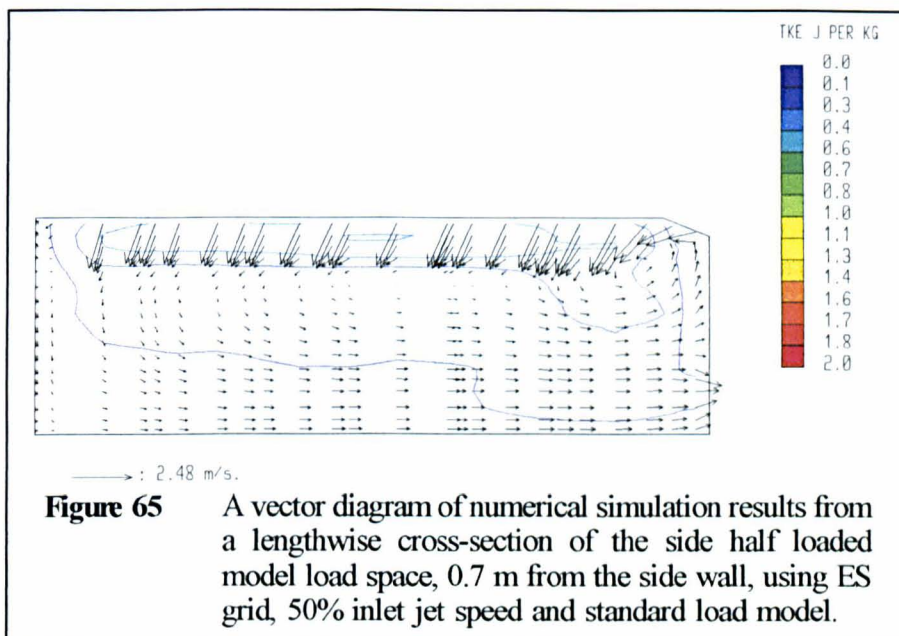
4.2.3 Side half loaded case

Mean velocity and Turbulent Kinetic Energy

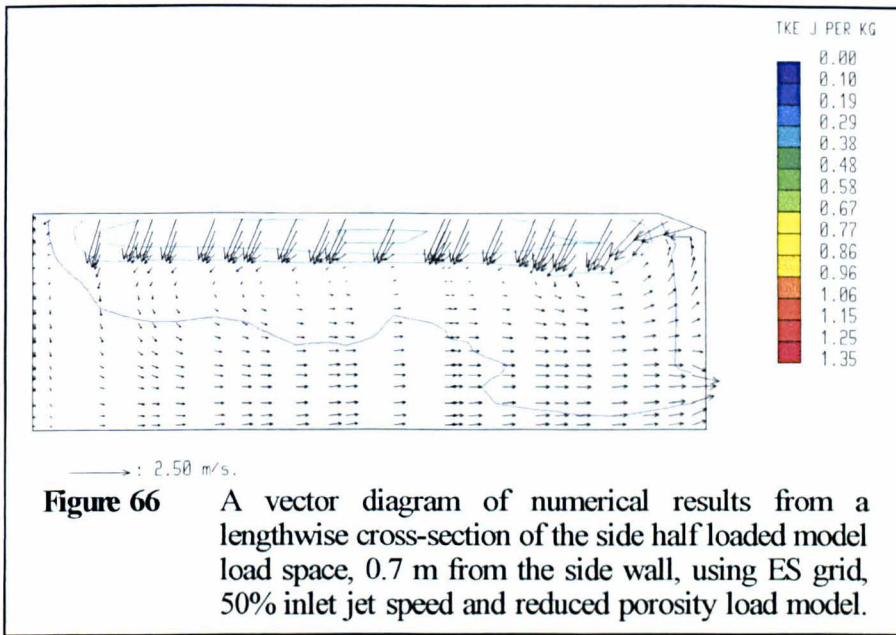


The experimental results for the standard lengthwise cross-section are given in figure 64. This shows that the open central section of the load space experiences a flow pattern similar to the empty load space case, with recirculation at the front, strong jet effects driving a rearward flow in the upper region and a forward flow toward the lower plenum chamber vents. The rearward circulation close to the ceiling is stronger in this case than in the empty case (*c.f.* figure 35), probably due to the restriction of the load space width by the presence of the load, but the jet effects are very similar

to the previous cases. This increase in flow velocity has also increased the movement of air in the rear portion of the load space, which in the empty case was almost stagnant.

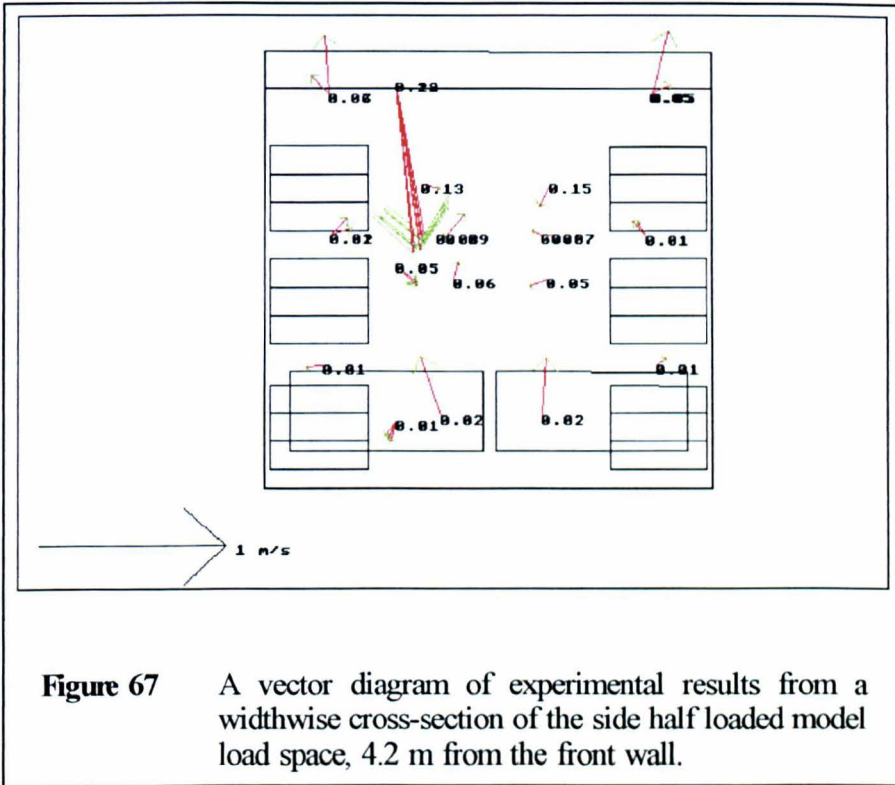


The numerical predictions of this case can be seen in figures 65 and 66, again reflecting the two loading models used. The results shown in these figures indicate no major differences from the use of the different loading models. The reduced porosity model has reduced the peak level of TKE in the domain, but the results here show that this does not translate into a general reduction of predicted levels throughout the load space. Minor changes in the flow pattern are evident, namely a reduction in the size of the interface zone between the inlet jets and the lower forward flow. This, and the consequent change in the shape of the front recirculation zone,

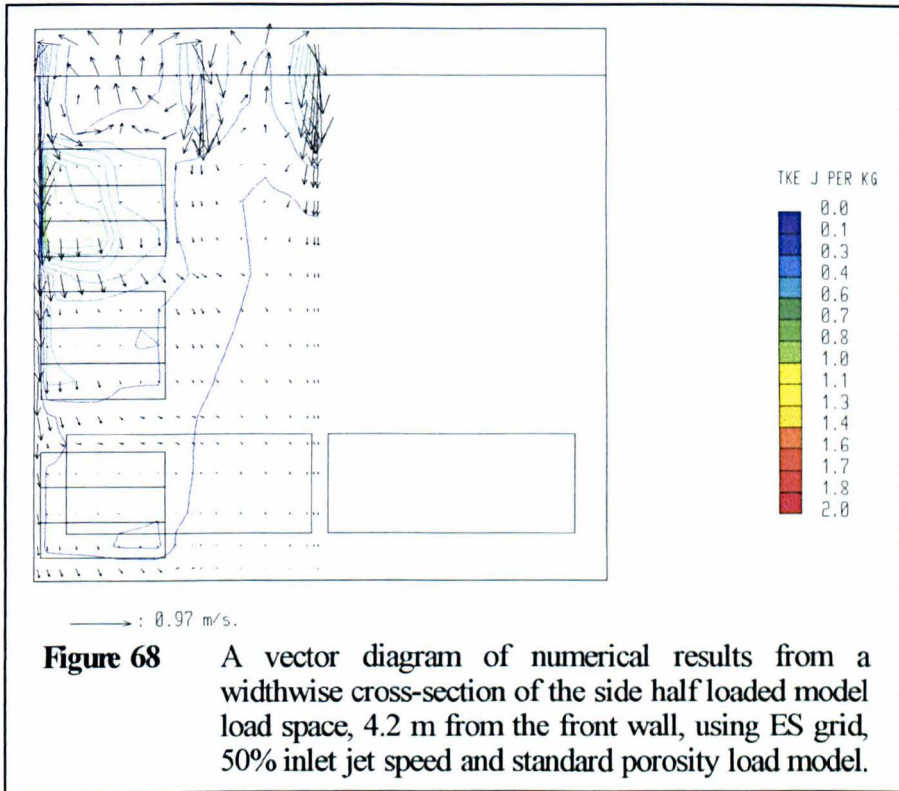


are due to the movement of air through the load from the wall jets and is therefore more clearly seen in the next figures.

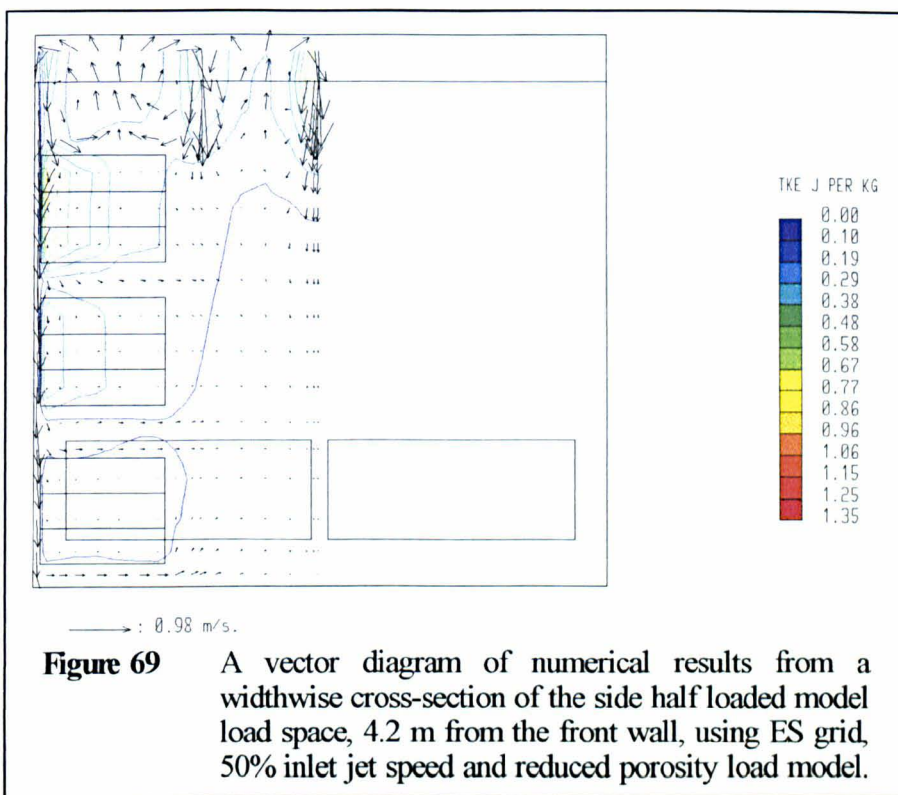
Considering the standard widthwise cross section (figure 67), it is apparent that much of the secondary circulation seen in the empty load space (figure 36) has been removed. This secondary movement was generated by the wall jets sustained momentum compared to the free jets. In this case the wall jet is affected by the presence of the load and thus the secondary circulation does not develop. This figure also indicates that the flow between the shelves is inward between the upper shelves and outward between the lower shelves, something which is not reflected by the numerical predictions shown in figures 68 and 69.



These numerical results, using the two different load models (see section 3.3.3), are significantly different in their predictions concerning the flow through the load. The standard load model, which allows air to move through the chick box base, promotes a transfer of vertical momentum from the wall jet, across the load and into the central region. This transfer then causes the change in the flow pattern seen in the previous cross sections of the numerical results (figures 65 and 66). The reduced porosity model (figure 69), which restricts further the movement through the chick box, does not allow for this transfer and, because of the changed velocity gradients, also does not predict the same high TKE values especially between the shelves of chick boxes. The direction of this flow has already

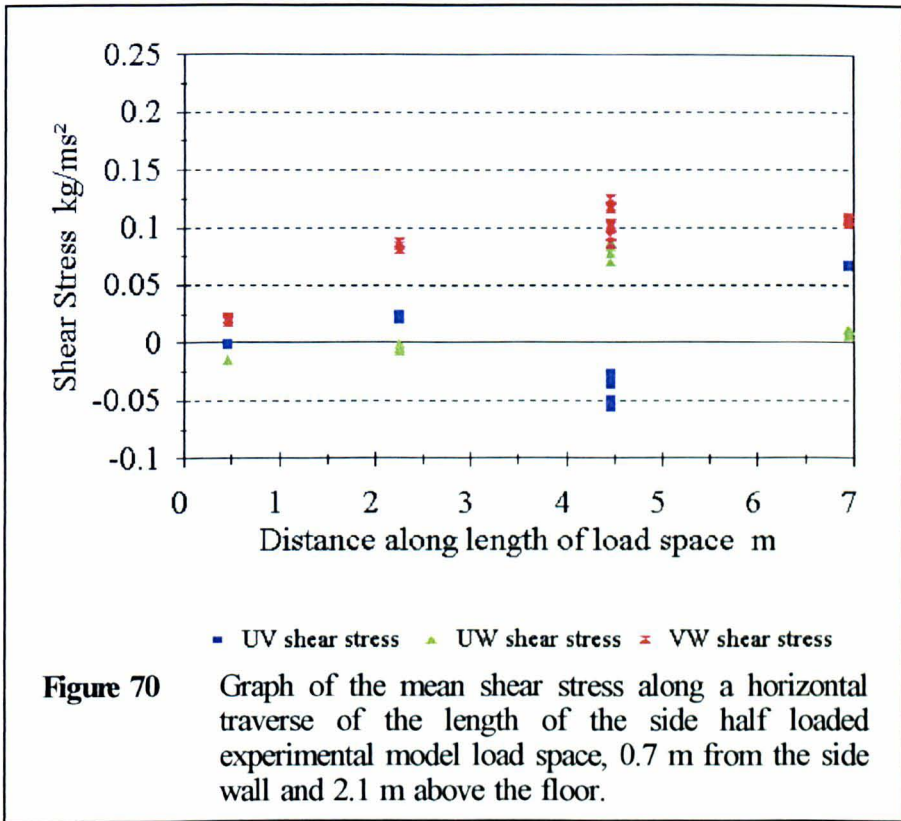


been mentioned as inconsistent with the observed values in the lower of these two spaces. It would be advantageous again in this situation, as in the previous case, to have more detailed information from the experiments about the flow in these confined spaces. Particularly in this case about the flow near the floor and wall, to measure the penetration of the wall jet when restricted by the load. As previously mentioned however a standard ultrasonic anemometer is impractical for this situation.



Mean Shear Stress

Figure 70 again shows the changing experimental shear stress results for a series of the fixed anemometer positions (numbers 3, 6, 9 and 12 shown in figure 17) along the length of the load space. In this case, as with the previous two cases, the UV shear changes little along the length of the load space. The UW component is somewhat different here, since it does not show the same rise between positions 3 and 6, the two locations nearest the front of the load space. Instead this rise occurs further back, suggesting that perhaps the channel between the two rows of the load, which generated the stronger mean velocities seen in figure 64, has moved this feature of the flow toward the rear of the load space. The other difference in this case is



the changed behaviour of the VW component of shear stress. Instead of the simple downward trend seen in the previous cases, there is an almost constant value except for the location nearest the front wall. The source of this change is unclear, but may be due to a flow interaction between the strong recirculation at the front of the load space and the recirculation cells above the load caused by the inlet jets.

4.2.4 Fully loaded case

Mean velocity and Turbulent Kinetic Energy

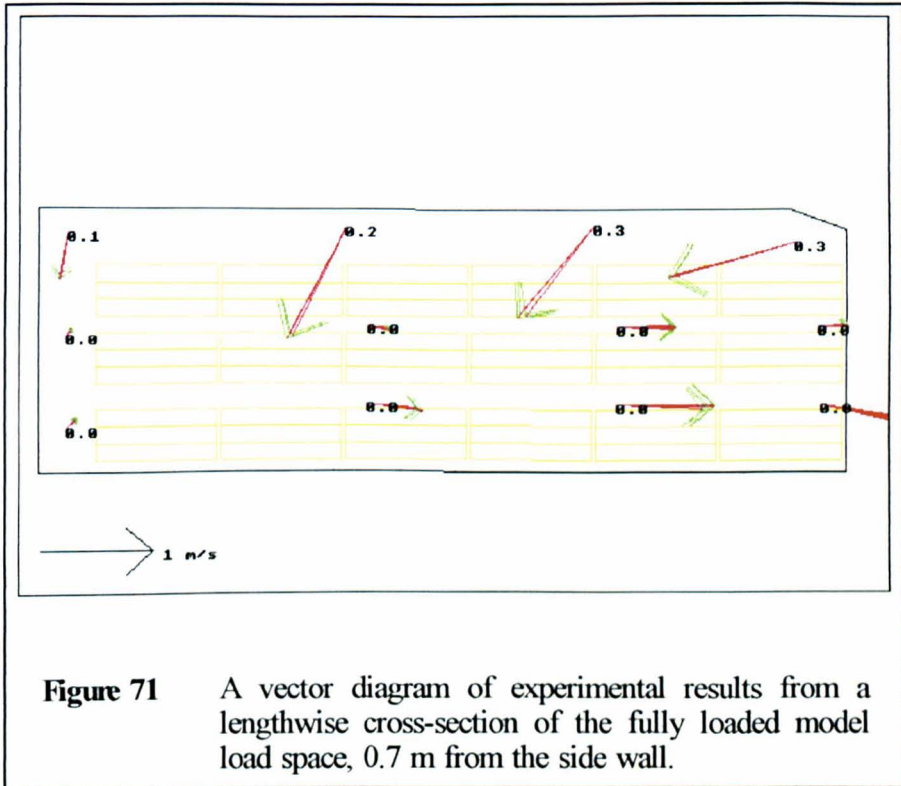
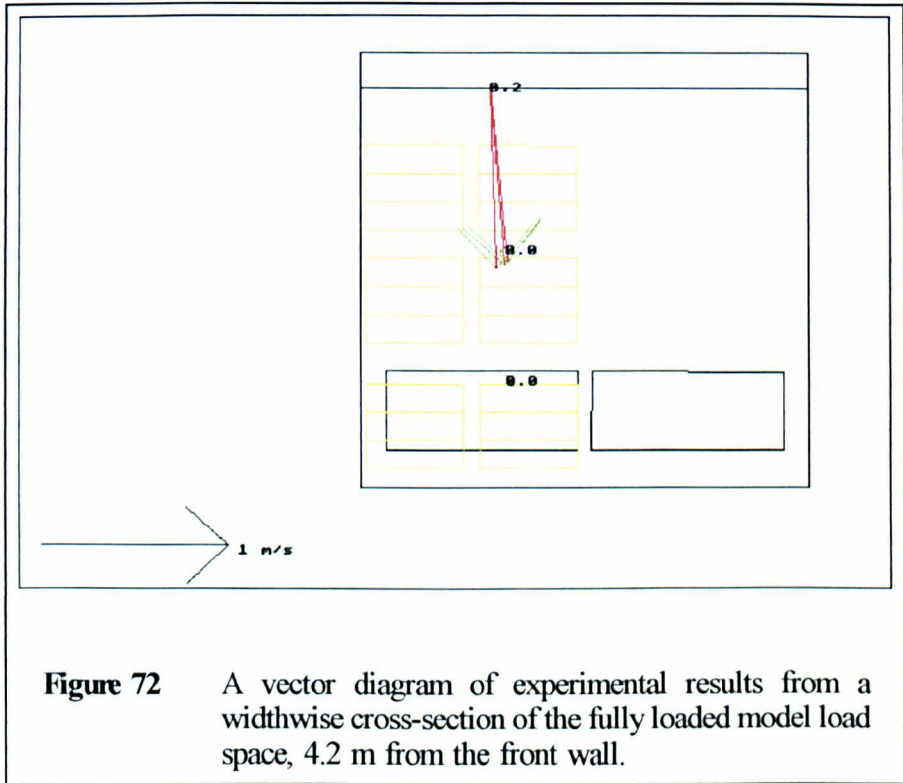


Figure 71 shows the experimental data collected in the fully loaded case from the standard lengthwise cross-section of the load space. The data collected in this case was of a more limited nature than in the previous cases, with fewer points being sampled but more repeats of each run. The flow pattern observed showed the air movement is again from back to front through the majority of the load, with only the jet dominated area above the load flowing from front to rear. Behind the load itself the data suggests a



possible recirculation zone forms before air moves into the load. TKE figures for positions inside the load are again very low because of the restrictions on air movement and eddy size, with values of up to 0.3 J kg^{-1} in the jets above the load. The experimental data for the other standard widthwise cross-section, figure 72, suggests that the presence of the full load has also largely removed the cross flow component between the shelves of chick boxes.

Numerical results for the same cross-sections, from the two simulations using 50% inlet jet speed with the two different loading models (section 3.3.3), are given in figures 73 - 76. These show the correct general

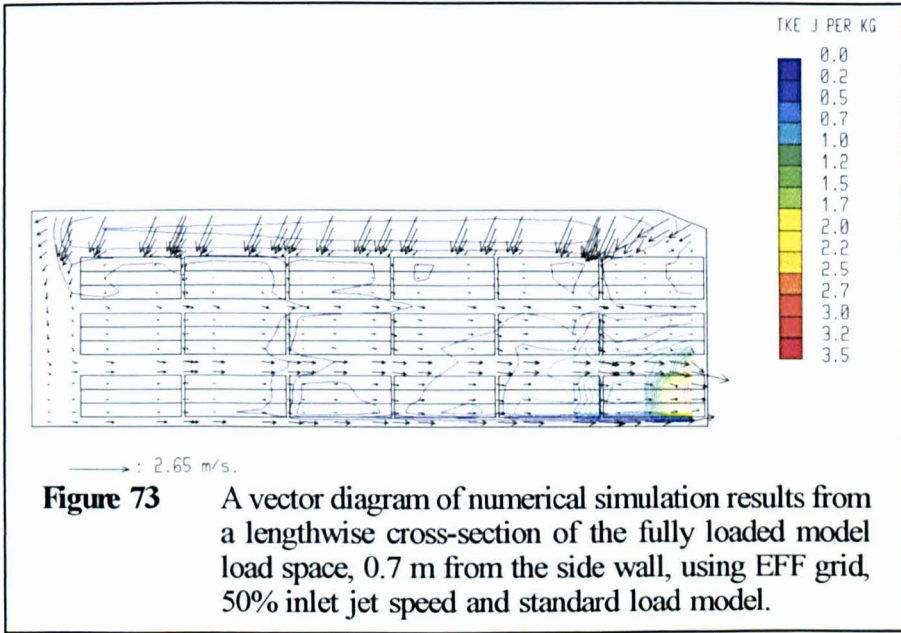


Figure 73 A vector diagram of numerical simulation results from a lengthwise cross-section of the fully loaded model load space, 0.7 m from the side wall, using EFF grid, 50% inlet jet speed and standard load model.

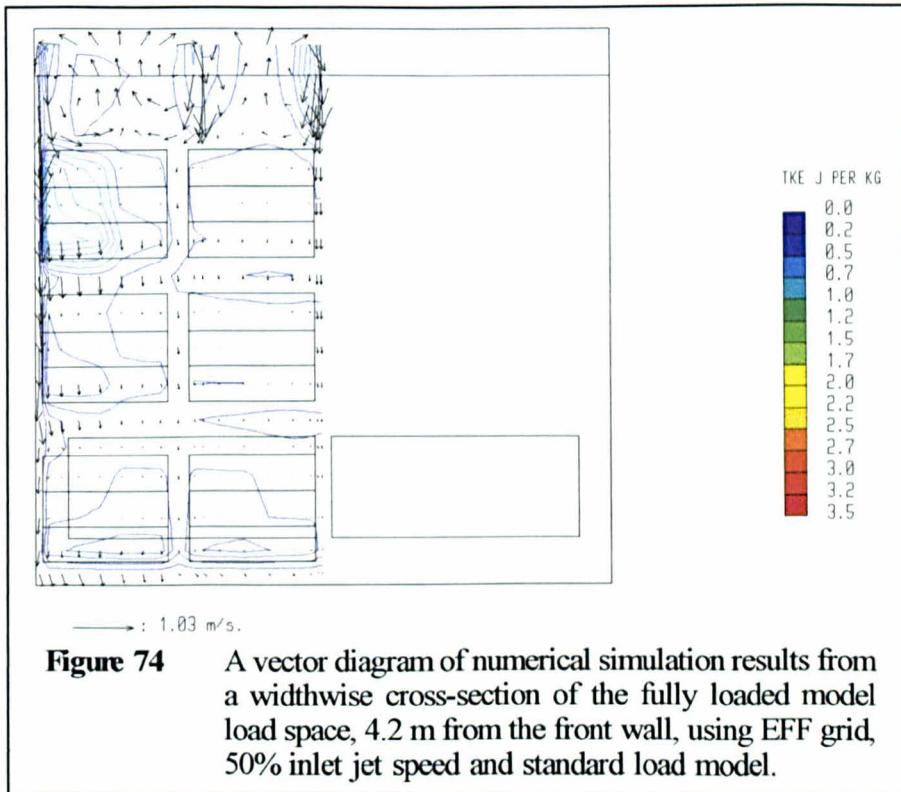
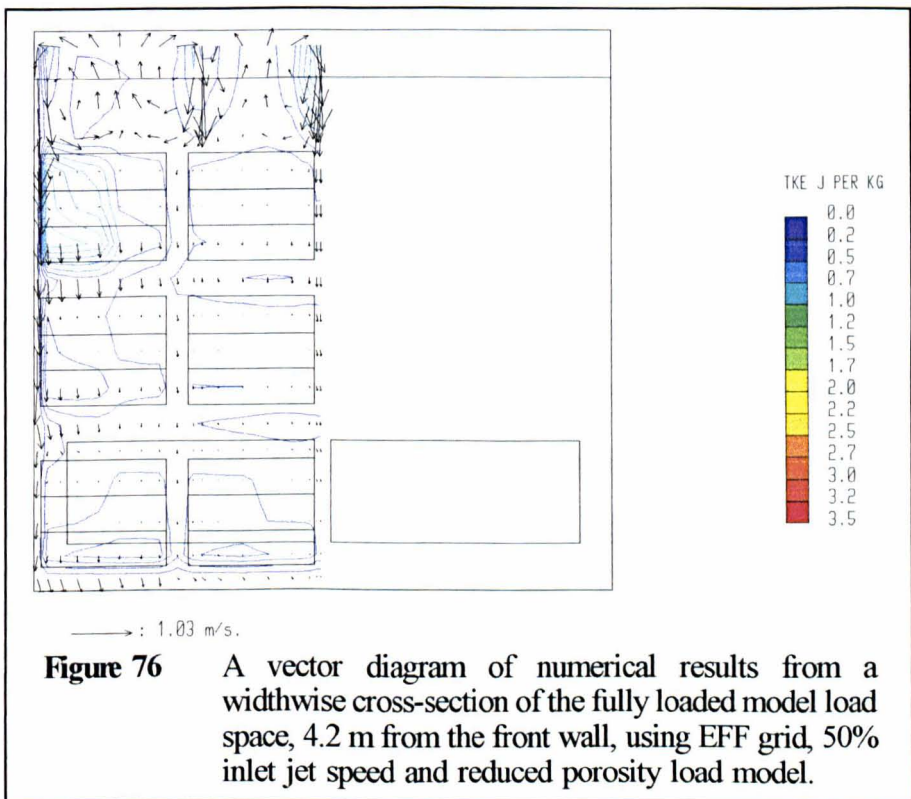
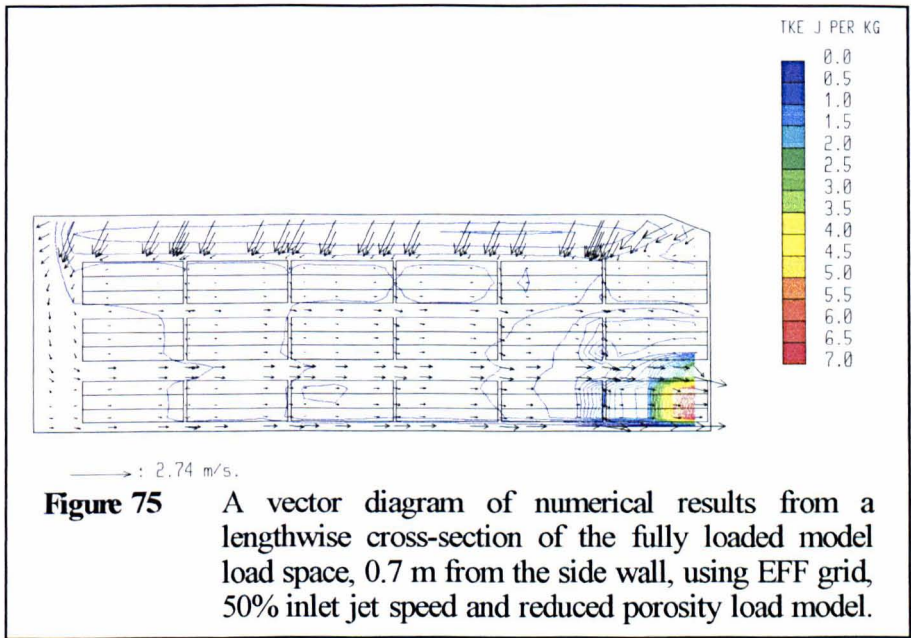


Figure 74 A vector diagram of numerical simulation results from a widthwise cross-section of the fully loaded model load space, 4.2 m from the front wall, using EFF grid, 50% inlet jet speed and standard load model.

flow pattern, although without a significant recirculation behind the load which may be due to insufficient grid resolution. Above the topmost chick



box in the front stack there is a recirculation zone predicted, which is driven by the inlet jets. This demonstrates that the topmost, jet dominated, region

is in this case mostly isolated from the lower flow through the load. Therefore a comparison of the predicted and measured values in this region will be a comparison of the jet boundary condition only. Such a comparison reveals that in the front section of the load space the inlet jet strength is under-predicted by ~25%, but that in the rest of the jets seem to be over-predicted by up to 50%. Also the angle of the inlet jets, taken as a constant in the numerical boundary conditions away from the front angled plate, does seem to change over the length of the load space, with an increasing vertical component toward the rear of the vehicle. This, together with the higher than observed values of TKE in this region, again suggest a lower inlet jet speed and variable jet angle would improve predictions. It must be remembered however, that these results are from 50% inlet jet speed simulations and that a further reduction would need to be justified in terms of the measured jet velocities (section 2.2.3).

The predicted velocities at locations other than above the load also tend to be over-predicted toward the rear of the load space, by up to 50%, and under-predicted toward the front by up to 35%. This is probably a feature of the channelling between layers of the load, and therefore of the loading model itself. Too much air being drawn through the load in the front stacks with an under-prediction of air penetration further back. This suggests a refinement of the load model may be necessary to more accurately model the solid-with-discrete-holes nature of the chick box,

rather than using a bulk porosity model. The differences in the two loading models used here, which concern vertical permeability, do not affect this result significantly, although the vertical flow from the wall jet through the load is effected as in the previous case.

The distribution of TKE is again poorly predicted in the presence of the load because of the artificial generation of TKE by velocity gradients at the load-channel boundaries. This is particularly true in the region of high velocity close to the front vent. Here the maximum TKE values are generated by both load models. In this case the reduced porosity model, which reduces vertical flow, increases the peak TKE prediction because of this artificial generation. Considering the wall jet-load interaction, however, the peak TKE value here is once again reduced by the reduced porosity model.

Mean Shear Stress

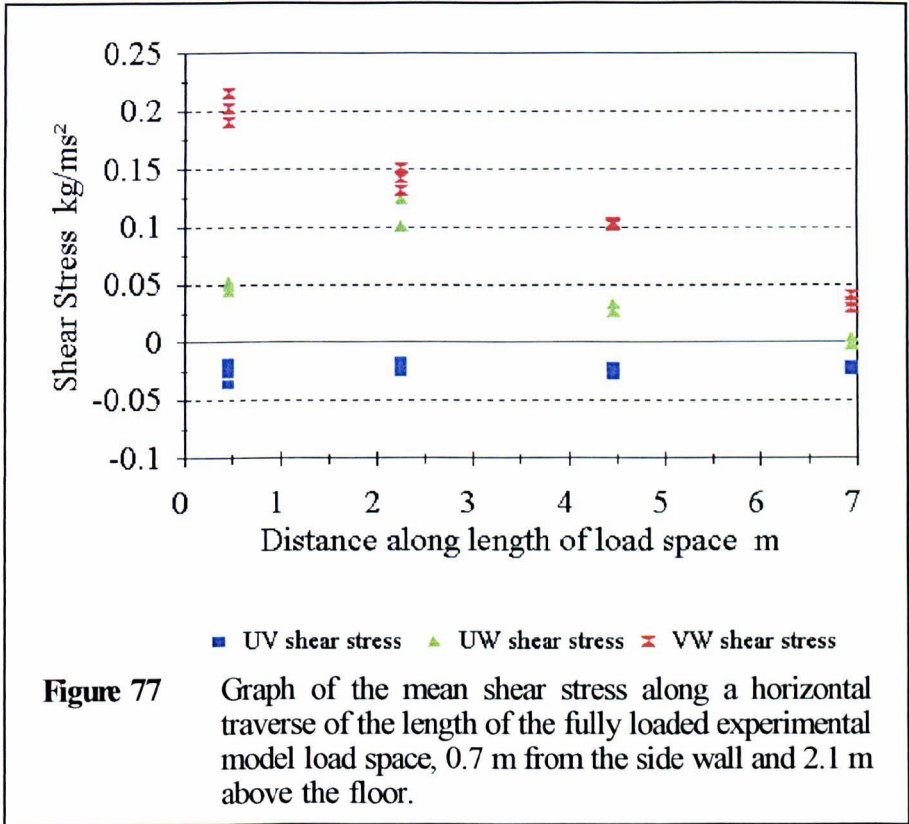


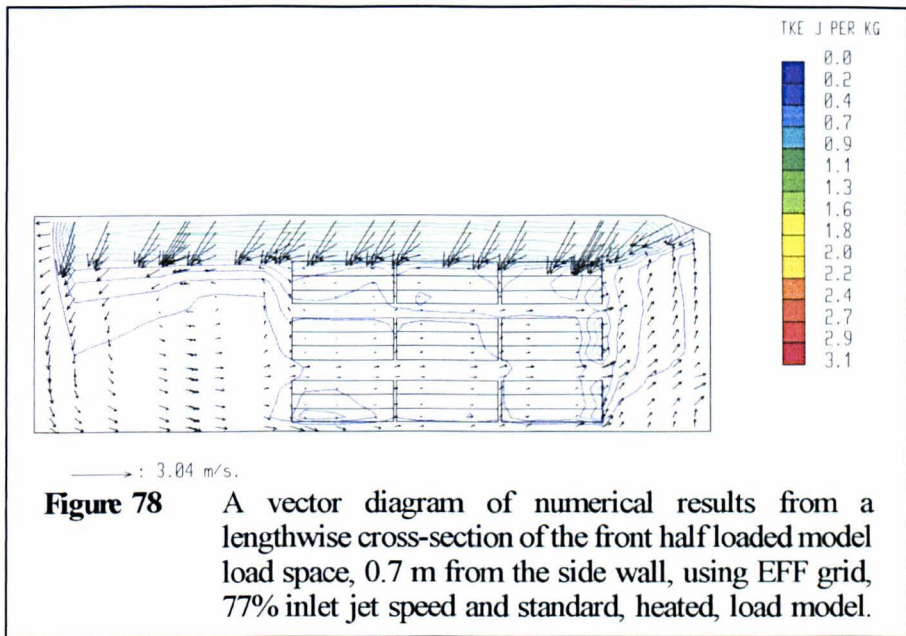
Figure 77 shows the changing experimental shear stress results for the series of the fixed anemometer positions (numbers 3, 6, 9 and 12 shown in figure 17) along the length of the load space. In this case, as with the empty load space case, the UV shear component is constant over the length of the load space, reflecting the proximity of the measuring position to an inlet jet. The UW component changes near the front angled plate where the jet angle is significantly different and the VW component again shows a clear downward trend along the length of the load space.

4.2.5 Non-isothermal numerical results

The results involving non-isothermal simulations cover two loading cases, the front half load and the fully loaded. In these cases there is no experimental data for comparison and therefore a volume flow rate of $\sim 5800 \text{ m}^3\text{hr}^{-1}$ (142 ach) was used, this higher flow rate being equivalent to the recirculation plus two fresh air fans found in the actual vehicle, also the underfloor ducts (see section 3.3.4) were included to allow excess air removal and to investigate the possibility that the ducts act as partial inlets. The heat load model used is given in section 3.3.3 and the inlet jet speed was based on the measured values (section 2.2.3) multiplied by 1.54 to increase the volume flow and reduced in these cases to 50% of the resultant value as in the isothermal cases. Thus values of 77% inlet jet speed which can be seen below which are the result of a 50% reduction of the 154% required to give the correct volume flow rate.

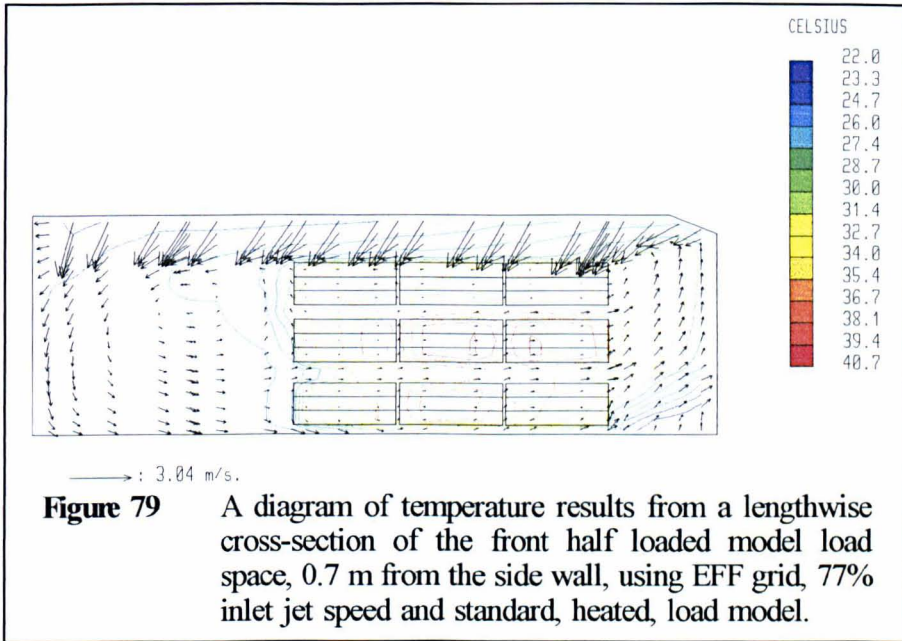
Front half loaded case

Figure 78 shows the results of velocity and TKE for the standard length-wise cross-section of the load space, using the standard load model in the front half loaded configuration and 77% inlet jet speed. In the velocity field the effect of the heat load can be seen in the reduction and change in position of the recirculation zone in front of the load (*c.f.* figure 57) because of the increased vertical movement when heated air exits the



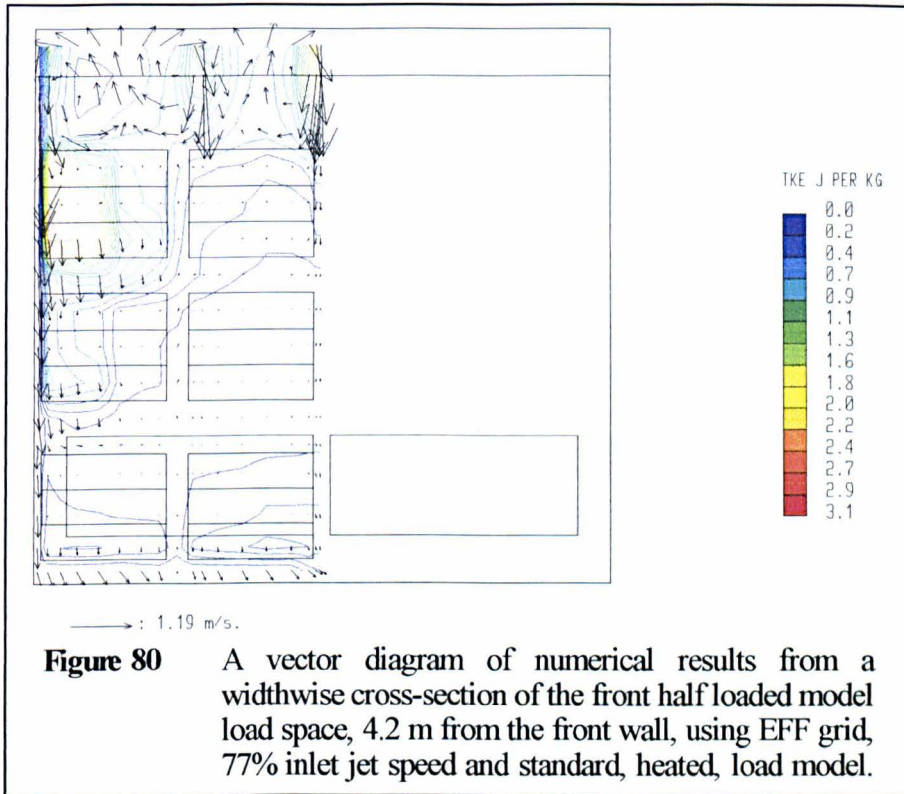
front of the load. This also gives rise to the drawing of air through the front of the floor ducts into the recirculation vent. This can be clearly seen on figure 79 where the velocity vectors are repeated with the contours of temperature at one degree Celsius intervals.

This figure shows the cold air being drawn from the base of the load space into the front vents and the heated air from the load being recirculated inside the load space. The recirculation zone behind the load is also effected by the inclusion of the floor vents, with air leaving the load space behind the load, and the increased flow rate which has increased the air movement in this space. The general pattern of the movement, however, both behind and within the load is unchanged from the isothermal simulations, with only minor variations where the thermal effects overcome small, previously



pressure driven effects, such as around the rear of the top shelf of chick boxes. The turbulence distribution in this simulation is also similar to the isothermal case, with a generally higher level close to the ceiling jets because of the higher flow rate used. The generation of peaks of TKE at the front of the load is again noticeable.

The results for the temperature field firstly illustrate the important role that stacking has on the dissipation of heat from the load and the insulating effect of large blocks of boxes. Also, considering the width-wise cross-section (figure 80), it is apparent that the vertical motion generated by the heat load is minor compared to the flow circulating from back to front through the space, in this case. The predicted levels of temperature amongst the load, however, seem rather high, since temperatures of up to 40°C



would certainly cause severe heat stress in day-old chicks. This suggests that the simple heat load model used here is inadequate to give realistic levels of temperature in this type of environment. However, the distribution of temperature may be reasonable and consideration of the results in terms of enthalpy may be more appropriate (see section 6).

Fully loaded case

In the second non-isothermal example the same heat load model was applied to a fully loaded case, with the same volume flow rate and open floor ducts. The load model used in this second example was the reduced

porosity model and the inlet jet speed was set to 77% of the measured values.

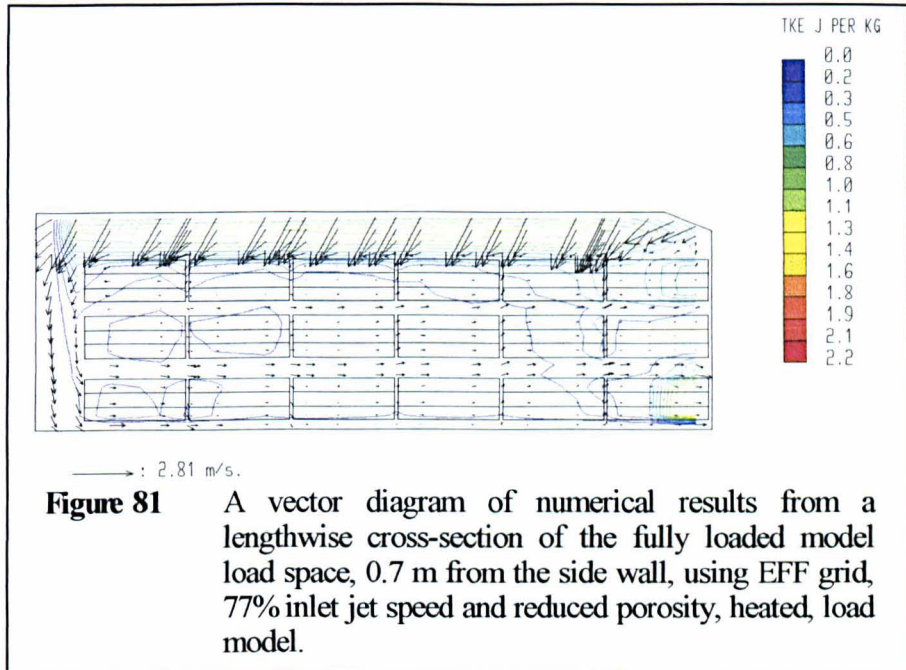
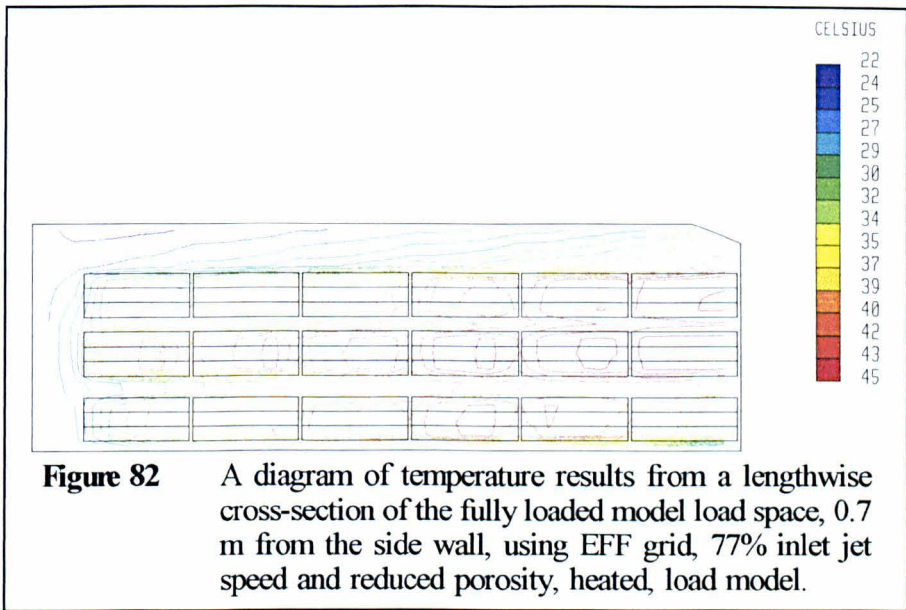
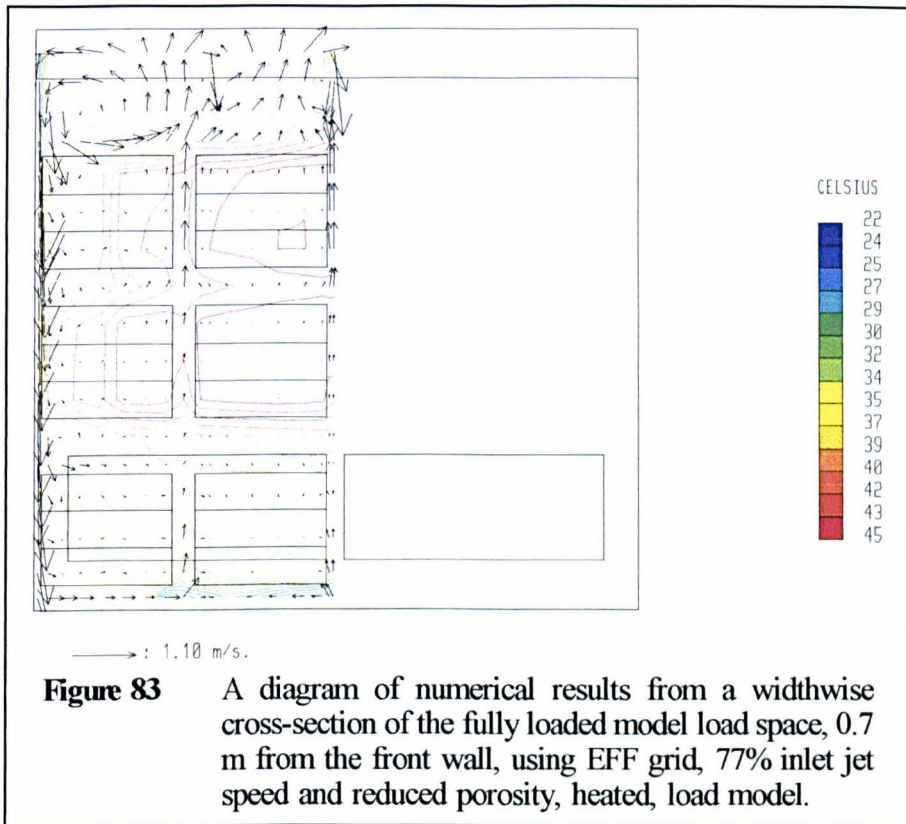


Figure 81 shows the results on the lengthwise cross-section beneath the inlet jet 0.7 m from the side wall. This figure is comparable to figure 75 in the isothermal examples and is clearly similar in the general flow, allowing for the higher flow rate and inlet jet speed. The heat load effects on the velocity field appear small in this case, with only a small general increase in vertical velocity due to buoyancy. There is a significant effect due to the presence of the open floor ducts which, as in the front half loaded case, act as an inlet near the front vents and as an outlet toward the rear of the load space. The effects of this are twofold; firstly the inflow of cool air reduces the temperature in the lowest stacks (figure 82); secondly



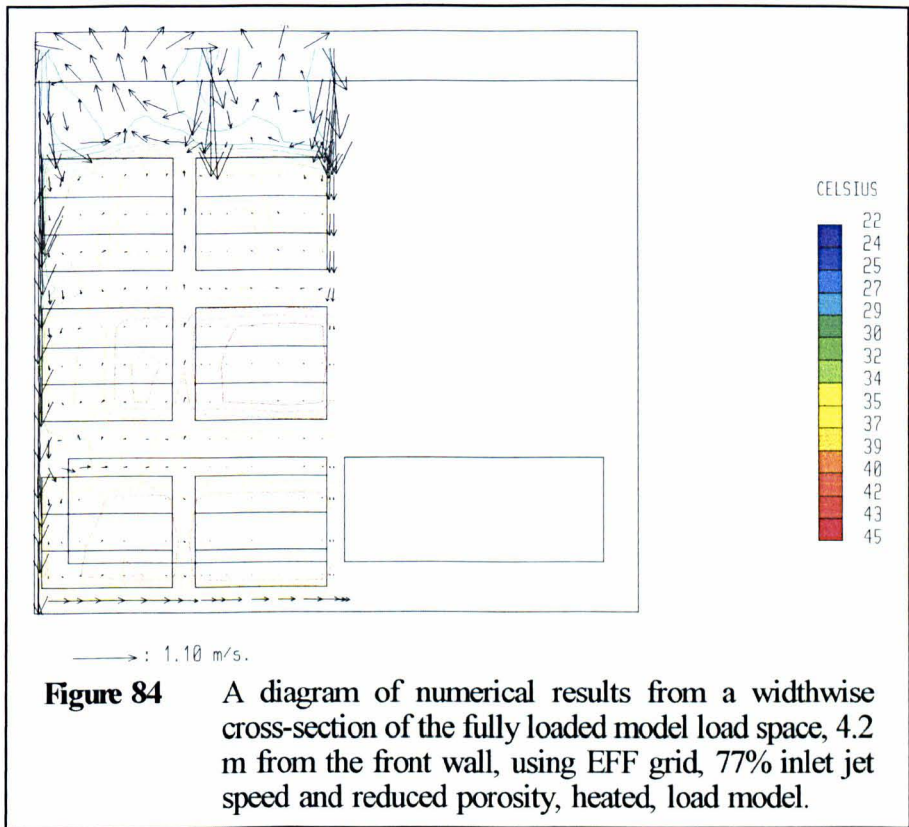
this opening in the floor provides a path of lower resistance for the air from the rear of the vehicle to escape, rather than passing through the load. Therefore the velocities seen within the load in this simulation are lower than the isothermal case despite the higher overall ventilation rate. As a consequence of this the TKE levels are also lower in this simulation than the isothermal case. The temperature predictions given in figure 82 are again of an extremely high level, but a believable distribution. A possible interpretation of these results is given in section 6.

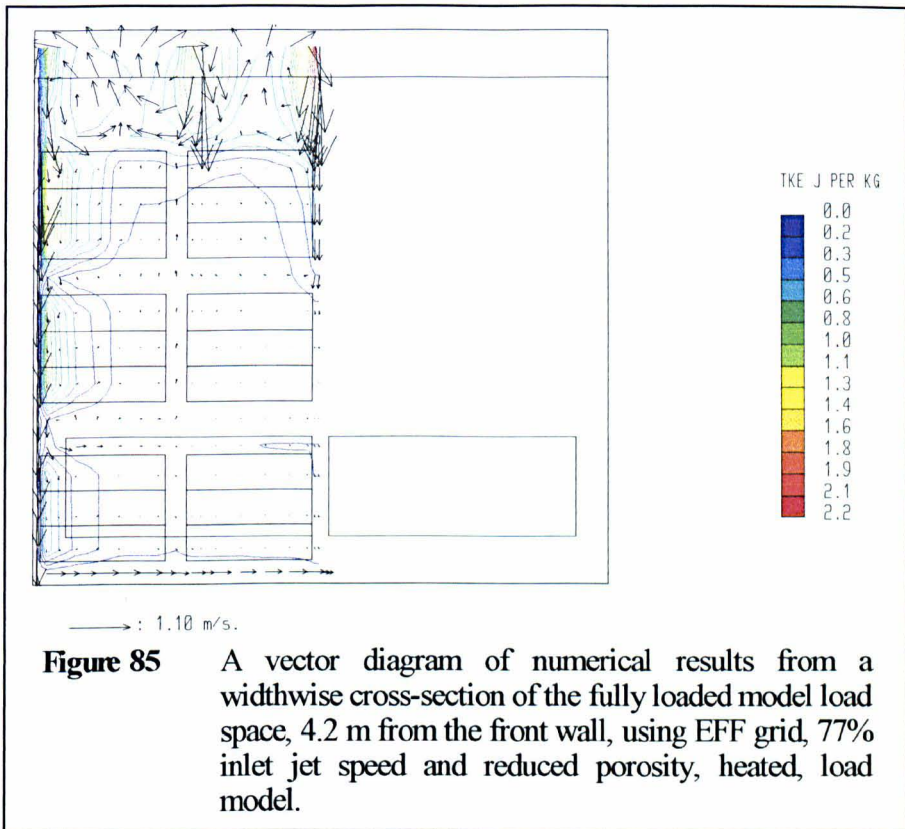
Figure 83 shows the flow and temperature fields on a widthwise cross-section through the front of the first stack of chick boxes next to the front wall of the load space. Visible at the base of this figure is the cooling flow entering through the underfloor vents. This flow, drawn by the low pressure of the front vents, reduces the temperature in this lowest stack of



chick boxes by $\sim 10^{\circ}\text{C}$ compared to the peak temperatures predicted in the stacks above. Between these upper stacks the up-flow is likely to be due to the recirculating flow rather than the buoyancy effects, which can be seen in the widthwise cross-section from the front of the fourth trolley (figure 84).

This cross-section also shows the peak temperature to be in the central stacks with no significant flow through the floor ducts. The turbulence distribution for this cross-section is very similar to the isothermal case and is given in figure 85.





4.2.6 Ventilation rate results

The ventilation rates calculated from the CFD mean velocity fields for the various numerical cases are given in appendix 5. These results are given in the form of a ventilation rate due to the mean flow through the space occupied by a pair of chick boxes stacked side by side on a trolley



Figure 86 A photograph of the arrangement of chick boxes within the model load space.

(see figure 86). This was found to be essentially the same as the value for individual chick boxes due to the orientation of the flow from rear to front

through the load space, and because of the grid structures used along the length of the vehicle, was more easily calculated.

Values are presented for each box pair space as a mean ventilation rate in m^3s^{-1} , calculated as the average of the net inflow and outflow values for the space. The continuity error, which is the difference between the net inflow and outflow values, is given in appendix 5. The sign associated with this error indicates whether the continuity error is positive, implying excess inflow, or negative, implying excess outflow from each box space. For more details see appendix 5.

Empty load space case

For the empty load space case, which indicates the "potential" ventilation rate for the load space with no resistance due to the load, five sets of simulation results were used to calculate ventilation rates. These were:

1. EFF grid with 100% inlet jet speed.
2. EFF grid with 66% inlet jet speed.
3. EFF grid with 50% inlet jet speed.
4. ES grid with 100% inlet jet speed.
5. ES grid with 50% inlet jet speed.

See section 3.4 for further details.

Table V A summary of the predicted ventilation rates for the empty load space case.

| Case Number | Open space ventilation rate m^3s^{-1} | | |
|-------------|---|--------|---------|
| | Minimum | Mean | Maximum |
| 1 | 0.0485 | 0.1866 | 0.3468 |
| 2 | 0.0312 | 0.1452 | 0.2921 |
| 3 | 0.0179 | 0.1105 | 0.2515 |
| 4 | 0.0283 | 0.1788 | 0.3872 |
| 5 | 0.0098 | 0.1040 | 0.2363 |

These simulations gave results which are summarised in table V. Clearly the range of predicted ventilation rates for all these simulations is large. Furthermore there is a significant difference in the values predicted by the two corresponding grid structures, particularly in areas of the flow where the grids are significantly different. This suggests that these predicted values are not completely grid independent, although similar trends and levels are predicted for many areas. For example the maximum ventilation rates, corresponding to the highest velocities, occur near the front vents, and the minimum values tend to occur in the topmost box spaces in the stacks close to the side or front wall. Since the differences in the predicted ventilation rate are particularly apparent close to the front of the load space, where the two grid structures differ most widely, it is also possible that the differences are due to the assumption that the ventilation rate can be calculated by using the mean cell centre velocity components as the

effective ventilation speeds through the appropriate cell faces without interpolation. This may give rise to different ventilation rate results for different grid structures because of the different control volumes over which the numerical calculation occurs.

Front half loaded case

In the front half loaded case, five sets of simulation results were again used for calculating ventilation rates. These were:

1. Standard load model and 100% inlet jet speed.
2. Reduced porosity load model and 100% inlet jet speed.
3. Standard load model and 50% inlet jet speed.
4. Reduced porosity load model and 50% inlet jet speed.
5. Standard load model, 100% inlet jet speed with $5800 \text{ m}^3\text{hr}^{-1}$

volume flow rate, heated load and open underfloor ducts.

See section 3.4 for further details.

The load model used in each CFD simulation was also used to provide the area porosities in the ventilation rate calculation, therefore preserving the effective areas for ventilation in each case. A summary of the results for these cases is given in table VI and it is interesting to note the relative insensitivity of these figures to the various models used compared to the variations within the individual simulations. This is particularly true for the positions of the maximum and minimum ventilation rates, which are

Table VI A summary of the predicted ventilation rates for the front half loaded model case.

| Case Number | Ventilation rate m^3s^{-1} | | | | |
|-------------|--|----------|---------|-----------------|----------------|
| | Box min | Box mean | Box max | Mean open space | Max open space |
| 1 | 0.0007 | 0.0023 | 0.0053 | 0.1481 | 0.3153 |
| 2 | 0.0006 | 0.0023 | 0.0043 | 0.1692 | 0.3900 |
| 3 | 0.0005 | 0.0018 | 0.0036 | 0.0917 | 0.2391 |
| 4 | 0.0007 | 0.0018 | 0.0032 | 0.0986 | 0.2799 |
| 5 | 0.0007 | 0.0020 | 0.0045 | 0.1694 | 0.3390 |

identical except in the heated model case.

The distribution of values throughout the load space is similar in each of the isothermal cases with above average ventilation rates in the topmost boxes of the lower two shelves and for the stacks nearest the front vents. The latter includes the maximum ventilation rate in each of the isothermal cases. The lowest ventilation rates tend to occur in boxes within the body of the stacks or on the topmost shelf, except in the non-isothermal case where the buoyancy tends to increase the ventilation rate for exposed boxes on the top shelf.

Side half loaded case

For the side half loaded case the ventilation rates were evaluated for two simulations, with the standard and reduced porosity load models respectively, both having 50% inlet jet speed. Summarised results for these

Table VII A summary of the predicted ventilation rates for the side half loaded model case.

| Case Number | Ventilation rate m^3s^{-1} | | | | |
|-------------|--|----------|---------|-----------------|----------------|
| | Box min | Box mean | Box max | Mean open space | Max open space |
| 1 | 0.0005 | 0.0017 | 0.0045 | 0.0683 | 0.1392 |
| 2 | 0.0003 | 0.0014 | 0.0030 | 0.0661 | 0.1424 |

two cases are given in table VII. As with the front half loaded case the variation between the loading models is small compared to the differences within each set, although generally the box ventilation rates in this configuration are slightly lower than for the previous case. This is probably due to the tendency of the air to bypass the boxes through the open channel in the centre of the load space, however in a non-isothermal case the extra exposed surface area of the box sides might improve the ventilation due to buoyancy.

Fully loaded case

The fully loaded simulations used to calculate ventilation rate were:

1. Standard load model with 50% inlet jet speed.
 2. Reduced porosity load model with 100% inlet jet speed.
 3. Reduced porosity load model with 50% inlet jet speed.
 4. Standard load model, 100% inlet jet speed with 5800 m³hr⁻¹ volume flow rate, heated load and open underfloor ducts.
 5. Reduced porosity load model, 100% inlet jet speed with 5800 m³hr⁻¹ volume flow rate, heated load and open underfloor ducts.
- See section 3.4 for more details.

Table VIII A summary of the predicted ventilation rates for the fully loaded model case.

| Case Number | Box ventilation rate m ³ s ⁻¹ | | |
|-------------|---|--------|---------|
| | Minimum | Mean | Maximum |
| 1 | 0.0004 | 0.0020 | 0.0066 |
| 2 | 0.0006 | 0.0021 | 0.0068 |
| 3 | 0.0004 | 0.0019 | 0.0070 |
| 4 | 0.0005 | 0.0021 | 0.0084 |
| 5 | 0.0003 | 0.0018 | 0.0085 |

Results for the ventilation rate calculation are summarised in table VIII. Variation between simulations in this case is again small with large variations of predicted values within the load. In both the isothermal and non-isothermal cases the boxes at the top of stacks tend to receive higher ventilation rates, with in the non-isothermal case above average ventilation

of boxes close to the front vents. The lowest ventilation rates again occur in the body of the stacks, especially on the top shelf. In the non-isothermal case the distribution pattern changes somewhat, with the maximum ventilation achieved among the topmost boxes at the rear of the vehicle. This is probably due to the presence of the open floor ducts rather than the heat load because this reduces the effect of the low pressure area from the front vents, reducing velocities in this region and therefore ventilation rate. The buoyancy effect does improve the ventilation rate for the exposed boxes on the top shelf.

4.3 Correlation and Spectral analysis results

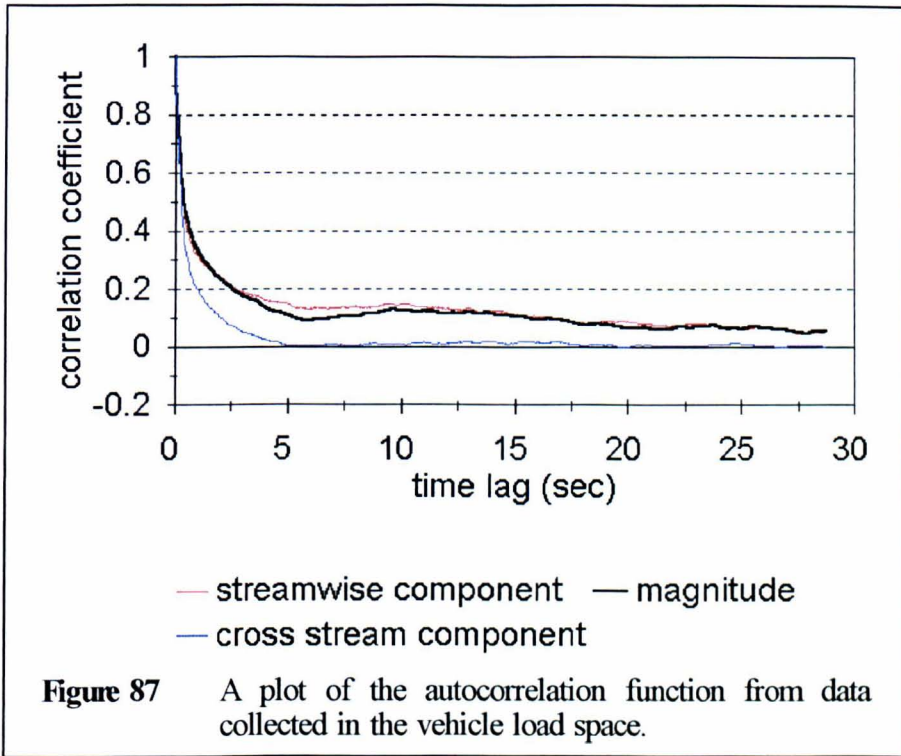
In this section the results are divided into sub-sections grouping the results by analysis method. Within each sub-section the different loading configurations are discussed in turn.

4.3.1 Autocorrelation results

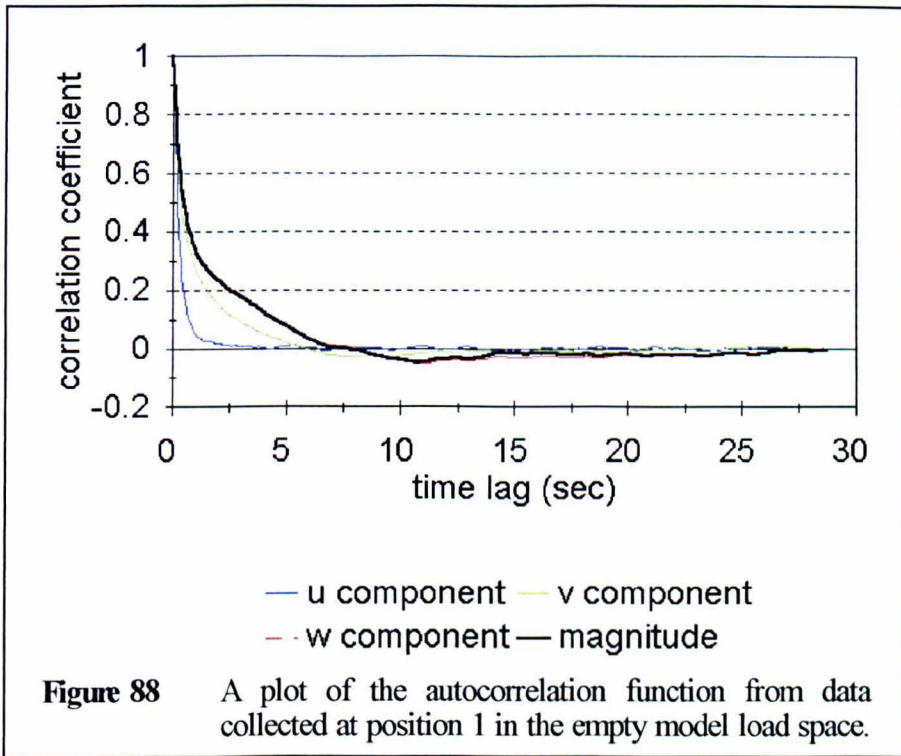
The autocorrelation function (see section 2.1.2) shows the correlation coefficient of time series with itself when a delay or time lag is introduced. It can be thought of as a measure of how predictable the time series is at points in the future, given previous data. Alternatively it can provide a measure of the energy containing eddy size in terms of the length scale. An estimate of the autocorrelation function can be calculated from any time series, however the statistical noise associated with such an estimate may reduce its usefulness. Therefore in this section the mean of a number of estimates, from a number of repeated runs, is presented where possible. This gives a smoothed estimate of the function from which more accurate information can be taken.

Empty load space case

A series of five 28.8 minute measurements from the actual vehicle modelled in this project were obtained, using the ultrasonic anemometer, at



a position directly upstream from the front vents. The autocorrelation function for this data can be seen in figure 87. This shows how the streamwise component, and therefore in this case also the magnitude, has a lengthy time period over which the time series correlates to some degree. This suggests that the flow is stable, though turbulent, since there is a decay in the correlation. In the cross-stream component correlation is only present with time lags of <5 seconds, which suggests turbulent fluctuations only in these directions. These values correspond to integral length scales of ~0.6 m for the cross-stream components and ~2.2 m for the streamwise component and magnitude, using the local mean velocity as the scaling value.



The autocorrelation function for the nearest equivalent position in the experimental model, position 1 on figure 17, is given in figure 88, using the standard coordinate system (figure 34) to label the components of velocity. Here the cross-stream component, the average of the u and v components, is very similar to that seen in the vehicle data. The streamwise component and magnitude, however, though again closely related, lose all correlation more quickly than in the vehicle data. This suggests that the flow in the model is less stable or more turbulent than the vehicle. This is also reflected in the integral length scales for this position which are ~0.4 m cross-stream and ~0.8 m for the magnitude. The reasons for this are unclear, although it may be due to the different materials/construction used in the model

vehicle, or the multiple fan arrangement used in place of the single vehicle recirculating fan, the latter of which seems the more likely.

The autocorrelation functions calculated from data for other positions within the empty model load space gave generally similar results to figure 88 and are therefore not given here. The integral length scales derived from these functions are summarised in table IX which also contains the equivalent data for the other loading cases.

Table IX Integral length scale summary

| | Velocity component | | | |
|---|--------------------|-------|-------|-----------|
| | u | v | w | magnitude |
| Vehicle data | | | | |
| Mean | 0.4 m | 0.7 m | 2.2 m | 2.2 m |
| Empty model load space (position 1) | | | | |
| Mean | 0.3 m | 0.6 m | 0.7 m | 0.8 m |
| Empty model load space (all positions) | | | | |
| Mean | 0.4 m | 0.5 m | 0.6 m | 0.6 m |
| SD | 0.3 m | 0.4 m | 0.5 m | 0.5 m |
| Maximum | 1.6 m | 2.2 m | 3.3 m | 3.4 m |
| Front half loaded model load space (all positions) | | | | |
| Mean | 0.2 m | 0.2 m | 0.2 m | 0.2 m |
| SD | 0.2 m | 0.2 m | 0.2 m | 0.2 m |
| Maximum | 2.0 m | 1.0 m | 1.1 m | 1.2 m |
| Side half loaded model load space (all positions) | | | | |
| Mean | 0.2 m | 0.2 m | 0.2 m | 0.3 m |
| SD | 0.2 m | 0.2 m | 0.2 m | 0.2 m |
| Maximum | 0.9 m | 0.8 m | 1.1 m | 0.9 m |
| Fully loaded model load space (all positions) | | | | |
| Mean | 0.3 m | 0.2 m | 0.4 m | 0.4 m |
| SD | 0.2 m | 0.2 m | 0.2 m | 0.2 m |
| Maximum | 1.1 m | 0.8 m | 0.9 m | 1.0 m |

SD = standard deviation of mean

Position 1 refers to figure 17

All positions means all data collected for the loading case

Front half loaded case

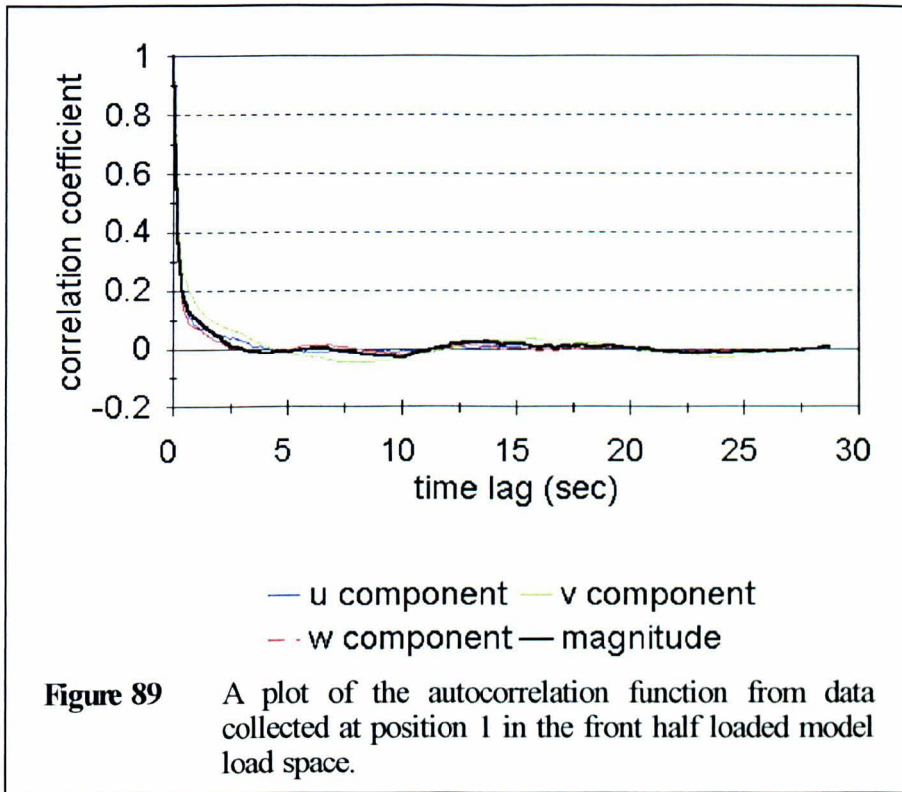
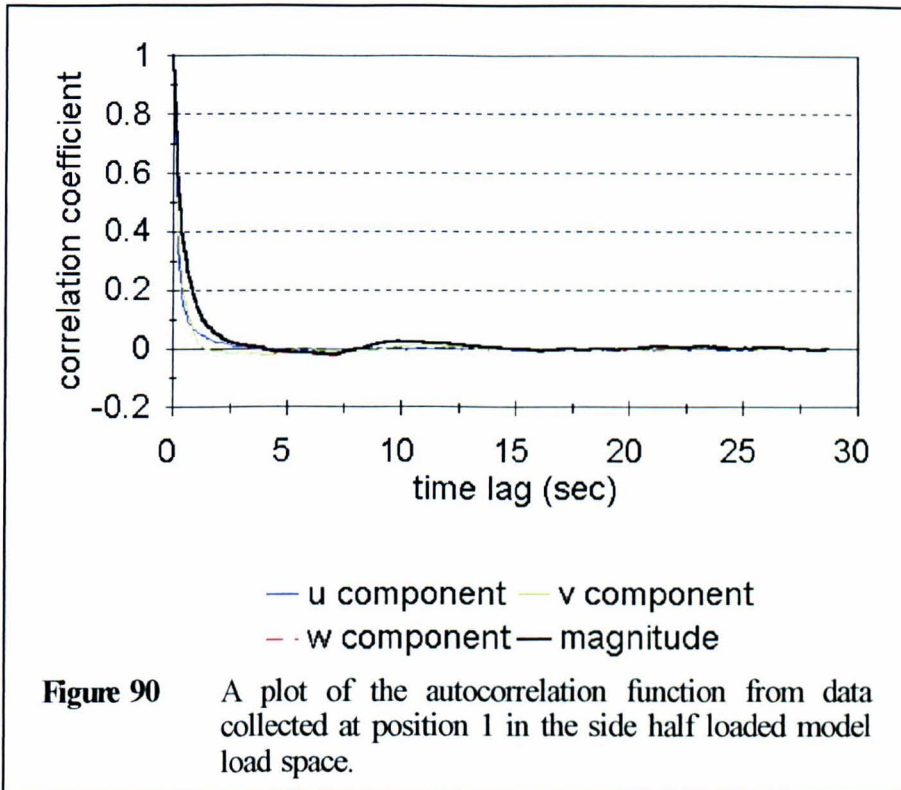


Figure 89 shows the autocorrelation function for position 1 (of figure 17) in the front half loaded model vehicle. This may be compared with figure 88 and indicates that the presence of the load significantly reduces the autocorrelation of the flow, destroying any larger scale structures. This is again representative of the results from throughout the load space and is reflected in the reduced integral length scales given in table IX.

Side half loaded case

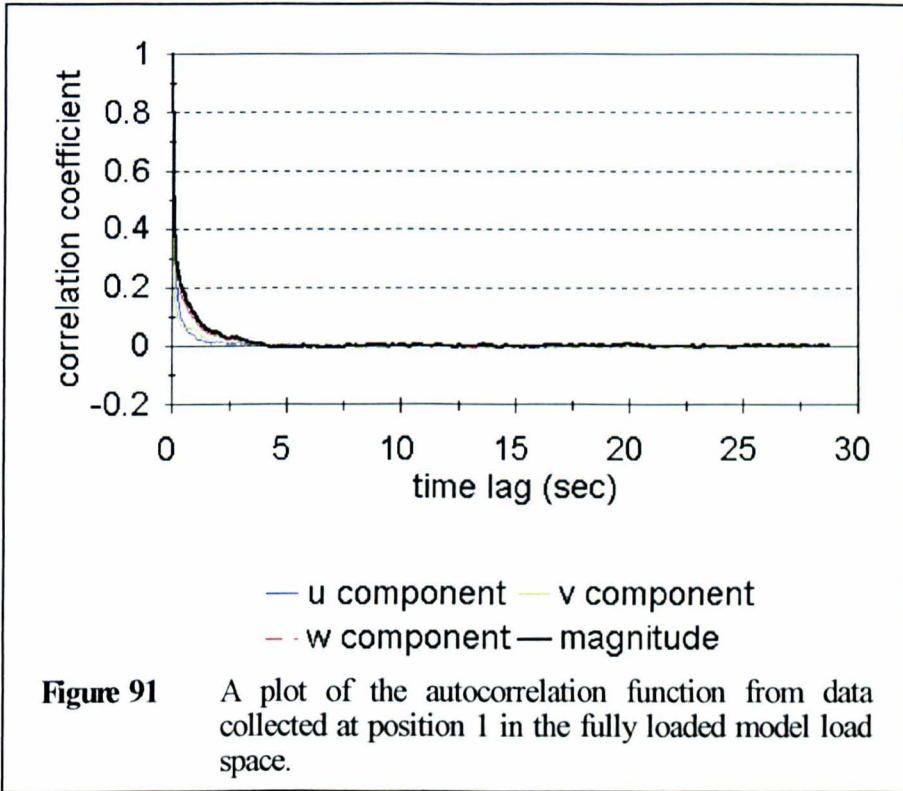
Figure 90 again shows the autocorrelation function for position 1, in this case for the side half loaded model. Comparison with the empty load



space case again indicates the presence of the load reduces the size of the turbulent structures within the flow. The one difference from the front half loaded case, however, is the smaller peak value of integral length scale seen in table IX. This suggests the scale of the u component fluctuations is being suppressed by the narrowing of the load space because of the presence of the load, where in the previous case the greater width of the open spaces allowed larger scale eddies. Similar autocorrelation functions are found throughout this load case.

Fully loaded case

Amongst the full load of empty chick boxes the size of turbulent



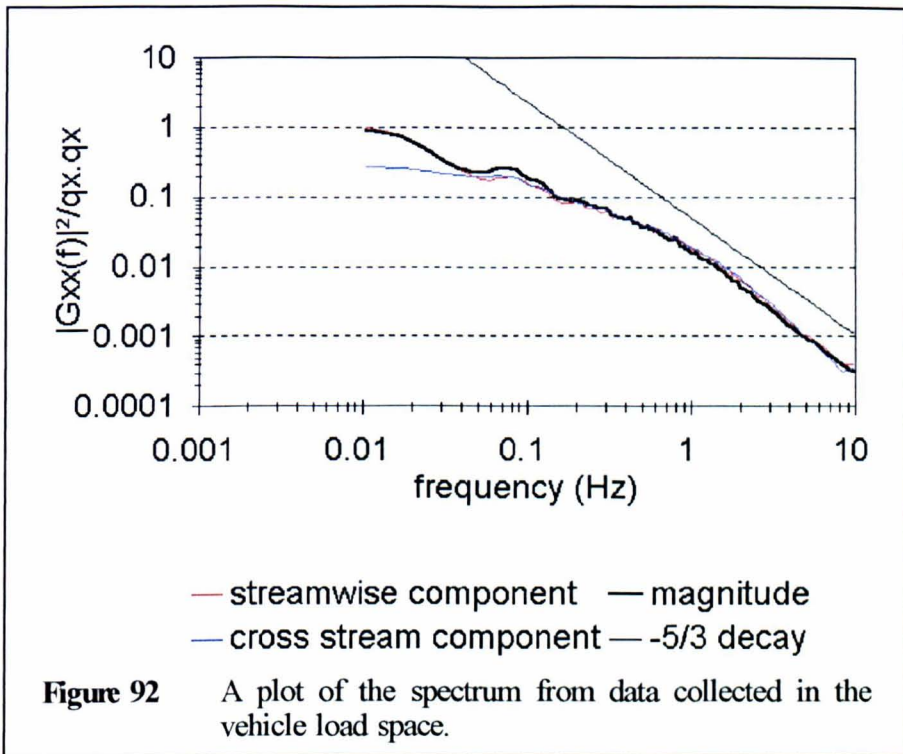
eddies will clearly be very constrained and this is reflected in the autocorrelation function for position 1 in this case (figure 91). Other positions throughout the load gave very similar results, as reflected by the integral length scale values given in table IX, even in the small open rear section of the load space.

4.3.2 Spectral analysis results

The autocorrelation function presents the data on the fluctuating component of the flow in the time domain, but it is useful to re-plot this same data in the frequency domain in order to assess the turbulent processes occurring in the flow. Therefore in this section the results for the spectrum and non-dimensional spectra are presented. Results are again smoothed by taking the average over repeated runs where possible and are normalised by the local mean magnitude of velocity or products thereof as appropriate (see section 2.1.2).

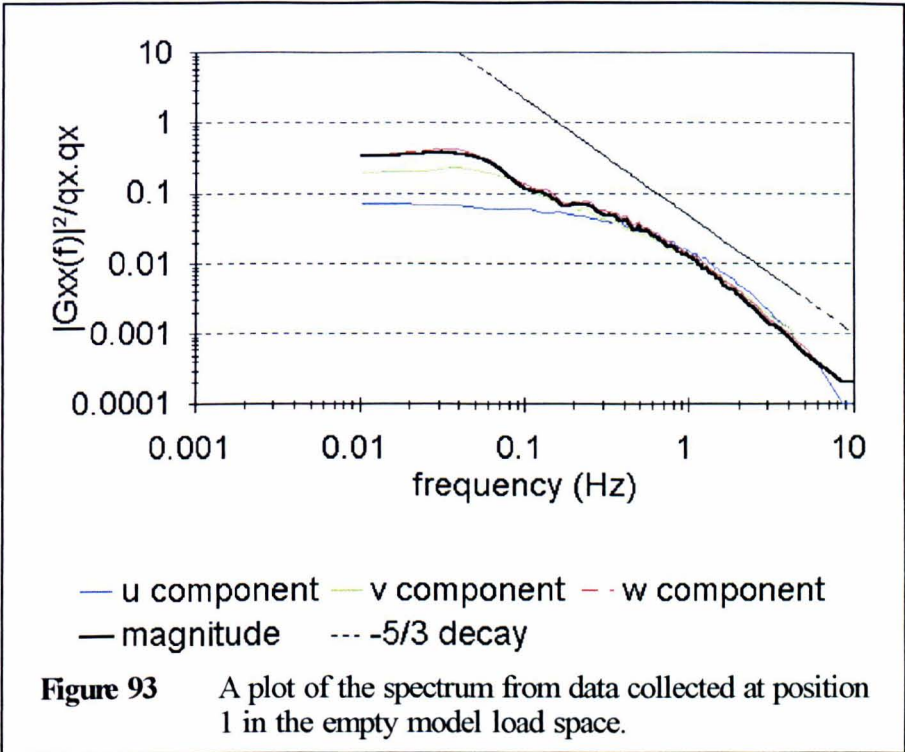
Empty load space case

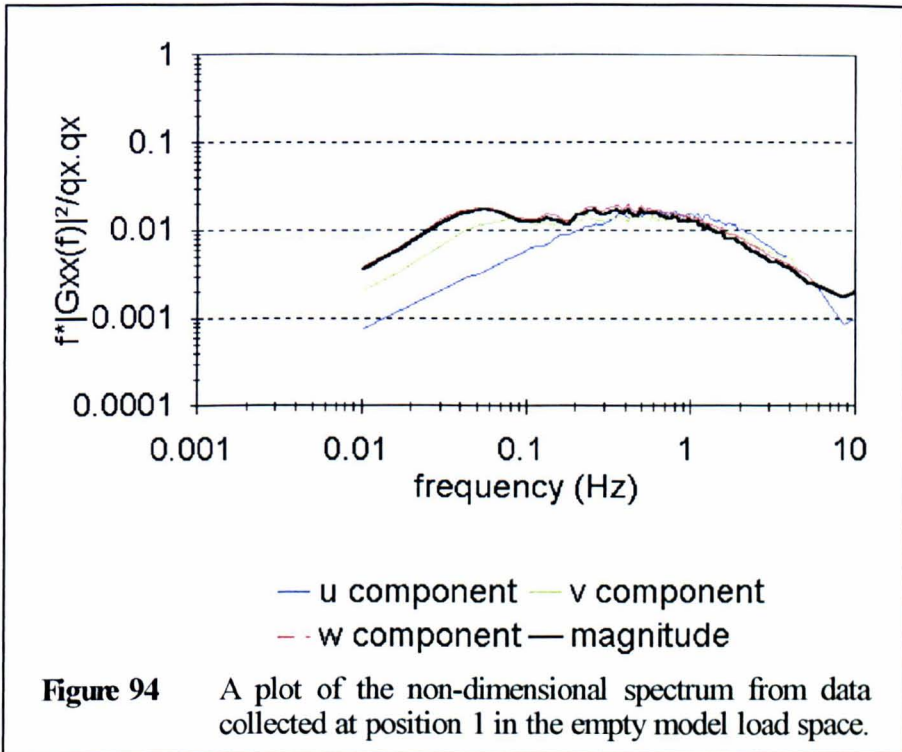
The data collected from the actual vehicle, analyzed in the frequency domain, gives rise to the spectrum seen in figure 92. This compares to the equivalent position 1 spectrum from the model load space given in figure 93. This suggests that the turbulent spectrum of the air flow in this situation has no particularly prominent features. This type of curve is typical of general turbulent flow, with an energy containing low frequency range which decays to higher frequency eddies in a cascade normally described as a $-5/3$ power law, called the inertial subrange, before dissipation. Although the results are presented here with a range of up to 10 Hz it must be remembered that the ultrasonic anemometers response at higher frequencies is not as accurate. In practice the upper limit for this instrument



in these low Reynolds number flows is 1-2 Hz and these results must be considered accordingly.

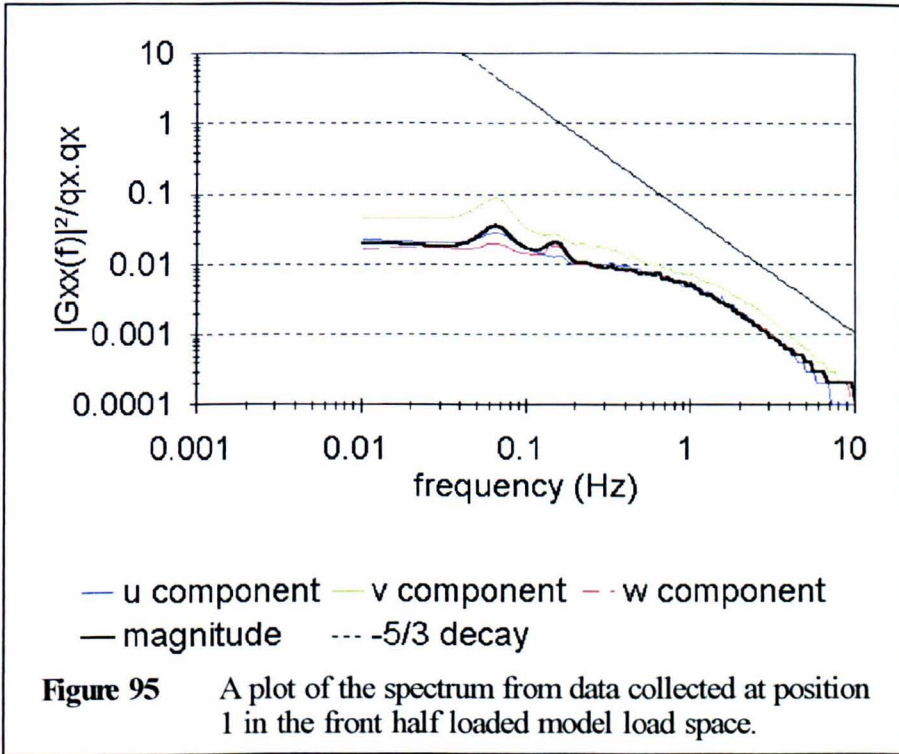
These figures suggest that the energy containing eddies have frequencies <0.3 Hz and that above this there is a normal $-5/3$ power law decay of turbulence. This is reflected in the non-dimensional spectrum (figure 94) for the empty model case given above, as is the conclusion that there are no prominent or dominant frequencies present in the turbulence. These conclusions are representative of the results from throughout the load space in this case.





Front half loaded case

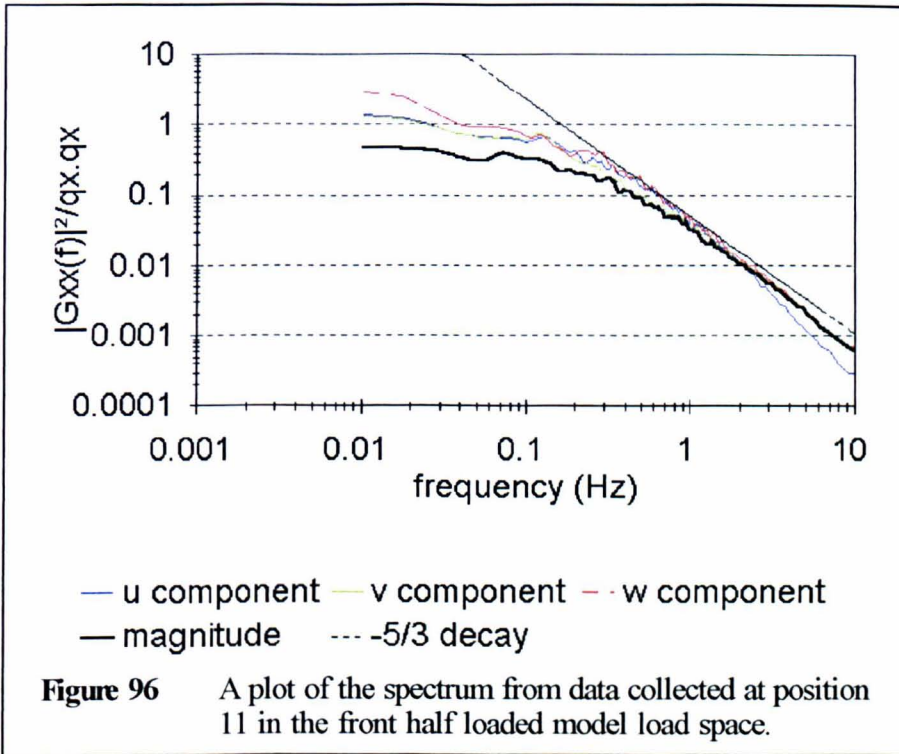
The spectrum from position 1 with the front half loaded configuration (figure 95) shows a generally flattened profile compared to the empty load space case (figure 93). This indicates that the presence of the load has increased the energy containing frequency range because of the restraints on eddy size. Two peaks have also arisen at ~0.065 Hz and ~0.15 Hz which would appear to be related to the v-component and w-component respectively. This would suggest that they are features of the recirculating zone associated with the open space at the front of the load in this configuration.



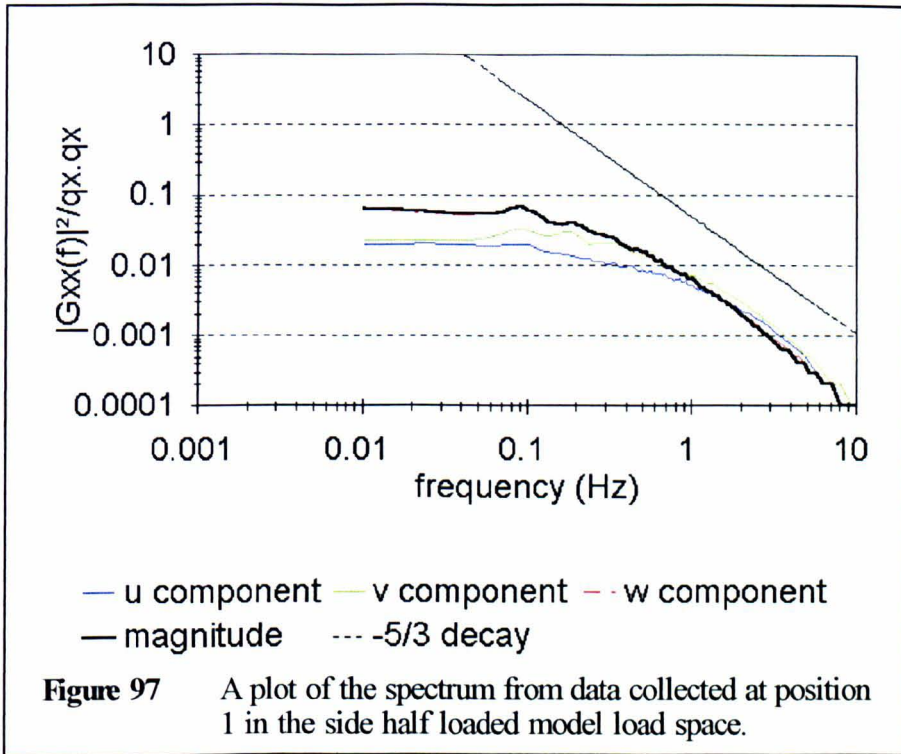
The suppression of the lower frequencies is less apparent in figure 96, which is the spectrum from position 11 in the rear, open, part of the load space. This shows the same low frequency energy containing range and inertial subrange as the empty case, again suggesting that the flattening of the spectrum is due to the presence of the load.

Side half loaded case

Figure 97 show the spectrum for position 1 of the side half loaded configuration. This shows some of the spectral flattening seen in the previous case, although not to the same extent. No noticeable peaks occur here, but one interesting feature is the difference in the shape of the spectra for the cross-stream components, that is the u and v components, as

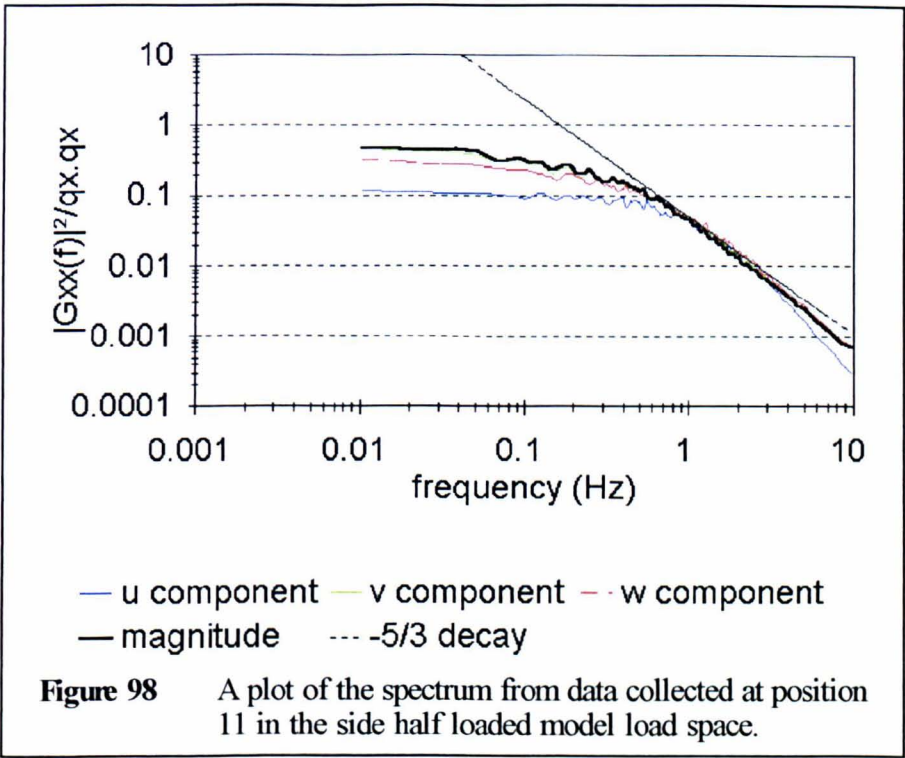


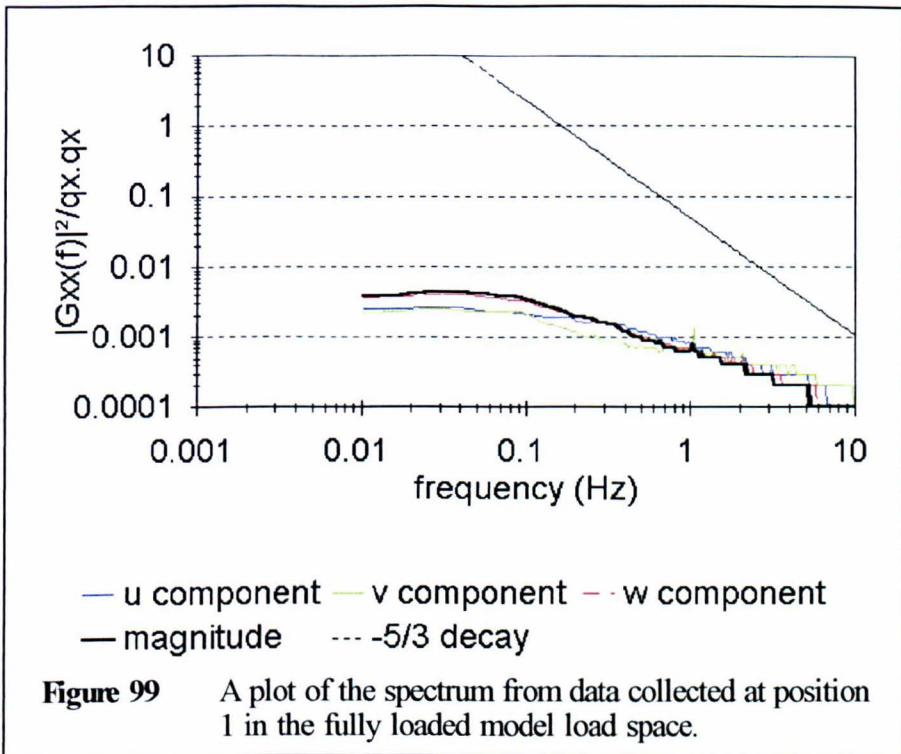
compared with the streamwise component. This may again suggest that the narrowing of the channel between the walls caused by the presence of the load is suppressing the large scale cross-stream component eddies and forcing energy into the higher frequencies. This effect can be seen throughout the load space, for example the spectrum from position 11 (figure 98) has some flattening of the u-component. One would not expect the same flattening in the other components in this case because of the different direction of the mean flow, which contains both v and w components.

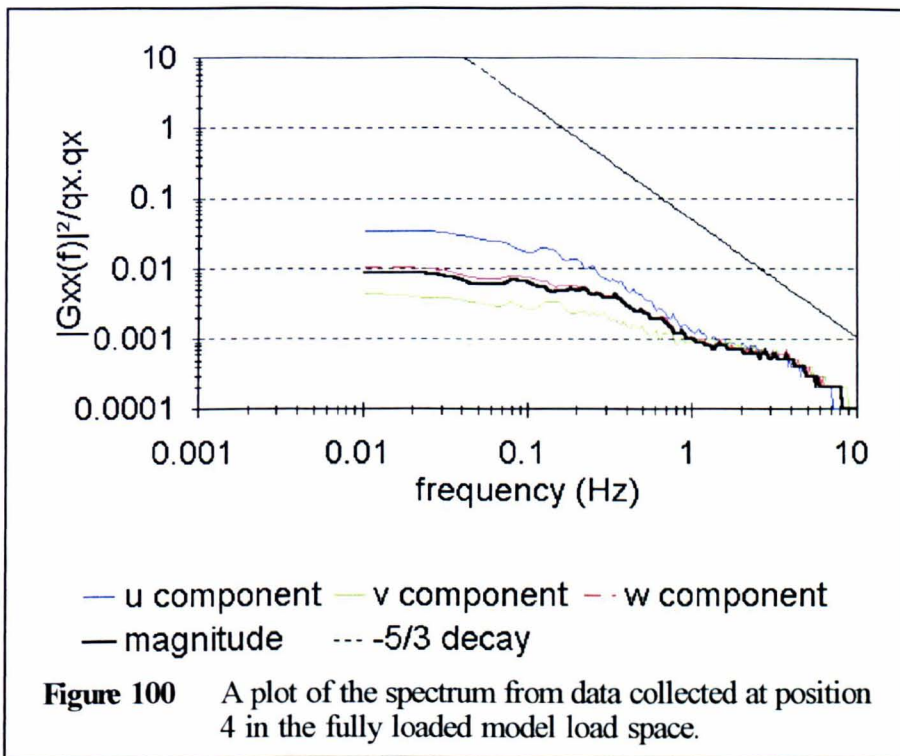


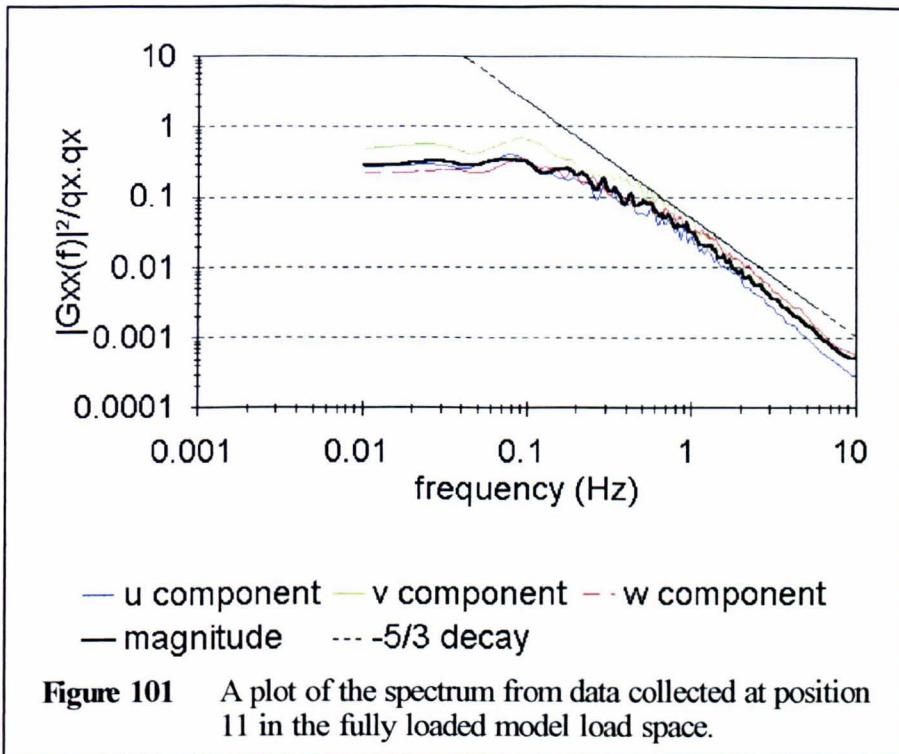
Fully loaded case

In this case, as can be seen from the spectrum of position 1 (figure 99), the turbulence levels in the confined spaces of a fully loaded vehicle are much reduced. Again one may note the separation of the spectra for the individual component at low frequencies. This can be seen most clearly in the spectrum for position 4 (figure 100) where the vertical, v-component, is particularly reduced and the cross-stream, u-component is increased. This corresponds to the restricted room vertically between the shelves compared to the open width of the space. This effect becomes less noticeable toward the rear of the load space, and in the open space behind the load a spectrum approaching that seen in the empty case is recovered (figure 101 from position 11).







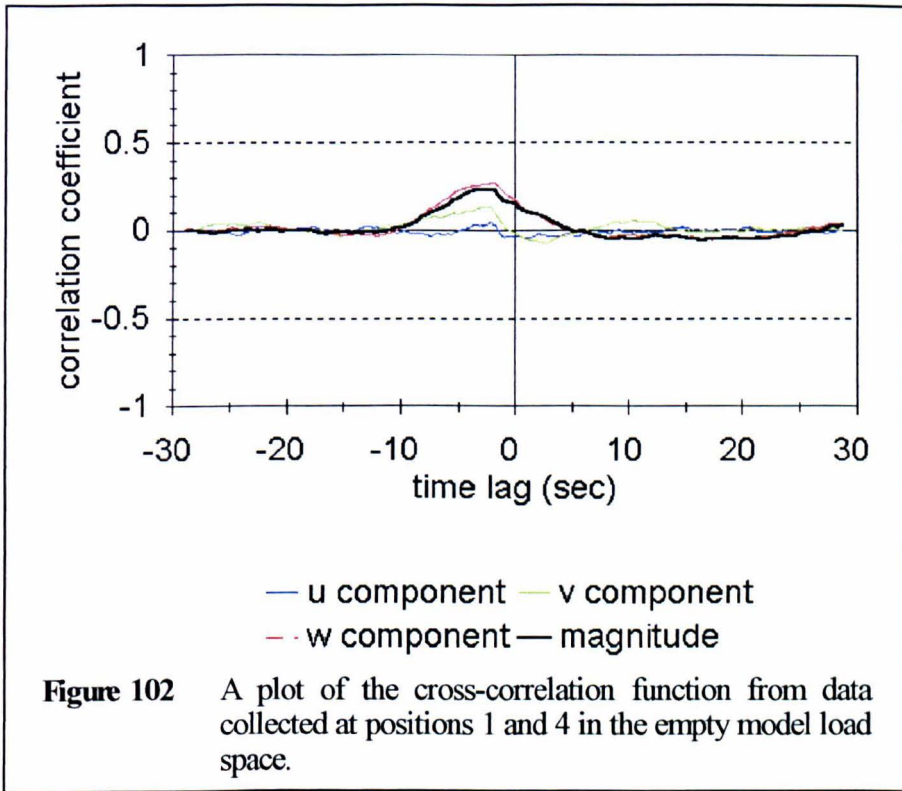


4.3.3 Cross-correlation and cross-spectral results

The cross-correlation function (see section 2.1.2) shows the correlation coefficient of a time series with another, spatially separate, simultaneously measured time series with a variable delay or time lag. Results given here are again smoothed were possible by averaging over repeated measurements.

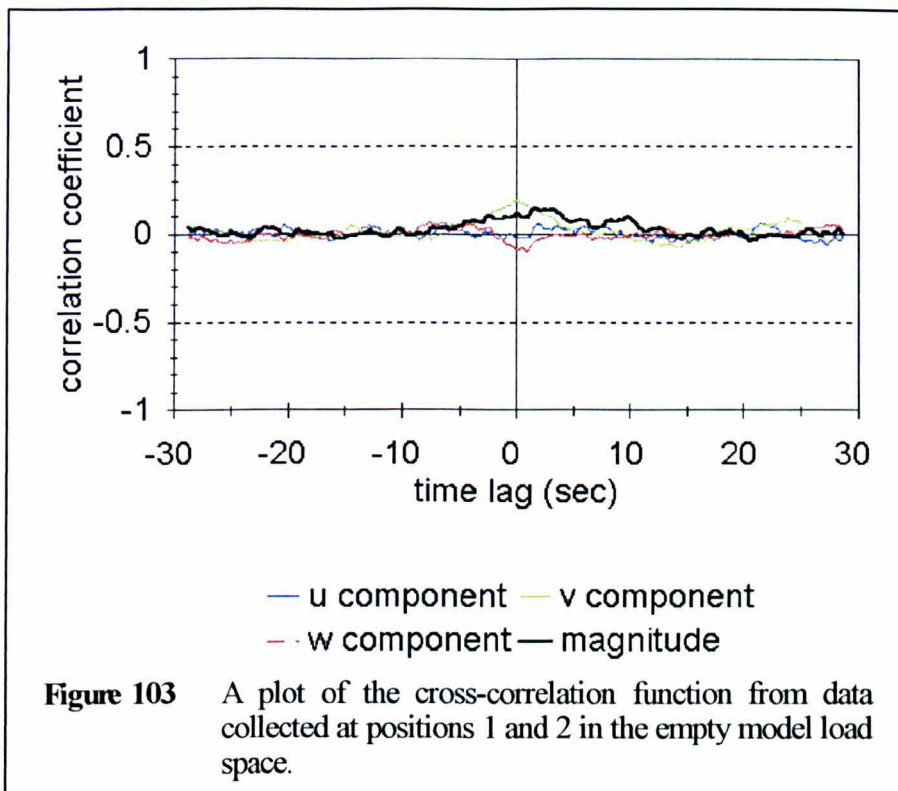
Empty load space case

The cross-correlation function between positions 4 and 1 (figure 17) is shown in figure 102. This indicates that there is a peak cross-correlation of ~ 0.25 between these positions at a time lag of $\sim (-2.5 \text{ s})$. The sign of this

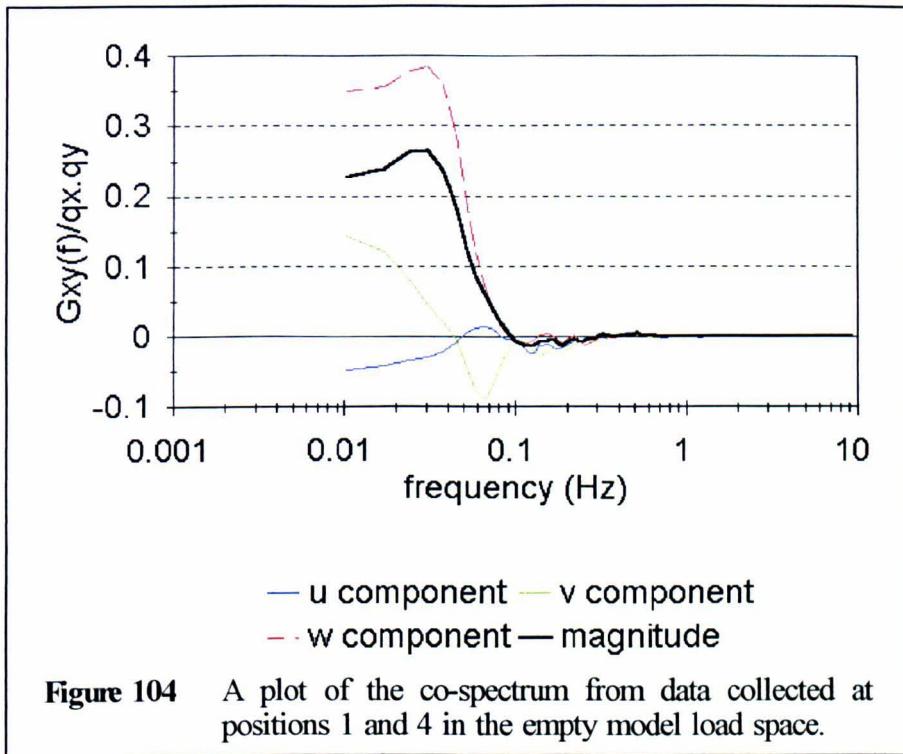


time delay indicates that the time series at position 4 is ahead of that at position 1, in that turbulent structures pass through 4 first, as is consistent with the mean flow field (figure 35). There is however a significant correlation at positive time delays, suggesting structures moving upstream. These may be large eddies present in the flow but possibly more likely are instabilities in the mean flow caused by the fan arrangement or other large scale effects.

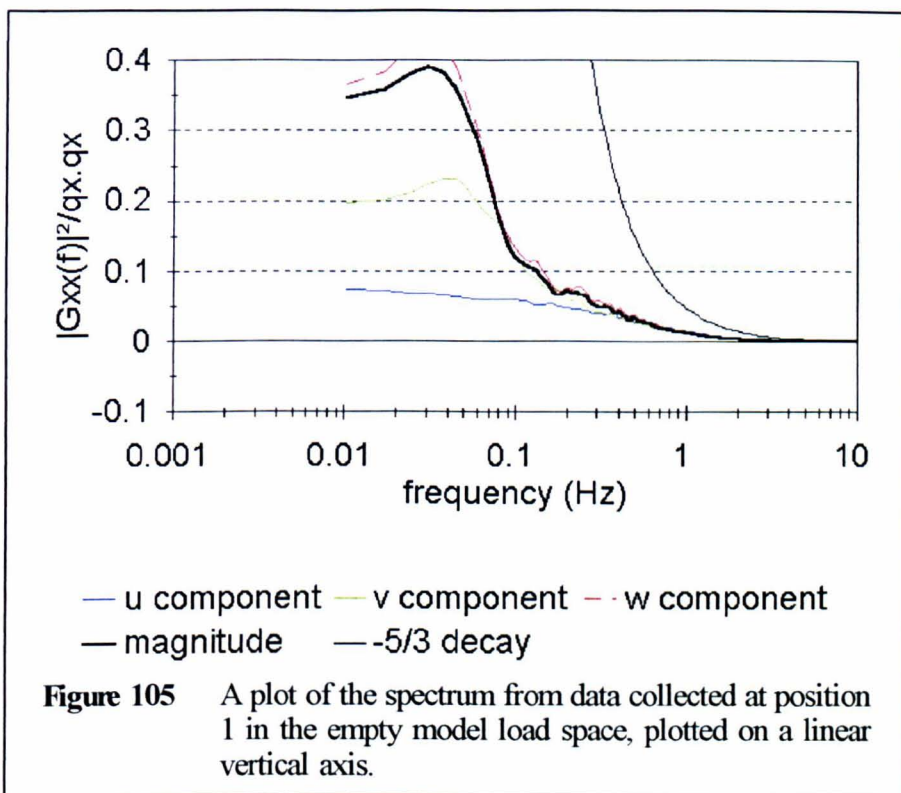
The maximum cross-correlation occurs in the streamwise component with the cross-stream components showing much lower correlations. It must be noted however that this level of correlation is not high given a spatial



separation of only 2 m, but is reasonable considering the length scales of turbulence of <1 m measured (table IX). Positions 4 and 1 in fact give the best correlation of any positions within the box. The result for position 2, for example (figure 103 - data from one run only), shows a peak cross-correlation coefficient of only ~ 0.2 and positions further separated show no significant correlation. The indeterminate time lag associated with this latter figure is partially due to the lack of smoothing but also may be due to the small proportion of the flow which actually passes between positions 1 and 2 because of the flow into the front vents (figure 35).



The cross-spectral analysis of such small correlations proved to be of little value because of the very large amounts of smoothing required to give a meaningful results. Figure 104 shows the only significant and meaningful result produced from this analysis. This is the co-spectrum from the correlation data for positions 4 and 1 and shows the frequencies which cross-correlate in phase between these positions. For comparison the spectrum for position 1 is re-plotted with a linear y-axis in figure 105. These figures suggest that the correlation which is present within the flow is confined to frequencies of <0.1 Hz. This very low frequency correlation may then be attributable to unsteady mean effects rather than turbulence.

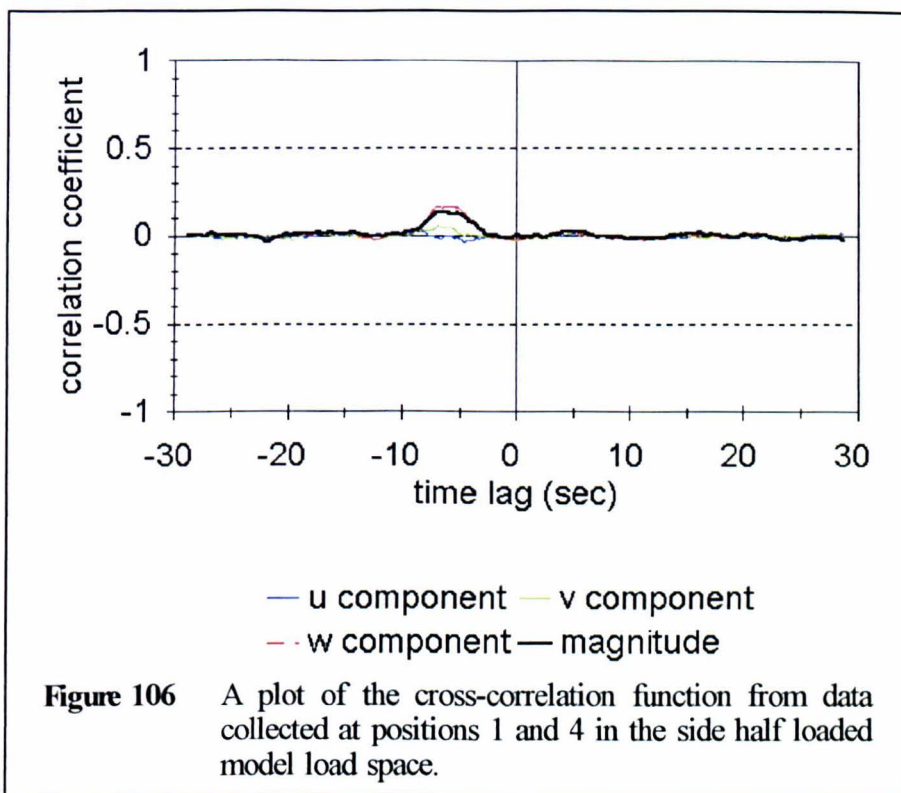


Front half loaded case

The presence of the load in this configuration was found to remove all cross-correlation from the flow, which is in line with the reduced integral length scale values shown in table IX.

Side half loaded case

The only significant cross-correlation found was between positions 4 and 1 (figure 106), which gives a peak cross-correlation coefficient of ~0.15 at (-5 s) to (-7 s) time delay. This is probably the same effect as seen in the empty load space case, present because of the clear movement of air between positions 4 and 1, but reduced and delayed because of the presence



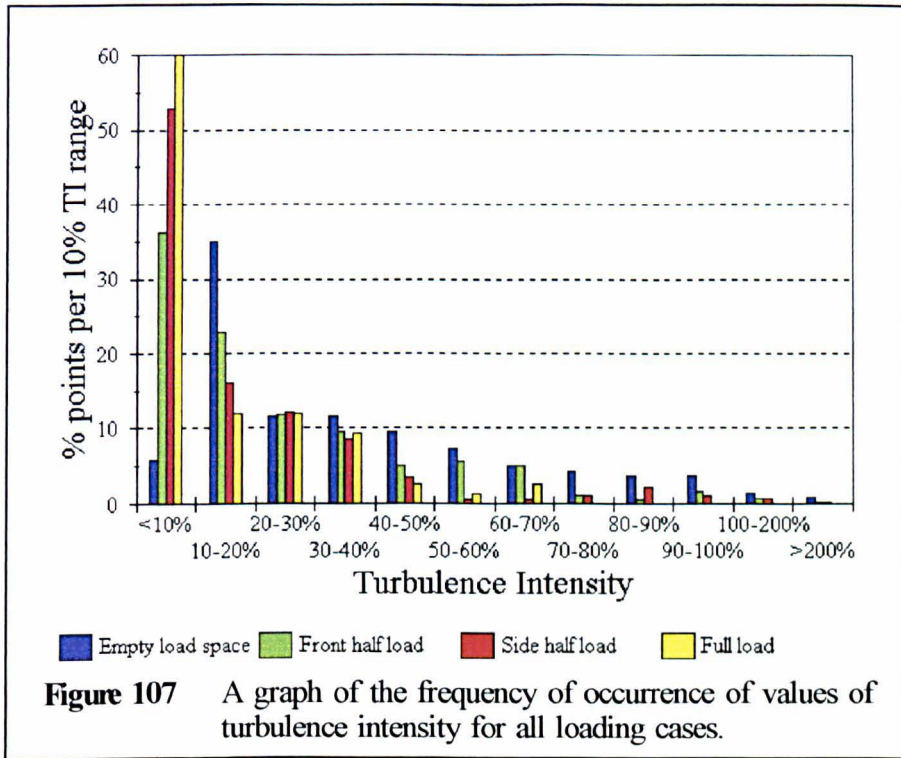
of the load.

Fully loaded case

Again no significant cross-correlations were found in this case.

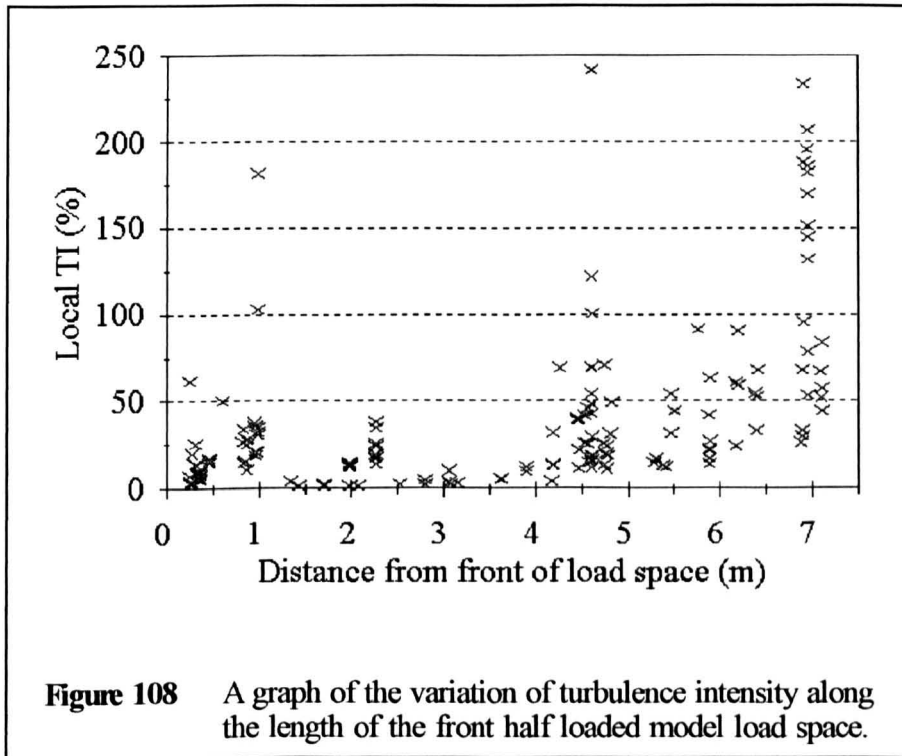
4.4 Discussion of experimental and numerical results

Turbulence intensity

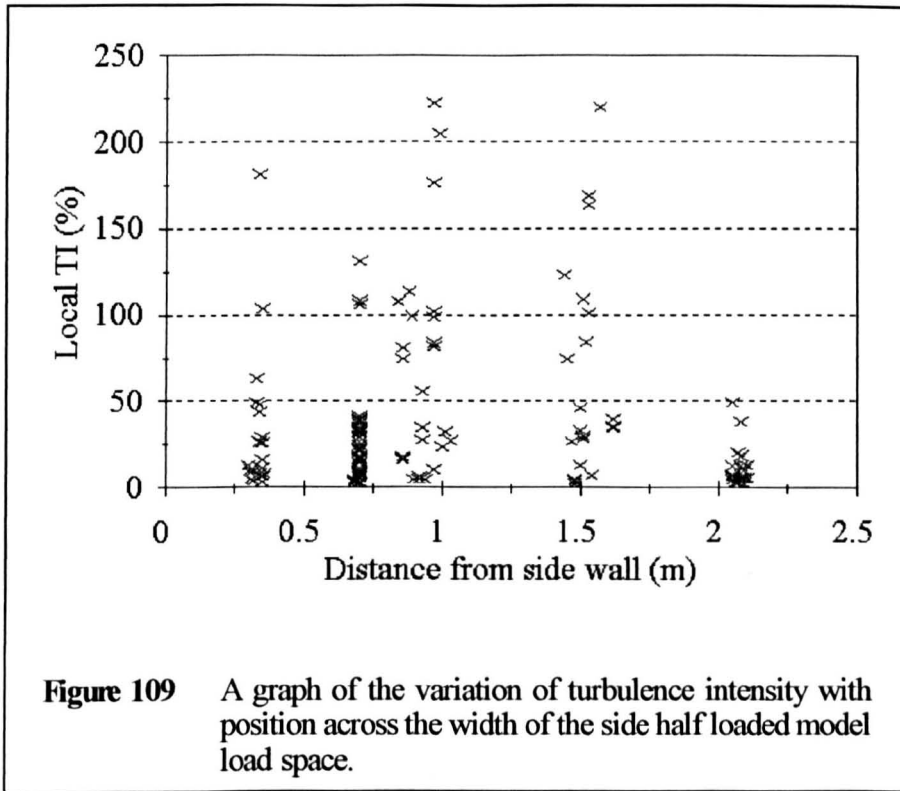


In section 4.2.1 the distribution of TKE was discussed in terms of the local turbulence intensity (TI). This allows the magnitude of the turbulent fluctuations to be expressed as a percentage of the mean magnitude and thus indicates the "variability" of the flow rather than the energy content (see section 2.1.2). The distribution of measured values of TI, for the various loading cases, is given in figure 107. This indicates that the majority of measurements have turbulence intensities of <30%, although values of >200% do occur in regions of low velocity.

The distribution of TI with position, for the empty load space case suggests a generally even distribution of TI throughout the load space, with maxima in areas of low velocity; such as the rear of the load space and in the mixing between the inlet jets and the lower forward flow region.



The effect of the load on TI can be assessed with reference to the two half loaded experimental arrangements. Figure 108 shows the variation of TI along the length of the load space in the front half loaded case and demonstrates the reduction in TI due to the load, in positions between ~1 m and ~4 m from the front of the load space, compared with the values in the open spaces in front of and behind the load. This suppression of turbulence is also visible in the side half loaded case (figure 109), where TI has been plotted against the distance from the side wall of the load space. The



previous results of mean velocity and TKE suggest that this effect is partially due to the increased mean magnitude of the flow in the loaded areas, especially in the front half loaded case, because of the channelling effect. This effect is also partially due to the reduction in TKE associated with the presence of the load.

Experimental measurements

The use of the ultrasonic anemometer in this study has confirmed that the instrument is well suited to the low Reynolds number flows typically found in this environment. There are however a number of points about its use which need to be considered. Firstly the instruments physical size has, as previously mentioned, limited the locations in which meaningful measurements can be taken. This has meant that validation of the ventilation rate results cannot be accomplished by this method without modifications. Furthermore, although the anemometer does measure the three components of air velocity simultaneously, its orientation within the flow is not a negligible concern. The arrangement of the long mounting body being such that measurements of flow along the length of the instrument should be avoided, and flow be kept to within $\pm 30^\circ$ of the perpendicular, according to the suppliers instructions. This limits the physical positioning of the instrument somewhat, and requires a knowledge of the flow prior to measurement. These drawbacks suggest that a smaller sensor head, which could be more conveniently located, preferably without rigid attachment to a mounting, might improve the range of experimental data which could be collected. Alternatively one might consider other measuring techniques, hot wire probes for example, for the less accessible areas of the load space, but these present other disadvantages such as the lack of robustness, directional uncertainty and low speed inaccuracy.

The validation of the ventilation rate results is also not a trivial problem, given the large number of possible, time varying, inlets and outlets to any individual chick box. This suggests that some type of tracer gas, or dissipation method, might be employed to overcome the detailed uncertainties. However, the recirculating nature of this particular type of ventilation system might then introduce the problem of recirculated tracer.

Numerical simulations

From the results presented in this chapter it would seem that some grid dependent effects remain in these calculations. This is perhaps not surprising given that the grids used were dictated in the main by the geometric constraints of the problem. It would be preferable to reduce the cell size, especially in the z direction, in order to remove the anisotropies in the grid and resolve the more detailed features of the flow more accurately. This however would require considerable further computing resources and would not in itself remove all the shortcomings seen in these results.

One particular area of concern is the ceiling jet holes, simulated in this study by a line source. The simplifications inherent in such an approach have clearly led to some problems in the results. Particularly the uncertainty associated with the jet penetration and the over-prediction of velocities in the rear section of the load space. The former of these is perhaps more

associated with the grid anisotropies discussed above, although the averaging inherent in the line source approach may be a cause of under-prediction. The latter problem is probably due to the specification of too high a mass and momentum source in the rear area of the load space. This is possibly due to the simplification of the inlets in terms of measured velocity and geometric hole area, without accounting for the possible effects of the tapering ducts within the false ceiling. To evaluate these a more detailed experimental approach would be required, to accurately assess the actual mass and momentum flow through such holes.

Another problem area for the numerical work was the prediction of turbulence. In the empty load space areas these problems seem to be due to inadequate resolution of velocity gradients and streamline curvature, which are well known problems associated with the $k-\epsilon$ model. Amongst the load itself, however, a more fundamental problem seems to occur, namely the generation of turbulence by velocity gradients at the boundary of porous media. This suggests the need for a more sophisticated model of turbulence which can account for restricted eddy sizes, damping by the load and limited contact between the higher speed external flow and the lower speed internal flow among the chick boxes. These features do not appear to be available in any current models.

5 Quantitative comparison of experimental and numerical results

5.1 Comparison methodology

The quantitative comparison of numerical simulation results with experimental data is a field which has received little study. Where validation against experimental results has been undertaken, this comparison is normally done on some restricted subset of the numerical domain, such as a cross section or traverse. Where flows are two dimensional, or where such a traverse can be considered representative of the important features of the flow, then this method is justified. In complex three dimensional flows, however, there is no clear progression from this technique which would allow the quantitative comparison of different numerical models to a set of experimental results. This objective requires that all the available experimental data be considered and a statistical goodness-of-fit parameter be derived for each set of numerical results, the comparative scores of such a parameter then being a measure of the models success. There are, however, a number of potential problems in such a strategy.

Experimental results used in such a comparison must reflect the important features of the flow if a meaningful comparison is to be achieved. The experimental data must also be extensive enough to represent the true mean and variance of the flow at the measuring positions, otherwise

comparison with any predicted values will be meaningless. Turbulence statistics also need careful consideration. The turbulent kinetic energy (TKE - k) derived from the experimental variance obviously requires that this variance be a representative sample of the turbulence, both in terms of a constant mean and in frequency content, not for example due to a periodicity in the flow. The dissipation rate of TKE (ϵ) cannot be directly measured and therefore an indirect method of verification must be used if required. One such method would be the comparison of measured and predicted length scales (l), where the latter is obtained from $l = \frac{k^{3/2}}{\epsilon}$. This however does pose the question of which experimental length scale is comparable to the prediction. Also the values of such a variable may not be meaningful for all points within the flow.

The comparison methodology adopted here seeks only to compare the available primitive variables, that is the three velocity components and the TKE, from both experiment and predictions. This allows differences in the data to be seen in terms of the components rather than compound variables such as length scale or turbulence intensity. The only exception to this is that the magnitude of velocity has also been included as a variable in the comparison as it was considered this might be more representative than the individual components in isolation. The basic principles however

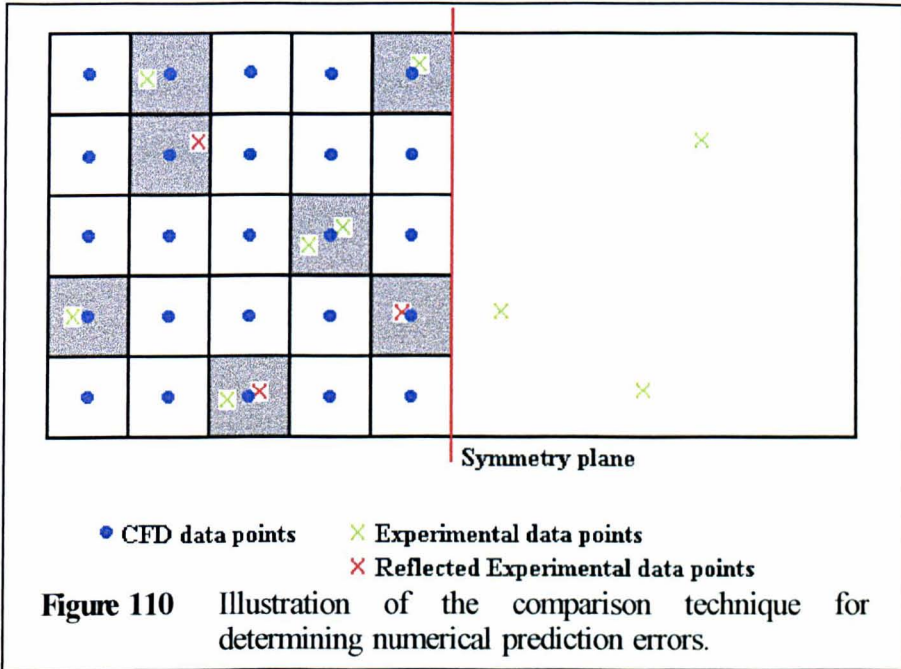
can be used to compare any variables over any domain or sub-domain of interest, and is therefore a truly three dimensional approach to comparison.

Given a set of experimental data, containing the means and variances of the velocity components at each specified position, and a set of numerical results, also specifying mean velocity components and TKE, the comparison procedure used was as follows:

1. Calculate the numerical grid cell containing the position of each experimental location (see note below concerning the symmetry plane).
2. Calculate the mean and standard deviation (SD) of means, for each variable considered, associated with any numerical cells which contain more than one experimental point.
3. For each numerical cell containing experimental data, calculate the error in the numerical predictions of the mean values of each variable in terms of absolute difference from the experimental results.

In the implementation of these comparison techniques the line of symmetry in the load space, used in the numerical simulation to reduce the domain, was incorporated by reflecting the experimental results in this plane. Any

cells which thereby held more than one experimental result were averaged in the way described above for repeated data points.



An illustration of this method is shown in figure 110. Here the numerical grid includes a line of symmetry (shown in red) through the centre of the experimental domain. The numerical cells and the locations of predictions (blue filled circles) are shown for this restricted domain. The locations of the experimental data are shown as green crosses. The experimental data which lies outside the numerical domain because of the line of symmetry is first reflected back into the domain across this line, giving the red crosses. Clearly part of this process will include a change of sign for any velocity component affected by this reflection. The numerical cell location of each cross, both red and green, is next calculated in order to determine which predicted value should be used for comparison with

each experimental data point. Clearly there can be some spatial discrepancy between the experimental and numerical locations and this might be overcome by interpolation of the numerical results, however this was not undertaken in the current trial both for simplicity and because the experimental data collected with the ultrasonic anemometer also contains an element of spatial averaging over the measuring volume (section 2.2.4).

Two cells in this picture each contain two experimental runs, as would any cell in which an experimental location had been repeated at two or more separate times. Within each of these cells the experimental data is averaged and the SD of the individual points calculated. This gives the SD of means, which is a measure of the experimental repeatability within that cell. Assuming, or having verified, that this SD of means does not vary with spatial location, *i.e.* throughout the grid, the repeatability of the experimental data does not depend on the location of measurement, then the average SD of means, over all numerical cells containing two or more experimental data points, gives an overall measure of experimental repeatability. If this measure did vary with spatial location, which was verified not to be true in these experiments, then either a spatially varying function would be needed to estimate the SD of means at all points within the numerical domain; or the experimental data would need to contain at least one repeat of every experimental data point so that the SD of means

could be calculated for every experimental location (see error analysis method B below).

Having calculated the repeatability, it is also necessary to replace the experimental results, in cells containing two or more experimental data points, with the average of these data points. This is because the variation measured by the SD is about the mean value. If one were to treat the spatial locations precisely, rather than grouping in units of numerical cells, with interpolation of the numerical results, then only repeated runs at single spatial locations would require this treatment. Finally the CFD error can be calculated for each numerical cell containing experimental data, either as single runs or the average of repeated runs discussed above. This gives a result for each cell shaded grey in the above illustration.

Once this error for each comparable position has been obtained it can be expressed in a number of ways:

- A. The prediction error can be expressed in terms of a simple percentage of measured values, for each variable, at each location, the goodness-of-fit parameter then being the percentage of points at which this error is within acceptable limits. This method is clearly the simplest type of analysis but does not allow for the experimental

error and will overstate the errors associated with small measured values.

B. Alternatively, using the estimate of experimental repeatability, that is the mean SD of means discussed above, the prediction error can be expressed as a number of SDs. The percentage of points falling within an acceptable experimental spread, say three or six SD, for each variable considered can then be used as a measure of goodness-of-fit for each variable. This measures the predicted values against the experimental results on an equal basis, allowing for the experimental variability. It is also possible, with these two methods, to plot the variation of error throughout the domain considered. The drawback is that one must know, or assume, that the SD of means does not vary with spatial location, otherwise the measure of repeatability must be calculated at each location, requiring at least two experimental runs per position. If data of this extent is available then an extension to this method would be to apply a Student's t-test at each position, the percentage falling within the percentile required then being the goodness-of-fit statistic.

C. The errors in the predicted values can also be expressed as an overall percentage or number of SDs. That is the total absolute error for the cells considered can be given as a fraction of the total

absolute sum of the measured values for each variable, or as a number of SDs. If N cells contain experimental data with measured values m_i and predicted values p_i then this overall error O can be

expressed $O = \frac{\sum_{i=1}^N |p_i - m_i|}{\sum_{j=1}^N |m_j|}$ as a percentage or as a number of SDs.

This gives an unbiased measure of the absolute error since the large percentages associated with small measured values do not occur. The drawback of this method, however, is the lack of information about the spatial distribution of the error, which may be valuable in improving the numerical model. There is also a problem of interpretation for this statistic which has no clear physical meaning and therefore no clearly defined boundaries of acceptability.

The proposals given in B and C above were implemented for this project in a BASIC program on the PC called "CINDERS" [Computational fluid dynamics and Experimental data comparison System]. The software also calculated the maximum, minimum and mean values of each set of the experimental results and the corresponding values for each associated set of numerical results and errors. This gave another, less direct, comparison in terms of the mean and extreme values achieved and predicted for each variable.

5.2 Comparison of cases

5.2.1 Empty load space case

The experimental data collected in this case amounted to 202 approximately ten minute runs with mean and extreme values shown in

Table X Summary of the experimental data collected in the empty model load space case.

| Variable | Minimum | Mean | Maximum | SD of Means* |
|--|---------|-------|---------|--------------|
| U component of velocity ms^{-1} | -0.48 | -0.02 | 0.73 | 0.076 |
| V component of velocity ms^{-1} | -0.94 | 0.01 | 0.67 | 0.098 |
| W component of velocity ms^{-1} | -0.94 | -0.08 | 1.02 | 0.125 |
| Magnitude of velocity ms^{-1} | 0.04 | 0.44 | 1.39 | 0.085 |
| Turbulent Kinetic Energy m^2s^{-2} | 0.02 | 0.11 | 0.33 | 0.023 |

* Mean Standard Deviation of means of numerical cells containing two or more experimental runs.

table X. This shows that the data collected represents a wide range of conditions with no bias toward positive or negative values apparent, since the mean experimental results for velocity lies in the centre of the range of

measured values and is approximately zero. The standard deviation values (SDs) show the repeatability of the experimental data collected.

Eight simulations of this case were completed, including grid independence tests, all of which achieved a volume flow rate of $3747 \pm 1 \text{ m}^3\text{hr}^{-1}$ which is well within the experimental range $3800 \pm 200 \text{ m}^3\text{hr}^{-1}$.

These eight simulations were:

1. EFF grid with 100% inlet jet speed.
2. EFF grid with 66% inlet jet speed.
3. EFF grid with 50% inlet jet speed.
4. ES grid with 100% inlet jet speed.
5. ES grid with 50% inlet jet speed.
6. X-doubled EFF grid with 50% inlet jets speed.
7. Y-doubled EFF grid with 50% inlet jets speed.
8. Z-doubled EFF grid with 50% inlet jets speed.

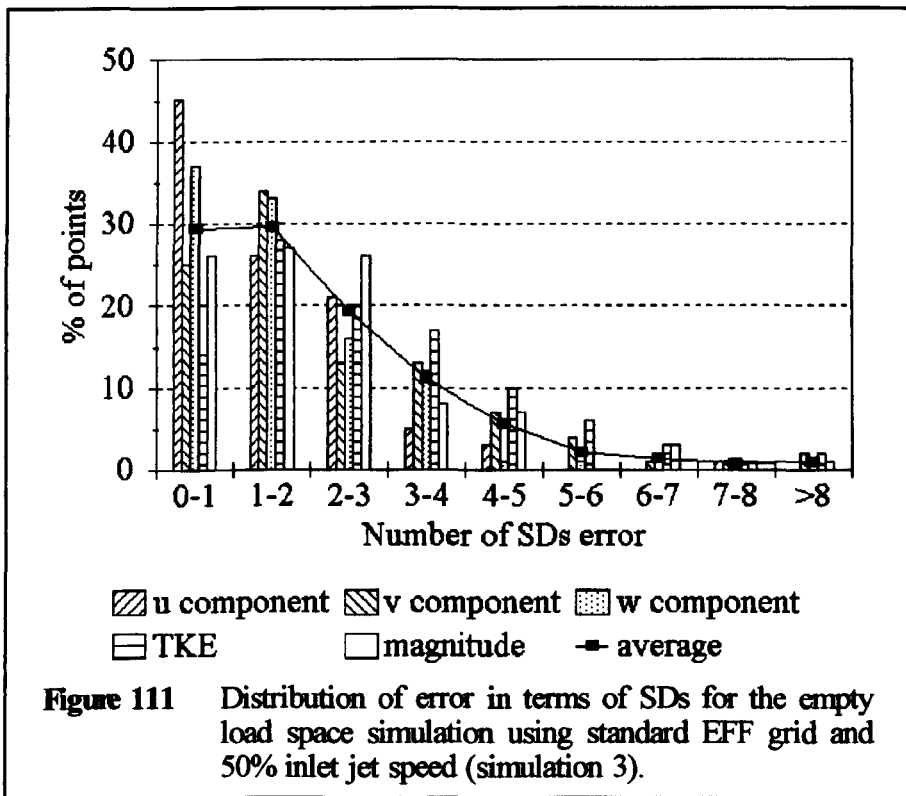
(See section 3.4 for more details.) These produced results with the mean and extreme values, for the positions of experimental data, shown in appendix 6, which contains the comparison output files for all the cases studied. The cells for which experimental data is available, numbered 107 out of 8874 in the standard grid cases, simulations 1 - 5 above and, 108-110 out of 17748 in simulations 6-8.

Comparison of the mean and ranges of the predicted results for the turbulent kinetic energy, shows that the mean and maximum values were reduced by 55% and 65% respectively, with an inlet jet speed of 50%. The peak TKE was also reduced by over 45% by either a doubling of the grid in any direction or by reducing the inlet jet speed to 66% of measured values. In all these cases however, the mean TKE for the measured positions also reduced by similar amounts, thus under-predicting the experimental mean value whilst also tending to over-predict the ranges. The velocity components varied much less with any changes to grid structure or inlet jet speed. The V-component shows a significant under-prediction of the minimum in all cases, with an under-prediction of the maximum in cases where the minimum improves, but with a generally acceptable mean value. The W-component again shows little variation and is within the correct range but the mean is generally under-predicted. These latter points contribute to the results for the magnitude, which although generally predicting the correct mean, over-predict both the minimum and maximum results.

The results in this form suggest that the broad ranges of variables are predicted and that for the most part problems occur with the outlying values, with the exception of the TKE. This is also seen in the CFD error results expressed as a number of SDs (appendix 6). Then the mean error for all variables in each simulation is ≤ 3 SDs, with a reduction to ~ 2 SDs in

simulations with 50% inlet jet speed. Maximum errors are also reduced, by 10 - 30% for velocity and 75% for TKE, by the reduction of inlet jet speed but are unaffected by the alterations in grid structure or resolution.

Overall levels of the errors, calculated as total absolute error divided by the total absolute measured values can also be seen to have reduced with reduced inlet jet speed (table XI). This measure again shows the significant effect of reducing inlet jet speed and the relative insensitivity to grid variations.



Finally the distribution of this error can be seen by categorising each point by the number of SDs error. This gives distribution curves such as

Table XI Overall total absolute errors as a fraction of total absolute measured values for simulations of the empty load space.

| Simulation | Velocity component | | | | TKE |
|------------|--------------------|-------------|------------|------------|------------|
| | U | V | W | Magnitude | |
| 1 | 112% | 143% | 101% | 54% | 67% |
| 2 | 93% | 117% | 83% | 43% | 59% |
| 3 | 86% | 107% | 59% | 42% | 59% |
| 4 | 111% | 136% | 87% | 46% | 71% |
| 5 | 84% | 105% | 71% | 41% | 55% |
| 6 | 86% | 114% | 75% | 42% | 65% |
| 7 | 104% | 105% | 92% | 45% | 66% |
| 8 | 88% | 117% | 81% | 44% | 60% |

Highlighted are the simulations with 50% inlet jet speed and standard grids. Simulations 6,7 and 8 also have 50% inlet jet speed with doubled grids and show no improvement. Simulation 7 also predicted a different overall flow pattern which is reflected in these results as generally higher overall errors.

These percentages indicate the total absolute CFD error, summed over all the numerical cells containing experimental data, divided by the total absolute measured value summed over these same cells. Thus a perfect prediction would have 0% total absolute error. Since the scaling of this statistic depends on the total absolute measured values, there is no clear comparison between the levels of individual variables, and the dominant flow variables (*i.e.* dominant flow direction velocity components) may tend to have smaller values because the total absolute sum of measured values is greater than that for other variables (*i.e.* directions).

figure 111, which applies to simulation 3, where the line shows the mean distribution for the variables. From this type of distribution data acceptable limits, in terms of numbers of SDs, can be set and the numbers of cells passing such criteria can be measured. The level at which these criteria

Table XII Fraction of points within 3 SDs of measured values for simulations of the empty load space.

| Simulation | Velocity component | | | | Turbulent Kinetic Energy |
|------------|--------------------|------------|------------|------------|--------------------------|
| | U | V | W | Magnitude | |
| 1 | 79% | 57% | 72% | 66% | 77% |
| 2 | 88% | 67% | 79% | 76% | 71% |
| 3 | 92% | 72% | 86% | 79% | 62% |
| 4 | 80% | 58% | 77% | 72% | 73% |
| 5 | 92% | 74% | 84% | 76% | 66% |
| 6 | 87% | 64% | 79% | 75% | 57% |
| 7 | 78% | 75% | 72% | 72% | 58% |
| 8 | 91% | 64% | 82% | 58% | 75% |

Highlighted are the simulations with 50% inlet jet speed and standard grids. Simulations 6,7 and 8 also have 50% inlet jet speed with doubled grids and show no improvement.

should be set is discussed in section 5.3, but a level of 3 SDs is used here as an indicator (table XII).

This distribution shows the improvement in velocity error values with reduced inlet jet speed and the worsening of the TKE values. This latter point ties in with the mean and range results which show the extreme values being improved by the reduction in jet velocity but the mean value also being reduced away from the experimental value. The overall error for TKE, however, does reduce with reduced jet velocity. This is presumably

because of the reduction in the extreme errors which contribute most to the total value.

5.2.2 Front half loaded case

The experimental data collected for this case consisted of 199 runs with the values shown in table XIII. Comparison with the data from the

Table XIII Summary of the experimental data collected in the front half loaded model load space case.

| Variable | Minimum | Mean | Maximum | SD of Means* |
|--|---------|-------|---------|--------------|
| U component of velocity ms^{-1} | -0.39 | 0.02 | 0.45 | 0.129 |
| V component of velocity ms^{-1} | -0.90 | -0.01 | 0.74 | 0.115 |
| W component of velocity ms^{-1} | -0.95 | -0.25 | 1.26 | 0.127 |
| Magnitude of velocity ms^{-1} | 0.09 | 0.46 | 1.26 | 0.102 |
| Turbulent Kinetic Energy m^2s^{-2} | 0.00 | 0.05 | 0.27 | 0.011 |

* Mean Standard Deviation of means of numerical cells containing two or more experimental runs.

empty model shows a slight increase in the W-component of velocity and reduction in TKE. This is presumably due to the presence of the load and the resultant changes in flow pattern (section 4.2.2).

For this case four simulations were completed, achieving the same flow rates as for the empty case. These were:

1. Standard load model and 100% inlet jet speed.
2. Reduced porosity load model and 100% inlet jet speed.
3. Standard load model and 50% inlet jet speed.
4. Reduced porosity load model and 50% inlet jet speed.

(See section 3.4 for more details.) The comparison output files are again shown in appendix 6. The experimental data in this case fell into 99 cells out of 8874 in the numerical grid.

Comparison of the mean and ranges of the predicted results suggests that the introduction of the reduced porosity load model does not change the overall statistics of the predicted flow significantly. The 50% reduction in the inlet jet velocity is again the dominant factor, with reductions in the ranges of the U and V-components of velocity by 45% and 20% respectively and in the mean magnitude by 25%. The mean and peak TKE are also reduced by 40% and 60% respectively. Compared to the experimental data the V-component of velocity is again under-predicted in the maximum and minimum values, with the W-component range also being under-predicted. The mean magnitude prediction is again generally correct but the maximum is over-predicted as is both the mean and maximum TKE.

The CFD error results expressed as a number of SDs suggests that the mean velocity is again predicted acceptably, with the mean error for each variable being ≤ 2 SDs and the maximum errors reduced over the empty case. The TKE results however have worsened with the introduction of the load, the mean error being at least 6.5 SDs with a maximum of at least 26.5 SDs, these figures being a 250% increase on the equivalent empty case.

Table XIV Overall total absolute errors as a fraction of total absolute measured values for simulations of the front half loaded load space.

| Simulation | Velocity component | | | | TKE |
|------------|--------------------|------------|------------|-----------|-------------|
| | U | V | W | Magnitude | |
| 1 | 114% | 112% | 52% | 37% | 277% |
| 2 | 123% | 105% | 55% | 40% | 236% |
| 3 | 103% | 87% | 50% | 40% | 150% |
| 4 | 103% | 81% | 49% | 36% | 134% |

Highlighted are the simulations with 50% inlet jet speed.

Overall levels of error, calculated as a fraction of measured values, for these four simulations can be seen in table XIV. The effect of inlet jet speed reduction is again visible compared to that of changing loading model, with reductions in V-component and TKE errors as would be expected.

Table XV Fraction of points within 3 SDs of measured values for simulations of the front half loaded load space.

| Simulation | Velocity component | | | | Turbulent Kinetic Energy |
|------------|--------------------|------------|------------|------------|--------------------------|
| | U | V | W | Magnitude | |
| 1 | 97% | 77% | 95% | 87% | 26% |
| 2 | 96% | 79% | 93% | 84% | 31% |
| 3 | 99% | 88% | 95% | 86% | 40% |
| 4 | 99% | 88% | 96% | 89% | 39% |

Highlighted are the simulations with 50% inlet jet speed.

Table XV shows the distribution of this error within the 3 SDs limit. In this case both the values for velocity and TKE have generally improved with a reduction in inlet jet speed. The largest change being in V-component as before. The improvement in TKE values with reduced jet speed, contrary to the result in the empty case, is due to the reduced experimental levels recorded in the presence of the load. The distribution of these levels, however, is clearly not as good as in the empty case.

5.2.3 Side half loaded case

Table XVI Summary of the experimental data collected in the side half loaded model load space case.

| Variable | Minimum | Mean | Maximum | SD of Means* |
|--|---------|-------|---------|--------------|
| U component of velocity ms^{-1} | -0.38 | -0.01 | 0.28 | 0.040 |
| V component of velocity ms^{-1} | -0.96 | 0.02 | 0.73 | 0.069 |
| W component of velocity ms^{-1} | -1.17 | -0.19 | 1.08 | 0.090 |
| Magnitude of velocity ms^{-1} | 0.05 | 0.51 | 1.23 | 0.076 |
| Turbulent Kinetic Energy m^2s^{-2} | 0.01 | 0.06 | 0.25 | 0.007 |

* Mean Standard Deviation of means of numerical cells containing two or more experimental runs.

For this case the experimental data amounted to 195 runs with the mean and range shown in table XVI. These values show little change from the front half loaded case, except in the smaller SD values (see section 5.3).

For this case two simulations were completed, with the same flow rates as previously. These were:

1. Standard load model.
2. Reduced porosity load model.

Both simulations used a 50% inlet jet speed, see section 3.4 for more details. The number of numerical cells covered by the experimental results in this case was 76 out of 8874 and the comparison output files are included in appendix 6.

Comparison of the mean and range of the predicted results shows no significant variation in the velocity variables for the two loading models except for a reduction in the mean predicted V-component of 55%, presumably due to the reduction in the flow through the model chick box floor with the reduced porosity model. The TKE however, is significantly effected, with a reduction in mean and peak predicted results of 25% and 35% respectively. As with the front half loaded case, however, the V-component is under-predicted, the W-component range is under-predicted and the TKE is over-predicted compared to the experimental ranges.

The mean CFD errors in terms of SDs are generally ≤ 3 in this case, with the only differences between the models again being the reduction in the V-component mean error from 3.0 SDs to 2.3 SDs, and the reduction in the mean and peak TKE errors by 35% and 65% respectively. The extra significance placed on the load model by these results probably arises because of the difference in the load configuration. In this case the load is placed along the walls of the load space, thus making the interaction between the wall jets and the load important and therefore the change in

load porosity significant. The previous case did not highlight this point because the load-jet interaction was confined to a half section of the wall, reducing its significance in line with the reduced information in that data set.

Table XVII Overall total absolute errors as a fraction of total absolute measured values for simulations of the side half loaded load space.

| Simulation | Velocity component | | | | TKE |
|------------|--------------------|------|-----|-----------|------|
| | U | V | W | Magnitude | |
| 1 | 77% | 100% | 52% | 44% | 131% |
| 2 | 79% | 78% | 51% | 45% | 86% |

Both these simulations used a 50% inlet jet speed.

Overall levels of the errors can be seen in table XVII and these seem to also follow the above comments as well as showing generally similar levels as the front half loaded case results. The reduction of TKE error is probably linked to the reduced predicted values between the shelves of chick boxes, which is closer to the experimental results than the overall high predicted otherwise (see section 4.2.3 figures 67-69).

Table XVIII shows the distribution of this error in terms of the number of points with error ≤ 3 SDs. The improvement in V-component is clear, with a less significant improvement in TKE because of the poor overall distribution of predictions.

Table XVIII Fraction of points within 3 SDs of measured values for simulations of the side half loaded load space.

| Simulation | Velocity component | | | | Turbulent Kinetic Energy |
|------------|--------------------|-----|-----|-----------|--------------------------|
| | U | V | W | Magnitude | |
| 1 | 80% | 62% | 76% | 62% | 24% |
| 2 | 80% | 80% | 76% | 61% | 28% |

Both these simulations used a 50% inlet jet speed.

5.2.4 Fully loaded case

Table XIX Summary of the experimental data collected in the fully loaded model load space case.

| Variable | Minimum | Mean | Maximum | SD of Means* |
|--|---------|-------|---------|--------------|
| U component of velocity ms^{-1} | -0.22 | 0.03 | 0.36 | 0.021 |
| V component of velocity ms^{-1} | -0.98 | -0.22 | 0.09 | 0.015 |
| W component of velocity ms^{-1} | -1.24 | -0.12 | 1.10 | 0.025 |
| Magnitude of velocity ms^{-1} | 0.15 | 0.62 | 1.27 | 0.026 |
| Turbulent Kinetic Energy m^2s^{-2} | 0.00 | 0.08 | 0.30 | 0.003 |

* Mean Standard Deviation of means of numerical cells containing two or more experimental runs.

The experimental data collected for this final case consisted of 75 runs which are summarised in table XIX. Compared to the front half loaded

case these experimental results are similar but with a reduced V-component range, presumably again because of the restricted flow pattern due to the presence of the load.

Three numerical simulations of this case were completed, achieving the same flow rate as previously. These were:

1. Standard load model with 50% inlet jet speed.
2. Reduced porosity load model with 100% inlet jet speed.
3. Reduced porosity load model with 50% inlet jet speed.

(See section 3.4 for more details.) The output files from the comparison are included in appendix 6 and the experimental data covered 13 cells from 8874 in the numerical grid.

Comparison of the ranges of the predicted values from each of the simulations again shows a greater significance attached to the reduced inlet jet speed. The introduction of the reduced porosity load model makes little change to the velocity predictions, except for a general reduction in the mean predicted magnitude by around 10%. The TKE however, is reduced by 25% in the mean and 35% in the maximum predictions. This presumably again reflects the reduction of levels between the shelves rather than an overall reduction in the predicted field (see section 4.2.4). The use of the 50% reduced inlet jet speed however makes significant reductions in all the velocity components, reducing the mean and maximum magnitude by 20%

overall. The mean TKE is also reduced by 25%. When compared to experimental results these predictions show a general under-prediction of each individual velocity component and a general over-prediction of the magnitude, due to many of the under-predictions being negative. TKE is also generally over-predicted. Mean CFD errors in this case are >5 SDs in all the simulations, with the mean TKE error >88 SDs and the minimum TKE error 4 SDs. This indicates a generally poor level of agreement with the experimental data, especially in the level of TKE. This problem, as discussed in section 4.2.4, is due to the artificial generation of TKE amongst the load because of velocity gradients. The increased significance of the loading model seen in the side half loaded case also does not appear here probably because of the lack of experimental points close to the wall.

Table XX Overall total absolute errors as a fraction of total absolute measured values for simulations of the fully loaded load space.

| Simulation | Velocity component | | | | TKE |
|------------|--------------------|------|-----|-----------|------|
| | U | V | W | Magnitude | |
| 1 | 98% | 79% | 40% | 35% | 387% |
| 2 | 109% | 105% | 52% | 51% | 693% |
| 3 | 97% | 75% | 46% | 38% | 535% |

Highlighted are the simulations with 50% inlet jet speed.

Overall levels of error are given in table XX. Once again the significance of the inlet jet velocity is greater than that of the loading

model, which does not reduce the overall TKE error in this case because of the large extreme values predicted with both models.

Table XXI Fraction of points within 3 SDs of measured values for simulations of the fully loaded load space.

| Simulation | Velocity component | | | | Turbulent Kinetic Energy |
|------------|--------------------|-----|-----|-----------|--------------------------|
| | U | V | W | Magnitude | |
| 1 | 46% | 31% | 38% | 38% | 0% |
| 2 | 46% | 38% | 38% | 23% | 0% |
| 3 | 54% | 46% | 46% | 46% | 0% |

Highlighted are the simulations with 50% inlet jet speed.

Finally table XXI shows the fraction of cells tested in which the CFD error is ≤ 3 SDs. Here the very small number of cells in the test mean that the differences amount to a one or two cell improvement. However the combination of reduced porosity load model and 50% inlet jet speed are again the most successful.

5.3 Discussion of comparison methodology and results

One of the most obvious features of the experimental data in the previous sections has been the large variation in the mean SD of means for the different cases (tables X, XIII, XVI and XIX). Although this must be

due at least in part to the different flow patterns measured and their stability at the measuring locations, there are no clear relationships between this variation and the global features of the flow. For example the relative stability of the velocity field in the side half loaded case compared to the front half loaded case suggests that the simple presence of that quantity of load is not sufficient explanation. It must be assumed therefore that either there is some detailed feature of the system, such as the exact load arrangement, which determines flow stability; or that the experimental data collected is unrepresentative in one or more of the cases. There are however similar numbers, distributions and numbers of repeated experimental runs in the empty, front half and side half loaded cases, which would suggest that the results are representative. This then leads to the conclusion that some loading arrangements can be better predicted than others and an error analysis technique such as this is required to determine the extent to which this is true in any given case.

Assuming this stability problem to be true, one might consider that the distributions of error, or the criteria for acceptance, should be based on some less variable parameter, say some function of the local velocity for example. This however does not then truly include the variability of the experimental data and introduces an "invisible" measure of acceptability into the derivation of the comparison results, rather than allowing the results to

be independent of any such inputs and acceptability criteria being applied only afterwards.

In the preceding sections an arbitrary acceptance level of 3 SDs was used for the CFD error and mention was made of the possibility of using a Students' t-test for significant difference if sufficient data was available, that is every point was repeated at least once. In trials with the data collected for the empty load space case, dividing the runs in half to obtain the repeats (see section 2.2.5), it was found that the SD of means calculated was 55% - 60% of the values given previously (section 5.2.1 table X). Since the experimental and numerical results were otherwise identical, ie. the CFD errors were identical, this effectively reduced the acceptance level of 3 SDs by ~60% with a consequent reduction in the percentage acceptance rate. However, the 3 SDs level of acceptance is arbitrary and one advantage of the t-test methodology is that an expected normal percentage acceptance can be calculated, or rather a level of acceptance can be defined which would, if the errors were normally distributed about the same mean, include a given percentage of points. For example, with one repeat of every experimental data point, 80% of errors would normally be within ± 3.08 SDs of the mean experimental value. This rises to 90% within ± 6.31 SDs. If two repeats of each point exist then the 80% boundary becomes ± 1.89 SDs and the 90% boundary ± 2.92 SDs (Spiegel 1968), the reduction being due to the increasing certainty attached to the experimental

mean. Considering the results with these criteria, it can be seen that overall the simulations have achieved a reasonable level of agreement with the experimental data for mean velocity in the first three cases. Agreement for TKE is less good, with particular problems when the load is introduced.

The final case of a fully loaded load space highlights one further point crucial to the success of any comparison technique, which is that no feature of the flow can be validated unless it appears in the experimental data set. The amount of data required therefore even in the simplest cases is quite extensive. Furthermore it is apparent from the preceding results that different error analysis techniques tend to highlight different shortcomings in the predictions, for example, the reduction of overall error in TKE with reduced inlet jet velocity, but also with a reduced fraction of points passing the 3 SDs test, in the front half loaded load space case. The conclusion from this is that although the extreme values of error decreased, the distribution was not improved. Also, in the empty load space case, the variation in flow pattern given by the simulation using a grid containing twice as many cells in the vertical direction, showed only slightly increased error values, which would not be explicable without a visual consideration of the changed predicted pattern. These points suggest that any error analysis technique can only be used to help quantify existing visual comparison and that various tests used in parallel can reveal various different features about the errors involved in predicting complex flows.

6 Implications

The implications of the results of this study will be discussed in this chapter. Section 6.1 deals with the general implications for the field of CFD simulations and the validation of CFD models. Section 6.2 deals with the problem of interpretation of the predicted temperatures from the numerical simulations, which is necessary because of the simplified heat load model used. Finally section 6.3 deals with the notable physical features of the ventilation system which affect the flow within the load space.

6.1 Implications for CFD studies

The results of this study have a number of implications in the wider context of CFD studies and their validation. Firstly in the area of problem specification, the complex geometry involved in this situation required simplifications to be made at the boundaries in order to render the problem into a soluble form (section 3.3.2). These simplifications have clearly had a significant effect on the solutions obtained, the variation of flow pattern with velocity specification at the ceiling jet holes for example. This suggests that a high level of user knowledge is required in order to obtain realistic results from general CFD software codes, especially where user supplied coding is required. Some of these simplifications were required because of the inability of the software to cope with the situation without an extremely

fine mesh, the false ceiling to load space transition for example. This indicates a requirement for CFD codes to cope robustly with such situations without a large concentration of resources in areas of lesser concern.

In general the study of internal flow situations will require a fine grid throughout a finite domain. The grids used in this study have been limited by available computing resources, which will clearly be a problem for most commercial companies especially in specialist areas, even with the increasing availability and power of computer workstations. This, combined with the requirement for CFD user knowledge, suggests that specialist resources and training is generally needed if good results are to be obtained.

The effects of the presence of the porous media in the flow are also clearly significant both in terms of the mean velocity and turbulence levels. A clear specification of the load in terms of bulk porosity is needed for these types of model and the effects of different specifications are significant both on the mean flow and the turbulence levels. In general turbulence values have been poorly predicted in his study, which suggests that the turbulence model used is inappropriate. However, there do not currently seem to be any alternatives which would significantly improve predictions given that the properties of turbulence in the presence of the porous load are not included in present models (Leschziner 1995).

Therefore, considering the possible shortcomings of the CFD model it is clear that careful validation is required. If the problem is such that the domain can be considered as two dimensional, or if a representative traverse or plane can be isolated, then traditional graph plotting methods alone can be adopted. Similarly, if quantitative accuracy is not a concern then visual interpretation of results is sufficient. However, in complex three dimensional flows, with complex geometry these conditions are unlikely to be satisfied, as in this case. Therefore a more general system of comparison with experimental data, as proposed here, should be adopted. The drawback to any such system is however the need for extensive experimental data for validation. Of the statistics suggested in section 5.1 it seems clear that the most useful is that which is based on the repeatability of the experimental data. This gives a physically and statistically meaningful goodness of fit parameter which can be related locally to the flow features and turbulence levels, thereby highlighting the areas of concern in the CFD modelling.

6.2 Interpretation of the predicted temperature results

The predicted temperature results for the heated front half and fully loaded cases (section 4.2.5) appear unrealistic in terms of the absolute values. This is considered to be due to the simple heat load model incorporated in to these simulations (section 3.3.3) which included a single value for heat production, 0.4 W per bird, neglecting environmental effects on heat production and the sensible/latent balance of heat loss (section 1.2). The environmental effects on heat production can only be allowed for by a more complex heat load model, which would require further information about chick physiology. The contribution of evaporative heat loss could also be dealt with in this way, including source terms for water vapour into the simulation and thereby explicitly expressing the latent component, if a suitable model for the water loss from a day-old chick could be developed. However, given that this was not possible in this study due to the constraints of time and the limits of current knowledge about the physiological responses of day-olds (section 1.2), one can reinterpret the simple "dry" air temperature predictions in terms of possible temperature and relative humidity (RH) combinations.

The predicted temperatures (T_p) given previously are calculated from the computed specific enthalpy field (E) by division by the specific heat capacity of dry air (C_p). Therefore, if the results are considered in terms of

specific enthalpy, one may assess the predicted enthalpy rise in terms of a dry, sensible, component (E_d) and an evaporative, latent, component (E_w) such that $E = E_d + E_w$. Assuming reasonable inlet conditions for the temperature and RH, one can then calculate the predicted temperature and moisture content of the air amongst the load.

Consider for example a predicted dry temperature (T_p) which gives a specific enthalpy $E = C_p T_p$. Given the base temperature, and therefore the base enthalpy (E_b), one can calculate the rise in enthalpy $\Delta E = E - E_b$. If one can also specify the associated rise in water content of the air, expressed as a vapour density (V_D), then the enthalpy rise due to this extra

moisture is $\Delta E_w \approx \frac{\Delta V_D}{\rho} (L + C_p^{water} T)$ where ρ is the density of dry air, L is the latent heat of vaporisation of water ($\sim 2500 \text{ kJ kg}^{-1}$) and C_p^{water} is the specific heat capacity of water vapour ($\sim 1.88 \text{ kJ kg}^{-1} \text{ K}^{-1}$). Therefore the

expression for enthalpy, $E \approx C_p T + \frac{V_D}{\rho} (L + C_p^{water} T)$ can be rearranged to give

the dry bulb temperature equivalent $T \approx \frac{E - \frac{V_D L}{\rho}}{\left(C_p + \frac{V_D}{\rho} C_p^{water} \right)}$. From this

temperature and vapour density the RH value can be calculated with reference to standard psychrometric tables.

Consider the total heat production of a day-old chick to be 0.5 W and the global ventilation rate through the load of 50 000 chicks to be

5800 m³hr⁻¹ (1.61 m³s⁻¹). Then the total heat production of the load is 25 kW and the dispersal of this heat by the global ventilation rate implies an average energy [enthalpy] rise of 15.5 kJ m⁻³ [13.4 kJ kg⁻¹]. Also consider that a day-old chick loses ~0.2 g hr⁻¹ body weight during transport [Mitchell (1996)] which is almost entirely due to water loss and therefore evaporative heat loss. Therefore in the example above, 50 000 birds and 5800 m³hr⁻¹ global ventilation rate, the moisture content of the air will be increased by, on average, 1.7 g m⁻³ in steady state conditions. Assuming inlet conditions of 22 °C and 50% RH, which is not unreasonable given that the air is partially recirculated and air conditioned, this implies an inlet enthalpy of 43.0 kJ kg⁻¹ and a vapour density (VD) of 9.7 g m⁻³. Therefore the average outlet conditions must be an enthalpy of 43.0 + 13.4 = 56.4 kJ kg⁻¹ and a vapour density of 9.7 + 1.7 = 11.4 g m⁻³, neglecting other heat losses etc.. Those outlet conditions are then equivalent to ~30 °C and 38% RH; however, the average conditions are not those which challenge the birds thermoregulatory system within a load, it is the local micro-environment conditions.

Therefore, consider the peak predicted temperature in the front half loaded model simulation of 40 °C, which equates to a specific enthalpy of 40.2 kJ kg⁻¹. In this case, however one must also consider that the simulated inlet conditions were 22 °C and 0% RH, which implies an inlet enthalpy of 22.1 kJ kg⁻¹ and therefore an enthalpy rise of 18.1 kJ kg⁻¹. Substituting the

more realistic inlet conditions, 22 °C and 50% RH, in terms of the enthalpy and VD, gives a peak predicted enthalpy of 61.1 kJ kg⁻¹ and assuming a peak moisture content rise of twice the average, a VD of 13.1 g m⁻³. This is equivalent to ~32 °C and 39% RH. In the fully loaded case the peak predicted temperature was 45 °C and following the same calculation the equivalent environment would be ~36 °C and 32% RH.

These figures provide a more realistic idea of predicted conditions inside the load and, physiological considerations would suggest (section 1.2), one which may be acceptable to the chicks on average. In terms of the thermoneutral range of chicks, 32 °C - 36 °C, suggested in section 1.2, one might conclude that even the peak predicted temperatures are acceptable. However, as previously discussed, the more recent study of Mitchell (1996) would suggest that evaluation in terms of "apparent equivalent temperature" (AET) is more appropriate. For the mean and peak conditions discussed above the AET values are 56 °, 62 ° and 67 °C respectively. The value of 56 ° for the average conditions would, according to Mitchell, cause minimum thermoregulatory stress and therefore be acceptable for journey times up to the capacity of the yolk sac to provide nourishment and water, normally 48 - 72 hours after hatching. The peak conditions, however, could lead to an elevation in deep body temperature and associated physiological stresses which would reduce the maximum acceptable transport time.

These results suggest that in normal conditions, with journey times limited by distance within the UK, chicks are unlikely to experience extreme environmental stress. There is, however, a variation of conditions within the load which potentially might allow some birds to be heat stressed. On longer journeys this may represent a serious challenge to the chicks physiology.

6.3 Implications for transporter design and ventilation rate

Predicted ventilation rates with the loaded, heated cases also vary widely, giving values of between 3 and 85 ml s⁻¹ per bird with a mean of 20 ml s⁻¹ per bird (section 4.2.6). This variation again indicates how the wide range of suggested ventilation rates given in table III is representative only of the variety of situations considered by the authors of the work summarised in that table. It is however important to notice that even the lowest predicted ventilation rates provide ~100 times the oxygen requirement of a day-old chick (table II) and therefore it is heat dissipation that is the major role of the ventilation system.

The ventilation rate achieved for a chick box in any given position within the load clearly depends on the design of the ventilation system and although in this study only one type and design of system was considered a number of interesting features were apparent. Consider, for example, the ceiling jet holes. These provide a surprisingly even distribution of air along the length of the load space because of the tapered ducts in the false ceiling. Also because of the angle of the issuing jets, the air within the load space is itself circulated from front to rear before being drawn forward by the recirculation fan vents. These vents provide the driving force for the dominant forward flow in the lower part of the load space and therefore through the load itself. The position, and size, of these vents is therefore a

dominant factor in the establishment of the flow pattern within the load space and of the ventilation rates achieved in the various layers of the load. This is demonstrated by the consistently high ventilation rates predicted close to the front vents and the low rates amongst the top shelf of chick boxes.

Another major factor in determining ventilation rate in these simulations was the inclusion of the floor ducts in the non-isothermal cases. These effectively allowed air to bypass the load and thus reduced the local ventilation rate despite significantly increased global ventilation rate. This is not to suggest that the simple removal of such ducts will improve conditions, only that the placement of such ducts needs to be considered in conjunction with the position of the load so that air is effectively delivered to the chick boxes. Also in these simulations a simple atmospheric pressure boundary condition was assumed at these floor ducts because the pressure field beneath the vehicle is unknown, but in reality the complex underbody flow of a transporter is likely to present a complex pressure field including both suction and overpressures. This will not negate these results, but will possibly lead to further unexpected features within the load space flow pattern.

The achieved local ventilation rate as a proportion of the global ventilation rate is also affected by the loading arrangement adopted within

the load space. The significant effect of channelling between the shelves of chick boxes has been discussed previously and it is this which provides high ventilation rates for boxes on the edges and top of stacks compared to those within the body of the load. The corresponding high temperatures within the body of the load are thus generated. These effects are compounded by the insulating and flow retarding properties of the chick box itself, which are a function of its design and may be a significant factor in defining conditions for day-old chicks [Henken *et al* (1987)].

Whatever the design effects of the chick box, however, the stacking of boxes is clearly an important factor, with increased ventilation rate where the top or sides of boxes are open to free moving air, especially where buoyant flows are present. Thus the optimum strategy must combine the provision of open space between boxes for ventilation without excessive channelling effects or bypassing because of open floor ducts.

7 Conclusions and recommendations for further work

This section contains a summary of the overall conclusions reached as a result of this work and a list of points which are recommended for inclusion in any future projects of this type. The detailed discussion of these points can be found in the preceding chapters.

7.1 Conclusions

Experimental measurements

1. The experimental measurements collected using the ultrasonic vector anemometer were successful in capturing the full spectrum of turbulence present in the air flow.
2. The size of the instrument however, precluded measurement amongst the load and in the confined spaces of the load space.
3. The physical modelling of the load space with the multiple fan arrangement rather than the single fan present in the actual vehicle was probably significant in producing the asymmetric effects seen in the results. This suggests fan arrangement is a significant factor to be considered in ventilation system design.
4. The design of the tapered false ceiling ducts is effective in producing relatively even ceiling jet speeds along the length of the vehicle load space.

5. The position, size and distribution of ceiling jet holes and recirculation vents are dominant in the establishment of the flow pattern in this vehicle design.
6. Significant experimental run times are required in this environment in order to achieve meaningful quasi-steady results, which indicates the unsteadiness of the overall flow.
7. The autocorrelation and length scale results suggest that the flow in the model vehicle is less stable than that in the actual transporter.
8. No prominent frequencies were seen in the spectra of either the model or the actual vehicle.
9. Turbulent kinetic energy (TKE) levels are generally high ($>0.1 \text{ J kg}^{-1}$) in the jet mixing region but are also significant in the lower sections of the empty load space. The presence of the load however reduces TKE to very low levels amongst the chick boxes.
10. The presence of the load also destroys any larger scale turbulent structures within the flow.
11. The unsteadiness of the flow in all cases meant that no significant cross-correlation was found between spatially separated points.

Numerical simulations

12. To include the detail of the false ceiling ducts and holes *etc.* would require an excessively fine grid and therefore simplifications are required for simulation purposes.

13. The results of the simulations are however sensitive to these type of boundary condition simplifications in the momentum equations although not to the values of turbulence model variables (k and ϵ).
14. The mean flow patterns predicted show similar qualitative features to the experimental results.
15. The simulation results generally over-predict the levels of TKE in the ceiling jets and under-predict the levels elsewhere in an empty load space.
16. The reduction of the simulated boundary condition jet inlet speed improves agreement with the experiment both in terms of the mean flow and TKE.
17. The grid independence of these results is not clear and some improvement in results is possible from the increased resolution of gradients within the jet region of the flow.
18. The simplification of the inlet jets to a line source is also likely to be a contributing factor in the under-prediction of the jet penetration as is the overly diffusive nature of the turbulence model used.
19. Load resistance is an important factor in the determination of the overall flow field, with loading arrangement and porosity model both giving significant effects.
20. TKE levels within the load are poorly represented due to the artificial generation of TKE within the porous media.
21. The secondary flow through the chick boxes in the fully loaded case is not in qualitative agreement with experiment, suggesting that the method of

bulk porosity as a description of the load may be overly simplified for largely blocked cases.

22. The limitations of the $k-\epsilon$ model are evident in these results and the need for a turbulence model capable of coping with the restricted flow and porous media problems encountered is highlighted.

Non-isothermal numerical simulations

23. The effect of the presence of the underfloor ducts may not be a simple one, with air flow both in and out of the vehicle by this route.

24. Vehicle underbody flow needs to be considered as this may have unforeseen effects on the internal environment of transporters if underfloor ducts are used.

25. Air heated by the load may be recirculated within the load space rather than be drawn into the air conditioning system, leading to raised temperatures in some areas of the load.

26. Flow patterns in the non-isothermal cases appear similar to those in the isothermal case because of the lack of large vertical openings allowing buoyant movement.

27. The simple heat load model used predicts very high temperatures which are considered to be unrealistic. Therefore either a more complex combined heat and moisture production model is required or the results need to be interpreted as change in enthalpy rather than temperature.

28. Enthalpy considerations suggest that the average thermal conditions predicted by the numerical model would be acceptable for journeys of up to 48 hours. The extremes of the predictions could however lead to physiological stress in some parts of the load thereby limiting this safe duration.

Ventilation rates

29. Wide variation in the predicted ventilation rates was found in each loading case, suggesting that air distribution is not even through the load.

30. Validation data for the ventilation rates are necessary to evaluate the contribution of turbulence to ventilation rate.

31. The results suggest that oxygen deprivation is not a significant problem with this design of vehicle. Heat dissipation is considered to be the major environmental factor which must be addressed by any control strategy.

32. Local ventilation rate is not a simple function of global ventilation rate because flow distribution in the load space is not uniform.

33. The stacking arrangement of chick boxes is significant in determining the conditions during transport.

Comparison of experimental and numerical data

34. A comparison methodology for complex three dimensional flows is presented, based on the cell by cell evaluation of numerical simulations with experimental data.

35. This method requires extensive experimental data in order to validate a numerical simulation adequately.

36. Comparison in terms of an acceptability criteria based on the repeatability of experimental measurements has been found to be most successful in this case.

37. The effect of loading arrangement on flow stability was found to be significant and therefore comparisons of loading arrangement should consider this effect and its implications for numerical simulations.

38. Statistical comparison demonstrates good agreement between the experimental and numerical results for the mean flow in the empty and partially loaded cases. Agreement for TKE and in the fully loaded cases was generally poor although in the latter the experimental data is less extensive.

39. Statistical comparison is valuable in giving a quantitative measure of accuracy for numerical simulations, although it should be used in conjunction with visual comparison of the flow field.

7.2 Recommendations for further work

This section contains a summary of the previously discussed points which are considered to be important in any future work of this type.

Experimental measurements

1. The inclusion of measurements in the confined spaces amongst the load.
2. Assessment of the effects of single and multiple fan systems.
3. Assessment of the possibility of simplifying the false ceiling design to reduce the resistance to flow.
4. The comparative study of different vehicle designs and ventilation systems.
5. The collection of underbody pressure data for commercial vehicles to assess the effect of open floor ducts on internal ventilation.
6. The collection of physiological data on the heat and moisture production of day-old chicks in a range of environmental conditions to allow a model of physiological response to be developed for numerical modelling.
7. The collection of ventilation rate data for individual chick boxes to allow validation of numerical models and to evaluate the contribution of turbulence to local ventilation.

Numerical simulations

1. The inclusion of the false ceiling *etc.* to reduce the boundary condition sensitivity.

2. Improvement of the grid resolution in important areas such as the inlet jets.
3. The inclusion of sinks for TKE within the modelled load to reduce over-predictions in this region.
4. Turbulence model development for porous media and restricted flow problems such as loaded chick transport vehicles.
5. Development of an improved model to describe the load which overcomes the problems associated with the bulk porosity model.
6. The inclusion of a heat and moisture production model to represent the presence of the birds and their effect on the environment.

7.3 General conclusions for CFD modelling

1. CFD modelling can be used successfully for predicting internal mean flows if sufficient care with boundary conditions is taken.
2. Turbulence levels are not predicted well in such flows by the k- ϵ model because of the well known problems associated with this model. Recent modifications to the model [Kato and Launder (1993), Craft *et al* (1995), Kawamoto (1996) and Murakami *et al* (1996)], although not developed for internal flows, may improve predictions because of more suitable behaviour in streamline curvature, pressure gradients *etc.*.
3. Porous media models based on bulk porosity coefficients may not be the most appropriate way of modelling obstructions in the flow if these obstructions are not homogeneous.
4. Where livestock is concerned sensible heat production/temperature alone is not sufficient to describe the thermal environment and moisture production/humidity must also be considered.
5. Validation data for numerical models of complex flows must be extensive and unbiased in location if general conclusions about the simulated flow are to be drawn. Validation methodology must also be equally unbiased and should account for the variability in experimental data.

References

- Abbot, M.B. and Basco, D.R. (1989). Computational fluid dynamics - an introduction for engineers. Longman Scientific and Technical.
- Acheson, D.J. (1990). Elementary Fluid Dynamics. Oxford University Press.
- Agriculture Canada (1989). Recommended code of practice for the care and handling of poultry from hatchery to processing plant. pp. 12-13.
- Alsam, H. and Wathes, C.M. (1991a). Conjoint preferences of chicks for heat and light intensity. *British Poultry Science* 32: 899-916.
- Alsam, H. and Wathes, C.M. (1991b). Thermal preferences of chicks brooded at different air temperatures. *British Poultry Science* 32: 917-927.
- Anon. (1988). Comfort and style for chicks on the move. *Poultry World* (April) p.17.
- Baker, C.J.; Dalley, S.J.; Yang, X.; Kettlewell, P.J. and Hoxey, R.P. (1996). An investigation of the aerodynamics and ventilation characteristics of poultry transport vehicles: Part II Wind tunnel experiments. Submitted to *Journal of Agricultural Engineering*.
- Bakken, G.S. (1991). Wind speed dependence of the overall thermal conductance of fur and feather insulation. *Journal of Thermal Biology* 16 (2): 121-126.
- Banks, S. (1983). Anatomy of a chick transporter. *World Poultry* (September) p.22.
- Bendat, J.S. and Piersol, A.G. (1980). *Engineering applications of correlation and spectral analysis*. John Wiley and Sons. New York.
- Berckmans, D.; Goedseels, V. and Geers, R. (1986). Development of a controller for livestock buildings based on an airflow rate measurement device. *Proceedings of the first European symposium on air conditioning and refrigeration*. Brussels. pp 61-68.
- Boon, C.R. (1978). Airflow patterns and temperature distributions in an experimental piggery. *Journal of Agricultural engineering research* 23: 129-139.
- Boon, C.R.; Andersen, M. and Harral, B.B. (1994). Dynamics of particulate pollutants in an experimental livestock building. *ASAE paper* 94-4586.
- Booty, J. (1982). Recommended practice for airfreighting poultry p.7 in *Papers from the conference on Airfreighting hatching eggs and day old poultry* eds Dr W.K.Smith. The West of Scotland Agricultural College, Auchincruive, Ayr, Scotland.
- Burger, R.E. (1989). Bird death at high temperatures. *Poultry Advisor* 22 (4): 21-24.
- Carpenter, G.A. (1981). Ventilation systems. pp.351-370 in Environmental aspects of housing for animal production. Eds. J.A.Clark. Butterworths, London.
- Charles, D.R. (1981). Practical ventilation and temperature control for poultry. pp.183-196 in Environmental aspects of housing for animal production. Eds. J.A.Clark. Butterworths, London.

- Charles, D.R. (1986). Temperature for broilers. *Worlds Poultry Science Journal* 42 (3): 249-258.
- Chow, C-Y. (1979). An introduction to computational fluid mechanics. John Wiley and Sons, New York.
- Craft, T.J.; Launder, B.E. and Suga, K. (1995). A non-linear eddy-viscosity model including sensitivity to stress anisotropy. *Proceedings 10th Turbulent shear flows symposium, Pennsylvania State University*.
- Daghir, N. (1988). Ten measures to overcome heat stress. *Poultry International* (January) p.19.
- Dalley, S.J.; Baker, C.J.; Yang, X.; Kettlewell, P.J. and Hoxey, R. (1996). An investigation of the aerodynamics and ventilation characteristics of poultry transport vehicles: Part III Internal flow field calculations. Submitted to *Journal of Agricultural Engineering*.
- Deaton, J.W. (1983). Alleviation of heat stress for avian egg production - a review. *Worlds Poultry Science Journal* 39 (3): 210-217.
- EU (1991). Council directive of 19th November 1991 on the protection of animals during transport. *Official Journal of the European Communities - Legislation* 34 (11th December): L340 17-27.
- Ernst, R.A.; Weathers, W.W. and Smith, J. (1984). Effects of heat stress on day-old broiler chicks. *Poultry Science* 63 (9): 1719-1721.
- Freeman, B.M. (1984). Transportation of poultry. *Worlds Poultry Science Journal* 40 (1): 19-30.
- Freitas, C.J. (1995). Perspective: Selected benchmarks from commercial CFD codes. *Trans. ASME. Journal of fluids engineering*. Vol. 117. pp. 208-218.
- Gill Instruments Ltd (1992). 3 axis research ultrasonic anemometer - Product specification issue 4.1. Solent House, Cannon Street, Lympington, Hampshire, SO41 9BR.
- Gould, A. (1996). Industrial perspectives of turbulence modelling and DNS. Presented to the High performance computational engineering in the UK meeting. Daresbury Laboratory, Cheshire, 18th-19th March.
- Heber, A.J. and Boon, C.R. (1993). Air velocity characteristics in an experimental livestock building with non-isothermal jet ventilation. *ASHRAE transactions* 99: 1139-1151.
- Henken, A.M.; Van der Hel, W.; Hoogerbrugge, A. and Scheele, C.W. (1987). Heat tolerance of one-day old chickens with special reference to conditions during air transport pp.261-287 in Energy metabolism in farm animals. Eds. A.M.Henken & M.W.Verstegen. Martinus Nijhoff.
- Henken, A.M. and Van der Hel, W. (1990). Give newly hatched chicks a safe flight. *Misset World Poultry* (February) pp.8-9.

- Henken, A.M.; Van der Hel, W. and Hamdy, A.M. (1991a). Effects of air humidity during incubation and age after hatch on heat tolerance of neonatal male and female chicks. *Poultry Science* 70: 1499-1506.
- Henken, A.M.; Van der Hel, W. and Hamdy, A.M. (1991b). Effects of incubation humidity and hatching time on heat tolerance of neonatal chicks: growth performance after heat exposure. *Poultry Science* 70: 1507-1515.
- Herbut, E.; Pietras, M. and Sokolowicz, Z. (1992). Effect of differentiated thermal conditions on heat production and feed consumption in chickens. *Roczniki Naukowe Zootechniki, Monografie I Rozprawy*. No. 31 pp. 295-303.
- Hinds, R.H. (1958). Baby chick transportation - problems and equipment. US dept of Agriculture report no. 267.
- Hoogerbrugge, A. and Ormel, H.J. (1982). Transport of day old chicks by air. pp.139-146 in Transport of animals intended for breeding, production and slaughter. Eds. R.Moss. Martinus Nijhoff.
- Hope, D. and Milholland, D. (1993). A three-dimensional ultrasonic anemometer to measure the performance of clean zone air delivery systems. *Journal of the IES*. 36 (6): 32-40.
- Hoxey, R.P.; Yang, X.; Baker, C.J. and Meehan, A.M. (1992). Preliminary research on the aerodynamic ventilation characteristics of chicken transporter lorries. Paper at Wind Engineering Society Conference 30th September. Cambridge, UK.
- Hoxey, R.P.; Kettlewell, P.J.; Meehan, A.M.; Baker, C.J. and Yang, X. (1996). An investigation of the aerodynamics and ventilation characteristics of poultry transport vehicles: Part I : Full-scale measurements. Submitted to *Journal of Agricultural Engineering*.
- Joshi, S.R. and Kulkarni, M.V. (1986). Hatchery management series - 6 - transport of chicks and sanitation of hatchery. *Poultry Advisor* 19 (2): 33-36.
- Kakaç, S.; Ramesh, K.S. and Aung, W. (1987). Handbook of single-phase convective heat transfer. John Wiley & Sons, New York.
- Kato, M. and Launder, B.E. (1993). The modelling of turbulent flow around stationary and vibrating square cylinders. *Proceedings 9th Symposium turbulent shear flows*. 10-4: 1-6.
- Kawamoto, S. (1996). Improved turbulence models for estimation of wind loading. Presented at the second international symposium on computational wind engineering, Colorado state University. August 4th-8th.
- Kettlewell, P.J. (1989). Physiological aspects of broiler transportation. *Worlds Poultry Science Journal* 46: 219-227.
- Launder, B.E. and Spalding, D.B. (1974). The numerical computation of turbulent flow. *Comp. meth. appl. mech. eng.*. Vol. 3. pp. 269-289.

- Leschziner, M.A. (1989). Modelling turbulent recirculating flows by finite volume methods - current status and future directions. *International Journal of Heat and Fluid Flow* 10 (3): 186-202.
- Leschziner, M.A. (1995). Modelling turbulence in physically complex flows. Invited keynote lecture. XXVI IAHR congress "Hydra 2000". London. Sept. 1995.
- Macleod, M.G. (1982). The effect of travel on day old chicks (Summary) pp. 3-5. in *Papers from the conference on Airfreighting hatching eggs and day old poultry* eds Dr W.K.Smith. The West of Scotland Agricultural College, Auchincruive, Ayr, Scotland.
- MAFF (1987). Codes of recommendations for the welfare of livestock: Domestic fowls. pp. 6-9.
- MAFF (1988). The Welfare of Poultry (Transport) Order 1988.
- MAFF (1993). Statistics - Hatching eggs and placings by hatcheries in the United Kingdom. 29th April.
- MAFF (1995). Statistics - Hatching eggs and placings by hatcheries in the United Kingdom. 3rd March.
- Mehta, U.B. (1991). Some aspects of uncertainty in CFD results. *Journal of Fluids Engineering - Transactions of the ASME* 113 (4): 538-543.
- Misson, B.H. (1976). The effects of temperature and RH on the thermoregulatory responses of grouped and isolated neonate chicks. *Journal of Agricultural Science* 86: 35-43.
- Mitchell, M.A. and Kettlewell, P.J. (1993). Catching and transport of broiler chickens. *Proceedings IVth European symposium on poultry welfare*. UFAW. pp 219-229.
- Mitchell, M.A. (1996). The thermal micro-environment experienced by one-day old chicks during road transportation: physiological responses during transport simulations. Private communication of unpublished report.
- Moreng, R.E. and Shaffner, C.S. (1951). Lethal internal temperatures for the chicken, from fertile egg to mature bird. *Poultry Science* 30 (2): 255-266.
- Mount, L.E. (1974). The concept of thermal neutrality. Chap. 21 in Heat loss from animals and man. (1974) Eds. Monteith, J.L. and Mount, L.E. Butterworths. London.
- Mount, L.E. (1979). Adaptation to thermal environment. Arnold. London.
- Muller, W. (1985). Ventilation requirements during air animal transport. Paper at 11th International Conference Animal Air Transportation Association. March 1985. Tampa, Florida, USA.
- Murakami, S.; Mochida, A.; Kondo, K.; Ishida, Y. and Tsuchiya, M. (1996). Development of new k- ϵ model for flow and pressure fields around bluff body. Presented at the second international symposium on computational wind engineering, Colorado state University. August 4th-8th.

Patankar, S.V. and Spalding, D.B. (1972). A calculation procedure for heat, mass and momentum transfer in three-dimensional parabolic flows. *International Journal of Heat and Mass Transfer*. 15: 1787-1806.

Patankar, S.V. (1980). Numerical heat transfer and fluid flow. Hemisphere publishing corporation.

Poczopko, P. (1981). The environmental physiology of juvenile animals pp. 109-130 in Environmental aspects of housing for animal production. Eds. J.A.Clark. Butterworths. London.

Prabakaran, R. (1990). Alleviating heat stress. *Poultry Advisor* 23 (3): 33-35.

Qureshi, A.A. (1991). Losses due to dehydrated broiler chicks. *Misset World Poultry* 7 (4): 75-79.

Randall, J.M. (1977). A handbook on the design of a ventilation system for livestock buildings using step control and automatic vents. NIAE report no. 28. Silsoe Research Institute, Wrest Park, Silsoe, Beds.

Randall, K. (1993). Poultry world annual market report. *Poultry World* (September) pp. 14-23.

Randall, K. (1995). Poultry world annual market report. *Poultry World* (September) pp. 14-24.

Roberts, D.H. (1987). Baby chicks require special care during flights. *Misset World Poultry* (December) pp. 48-50.

Sainsbury, D.W.B. (1981). Health problems in intensive animal production. pp.439-454 in Environmental aspects of housing for animal production. Eds. J.A.Clark. Butterworths. London.

Singh, S.K. (1988). Coping with high temperatures. *Poultry International* (January) pp. 16-18.

Spiegel, M.R. (1968). Mathematical Handbook of formulas and tables. Schaum's outline series. McGraw-Hill.

Tamlyn, J. and Starr, J.R. (1987). Monitoring environment during transportation of day-olds. *International Hatchery Practice* 1 (6): 11-17.

Tennekes, and Lumley,. (1972). A first course in turbulence. MIT press.

Turner, L.W.; Gates, R.S.; Turner, G.M. and Tuttle, J.W. (1992). Heat and moisture production of day-old chicks. submitted to *Trans ASAE*.

UMIST (1995). Turbulence modelling for CFD. 20th-23rd June and 5th-8th Sept. course notes.

UMIST (1996). Proceedings of the 7th Biennial Colloquium on Computational Fluid Dynamics. 2nd-3rd May.

Van der Hel, W.; Henken, A.M.; Verstegen, M.W. and Brandsma, H.A. (1991). The upper critical ambient temperature in neonatal chicks. *Poultry Science* 70: 1882-1887.

Wathes, C.M. (1981). Insulation of animal houses. pp.379-412 in Environmental aspects of housing for animal production. Eds. J.A.Clark. Butterworths. London.

Wathes, C.M. (1992). Ventilation. pp.83-91 in Farm animals & the environment. Eds. C.J.C.Phillips and D.Piggins. CAB International, Wallingford.

Williams, C.; Godfrey, G.F. and Thompson, R.B. (1951). The effect of rapidity of hatching on growth, egg production, mortality and sex ratios in the domestic fowl. *Poultry Science* 30 (4): 599-606.

Wilson, W.O. and Plaister, T.H. (1951). Breed differences in heat tolerance of day old baby chicks. *Poultry Science* 30 (4): 625-627.

World Meteorological Organization. (1989). Animal health and production at extremes of weather. Technical note no.191. WMO Report no. 685.

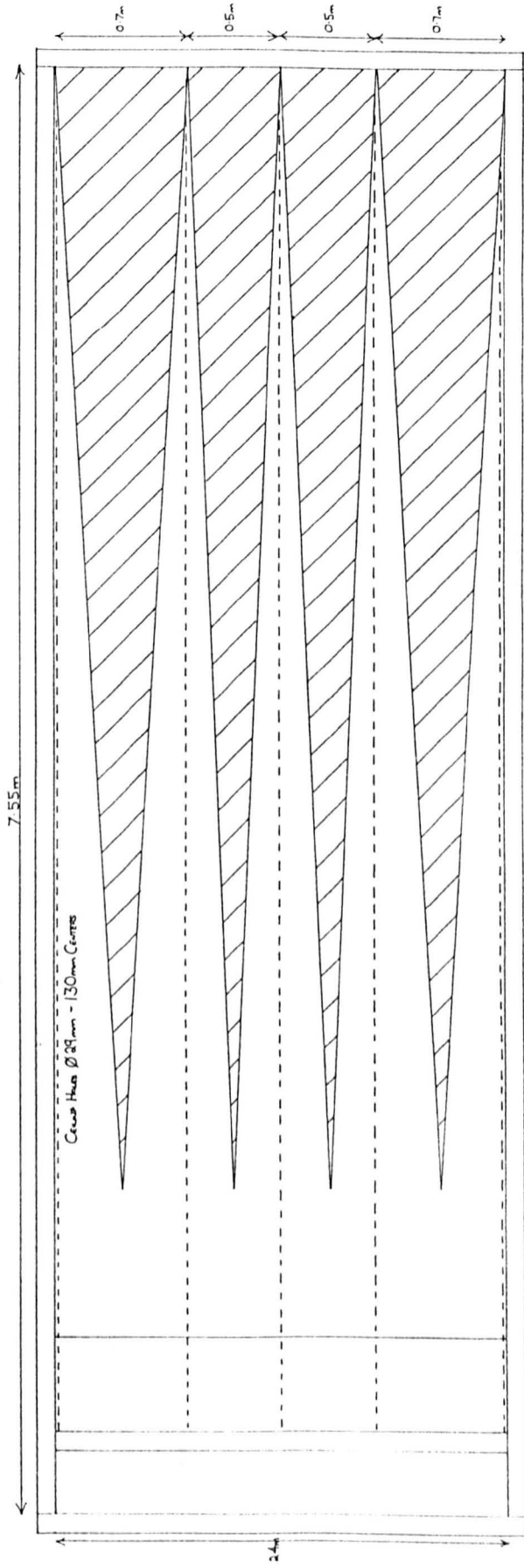
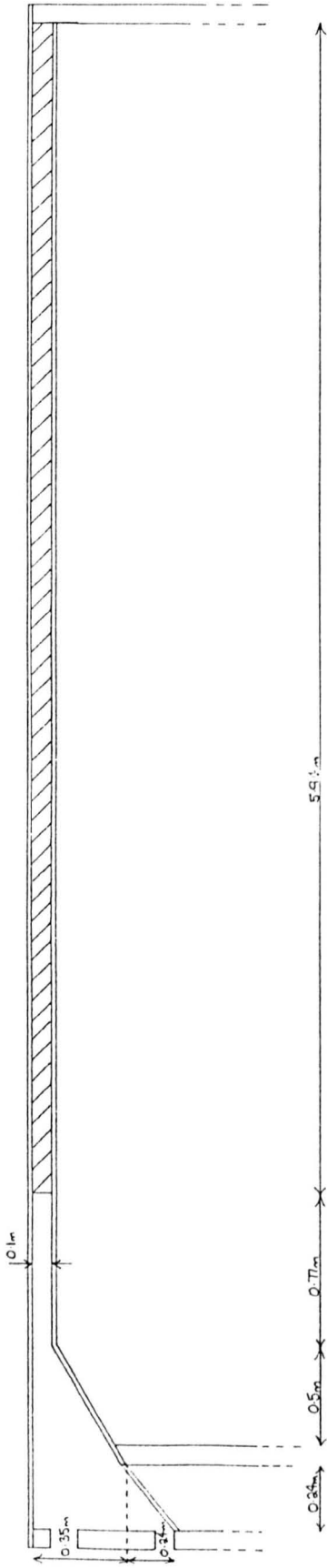
Yost, M.G. and Spear, R.C. (1992). Measuring indoor airflow patterns by using a sonic vector anemometer. *American Industrial Hygiene Association Journal* 53 (11): 677-680

Appendices

appendix 1 Experimental model construction

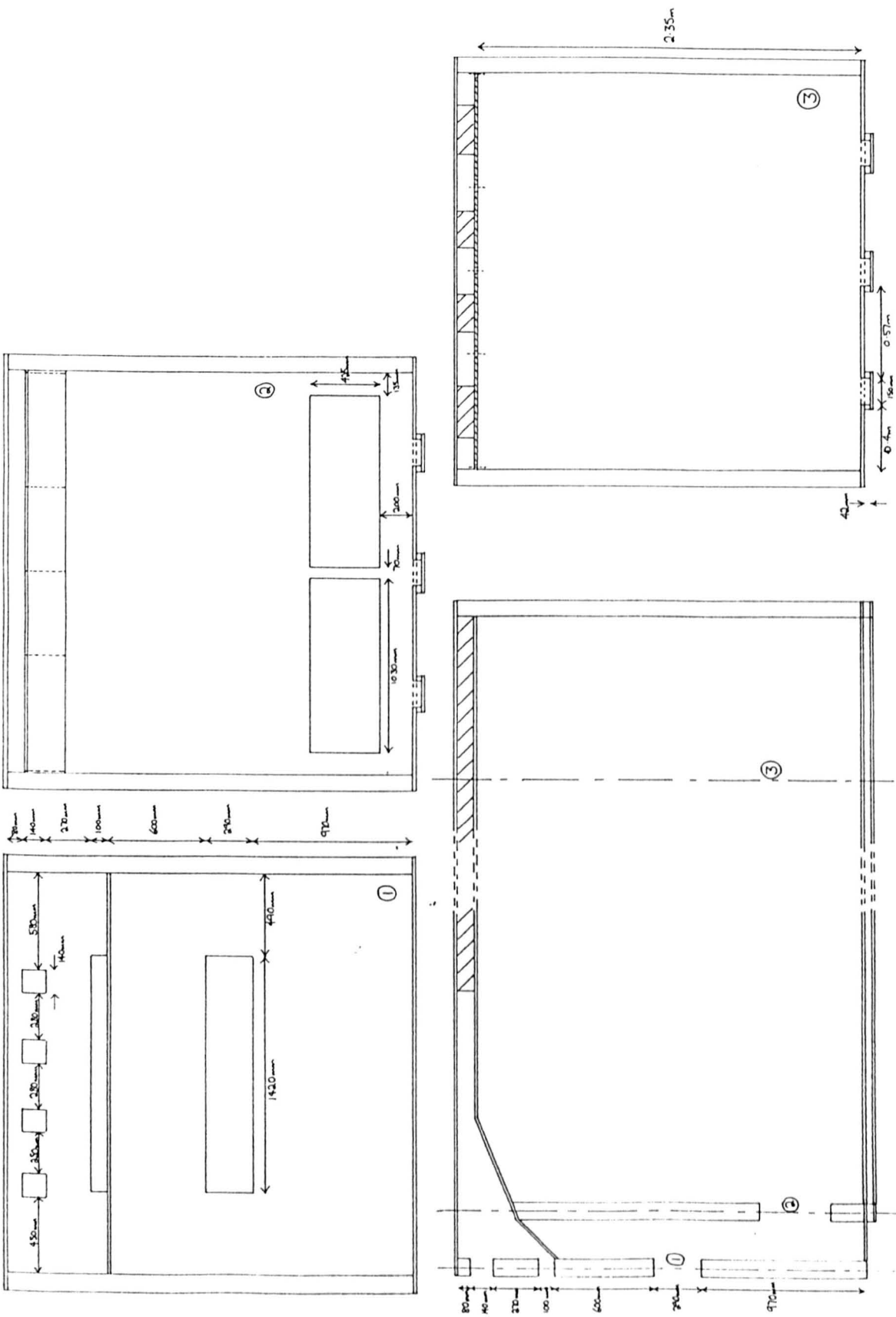
In this section the plans detailing the full scale experimental model construction are given. The model framework was constructed from 4" × 2" softwood clad with ¼" plywood for the false ceiling and ¾" sterling board elsewhere. The inside of the model was painted with standard emulsion to seal the surface and the construction joints were sealed with silicon sealant to create a nominally airtight container. Around the door, a standard hardwood internal door in the rear of the load space, draught excluder was used to give a nominal seal. This technique was also used around the metal fan hood in conjunction with silicon sealant. The floor ducts were sealed with sterling board cover plates and cloth backed plastic masking tape.

Figure A1.1 shows the measurements concerning the false ceiling space and figure A1.2 shows the relationship between this and the load space. The floor duct cover detail is given in figure A1.3, although these were not used in these experiments. Figure A1.4 shows the metal cover which is present in the vehicle and which is used to restrict the air flow through the centre three rows of holes on the angled ceiling plate at the front of the load space. Figures A1.5 and A1.6 show views of the fan rig which was used to mount the recirculation fans used in these experiments. Above the outlets of the fan rig was a metal cover plate which directed the air into the false ceiling space, this cover is detailed in figure A1.7. Finally figure A1.8 is a diagram of the trolley used throughout these experiments to hold the empty chick boxes with the load space. This was constructed from 30 mm × 3 mm × 90° angle steel bar and mounted on either flat plates (shown) or casters.



AQUINN LAB. VEHICLE - CEILING DETAIL (PLAN & SIDE VIEW c/s) 28th - 6 - 93

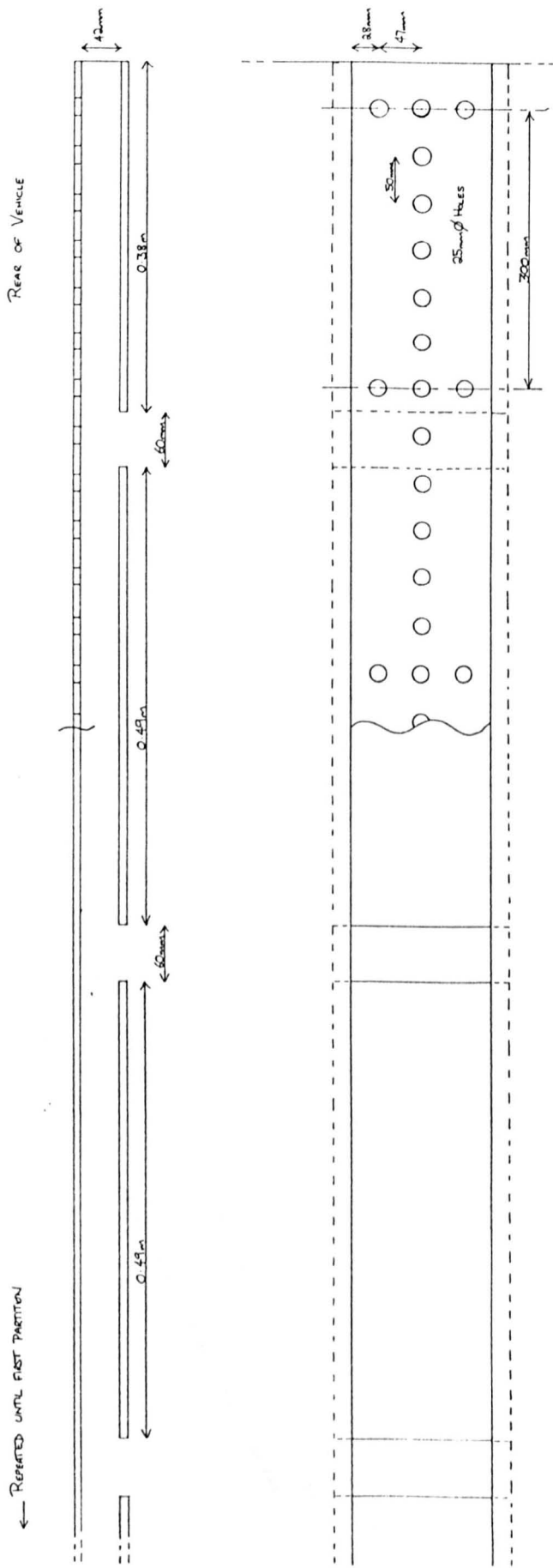
Figure A1.1 Vehicle model plan



28th-6-93

AQUINN LAB. VEHICLE ~ SIDE AND END VIEW c/s.

Figure A1.2 Vehicle model plan



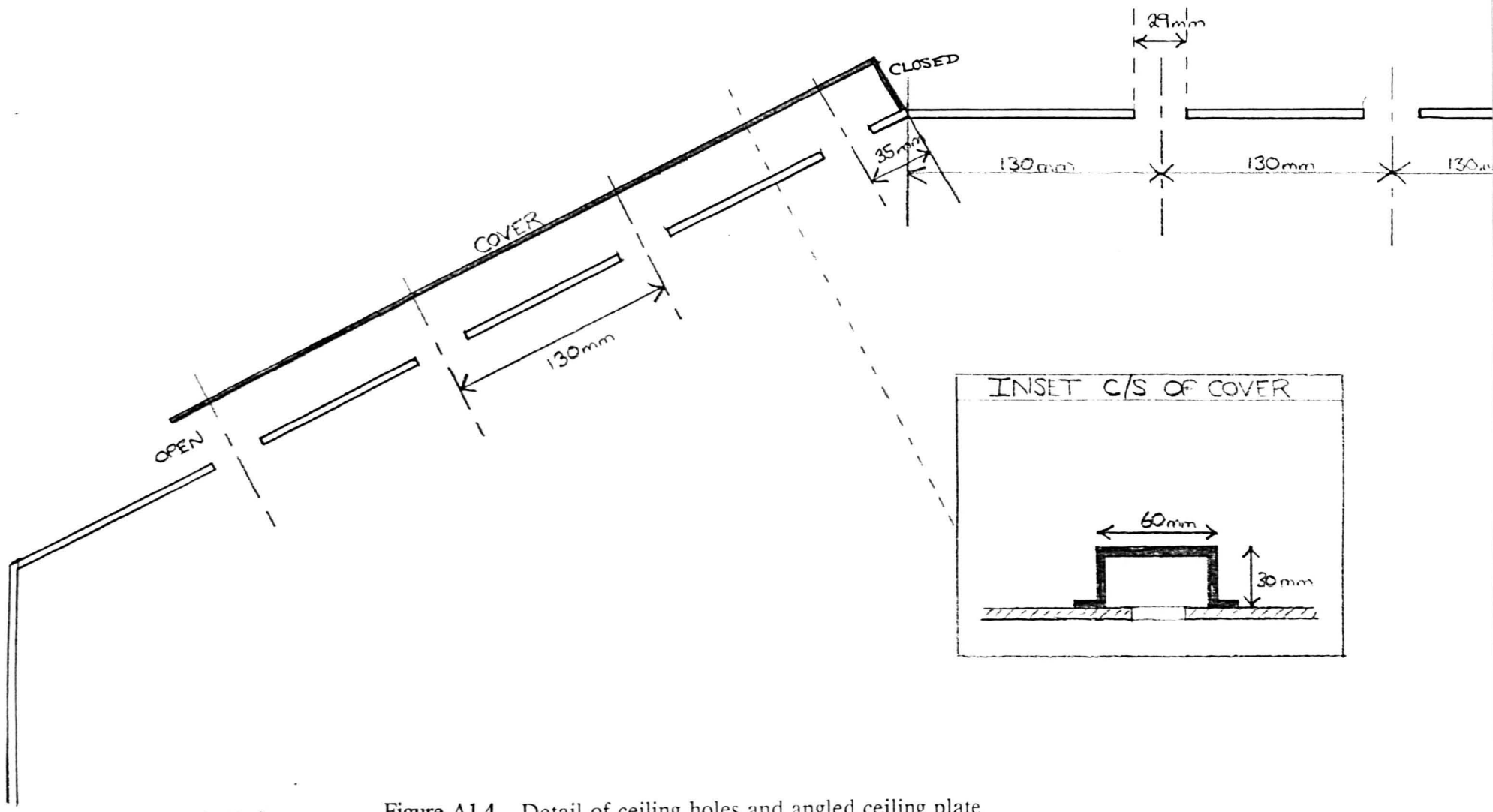
28th-6-93

(PLAN & SIDE VIEW c/s)

LAB. VEHICLE - FLOOR DUCT DETAIL

A QUINN

Figure A1.3 Vehicle model plan



A QUINN

Figure A1.4 Detail of ceiling holes and angled ceiling plate

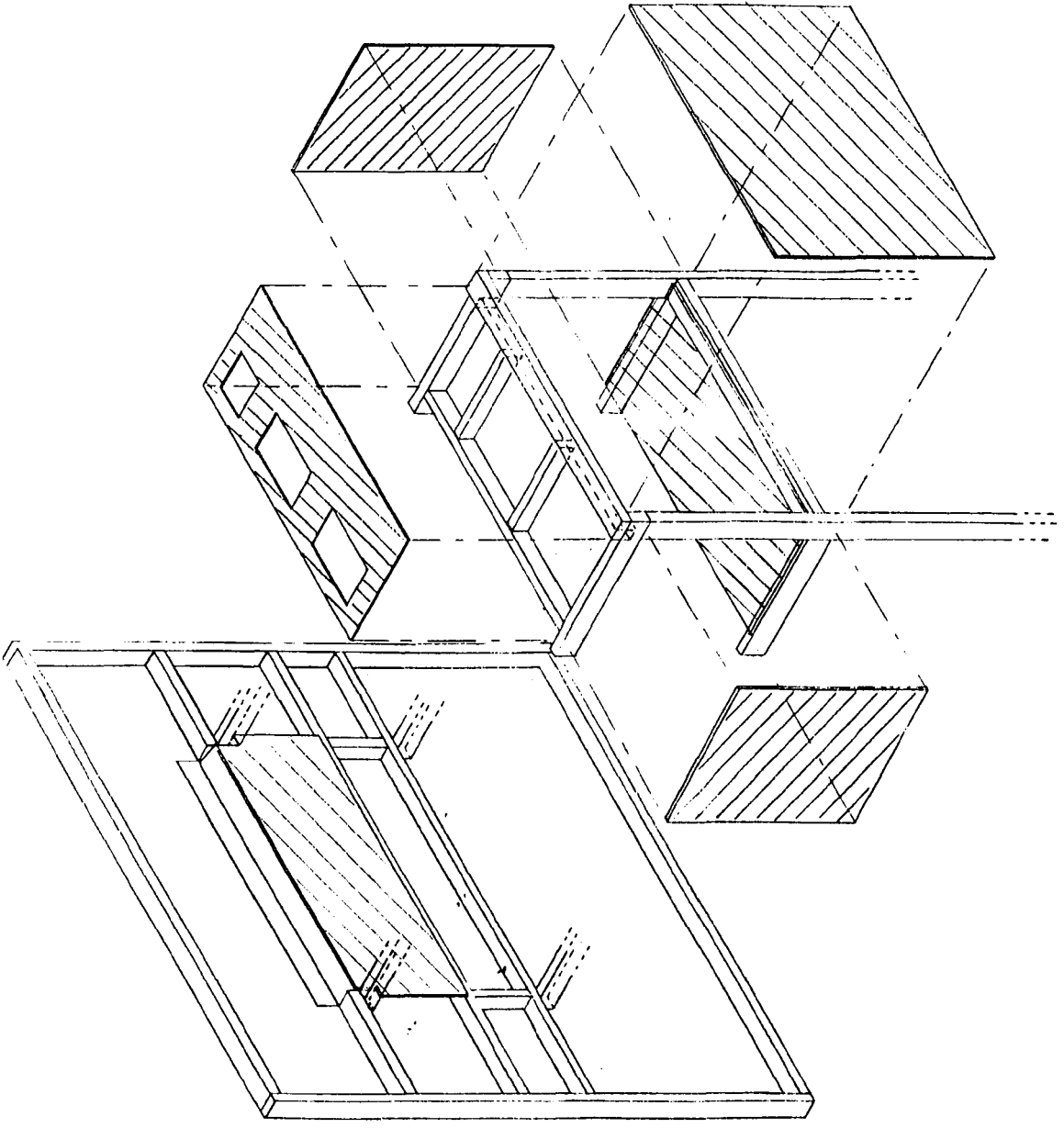


Figure A1.5 Fan mounting rig

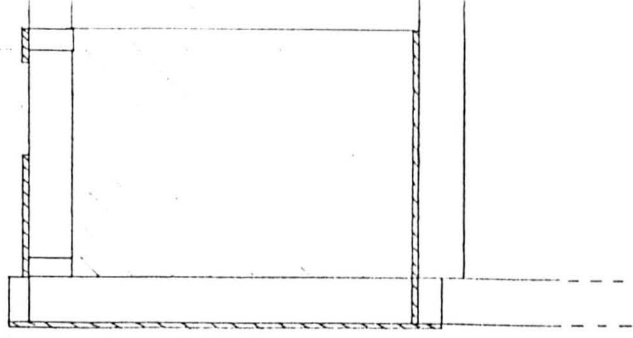
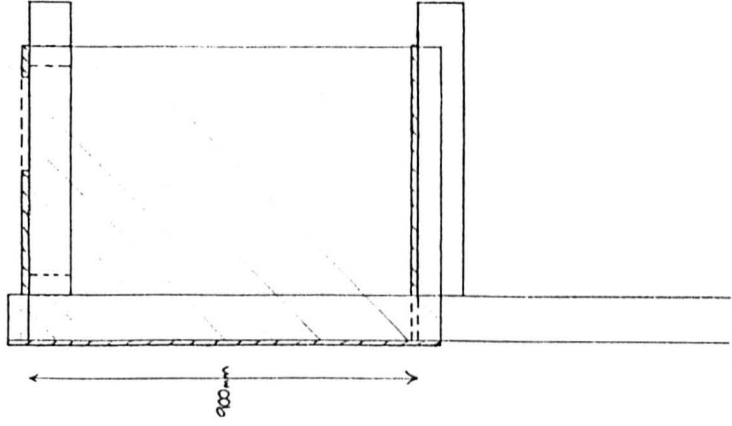
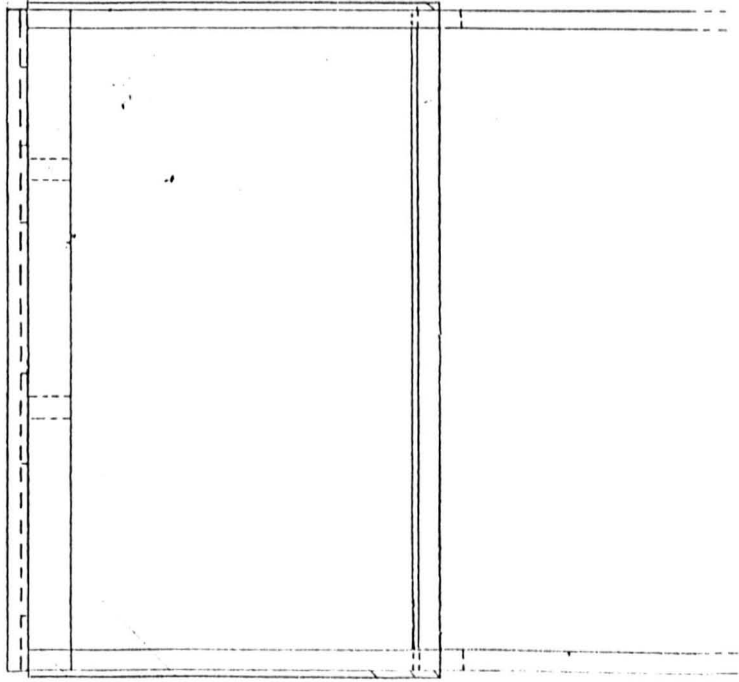
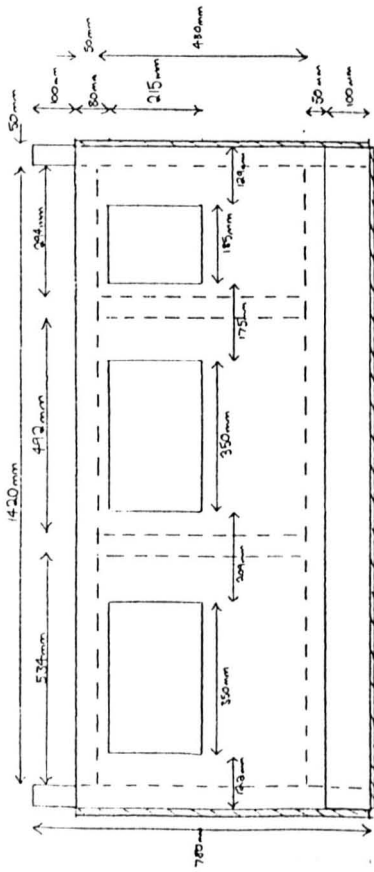


Figure A1.6 Fan mounting rig plan

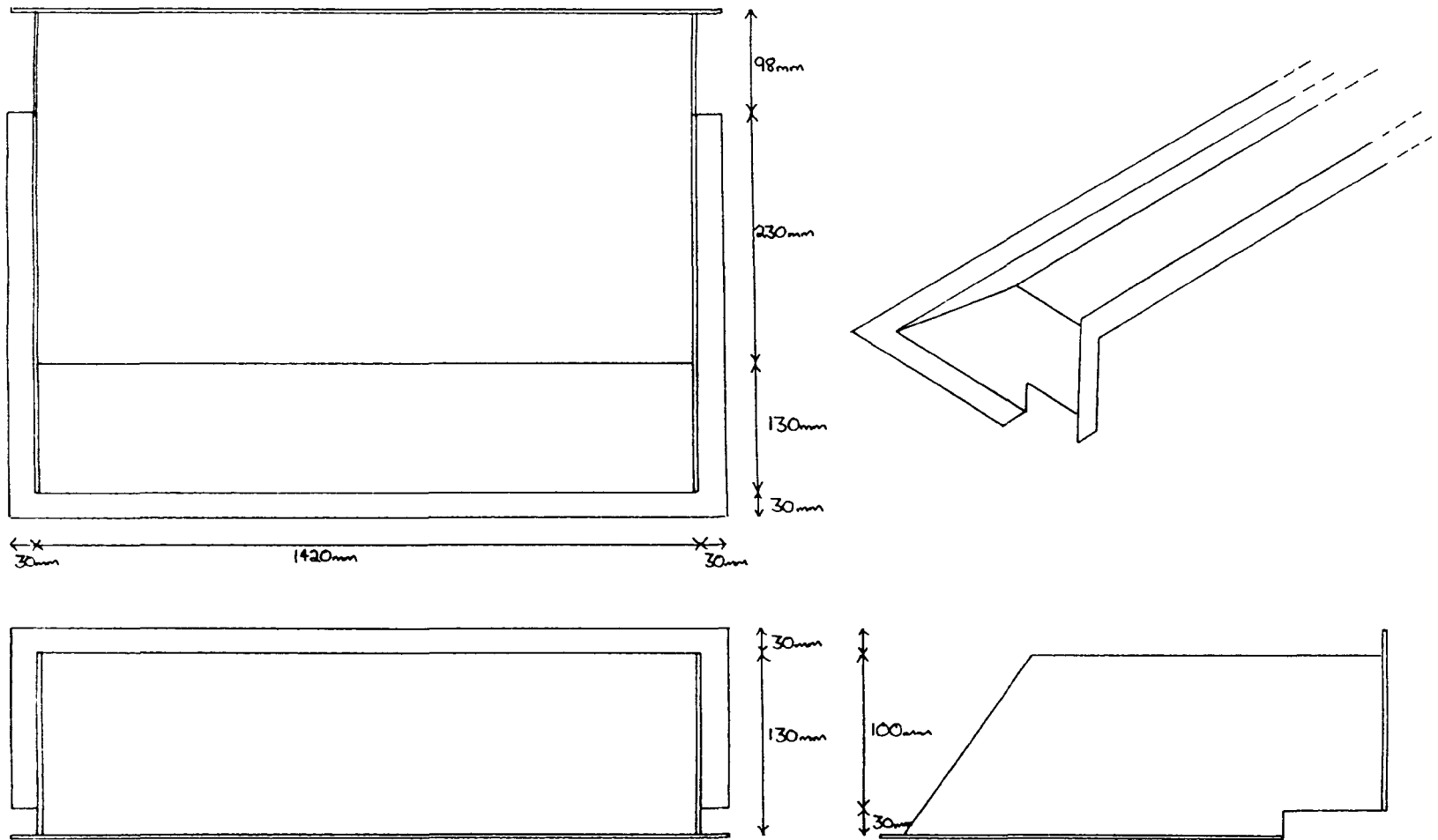
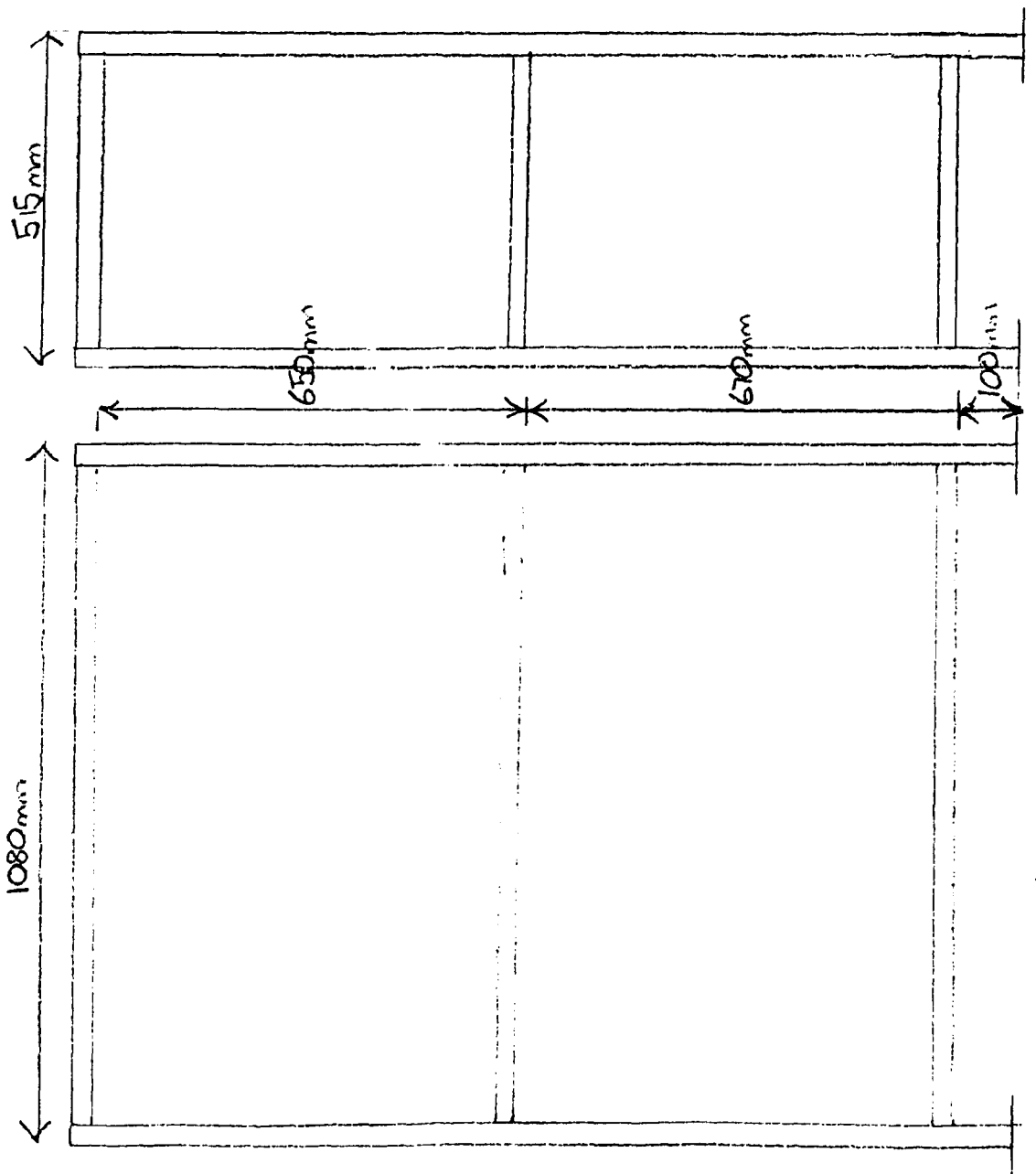
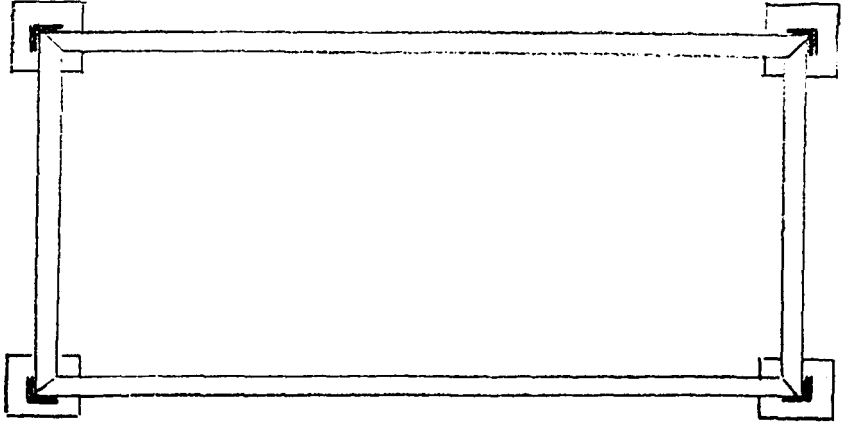


Figure A1.7 Diagram of the plate used to deflect the fan output into the model vehicle.
This plate is mounted on top of the fan rig.



PLAN VIEW



1ST JURY

Figure A1.8 Diagram of a trolley

appendix 2 Experimental data

In this section the experimental data collected in all the loading cases is summarised and the data files and archive format given. In the first part the summary files for the experimental data are given for the four loading cases. These contain one line for each 9.6 minute experimental data collecting run, the meaning of which is given below.

column 1 - run number of data

column 2 - zero

column 3 - measurement position in the standard x direction

column 4 - measurement position in the standard y direction

column 5 - measurement position in the standard z direction

The standard co-ordinate system is given in figure 34

column 6 - mean u velocity component

column 7 - mean v velocity component

column 8 - mean w velocity component

column 9 - variance of u component

column 10 - variance of v component

column 11 - variance of w component

Experimental data summary file for empty model load space

| | | | | | | | | | | |
|----|---|-------|-------|-------|---------|---------|---------|--------|--------|--------|
| 1 | 0 | 0.300 | 0.250 | 0.300 | 0.0996 | 0.1450 | -0.6350 | 0.0193 | 0.0205 | 0.0328 |
| 2 | 0 | 0.895 | 0.250 | 0.300 | 0.0915 | 0.2325 | -0.5188 | 0.0320 | 0.0184 | 0.0373 |
| 3 | 0 | 1.515 | 0.250 | 0.300 | -0.0497 | 0.2246 | -0.5755 | 0.0399 | 0.0148 | 0.0307 |
| 4 | 0 | 0.300 | 0.250 | 0.875 | 0.0750 | 0.0194 | -0.6292 | 0.0264 | 0.0323 | 0.0523 |
| 5 | 0 | 0.895 | 0.250 | 0.885 | 0.1333 | 0.1439 | -0.6221 | 0.0362 | 0.0314 | 0.0438 |
| 6 | 0 | 0.290 | 0.250 | 1.410 | 0.0628 | -0.0374 | -0.6017 | 0.0278 | 0.0362 | 0.0614 |
| 7 | 0 | 0.890 | 0.250 | 1.415 | 0.1469 | 0.1069 | -0.6214 | 0.0406 | 0.0370 | 0.0487 |
| 8 | 0 | 2.100 | 0.250 | 1.415 | -0.0351 | 0.0346 | -0.7735 | 0.0277 | 0.0273 | 0.0345 |
| 9 | 0 | 0.295 | 0.250 | 2.530 | 0.0973 | -0.0506 | -0.4190 | 0.0263 | 0.0249 | 0.0390 |
| 10 | 0 | 0.900 | 0.250 | 2.530 | 0.2303 | 0.0729 | -0.4652 | 0.0445 | 0.0297 | 0.0393 |
| 11 | 0 | 0.300 | 0.250 | 3.640 | 0.0671 | 0.0090 | -0.2635 | 0.0128 | 0.0184 | 0.0484 |
| 12 | 0 | 0.890 | 0.250 | 3.630 | 0.1531 | 0.1094 | -0.3693 | 0.0354 | 0.0166 | 0.0413 |
| 13 | 0 | 1.515 | 0.250 | 3.640 | 0.0513 | 0.1285 | -0.5169 | 0.0316 | 0.0114 | 0.0249 |
| 14 | 0 | 0.295 | 0.250 | 4.725 | -0.0182 | 0.0293 | -0.2759 | 0.0096 | 0.0113 | 0.0248 |
| 15 | 0 | 0.885 | 0.250 | 4.725 | 0.0279 | 0.0763 | -0.3512 | 0.0256 | 0.0155 | 0.0183 |
| 16 | 0 | 2.100 | 0.250 | 4.730 | 0.0314 | 0.0465 | -0.4525 | 0.0102 | 0.0084 | 0.0108 |
| 17 | 0 | 0.295 | 0.250 | 5.850 | 0.0381 | -0.0225 | -0.0516 | 0.0153 | 0.0196 | 0.0256 |
| 18 | 0 | 0.885 | 0.250 | 5.845 | 0.0734 | 0.0910 | -0.1581 | 0.0187 | 0.0113 | 0.0148 |
| 19 | 0 | 0.855 | 0.250 | 6.920 | 0.0449 | 0.0214 | 0.0046 | 0.0198 | 0.0107 | 0.0104 |
| 20 | 0 | 0.665 | 0.350 | 6.920 | 0.0628 | -0.0377 | -0.0149 | 0.0251 | 0.0178 | 0.0159 |
| 21 | 0 | 0.295 | 0.775 | 5.845 | 0.1035 | -0.1340 | 0.1476 | 0.0362 | 0.0510 | 0.0486 |
| 22 | 0 | 0.890 | 0.775 | 5.845 | -0.0587 | 0.1810 | -0.1757 | 0.0252 | 0.0192 | 0.0192 |
| 23 | 0 | 2.105 | 0.775 | 5.840 | -0.0394 | 0.1037 | -0.2081 | 0.0199 | 0.0164 | 0.0220 |
| 24 | 0 | 1.505 | 0.775 | 4.735 | -0.0169 | 0.1257 | -0.3101 | 0.0376 | 0.0335 | 0.0378 |
| 25 | 0 | 0.895 | 0.775 | 4.735 | -0.0270 | 0.1099 | -0.2693 | 0.0343 | 0.0343 | 0.0367 |
| 26 | 0 | 0.300 | 0.775 | 4.735 | 0.0446 | -0.0217 | -0.0600 | 0.0401 | 0.0414 | 0.0437 |
| 27 | 0 | 0.300 | 0.775 | 3.635 | 0.1119 | -0.0290 | -0.0580 | 0.0420 | 0.0523 | 0.0751 |

| | | | | | | | | | | |
|----|---|-------|-------|-------|---------|---------|---------|--------|--------|--------|
| 28 | 0 | 0.895 | 0.775 | 3.620 | -0.0121 | 0.1818 | -0.3763 | 0.0439 | 0.0355 | 0.0311 |
| 29 | 0 | 0.305 | 0.775 | 2.520 | -0.0870 | -0.1502 | -0.3298 | 0.0770 | 0.0637 | 0.0618 |
| 30 | 0 | 0.900 | 0.775 | 2.520 | -0.1881 | 0.0831 | -0.5714 | 0.0425 | 0.0392 | 0.0411 |
| 31 | 0 | 2.100 | 0.775 | 2.515 | 0.0248 | -0.0141 | -0.3706 | 0.0505 | 0.0508 | 0.0408 |
| 32 | 0 | 1.505 | 0.775 | 1.415 | -0.0955 | 0.1052 | -0.8993 | 0.0391 | 0.0634 | 0.0366 |
| 33 | 0 | 0.900 | 0.775 | 1.410 | -0.1717 | -0.0130 | -0.7571 | 0.0678 | 0.0600 | 0.0660 |
| 34 | 0 | 0.300 | 0.775 | 1.410 | 0.0050 | -0.1118 | -0.5116 | 0.0727 | 0.0557 | 0.0862 |
| 35 | 0 | 0.300 | 0.775 | 0.860 | -0.1648 | 0.2174 | -0.6572 | 0.0503 | 0.0559 | 0.0725 |
| 36 | 0 | 0.825 | 0.775 | 0.880 | -0.1317 | 0.1601 | -0.6772 | 0.0742 | 0.0495 | 0.0618 |
| 37 | 0 | 0.300 | 0.775 | 0.305 | -0.2546 | 0.3164 | -0.2731 | 0.0617 | 0.0533 | 0.0798 |
| 38 | 0 | 0.905 | 0.775 | 0.300 | -0.2167 | 0.2021 | -0.4784 | 0.0302 | 0.0338 | 0.0431 |
| 39 | 0 | 2.110 | 0.775 | 0.305 | -0.0151 | 0.1517 | -0.3625 | 0.0455 | 0.0657 | 0.0831 |
| 40 | 0 | 0.300 | 0.805 | 0.300 | -0.1271 | 0.1415 | -0.2707 | 0.0586 | 0.0735 | 0.0782 |
| 41 | 0 | 2.110 | 0.805 | 0.305 | 0.0673 | 0.1855 | -0.3804 | 0.0523 | 0.0780 | 0.0729 |
| 42 | 0 | 1.920 | 0.810 | 6.930 | 0.1210 | -0.1361 | -0.0266 | 0.0192 | 0.0272 | 0.0165 |
| 43 | 0 | 0.485 | 0.810 | 6.935 | 0.0985 | -0.0248 | 0.0387 | 0.0336 | 0.0302 | 0.0335 |
| 44 | 0 | 0.300 | 1.245 | 0.595 | 0.0005 | 0.4443 | 0.1878 | 0.0894 | 0.0492 | 0.0736 |
| 45 | 0 | 0.900 | 1.245 | 0.600 | -0.1726 | 0.4552 | -0.4339 | 0.0518 | 0.0390 | 0.0681 |
| 46 | 0 | 0.300 | 1.245 | 1.705 | 0.2042 | -0.0119 | -0.1461 | 0.1017 | 0.0922 | 0.0749 |
| 47 | 0 | 0.900 | 1.245 | 1.710 | -0.0420 | -0.3610 | -0.1443 | 0.1312 | 0.0965 | 0.0939 |
| 48 | 0 | 2.095 | 1.245 | 1.710 | -0.1354 | -0.2514 | -0.1255 | 0.1224 | 0.1000 | 0.0671 |
| 49 | 0 | 0.895 | 1.245 | 2.815 | -0.0932 | -0.1532 | 0.0529 | 0.0609 | 0.1151 | 0.1402 |
| 50 | 0 | 0.305 | 1.245 | 2.815 | -0.0088 | -0.2338 | 0.1024 | 0.0821 | 0.0956 | 0.0975 |
| 51 | 0 | 0.295 | 1.245 | 3.920 | 0.0798 | -0.0802 | 0.1332 | 0.0622 | 0.0626 | 0.0635 |
| 52 | 0 | 0.895 | 1.245 | 3.915 | -0.0602 | -0.0555 | -0.0371 | 0.0502 | 0.0830 | 0.0612 |
| 53 | 0 | 1.490 | 1.245 | 3.910 | 0.0881 | -0.0292 | -0.1321 | 0.0616 | 0.0868 | 0.0712 |
| 54 | 0 | 0.895 | 1.245 | 5.025 | -0.1006 | -0.2046 | 0.0732 | 0.0387 | 0.0635 | 0.0440 |
| 55 | 0 | 0.290 | 1.245 | 5.030 | 0.1089 | -0.1394 | 0.2866 | 0.0718 | 0.0602 | 0.0635 |
| 56 | 0 | 0.290 | 1.245 | 6.150 | 0.2147 | -0.1765 | 0.3538 | 0.0606 | 0.0672 | 0.0543 |
| 57 | 0 | 0.890 | 1.245 | 6.135 | -0.1146 | -0.0511 | 0.0545 | 0.0210 | 0.0716 | 0.0512 |
| 58 | 0 | 1.500 | 1.245 | 6.130 | 0.2296 | -0.2685 | 0.1531 | 0.0330 | 0.0571 | 0.0368 |
| 59 | 0 | 0.890 | 1.245 | 3.915 | -0.0476 | -0.0769 | -0.0306 | 0.0421 | 0.0775 | 0.0615 |
| 60 | 0 | 0.890 | 1.245 | 3.915 | -0.0628 | -0.1254 | 0.0141 | 0.0441 | 0.0682 | 0.0486 |
| 61 | 0 | 0.470 | 1.265 | 0.300 | -0.1857 | 0.5486 | -0.2190 | 0.0576 | 0.0395 | 0.0532 |
| 62 | 0 | 0.900 | 1.265 | 0.295 | -0.1831 | 0.5853 | -0.3689 | 0.0380 | 0.0315 | 0.0481 |
| 63 | 0 | 0.475 | 1.265 | 0.865 | 0.2510 | 0.3096 | 0.0257 | 0.1000 | 0.0780 | 0.1025 |
| 64 | 0 | 0.480 | 1.265 | 1.410 | 0.2556 | 0.1438 | -0.2017 | 0.1136 | 0.0798 | 0.0982 |
| 65 | 0 | 0.475 | 1.265 | 2.525 | -0.2671 | -0.3385 | 0.1539 | 0.0611 | 0.0946 | 0.1003 |
| 66 | 0 | 0.470 | 1.265 | 3.620 | -0.0174 | 0.0332 | -0.0248 | 0.0527 | 0.0652 | 0.0535 |
| 67 | 0 | 0.475 | 1.265 | 4.725 | -0.0712 | -0.0445 | 0.1096 | 0.0503 | 0.0660 | 0.0603 |
| 68 | 0 | 0.470 | 1.265 | 5.850 | -0.0565 | 0.0363 | 0.1319 | 0.0487 | 0.0429 | 0.0568 |
| 69 | 0 | 0.470 | 1.265 | 6.925 | 0.0987 | 0.1041 | -0.0234 | 0.0383 | 0.0274 | 0.0346 |
| 70 | 0 | 0.885 | 1.265 | 3.910 | -0.1035 | -0.0420 | -0.0415 | 0.0507 | 0.0823 | 0.0782 |
| 71 | 0 | 0.885 | 1.265 | 3.910 | -0.0528 | -0.0107 | -0.0302 | 0.0500 | 0.0830 | 0.0775 |
| 72 | 0 | 0.485 | 1.690 | 0.320 | -0.2723 | 0.6706 | -0.0209 | 0.0373 | 0.0368 | 0.0471 |
| 73 | 0 | 0.475 | 1.690 | 0.870 | 0.0212 | 0.5099 | 0.2396 | 0.0738 | 0.0754 | 0.0964 |
| 74 | 0 | 0.475 | 1.690 | 1.415 | -0.1375 | -0.0176 | 0.3308 | 0.1268 | 0.2435 | 0.1736 |
| 75 | 0 | 0.865 | 1.690 | 0.310 | -0.2188 | 0.6725 | -0.1515 | 0.0423 | 0.0288 | 0.0554 |
| 76 | 0 | 0.870 | 1.690 | 0.865 | 0.0640 | 0.3365 | -0.2003 | 0.0697 | 0.0516 | 0.0681 |
| 77 | 0 | 0.875 | 1.690 | 1.415 | 0.1140 | -0.4014 | 0.4810 | 0.1625 | 0.1852 | 0.1301 |
| 78 | 0 | 0.865 | 1.690 | 2.520 | -0.1854 | -0.1940 | 0.4198 | 0.1133 | 0.1199 | 0.1191 |
| 79 | 0 | 0.475 | 1.690 | 2.530 | -0.4172 | -0.1523 | 0.3289 | 0.0914 | 0.1539 | 0.1179 |
| 80 | 0 | 0.470 | 1.690 | 3.625 | -0.4424 | 0.0577 | 0.3238 | 0.0714 | 0.1287 | 0.0923 |

| | | | | | | | | | | |
|-----|---|-------|-------|-------|---------|---------|---------|--------|--------|--------|
| 81 | 0 | 0.900 | 1.690 | 3.630 | -0.2108 | -0.0081 | 0.2571 | 0.0963 | 0.1037 | 0.0750 |
| 82 | 0 | 0.470 | 1.690 | 4.735 | -0.3945 | 0.2166 | 0.2379 | 0.0704 | 0.0906 | 0.0866 |
| 83 | 0 | 0.890 | 1.690 | 4.725 | 0.0593 | -0.2474 | 0.2069 | 0.0637 | 0.1659 | 0.0664 |
| 84 | 0 | 0.465 | 1.690 | 5.855 | -0.2269 | 0.4749 | 0.0241 | 0.0571 | 0.0400 | 0.0730 |
| 85 | 0 | 0.900 | 1.690 | 5.840 | 0.0571 | -0.3517 | 0.2072 | 0.0607 | 0.1602 | 0.0782 |
| 86 | 0 | 0.930 | 1.690 | 6.885 | 0.1620 | -0.2270 | 0.0945 | 0.0597 | 0.1182 | 0.0786 |
| 87 | 0 | 0.470 | 1.690 | 6.920 | -0.0327 | 0.4382 | -0.2640 | 0.0428 | 0.0280 | 0.0491 |
| 88 | 0 | 1.940 | 1.690 | 5.870 | 0.2496 | 0.5314 | -0.0421 | 0.0618 | 0.0490 | 0.0663 |
| 89 | 0 | 1.940 | 1.690 | 3.620 | 0.4186 | 0.2855 | 0.0819 | 0.0747 | 0.1253 | 0.0989 |
| 90 | 0 | 1.940 | 1.690 | 3.620 | 0.3463 | 0.2515 | 0.0400 | 0.0737 | 0.1067 | 0.0884 |
| 91 | 0 | 1.925 | 1.690 | 1.440 | 0.2252 | -0.1663 | 0.2059 | 0.1316 | 0.2484 | 0.2139 |
| 92 | 0 | 0.905 | 1.245 | 3.925 | -0.0901 | -0.0870 | 0.0138 | 0.0406 | 0.0807 | 0.0598 |
| 93 | 0 | 0.905 | 1.245 | 3.925 | -0.0927 | -0.0934 | 0.0037 | 0.0423 | 0.0866 | 0.0728 |
| 94 | 0 | 0.905 | 1.245 | 3.925 | -0.0911 | -0.0500 | -0.0315 | 0.0461 | 0.0793 | 0.0659 |
| 95 | 0 | 0.910 | 1.245 | 0.590 | -0.1959 | 0.4464 | -0.5626 | 0.0529 | 0.0450 | 0.0842 |
| 96 | 0 | 0.910 | 1.245 | 0.590 | -0.1875 | 0.4598 | -0.5625 | 0.0545 | 0.0424 | 0.0791 |
| 97 | 0 | 0.910 | 1.245 | 0.590 | -0.2101 | 0.4389 | -0.5843 | 0.0608 | 0.0438 | 0.0771 |
| 98 | 0 | 0.910 | 1.970 | 0.490 | -0.0859 | 0.5637 | 0.2159 | 0.0358 | 0.0240 | 0.0582 |
| 99 | 0 | 0.700 | 1.970 | 1.220 | 0.1132 | -0.9351 | 1.0221 | 0.0810 | 0.1865 | 0.1283 |
| 100 | 0 | 0.120 | 1.730 | 4.185 | 0.2468 | -0.2668 | 0.7499 | 0.1048 | 0.1320 | 0.1313 |
| 101 | 0 | 0.265 | 1.730 | 4.185 | -0.1838 | 0.4784 | 0.3494 | 0.0959 | 0.0599 | 0.1131 |
| 102 | 0 | 0.420 | 1.730 | 4.185 | -0.3995 | 0.3429 | 0.3435 | 0.0996 | 0.1145 | 0.1407 |
| 103 | 0 | 0.565 | 1.730 | 4.185 | -0.5207 | 0.0088 | 0.2977 | 0.1064 | 0.2246 | 0.1569 |
| 104 | 0 | 0.705 | 1.730 | 4.185 | -0.3067 | -0.5330 | 0.4092 | 0.0720 | 0.3631 | 0.1440 |
| 105 | 0 | 0.950 | 1.730 | 4.185 | 0.0142 | 0.0112 | 0.2753 | 0.1315 | 0.1560 | 0.1102 |
| 106 | 0 | 1.000 | 1.730 | 4.185 | -0.1447 | -0.1578 | 0.2809 | 0.1587 | 0.1508 | 0.0947 |
| 107 | 0 | 1.100 | 1.730 | 4.185 | -0.1630 | -0.3859 | 0.3593 | 0.1224 | 0.2222 | 0.1078 |
| 108 | 0 | 1.195 | 1.730 | 4.185 | -0.0212 | -0.6928 | 0.4036 | 0.0768 | 0.2437 | 0.1054 |
| 109 | 0 | 0.120 | 1.730 | 4.185 | 0.2591 | -0.2179 | 0.7862 | 0.1063 | 0.1408 | 0.1321 |
| 110 | 0 | 0.350 | 1.730 | 4.185 | -0.2867 | 0.4962 | 0.3233 | 0.1048 | 0.0837 | 0.1351 |
| 111 | 0 | 0.840 | 1.730 | 4.185 | 0.0303 | -0.1848 | 0.3706 | 0.0803 | 0.2413 | 0.1167 |
| 112 | 0 | 1.300 | 1.730 | 4.185 | 0.1547 | -0.4024 | 0.3250 | 0.0974 | 0.2345 | 0.1071 |
| 113 | 0 | 1.395 | 1.730 | 4.185 | 0.1021 | -0.0550 | 0.1913 | 0.1286 | 0.1589 | 0.0958 |
| 114 | 0 | 1.450 | 1.730 | 4.185 | -0.0476 | -0.1049 | 0.1593 | 0.0976 | 0.1576 | 0.0924 |
| 115 | 0 | 1.545 | 1.730 | 4.185 | -0.0059 | -0.3715 | 0.1942 | 0.0762 | 0.2616 | 0.1094 |
| 116 | 0 | 1.700 | 1.730 | 4.185 | 0.4767 | -0.4531 | 0.1474 | 0.0716 | 0.3104 | 0.1140 |
| 117 | 0 | 1.850 | 1.730 | 4.185 | 0.4518 | 0.1595 | 0.0439 | 0.1131 | 0.2265 | 0.0957 |
| 118 | 0 | 2.000 | 1.730 | 4.185 | 0.2587 | 0.5586 | -0.0160 | 0.0813 | 0.0799 | 0.0984 |
| 119 | 0 | 2.055 | 1.730 | 4.185 | 0.1652 | 0.6111 | -0.0478 | 0.0745 | 0.0623 | 0.0862 |
| 120 | 0 | 2.100 | 1.730 | 4.185 | 0.1319 | 0.6292 | -0.0665 | 0.0839 | 0.0672 | 0.0913 |
| 121 | 0 | 2.280 | 1.730 | 4.185 | -0.2526 | -0.3346 | 0.3620 | 0.0902 | 0.1953 | 0.1143 |
| 122 | 0 | 2.055 | 1.730 | 4.185 | 0.2192 | 0.6252 | -0.0491 | 0.0797 | 0.0703 | 0.0909 |
| 123 | 0 | 2.280 | 1.730 | 4.185 | -0.1790 | -0.3139 | 0.3848 | 0.0802 | 0.1503 | 0.1434 |
| 124 | 0 | 0.950 | 0.070 | 4.185 | 0.1330 | 0.0503 | -0.5667 | 0.0373 | 0.0118 | 0.0503 |
| 125 | 0 | 0.950 | 0.250 | 4.185 | 0.1065 | 0.0370 | -0.5822 | 0.0299 | 0.0255 | 0.0382 |
| 126 | 0 | 0.950 | 0.415 | 4.185 | 0.0801 | 0.0375 | -0.5106 | 0.0312 | 0.0422 | 0.0431 |
| 127 | 0 | 0.950 | 0.605 | 4.185 | 0.0816 | 0.0301 | -0.4416 | 0.0331 | 0.0502 | 0.0467 |
| 128 | 0 | 0.950 | 0.760 | 4.185 | 0.0143 | 0.0041 | -0.3172 | 0.0355 | 0.0655 | 0.0584 |
| 129 | 0 | 0.950 | 0.890 | 4.185 | 0.0189 | -0.0557 | -0.2171 | 0.0341 | 0.0793 | 0.0583 |
| 130 | 0 | 0.950 | 1.030 | 4.185 | -0.0278 | -0.1357 | -0.0896 | 0.0390 | 0.0944 | 0.0724 |
| 131 | 0 | 0.950 | 1.175 | 4.185 | -0.0552 | -0.0983 | 0.0059 | 0.0477 | 0.1184 | 0.0872 |
| 132 | 0 | 0.950 | 1.350 | 4.185 | -0.1419 | -0.2480 | 0.2380 | 0.0563 | 0.1365 | 0.0763 |
| 133 | 0 | 0.950 | 1.540 | 4.185 | -0.1038 | -0.1422 | 0.3010 | 0.0786 | 0.1433 | 0.0843 |

134 0 0.950 1.540 4.185 -0.1464 -0.2002 0.3078 0.0897 0.1556 0.0999
135 0 0.950 1.660 4.185 -0.0419 -0.1303 0.2999 0.1090 0.1329 0.0968
136 0 0.950 1.870 4.185 0.1504 -0.0276 0.2198 0.0734 0.1415 0.0821
137 0 0.950 1.980 4.185 0.1634 -0.0173 0.1448 0.0623 0.1426 0.0687
138 0 0.950 2.110 4.185 0.0645 -0.0279 0.0004 0.0282 0.0608 0.0457
139 0 0.950 2.250 4.185 0.1201 -0.0754 -0.0112 0.0301 0.0262 0.0440
140 0 0.300 0.775 0.900 0.0734 -0.0441 -0.2763 0.0819 0.1151 0.1889
141 0 0.900 0.775 0.900 -0.1165 0.1936 -0.8189 0.0674 0.0565 0.0908
142 0 0.900 0.775 1.200 -0.1573 0.0762 -0.9355 0.0687 0.0814 0.0867
143 0 1.500 0.775 1.200 -0.1254 0.1984 -1.0864 0.0504 0.0786 0.0630
144 0 1.500 0.775 1.200 -0.1056 0.1818 -0.9972 0.0514 0.0718 0.0711
145 0 0.300 0.775 1.200 0.1666 -0.3104 -0.3290 0.0923 0.1288 0.1675
146 0 0.300 0.775 2.500 -0.1361 -0.3854 -0.3641 0.0838 0.0853 0.1023
147 0 0.900 0.775 2.500 -0.1323 -0.0646 -0.6081 0.0569 0.1305 0.0968
148 0 2.100 0.775 2.500 0.0271 -0.1461 -0.3352 0.0663 0.1056 0.0885
149 0 1.500 0.775 4.795 0.0207 -0.0985 -0.2450 0.0367 0.0712 0.0694
150 0 0.900 0.775 4.785 -0.0232 -0.0400 -0.2947 0.0279 0.0633 0.0649
151 0 0.300 0.775 4.795 0.0384 -0.1886 0.0038 0.0416 0.0618 0.0711
152 0 0.300 0.775 5.855 0.0962 -0.2260 0.1244 0.0428 0.0720 0.0834
153 0 0.900 0.775 5.855 -0.0526 -0.0300 -0.1732 0.0205 0.0611 0.0504
154 0 1.500 0.775 5.855 0.1178 -0.0975 -0.0924 0.0275 0.0588 0.0422
155 0 0.700 2.125 6.950 0.2451 -0.0066 0.2049 0.0538 0.1406 0.1399
156 0 0.700 2.125 6.950 0.2523 -0.0215 0.2179 0.0511 0.1384 0.1370
157 0 0.700 1.200 0.270 -0.3154 0.6498 -0.2976 0.0566 0.0572 0.0721
158 0 0.700 2.050 0.460 0.0088 0.2464 1.0015 0.0726 0.1732 0.3129
159 0 0.700 0.400 2.270 0.0312 -0.1957 -0.6574 0.0740 0.1274 0.1030
160 0 0.700 0.405 2.270 0.0158 -0.0735 -0.6743 0.0778 0.1212 0.0992
161 0 0.700 0.405 2.270 0.0221 -0.1033 -0.6675 0.0793 0.1308 0.1173
162 0 0.700 0.405 2.270 0.0251 -0.1135 -0.6170 0.0846 0.1302 0.1209
163 0 0.700 0.405 2.270 0.0519 -0.1904 -0.6470 0.0731 0.1139 0.0980
164 0 0.700 0.405 2.270 0.0254 -0.1979 -0.6652 0.0703 0.1237 0.0997
165 0 0.700 0.405 2.270 0.0365 -0.1841 -0.6955 0.0694 0.1243 0.0957
166 0 0.700 1.210 2.260 -0.2797 -0.6123 0.0465 0.0993 0.2083 0.1279
167 0 0.700 2.190 2.260 0.1367 -0.7547 0.4289 0.2284 0.2203 0.2106
168 0 0.700 0.360 4.475 0.0665 0.0018 -0.4175 0.0372 0.0345 0.0483
169 0 0.700 1.205 4.470 -0.0756 -0.0266 -0.0212 0.0535 0.1142 0.0751
170 0 0.700 2.180 4.465 0.7269 -0.4511 0.0404 0.0797 0.1855 0.1613
171 0 0.700 0.395 6.960 0.0279 -0.0451 -0.0820 0.0353 0.0296 0.0220
172 0 0.700 1.200 6.960 -0.0449 0.0209 -0.1073 0.0424 0.0623 0.0441
173 0 0.700 1.200 6.960 0.0116 0.0686 -0.1086 0.0419 0.0526 0.0409
174 0 0.700 1.200 6.960 -0.0042 0.0342 -0.0999 0.0522 0.0654 0.0428
175 0 0.700 1.200 6.960 0.0092 0.0606 -0.0744 0.0472 0.0574 0.0459
176 0 0.700 1.200 6.960 -0.0056 -0.0091 -0.1088 0.0351 0.0412 0.0353
177 0 0.700 1.200 6.960 -0.0022 -0.0443 -0.1093 0.0379 0.0473 0.0353
178 0 0.700 1.200 6.960 -0.0158 -0.0406 -0.1016 0.0398 0.0555 0.0379
179 0 0.700 2.125 6.950 0.2292 0.0265 0.2208 0.0539 0.1309 0.1432
180 0 0.685 0.395 0.265 -0.0297 0.1856 -0.7845 0.0415 0.0527 0.0696
181 0 0.685 0.395 0.265 -0.0235 0.1670 -0.7283 0.0385 0.0500 0.0653
182 0 0.685 0.395 0.265 -0.0437 0.1679 -0.7507 0.0365 0.0507 0.0609
183 0 0.685 0.395 0.265 -0.0499 0.2476 -0.7985 0.0338 0.0394 0.0500
184 0 0.685 0.395 0.265 -0.0422 0.2286 -0.7703 0.0335 0.0423 0.0548
185 0 0.685 0.395 0.265 -0.0434 0.2370 -0.7690 0.0366 0.0417 0.0544
186 0 0.685 0.395 0.265 -0.0527 0.1762 -0.7549 0.0373 0.0479 0.0599

| | | | | | | | | | | |
|-----|---|-------|-------|-------|---------|--------|---------|--------|--------|--------|
| 187 | 0 | 0.685 | 0.395 | 0.265 | -0.0559 | 0.2089 | -0.7687 | 0.0363 | 0.0466 | 0.0561 |
| 188 | 0 | 0.685 | 0.395 | 0.265 | -0.0603 | 0.2063 | -0.7637 | 0.0363 | 0.0436 | 0.0578 |
| 189 | 0 | 0.685 | 0.395 | 0.265 | -0.0522 | 0.2035 | -0.7654 | 0.0377 | 0.0473 | 0.0636 |
| 190 | 0 | 0.685 | 0.395 | 0.265 | -0.0582 | 0.2152 | -0.7837 | 0.0352 | 0.0471 | 0.0549 |
| 191 | 0 | 0.685 | 0.395 | 0.265 | -0.0601 | 0.1950 | -0.7521 | 0.0370 | 0.0432 | 0.0564 |
| 192 | 0 | 0.685 | 0.395 | 0.265 | -0.0458 | 0.1927 | -0.7791 | 0.0355 | 0.0444 | 0.0590 |
| 193 | 0 | 0.685 | 0.395 | 0.265 | -0.0592 | 0.2468 | -0.7817 | 0.0358 | 0.0436 | 0.0604 |
| 194 | 0 | 0.685 | 0.395 | 0.265 | -0.0314 | 0.2330 | -0.7838 | 0.0356 | 0.0441 | 0.0595 |
| 195 | 0 | 0.685 | 0.395 | 0.265 | -0.0578 | 0.2231 | -0.7489 | 0.0400 | 0.0414 | 0.0563 |
| 196 | 0 | 0.685 | 0.395 | 0.265 | -0.0562 | 0.2350 | -0.7726 | 0.0342 | 0.0441 | 0.0560 |
| 197 | 0 | 0.685 | 0.395 | 0.265 | -0.0507 | 0.2470 | -0.7983 | 0.0349 | 0.0457 | 0.0594 |
| 198 | 0 | 0.685 | 0.395 | 0.265 | -0.0474 | 0.2226 | -0.7640 | 0.0344 | 0.0491 | 0.0552 |
| 199 | 0 | 0.685 | 0.395 | 0.265 | -0.0375 | 0.2041 | -0.7914 | 0.0369 | 0.0450 | 0.0693 |
| 200 | 0 | 0.685 | 0.395 | 0.265 | -0.0379 | 0.1991 | -0.7821 | 0.0406 | 0.0484 | 0.0616 |
| 201 | 0 | 0.685 | 0.395 | 0.265 | -0.0465 | 0.1838 | -0.7798 | 0.0390 | 0.0489 | 0.0624 |
| 202 | 0 | 0.685 | 0.395 | 0.265 | -0.0466 | 0.2439 | -0.7682 | 0.0360 | 0.0413 | 0.0589 |

Experimental data summary file for front half loaded model load space

| | | | | | | | | | | |
|-----|---|-------|-------|-------|---------|---------|---------|--------|--------|--------|
| 300 | 0 | 0.580 | 0.700 | 1.430 | -0.0402 | -0.1817 | -0.9071 | 0.0057 | 0.0117 | 0.0064 |
| 301 | 0 | 0.580 | 0.700 | 1.430 | -0.0376 | -0.1816 | -0.9073 | 0.0060 | 0.0103 | 0.0064 |
| 302 | 0 | 0.580 | 0.700 | 1.430 | -0.0294 | -0.1744 | -0.9110 | 0.0062 | 0.0112 | 0.0069 |
| 303 | 0 | 1.210 | 0.700 | 1.980 | -0.0265 | -0.4407 | -0.4302 | 0.0078 | 0.0492 | 0.0508 |
| 304 | 0 | 1.210 | 0.700 | 1.980 | -0.0259 | -0.4343 | -0.4376 | 0.0073 | 0.0471 | 0.0508 |
| 305 | 0 | 1.210 | 0.700 | 1.980 | -0.0068 | -0.4784 | -0.4033 | 0.0068 | 0.0506 | 0.0408 |
| 306 | 0 | 1.210 | 0.700 | 1.980 | 0.0097 | -0.4754 | -0.4168 | 0.0068 | 0.0545 | 0.0334 |
| 307 | 0 | 1.210 | 0.700 | 3.065 | 0.0194 | -0.4512 | -0.2252 | 0.0057 | 0.0215 | 0.0239 |
| 308 | 0 | 1.200 | 0.700 | 4.185 | -0.0861 | -0.1700 | -0.3479 | 0.0098 | 0.0552 | 0.0348 |
| 309 | 0 | 0.590 | 0.700 | 3.625 | -0.1367 | -0.0295 | -0.4378 | 0.0080 | 0.0062 | 0.0072 |
| 310 | 0 | 0.590 | 0.700 | 3.625 | -0.1313 | -0.0262 | -0.4433 | 0.0096 | 0.0076 | 0.0065 |
| 311 | 0 | 0.600 | 0.700 | 2.525 | 0.0235 | -0.0878 | 0.6456 | 0.0036 | 0.0090 | 0.0059 |
| 312 | 0 | 1.830 | 0.700 | 1.980 | -0.0015 | -0.0093 | -0.7755 | 0.0047 | 0.0051 | 0.0066 |
| 313 | 0 | 1.830 | 0.700 | 3.075 | -0.0499 | 0.0719 | -0.6260 | 0.0039 | 0.0070 | 0.0060 |
| 314 | 0 | 1.820 | 0.700 | 4.175 | -0.0538 | 0.0290 | -0.5532 | 0.0107 | 0.0053 | 0.0067 |
| 315 | 0 | 1.820 | 0.700 | 4.175 | -0.0441 | 0.0223 | -0.5616 | 0.0111 | 0.0057 | 0.0072 |
| 316 | 0 | 1.820 | 0.700 | 4.175 | -0.0492 | 0.0183 | -0.5637 | 0.0117 | 0.0056 | 0.0067 |
| 317 | 0 | 2.280 | 0.700 | 4.185 | -0.2103 | -0.2103 | -0.4953 | 0.0520 | 0.0194 | 0.0159 |
| 318 | 0 | 2.280 | 0.700 | 4.185 | -0.2169 | -0.2172 | -0.4949 | 0.0515 | 0.0196 | 0.0165 |
| 319 | 0 | 2.280 | 0.700 | 3.065 | 0.0259 | -0.0580 | -0.6724 | 0.0091 | 0.0092 | 0.0119 |
| 320 | 0 | 0.720 | 0.680 | 0.320 | -0.0594 | -0.0986 | -0.5826 | 0.0228 | 0.0209 | 0.0489 |
| 321 | 0 | 0.900 | 0.680 | 0.360 | -0.0180 | 0.0481 | -0.7089 | 0.0114 | 0.0123 | 0.0224 |
| 322 | 0 | 1.200 | 0.680 | 0.330 | 0.0029 | -0.0709 | -0.4648 | 0.0131 | 0.0091 | 0.0172 |
| 323 | 0 | 1.200 | 0.680 | 0.330 | 0.0162 | -0.1035 | -0.4749 | 0.0140 | 0.0094 | 0.0169 |
| 324 | 0 | 1.200 | 0.680 | 0.330 | 0.0205 | -0.0957 | -0.4689 | 0.0158 | 0.0105 | 0.0184 |
| 325 | 0 | 0.900 | 0.260 | 0.360 | 0.1002 | 0.1978 | -0.4728 | 0.0106 | 0.0095 | 0.0091 |
| 326 | 0 | 1.090 | 0.260 | 0.350 | 0.0239 | 0.1131 | -0.5332 | 0.0130 | 0.0126 | 0.0144 |
| 327 | 0 | 1.090 | 0.260 | 0.350 | 0.0186 | 0.1056 | -0.5253 | 0.0130 | 0.0126 | 0.0131 |
| 328 | 0 | 1.090 | 0.260 | 0.350 | 0.0118 | 0.1141 | -0.5237 | 0.0138 | 0.0124 | 0.0126 |
| 329 | 0 | 1.310 | 0.260 | 0.360 | 0.0467 | -0.1017 | -0.4584 | 0.0050 | 0.0138 | 0.0143 |
| 330 | 0 | 1.310 | 0.260 | 0.360 | 0.0409 | -0.1044 | -0.4644 | 0.0053 | 0.0141 | 0.0141 |
| 331 | 0 | 1.310 | 0.260 | 0.360 | 0.0415 | -0.0927 | -0.4770 | 0.0051 | 0.0147 | 0.0168 |
| 332 | 0 | 2.280 | 0.260 | 0.360 | -0.1156 | -0.3390 | -0.4971 | 0.0232 | 0.0290 | 0.0192 |
| 333 | 0 | 1.700 | 0.930 | 0.310 | -0.0785 | 0.0584 | -0.4517 | 0.0138 | 0.0190 | 0.0251 |

334 0 0.290 0.930 0.310 -0.3864 0.1840 -0.3114 0.0429 0.0286 0.0703
335 0 0.900 0.930 0.830 0.3057 0.0169 -0.2289 0.0143 0.0164 0.0111
336 0 1.200 0.980 0.830 0.0308 -0.2430 -0.2648 0.0236 0.0467 0.0179
337 0 0.120 0.980 0.870 0.1374 -0.9634 -0.1150 0.0324 0.0898 0.0791
338 0 0.300 0.980 0.890 0.2134 -0.4694 -0.3225 0.0393 0.1228 0.0489
339 0 0.900 0.980 0.870 0.2218 0.0612 -0.2869 0.0360 0.0231 0.0160
340 0 1.500 0.980 0.875 -0.1719 0.0643 -0.2378 0.0236 0.0107 0.0110
341 0 2.100 0.980 0.820 -0.1484 -0.5094 -0.4478 0.0521 0.1421 0.0597
342 0 2.280 0.980 0.860 -0.1098 -0.7614 -0.2864 0.0421 0.0783 0.0823
343 0 2.280 1.580 0.960 -0.2275 -0.5883 0.1161 0.0756 0.1235 0.0948
344 0 2.100 1.580 0.960 -0.1702 -0.1899 -0.6525 0.0647 0.0654 0.0749
345 0 1.800 1.580 0.950 -0.0876 -0.0315 -0.0026 0.0611 0.0717 0.0623
346 0 1.500 1.580 0.950 -0.1091 -0.4726 -0.3421 0.0756 0.0760 0.1123
347 0 1.200 1.580 0.990 0.0649 -0.2624 -0.0393 0.1197 0.0897 0.0616
348 0 0.900 1.580 0.970 0.0354 -0.6826 -0.5093 0.0831 0.0770 0.1063
349 0 0.600 1.580 0.990 0.0800 -0.3284 -0.0186 0.0652 0.1101 0.0594
350 0 0.300 1.580 0.980 -0.0058 -0.2305 -0.6253 0.0421 0.0750 0.0654
351 0 0.120 1.580 0.990 0.1078 -0.6249 -0.0364 0.0752 0.0934 0.0773
352 0 0.120 1.580 0.990 0.1071 -0.5804 -0.0642 0.0696 0.0966 0.0765
353 0 0.120 1.580 0.990 0.1017 -0.6137 -0.0663 0.0736 0.0971 0.0796
354 0 0.120 1.620 0.250 0.4497 -0.0451 0.1330 0.0977 0.1039 0.0695
355 0 0.890 1.620 0.250 -0.1530 0.7412 -0.2883 0.0339 0.0200 0.0377
356 0 0.890 1.620 0.600 0.1470 0.4025 -0.0891 0.1008 0.0462 0.0455
357 0 0.330 0.280 4.755 0.1690 0.0911 -0.1414 0.0211 0.0272 0.0319
358 0 0.920 0.280 4.765 0.1131 0.1316 -0.2992 0.0131 0.0109 0.0232
359 0 1.530 0.280 4.775 0.1068 0.1172 -0.3773 0.0144 0.0077 0.0138
360 0 0.320 0.280 5.465 0.1433 -0.0818 -0.1922 0.0137 0.0215 0.0346
361 0 0.940 0.280 5.415 0.2135 0.0505 -0.4046 0.0178 0.0140 0.0189
362 0 1.570 0.280 5.375 0.1402 0.1297 -0.4475 0.0219 0.0182 0.0195
363 0 0.330 0.280 5.885 0.0586 -0.0856 -0.2930 0.0123 0.0126 0.0175
364 0 0.930 0.280 5.885 0.1706 -0.0567 -0.3422 0.0206 0.0156 0.0138
365 0 1.550 0.280 5.885 0.1169 0.1083 -0.4445 0.0340 0.0418 0.0255
366 0 2.065 0.280 6.405 0.0700 -0.1342 -0.1041 0.0146 0.0180 0.0134
367 0 0.940 0.280 6.395 0.1541 -0.1304 -0.1687 0.0175 0.0406 0.0144
368 0 0.910 0.280 6.395 0.2100 0.0169 -0.3242 0.0220 0.0561 0.0200
369 0 2.060 0.280 6.375 -0.0608 -0.1068 -0.3205 0.0467 0.0558 0.0261
370 0 2.050 0.280 5.895 -0.0396 -0.0424 -0.4754 0.0378 0.0555 0.0299
371 0 2.075 0.280 5.285 0.0137 0.0667 -0.5041 0.0257 0.0203 0.0284
372 0 2.075 0.280 6.910 -0.0046 -0.1713 -0.1072 0.0326 0.0287 0.0167
373 0 1.500 0.280 6.900 0.2624 0.0967 -0.1336 0.0174 0.0265 0.0132
374 0 1.510 0.280 6.900 0.1756 -0.0628 -0.0359 0.0141 0.0165 0.0184
375 0 0.300 0.280 6.900 0.2069 -0.2529 -0.0099 0.0164 0.0361 0.0188
376 0 2.090 0.280 4.785 -0.0221 0.0961 -0.3442 0.0152 0.0106 0.0206
377 0 2.090 0.650 4.775 0.0338 0.1400 -0.3011 0.0149 0.0122 0.0266
378 0 2.100 0.650 5.895 0.0036 -0.1637 -0.3316 0.0473 0.0625 0.0621
379 0 1.520 0.650 4.755 0.0553 0.2232 -0.3314 0.0153 0.0102 0.0172
380 0 1.500 0.650 5.885 -0.0487 0.0421 -0.5000 0.0254 0.0258 0.0162
381 0 0.900 0.650 4.745 -0.0067 0.2211 -0.1973 0.0143 0.0130 0.0175
382 0 0.890 0.650 5.875 0.1626 -0.0328 -0.2216 0.0190 0.0227 0.0222
383 0 0.300 0.650 6.885 0.1451 -0.3518 0.2097 0.0332 0.0396 0.0259
384 0 0.930 0.650 6.915 0.0900 -0.0455 0.0537 0.0177 0.0276 0.0157
385 0 1.520 0.650 6.915 0.0718 0.0011 -0.1272 0.0271 0.0343 0.0191
386 0 0.325 0.650 5.765 0.1024 -0.1372 0.0011 0.0144 0.0232 0.0160

387 0 0.320 0.650 4.705 -0.0277 0.0890 -0.0217 0.0173 0.0282 0.0123
388 0 2.090 0.650 6.960 -0.0197 -0.2472 -0.0464 0.0314 0.0493 0.0189
389 0 2.090 0.960 4.625 -0.0239 0.2893 -0.1645 0.0128 0.0141 0.0134
390 0 1.500 0.960 4.605 -0.0446 0.2757 -0.1607 0.0111 0.0100 0.0101
391 0 0.900 0.960 4.605 -0.1567 0.2504 -0.0618 0.0090 0.0154 0.0098
392 0 0.330 0.960 4.610 -0.1180 0.1379 -0.0157 0.0124 0.0256 0.0078
393 0 0.320 1.285 4.610 -0.1176 0.1040 0.0043 0.0212 0.0254 0.0134
394 0 0.120 1.285 4.605 0.0841 -0.3599 0.2630 0.0563 0.0825 0.0379
395 0 0.120 1.285 4.605 0.0914 -0.3561 0.2611 0.0541 0.0819 0.0381
396 0 0.120 1.285 4.605 0.1506 -0.3248 0.2453 0.0651 0.0901 0.0475
397 0 0.120 1.285 4.605 0.1664 -0.3219 0.2728 0.0621 0.0820 0.0544
398 0 0.605 1.290 4.605 -0.1620 0.1519 -0.0047 0.0152 0.0276 0.0258
399 0 0.900 1.290 4.615 -0.1931 0.2715 -0.1162 0.0112 0.0175 0.0118
400 0 1.200 1.290 4.615 -0.1119 0.1693 -0.0738 0.0102 0.0533 0.0300
401 0 1.520 1.290 4.605 0.0122 0.3351 -0.1952 0.0105 0.0127 0.0114
402 0 1.810 1.290 4.585 -0.0934 0.3332 -0.1820 0.0169 0.0152 0.0130
403 0 2.100 1.290 4.615 -0.1503 0.2948 -0.1110 0.0252 0.0271 0.0195
404 0 2.280 1.290 4.605 -0.1176 0.1197 -0.0430 0.0266 0.0893 0.0293
405 0 2.280 1.290 4.605 -0.1098 0.1146 -0.0286 0.0279 0.1202 0.0294
406 0 2.280 1.290 4.605 -0.1089 0.1274 -0.0362 0.0284 0.1052 0.0319
407 0 2.280 1.290 4.605 -0.0938 0.1460 -0.0420 0.0266 0.1027 0.0304
408 0 2.110 1.645 4.565 -0.1588 0.5763 -0.0119 0.0713 0.0636 0.0462
409 0 2.040 1.645 5.305 0.1639 0.6054 0.1013 0.0517 0.0436 0.0389
410 0 2.100 1.645 6.195 -0.0541 0.3401 -0.1973 0.0551 0.0595 0.0716
411 0 1.480 1.645 6.175 -0.0179 -0.4248 0.2090 0.0528 0.1618 0.0566
412 0 1.500 1.645 5.355 -0.0124 -0.0356 0.1035 0.0492 0.1612 0.0692
413 0 1.490 1.645 4.535 -0.1394 0.3531 -0.1341 0.0297 0.0771 0.0278
414 0 0.920 1.645 4.535 -0.2124 0.3746 -0.1373 0.0349 0.0489 0.0218
415 0 0.860 1.645 5.505 -0.3181 -0.0998 0.3861 0.0845 0.0875 0.0580
416 0 0.930 1.645 6.195 0.1374 -0.2938 0.2273 0.0742 0.1284 0.0803
417 0 0.320 1.645 7.115 0.4093 0.0311 0.0481 0.0402 0.0710 0.0406
418 0 0.310 1.645 6.175 -0.2675 0.3050 0.4635 0.0808 0.0407 0.0624
419 0 0.320 1.645 5.465 -0.3597 0.0483 0.4382 0.0750 0.0641 0.0638
420 0 0.900 1.645 7.115 0.1814 0.2414 -0.0579 0.0505 0.0640 0.0437
421 0 0.900 1.645 7.115 0.2693 0.2279 0.0912 0.0503 0.0658 0.0367
422 0 0.900 1.645 7.115 0.1559 0.2394 -0.1363 0.0405 0.0460 0.0278
423 0 1.510 1.645 7.105 0.3133 -0.2565 0.0891 0.0357 0.0938 0.0489
424 0 2.080 1.645 7.100 0.2565 0.0885 -0.1092 0.0336 0.0429 0.0386
425 0 0.300 1.645 4.565 -0.1849 0.2876 -0.0382 0.0324 0.0446 0.0323
426 0 0.940 2.120 4.825 -0.0836 0.4652 0.1920 0.0491 0.1501 0.0568
427 0 1.460 2.120 4.815 -0.0921 0.6113 0.0948 0.0550 0.1323 0.0556
428 0 1.980 1.300 4.265 0.0949 -0.0150 0.1048 0.0101 0.0051 0.0127
429 0 1.980 1.300 3.155 -0.0282 0.0412 0.5387 0.0052 0.0046 0.0069
430 0 1.980 1.300 2.070 -0.0109 -0.0911 0.7961 0.0050 0.0054 0.0100
431 0 1.050 1.300 1.350 -0.0039 0.1120 0.8904 0.0141 0.0205 0.0229
432 0 0.300 0.660 1.710 -0.0091 0.1399 0.7177 0.0081 0.0045 0.0123
433 0 0.300 0.660 1.710 -0.0223 0.1396 0.7272 0.0081 0.0051 0.0126
434 0 0.300 0.660 1.710 -0.0217 0.1454 0.7173 0.0082 0.0047 0.0128
435 0 0.300 0.660 1.710 0.0201 0.1114 0.7829 0.0074 0.0046 0.0122
436 0 0.890 0.660 1.710 -0.0069 0.1212 0.9472 0.0063 0.0050 0.0143
437 0 0.900 0.660 2.805 -0.0491 0.0928 0.6073 0.0088 0.0068 0.0190
438 0 0.310 0.660 2.805 0.0107 0.0186 0.6913 0.0066 0.0047 0.0089
439 0 0.310 0.660 3.905 -0.1588 -0.0371 0.3141 0.0104 0.0073 0.0128

| | | | | | | | | | | |
|-----|---|-------|-------|-------|---------|---------|---------|--------|--------|--------|
| 440 | 0 | 0.900 | 0.660 | 3.905 | -0.1423 | 0.0085 | 0.5001 | 0.0160 | 0.0121 | 0.0232 |
| 441 | 0 | 0.700 | 1.200 | 0.270 | -0.1774 | 0.2195 | -0.5035 | 0.0360 | 0.0228 | 0.0724 |
| 442 | 0 | 0.700 | 2.050 | 0.460 | 0.0566 | 0.0218 | 1.2758 | 0.0622 | 0.1644 | 0.2510 |
| 443 | 0 | 0.700 | 2.050 | 0.460 | 0.0624 | 0.0152 | 1.2782 | 0.0613 | 0.1629 | 0.2512 |
| 444 | 0 | 0.700 | 2.050 | 0.460 | 0.0570 | 0.0244 | 1.2511 | 0.0649 | 0.1678 | 0.2570 |
| 445 | 0 | 0.700 | 2.050 | 0.460 | 0.0386 | 0.0287 | 1.2169 | 0.0657 | 0.1704 | 0.2583 |
| 446 | 0 | 0.700 | 0.400 | 2.270 | -0.0497 | -0.0102 | -0.0963 | 0.0011 | 0.0016 | 0.0014 |
| 447 | 0 | 0.700 | 0.400 | 2.270 | -0.0470 | -0.0226 | -0.1037 | 0.0009 | 0.0016 | 0.0012 |
| 448 | 0 | 0.700 | 0.400 | 2.270 | -0.0394 | -0.0186 | -0.0545 | 0.0009 | 0.0016 | 0.0012 |
| 449 | 0 | 0.700 | 0.400 | 2.270 | -0.0404 | -0.0245 | -0.0583 | 0.0010 | 0.0017 | 0.0012 |
| 450 | 0 | 0.700 | 0.400 | 2.270 | -0.0392 | -0.0318 | -0.0721 | 0.0010 | 0.0018 | 0.0012 |
| 451 | 0 | 0.700 | 0.400 | 2.270 | -0.0433 | -0.0374 | -0.0801 | 0.0011 | 0.0020 | 0.0015 |
| 452 | 0 | 0.700 | 0.400 | 2.270 | -0.0486 | -0.0359 | -0.0833 | 0.0010 | 0.0017 | 0.0014 |
| 453 | 0 | 0.700 | 1.210 | 2.260 | 0.0604 | -0.0961 | -0.2717 | 0.0081 | 0.0109 | 0.0104 |
| 454 | 0 | 0.700 | 2.190 | 2.260 | -0.1121 | -0.8981 | 0.7440 | 0.1641 | 0.1594 | 0.2166 |
| 455 | 0 | 0.700 | 0.360 | 4.475 | -0.0521 | 0.2731 | -0.1522 | 0.0146 | 0.0155 | 0.0130 |
| 456 | 0 | 0.700 | 1.205 | 4.470 | -0.3166 | 0.3125 | -0.1234 | 0.0128 | 0.0273 | 0.0076 |
| 457 | 0 | 0.700 | 2.180 | 4.465 | -0.0626 | -0.7577 | 0.1581 | 0.1625 | 0.1368 | 0.1792 |
| 458 | 0 | 0.700 | 2.180 | 4.465 | -0.0286 | -0.7753 | 0.1518 | 0.1561 | 0.1316 | 0.1942 |
| 459 | 0 | 0.700 | 2.180 | 4.465 | -0.0278 | -0.7481 | 0.1296 | 0.1530 | 0.1350 | 0.1733 |
| 460 | 0 | 0.700 | 2.180 | 4.465 | -0.0426 | -0.7644 | 0.1638 | 0.1538 | 0.1400 | 0.1909 |
| 461 | 0 | 0.700 | 0.395 | 6.960 | 0.1944 | -0.1227 | -0.0201 | 0.0192 | 0.0208 | 0.0168 |
| 462 | 0 | 0.700 | 1.200 | 6.960 | -0.0119 | 0.1418 | 0.0538 | 0.0301 | 0.0280 | 0.0376 |
| 463 | 0 | 0.700 | 1.200 | 6.960 | 0.0002 | 0.1495 | 0.0792 | 0.0299 | 0.0286 | 0.0386 |
| 464 | 0 | 0.700 | 1.200 | 6.960 | 0.0045 | 0.1451 | 0.0711 | 0.0316 | 0.0268 | 0.0369 |
| 465 | 0 | 0.700 | 1.200 | 6.960 | 0.0049 | 0.1524 | 0.0618 | 0.0301 | 0.0295 | 0.0411 |
| 466 | 0 | 0.700 | 1.200 | 6.960 | -0.0132 | 0.1786 | 0.0478 | 0.0288 | 0.0260 | 0.0357 |
| 467 | 0 | 0.700 | 1.200 | 6.960 | 0.0097 | 0.1635 | 0.0439 | 0.0274 | 0.0247 | 0.0349 |
| 468 | 0 | 0.700 | 1.200 | 6.960 | -0.0071 | 0.1757 | 0.0608 | 0.0306 | 0.0283 | 0.0413 |
| 469 | 0 | 0.700 | 2.125 | 6.950 | 0.2224 | -0.0006 | 0.1584 | 0.0472 | 0.1039 | 0.1409 |
| 471 | 0 | 0.685 | 0.395 | 0.265 | -0.0411 | 0.2108 | -0.7320 | 0.0073 | 0.0150 | 0.0073 |
| 472 | 0 | 0.685 | 0.395 | 0.265 | -0.0294 | 0.1444 | -0.6633 | 0.0081 | 0.0127 | 0.0087 |
| 473 | 0 | 0.685 | 0.395 | 0.265 | -0.0375 | 0.1500 | -0.6496 | 0.0086 | 0.0127 | 0.0086 |
| 474 | 0 | 0.685 | 0.395 | 0.265 | -0.0298 | 0.1406 | -0.6403 | 0.0080 | 0.0131 | 0.0084 |
| 475 | 0 | 0.685 | 0.395 | 0.265 | -0.0192 | 0.1360 | -0.6265 | 0.0074 | 0.0115 | 0.0081 |
| 476 | 0 | 0.685 | 0.395 | 0.265 | -0.0926 | 0.2982 | -0.7422 | 0.0153 | 0.0207 | 0.0131 |
| 477 | 0 | 0.685 | 0.395 | 0.265 | -0.0858 | 0.3160 | -0.7461 | 0.0151 | 0.0186 | 0.0143 |
| 478 | 0 | 0.685 | 0.395 | 0.265 | -0.0742 | 0.3338 | -0.7770 | 0.0147 | 0.0215 | 0.0133 |
| 479 | 0 | 0.685 | 0.395 | 0.265 | -0.0710 | 0.3144 | -0.7728 | 0.0143 | 0.0211 | 0.0134 |
| 480 | 0 | 0.685 | 0.395 | 0.265 | -0.0758 | 0.3394 | -0.7847 | 0.0151 | 0.0196 | 0.0138 |
| 481 | 0 | 0.685 | 0.395 | 0.265 | -0.0850 | 0.3276 | -0.7863 | 0.0161 | 0.0217 | 0.0142 |
| 482 | 0 | 0.685 | 0.395 | 0.265 | -0.0767 | 0.3299 | -0.7874 | 0.0155 | 0.0200 | 0.0128 |
| 483 | 0 | 0.685 | 0.395 | 0.265 | -0.0755 | 0.3222 | -0.7589 | 0.0125 | 0.0160 | 0.0117 |
| 484 | 0 | 0.685 | 0.395 | 0.265 | -0.0150 | 0.1661 | -0.7026 | 0.0071 | 0.0167 | 0.0087 |
| 485 | 0 | 0.685 | 0.395 | 0.265 | -0.0309 | 0.2017 | -0.6699 | 0.0082 | 0.0183 | 0.0095 |
| 486 | 0 | 0.685 | 0.395 | 0.265 | -0.0517 | 0.2152 | -0.6960 | 0.0081 | 0.0179 | 0.0090 |
| 487 | 0 | 0.685 | 0.395 | 0.265 | -0.0489 | 0.2114 | -0.6927 | 0.0080 | 0.0159 | 0.0081 |
| 488 | 0 | 0.685 | 0.395 | 0.265 | -0.0562 | 0.2168 | -0.6926 | 0.0076 | 0.0152 | 0.0082 |
| 489 | 0 | 0.685 | 0.395 | 0.265 | -0.0618 | 0.2198 | -0.6862 | 0.0071 | 0.0140 | 0.0074 |
| 490 | 0 | 0.685 | 0.395 | 0.265 | -0.0693 | 0.2181 | -0.6713 | 0.0067 | 0.0141 | 0.0063 |
| 491 | 0 | 0.685 | 0.395 | 0.265 | -0.0731 | 0.2275 | -0.6688 | 0.0063 | 0.0133 | 0.0065 |
| 492 | 0 | 0.685 | 0.395 | 0.265 | -0.0713 | 0.2175 | -0.6612 | 0.0066 | 0.0147 | 0.0062 |
| 493 | 0 | 0.685 | 0.395 | 0.265 | -0.0667 | 0.2104 | -0.6569 | 0.0060 | 0.0135 | 0.0067 |

494 0 0.685 0.395 0.265 -0.0605 0.2105 -0.6467 0.0064 0.0133 0.0075
495 0 0.685 0.395 0.265 -0.0632 0.2088 -0.6517 0.0070 0.0137 0.0073
496 0 0.685 0.395 0.265 -0.0657 0.2075 -0.6662 0.0073 0.0143 0.0077
497 0 0.685 0.395 0.265 -0.0690 0.2016 -0.6815 0.0072 0.0144 0.0077
498 0 0.685 0.395 0.265 -0.0756 0.1851 -0.6855 0.0075 0.0153 0.0085
499 0 0.685 0.395 0.265 -0.0579 0.1700 -0.6584 0.0079 0.0150 0.0079

Experimental data file for side half loaded model load space

500 0 2.080 0.660 1.130 -0.0411 0.1457 0.6430 0.0149 0.0087 0.0229
501 0 2.090 0.660 2.240 0.0703 0.0832 0.6958 0.0092 0.0063 0.0104
502 0 2.090 0.660 3.350 -0.0371 0.0524 0.4195 0.0047 0.0053 0.0108
503 0 2.100 0.660 4.460 -0.0523 0.0467 0.3812 0.0039 0.0043 0.0085
504 0 2.100 0.660 5.545 -0.0549 0.0754 0.2175 0.0031 0.0041 0.0070
505 0 2.090 0.660 6.645 0.0747 0.1975 0.1413 0.0062 0.0037 0.0031
506 0 0.300 0.660 6.645 -0.0284 0.1614 0.1589 0.0060 0.0035 0.0035
507 0 0.310 0.660 5.545 0.0444 0.0848 0.2861 0.0032 0.0049 0.0085
508 0 0.310 0.660 4.460 0.0939 -0.0061 0.4618 0.0050 0.0067 0.0097
509 0 0.320 0.660 3.350 0.1087 0.0398 0.5934 0.0061 0.0072 0.0156
510 0 0.320 0.660 2.240 -0.0538 0.1489 0.7120 0.0141 0.0095 0.0164
511 0 0.310 0.660 1.130 0.0305 0.1676 0.5437 0.0127 0.0133 0.0410
512 0 0.970 1.120 1.120 -0.0139 0.0020 -0.9432 0.0542 0.0600 0.0724
513 0 1.000 1.120 1.980 -0.1747 -0.1451 -0.6511 0.0686 0.0690 0.0876
514 0 1.030 1.120 2.870 0.1093 0.1163 -0.5166 0.0413 0.0440 0.0720
515 0 1.010 1.120 4.145 0.0202 0.0983 -0.4068 0.0293 0.0385 0.0456
516 0 0.990 1.120 5.235 0.0176 0.0181 -0.1315 0.0229 0.0266 0.0238
517 0 0.970 1.120 6.285 0.0565 -0.1590 0.1002 0.0213 0.0311 0.0236
518 0 0.970 1.120 6.285 0.0489 -0.1668 0.1111 0.0198 0.0266 0.0247
519 0 0.970 1.120 6.285 0.0599 -0.1680 0.1040 0.0238 0.0361 0.0272
520 0 1.500 1.120 6.435 -0.0755 -0.2356 0.1408 0.0197 0.0333 0.0211
521 0 1.490 1.120 5.345 -0.0524 -0.0232 -0.0400 0.0185 0.0254 0.0235
522 0 1.510 1.120 4.175 -0.0958 -0.0360 -0.1960 0.0260 0.0316 0.0486
523 0 1.510 1.120 3.030 -0.0087 0.0076 -0.4240 0.0295 0.0247 0.0458
524 0 1.510 1.120 1.950 -0.0188 -0.1829 -0.5312 0.0597 0.0528 0.0769
525 0 1.500 1.120 0.900 -0.0397 -0.0064 -0.8163 0.0445 0.0492 0.0768
526 0 0.900 0.390 1.150 0.0060 0.0057 -1.0260 0.0312 0.0278 0.0322
527 0 0.920 0.390 2.190 0.0126 -0.0911 -0.8334 0.0258 0.0383 0.0287
528 0 0.920 0.390 3.375 -0.0363 0.1150 -0.6572 0.0154 0.0246 0.0141
529 0 0.940 0.390 4.395 -0.1065 0.3198 -0.5772 0.0085 0.0134 0.0180
530 0 0.920 0.390 5.565 0.0154 0.1078 -0.5200 0.0085 0.0109 0.0078
531 0 0.930 0.390 6.645 0.0136 -0.0791 -0.1990 0.0062 0.0109 0.0083
532 0 1.470 0.390 6.645 -0.0374 -0.0724 -0.2318 0.0080 0.0147 0.0092
533 0 1.480 0.390 5.535 -0.0755 0.1271 -0.5752 0.0082 0.0113 0.0121
534 0 1.480 0.390 4.415 0.0272 0.3148 -0.8125 0.0076 0.0099 0.0179
535 0 1.480 0.390 3.350 0.0981 0.2756 -0.7247 0.0128 0.0170 0.0218
536 0 1.480 0.390 2.300 0.0707 0.1342 -0.8993 0.0178 0.0243 0.0198
537 0 1.480 0.390 1.230 0.0183 0.2082 -1.1687 0.0199 0.0285 0.0205
538 0 2.050 1.360 6.995 -0.0038 0.0964 -0.1025 0.0055 0.0043 0.0097
539 0 1.450 1.360 6.985 0.0851 -0.2017 0.1539 0.0321 0.0261 0.0480
540 0 1.440 1.360 5.835 -0.0250 -0.0912 0.1974 0.0368 0.0358 0.0450
541 0 2.050 1.360 5.865 -0.0885 0.0698 -0.3546 0.0029 0.0030 0.0072
542 0 1.480 1.360 4.755 -0.0488 0.0296 -0.0002 0.0310 0.0348 0.0456
543 0 2.050 1.360 4.785 -0.0503 0.0699 -0.3407 0.0031 0.0033 0.0095

| | | | | | | | | | | |
|-----|---|-------|-------|-------|---------|---------|---------|--------|--------|--------|
| 544 | 0 | 1.540 | 1.360 | 3.640 | -0.0227 | -0.0052 | -0.0427 | 0.0380 | 0.0433 | 0.0564 |
| 545 | 0 | 2.050 | 1.360 | 3.640 | -0.0759 | 0.0777 | -0.2765 | 0.0043 | 0.0040 | 0.0134 |
| 546 | 0 | 1.530 | 1.360 | 2.570 | 0.0878 | -0.0033 | -0.2227 | 0.0547 | 0.0552 | 0.0834 |
| 547 | 0 | 2.050 | 1.360 | 2.560 | 0.1303 | -0.0050 | -0.4373 | 0.0081 | 0.0037 | 0.0173 |
| 548 | 0 | 1.500 | 1.360 | 1.450 | -0.1751 | -0.3067 | -0.5959 | 0.1158 | 0.1115 | 0.0892 |
| 549 | 0 | 2.060 | 1.360 | 1.450 | -0.0652 | 0.0702 | -0.8238 | 0.0117 | 0.0089 | 0.0237 |
| 550 | 0 | 0.340 | 1.360 | 0.230 | -0.3480 | 0.5705 | 0.0736 | 0.0247 | 0.0146 | 0.0294 |
| 551 | 0 | 0.350 | 1.360 | 1.410 | 0.1364 | 0.1190 | -0.6982 | 0.0054 | 0.0077 | 0.0207 |
| 552 | 0 | 0.930 | 1.360 | 1.380 | 0.1183 | -0.3238 | -0.4900 | 0.0793 | 0.0868 | 0.0845 |
| 553 | 0 | 0.970 | 1.360 | 2.500 | 0.0391 | -0.1934 | -0.1602 | 0.0835 | 0.0974 | 0.1060 |
| 554 | 0 | 0.350 | 1.360 | 2.520 | -0.0787 | 0.0431 | -0.3800 | 0.0099 | 0.0050 | 0.0189 |
| 555 | 0 | 0.350 | 1.360 | 3.650 | 0.0921 | 0.0966 | -0.0482 | 0.0092 | 0.0098 | 0.0227 |
| 556 | 0 | 0.970 | 1.360 | 3.600 | 0.1042 | 0.1196 | -0.1636 | 0.0437 | 0.0408 | 0.0988 |
| 557 | 0 | 0.350 | 1.360 | 4.735 | 0.1160 | 0.0401 | -0.1975 | 0.0057 | 0.0060 | 0.0164 |
| 558 | 0 | 0.920 | 1.360 | 4.695 | 0.0524 | 0.0004 | 0.0463 | 0.0414 | 0.0462 | 0.0652 |
| 559 | 0 | 0.350 | 1.360 | 5.845 | 0.1046 | 0.0749 | -0.1880 | 0.0026 | 0.0031 | 0.0110 |
| 560 | 0 | 0.970 | 1.360 | 5.845 | 0.0399 | -0.1127 | 0.2647 | 0.0435 | 0.0438 | 0.0502 |
| 561 | 0 | 0.350 | 1.360 | 6.915 | -0.0018 | 0.1502 | -0.0841 | 0.0044 | 0.0065 | 0.0062 |
| 562 | 0 | 0.930 | 1.360 | 6.915 | -0.0731 | -0.2216 | 0.2114 | 0.0391 | 0.0279 | 0.0438 |
| 563 | 0 | 2.070 | 1.360 | 0.180 | 0.3792 | 0.7020 | 0.2411 | 0.0319 | 0.0162 | 0.0256 |
| 564 | 0 | 1.540 | 1.360 | 0.170 | 0.3320 | 0.7342 | -0.3179 | 0.0254 | 0.0229 | 0.0602 |
| 565 | 0 | 1.620 | 1.635 | 0.640 | -0.1757 | 0.3733 | -0.0729 | 0.0254 | 0.0401 | 0.0725 |
| 566 | 0 | 1.620 | 1.635 | 0.640 | -0.1889 | 0.3895 | -0.0680 | 0.0255 | 0.0412 | 0.0671 |
| 567 | 0 | 1.620 | 1.635 | 0.640 | -0.1799 | 0.3594 | -0.0598 | 0.0230 | 0.0355 | 0.0586 |
| 568 | 0 | 1.570 | 1.635 | 1.950 | -0.1164 | -0.1761 | 0.1861 | 0.0941 | 0.1490 | 0.1054 |
| 569 | 0 | 1.560 | 1.635 | 3.055 | 0.0181 | 0.1390 | -0.0786 | 0.0548 | 0.1169 | 0.0904 |
| 570 | 0 | 1.530 | 1.635 | 4.035 | -0.0618 | -0.1198 | 0.2668 | 0.0650 | 0.1387 | 0.0878 |
| 571 | 0 | 1.530 | 1.635 | 5.125 | -0.1115 | -0.0982 | 0.3177 | 0.0699 | 0.1022 | 0.0765 |
| 572 | 0 | 1.520 | 1.635 | 6.215 | -0.1551 | -0.1002 | 0.3114 | 0.0677 | 0.0923 | 0.0606 |
| 573 | 0 | 0.860 | 1.635 | 6.045 | 0.0860 | -0.0068 | 0.3831 | 0.0692 | 0.0846 | 0.0751 |
| 574 | 0 | 0.890 | 1.635 | 5.145 | 0.0875 | 0.0067 | 0.3456 | 0.0862 | 0.0859 | 0.0798 |
| 575 | 0 | 0.840 | 1.635 | 3.825 | 0.1026 | -0.0244 | 0.3301 | 0.0748 | 0.0988 | 0.0853 |
| 576 | 0 | 0.880 | 1.635 | 2.730 | -0.0050 | -0.1329 | 0.3282 | 0.0923 | 0.0970 | 0.0942 |
| 577 | 0 | 0.860 | 1.635 | 1.660 | -0.1203 | -0.3170 | 0.2896 | 0.1113 | 0.0855 | 0.1244 |
| 578 | 0 | 0.860 | 1.635 | 0.490 | 0.1378 | 0.5544 | -0.2643 | 0.0546 | 0.0346 | 0.0498 |
| 579 | 0 | 0.860 | 1.635 | 0.490 | 0.1612 | 0.5551 | -0.2434 | 0.0535 | 0.0301 | 0.0450 |
| 580 | 0 | 0.860 | 1.635 | 0.490 | 0.1606 | 0.5561 | -0.2630 | 0.0532 | 0.0338 | 0.0441 |
| 581 | 0 | 2.070 | 2.120 | 0.250 | 0.2568 | 0.4461 | 0.6785 | 0.0160 | 0.0177 | 0.0132 |
| 582 | 0 | 2.080 | 2.120 | 1.420 | 0.1030 | 0.2316 | 0.7770 | 0.0654 | 0.0832 | 0.0908 |
| 583 | 0 | 2.070 | 2.120 | 2.530 | -0.0291 | 0.4165 | 0.2301 | 0.0188 | 0.0397 | 0.0332 |
| 584 | 0 | 2.070 | 2.120 | 3.630 | 0.1137 | 0.0564 | -0.0186 | 0.0183 | 0.0438 | 0.0351 |
| 585 | 0 | 2.080 | 2.120 | 4.740 | 0.0889 | 0.3446 | -0.1098 | 0.0229 | 0.0526 | 0.0292 |
| 586 | 0 | 2.080 | 2.120 | 5.835 | 0.1340 | 0.5996 | -0.2936 | 0.0431 | 0.0386 | 0.0335 |
| 587 | 0 | 0.330 | 2.120 | 6.965 | -0.1544 | 0.1444 | -0.0641 | 0.0164 | 0.0329 | 0.0120 |
| 588 | 0 | 0.330 | 2.120 | 6.325 | -0.0282 | 0.2172 | -0.2145 | 0.0221 | 0.0401 | 0.0308 |
| 589 | 0 | 0.340 | 2.120 | 5.785 | -0.1581 | 0.2879 | -0.0630 | 0.0262 | 0.0488 | 0.0308 |
| 590 | 0 | 0.340 | 2.120 | 4.710 | -0.0949 | 0.1079 | 0.1123 | 0.0218 | 0.0772 | 0.0216 |
| 591 | 0 | 0.340 | 2.120 | 3.600 | -0.0160 | 0.3230 | 0.2153 | 0.0258 | 0.0640 | 0.0412 |
| 592 | 0 | 0.340 | 2.120 | 2.440 | -0.0086 | 0.2344 | 0.3330 | 0.0200 | 0.0250 | 0.0419 |
| 593 | 0 | 0.350 | 2.120 | 1.350 | -0.1300 | 0.0282 | 1.1055 | 0.0576 | 0.0447 | 0.0492 |
| 594 | 0 | 0.360 | 2.120 | 0.880 | -0.3246 | 0.1322 | 1.0764 | 0.0895 | 0.0419 | 0.0752 |
| 650 | 0 | 0.700 | 1.200 | 0.270 | -0.3913 | 0.6066 | -0.5853 | 0.0296 | 0.0225 | 0.0557 |
| 651 | 0 | 0.700 | 1.200 | 0.270 | -0.3858 | 0.6059 | -0.5800 | 0.0288 | 0.0217 | 0.0503 |

| | | | | | | | | | | |
|-----|---|-------|-------|-------|---------|---------|---------|--------|--------|--------|
| 652 | 0 | 0.700 | 1.200 | 0.270 | -0.3698 | 0.5943 | -0.5670 | 0.0270 | 0.0213 | 0.0494 |
| 653 | 0 | 0.700 | 2.050 | 0.460 | -0.0683 | 0.3749 | 0.5142 | 0.0393 | 0.0366 | 0.0612 |
| 654 | 0 | 0.700 | 2.050 | 0.460 | -0.0617 | 0.3668 | 0.5056 | 0.0374 | 0.0389 | 0.0617 |
| 655 | 0 | 0.700 | 2.050 | 0.460 | -0.0659 | 0.3646 | 0.5110 | 0.0389 | 0.0384 | 0.0624 |
| 656 | 0 | 0.700 | 2.050 | 0.460 | -0.0628 | 0.3803 | 0.5449 | 0.0394 | 0.0393 | 0.0630 |
| 657 | 0 | 0.700 | 2.050 | 0.460 | -0.0801 | 0.3698 | 0.5080 | 0.0394 | 0.0374 | 0.0562 |
| 658 | 0 | 0.700 | 2.050 | 0.460 | -0.0780 | 0.3604 | 0.4971 | 0.0394 | 0.0383 | 0.0606 |
| 659 | 0 | 0.700 | 0.400 | 2.270 | -0.0441 | -0.3277 | -0.7593 | 0.0215 | 0.0400 | 0.0676 |
| 660 | 0 | 0.700 | 0.400 | 2.270 | -0.0295 | -0.3402 | -0.7640 | 0.0188 | 0.0375 | 0.0571 |
| 661 | 0 | 0.700 | 0.400 | 2.270 | -0.0296 | -0.3611 | -0.7580 | 0.0181 | 0.0383 | 0.0550 |
| 662 | 0 | 0.700 | 1.210 | 2.260 | 0.0255 | -0.5549 | 0.1619 | 0.0564 | 0.0728 | 0.0680 |
| 663 | 0 | 0.700 | 1.210 | 2.260 | 0.0372 | -0.5741 | 0.1392 | 0.0573 | 0.0718 | 0.0744 |
| 664 | 0 | 0.700 | 1.210 | 2.260 | 0.0336 | -0.5705 | 0.1430 | 0.0549 | 0.0736 | 0.0701 |
| 665 | 0 | 0.700 | 2.190 | 2.260 | 0.2815 | -0.6373 | 0.3180 | 0.1373 | 0.1066 | 0.1369 |
| 666 | 0 | 0.700 | 2.190 | 2.260 | 0.2822 | -0.6477 | 0.3076 | 0.1309 | 0.1084 | 0.1387 |
| 667 | 0 | 0.700 | 2.190 | 2.260 | 0.2773 | -0.6125 | 0.2751 | 0.1240 | 0.1023 | 0.1293 |
| 668 | 0 | 0.700 | 0.400 | 2.270 | -0.0266 | -0.3479 | -0.7654 | 0.0199 | 0.0364 | 0.0647 |
| 669 | 0 | 0.700 | 0.400 | 2.270 | -0.0265 | -0.3589 | -0.7706 | 0.0183 | 0.0347 | 0.0581 |
| 670 | 0 | 0.700 | 0.400 | 2.270 | -0.0022 | -0.3757 | -0.7367 | 0.0191 | 0.0358 | 0.0655 |
| 671 | 0 | 0.700 | 0.400 | 2.270 | -0.0075 | -0.3881 | -0.7537 | 0.0178 | 0.0327 | 0.0600 |
| 672 | 0 | 0.700 | 0.360 | 4.475 | -0.0568 | -0.0786 | -0.6842 | 0.0076 | 0.0079 | 0.0112 |
| 673 | 0 | 0.700 | 0.360 | 4.475 | -0.0413 | -0.0977 | -0.6870 | 0.0070 | 0.0075 | 0.0094 |
| 674 | 0 | 0.700 | 0.360 | 4.475 | -0.0283 | -0.1167 | -0.6896 | 0.0064 | 0.0066 | 0.0089 |
| 675 | 0 | 0.700 | 1.205 | 4.470 | 0.1040 | -0.1006 | -0.1322 | 0.0223 | 0.0365 | 0.0419 |
| 676 | 0 | 0.700 | 1.205 | 4.470 | 0.1130 | -0.1179 | -0.1355 | 0.0214 | 0.0349 | 0.0408 |
| 677 | 0 | 0.700 | 1.205 | 4.470 | 0.1161 | -0.1073 | -0.1391 | 0.0214 | 0.0323 | 0.0404 |
| 678 | 0 | 0.700 | 2.180 | 4.465 | 0.1536 | -0.8159 | 0.3814 | 0.1275 | 0.1230 | 0.1870 |
| 679 | 0 | 0.700 | 2.180 | 4.465 | 0.1402 | -0.8355 | 0.3502 | 0.1069 | 0.1133 | 0.1542 |
| 680 | 0 | 0.700 | 2.180 | 4.465 | 0.1428 | -0.8556 | 0.3822 | 0.1287 | 0.1208 | 0.1813 |
| 681 | 0 | 0.700 | 2.180 | 4.465 | 0.0999 | -0.8834 | 0.4867 | 0.1220 | 0.1339 | 0.1975 |
| 682 | 0 | 0.700 | 2.180 | 4.465 | 0.1305 | -0.9017 | 0.4786 | 0.1257 | 0.1395 | 0.1929 |
| 683 | 0 | 0.700 | 2.180 | 4.465 | 0.1280 | -0.8852 | 0.4400 | 0.1193 | 0.1313 | 0.1973 |
| 684 | 0 | 0.700 | 2.180 | 4.465 | 0.0957 | -0.9106 | 0.4742 | 0.1290 | 0.1260 | 0.1992 |
| 685 | 0 | 0.700 | 0.395 | 6.960 | -0.0440 | -0.2612 | -0.1041 | 0.0061 | 0.0124 | 0.0097 |
| 686 | 0 | 0.700 | 0.395 | 6.960 | -0.0437 | -0.2755 | -0.1275 | 0.0062 | 0.0108 | 0.0098 |
| 687 | 0 | 0.700 | 0.395 | 6.960 | -0.0238 | -0.2975 | -0.1340 | 0.0054 | 0.0099 | 0.0091 |
| 688 | 0 | 0.700 | 1.200 | 6.960 | -0.0217 | -0.3474 | 0.1236 | 0.0175 | 0.0286 | 0.0326 |
| 689 | 0 | 0.700 | 1.200 | 6.960 | -0.0182 | -0.3232 | 0.1046 | 0.0180 | 0.0293 | 0.0281 |
| 690 | 0 | 0.700 | 1.200 | 6.960 | -0.0260 | -0.3070 | 0.1010 | 0.0189 | 0.0277 | 0.0267 |
| 691 | 0 | 0.700 | 1.200 | 6.960 | -0.0195 | -0.3123 | 0.0975 | 0.0194 | 0.0318 | 0.0279 |
| 692 | 0 | 0.700 | 1.200 | 6.960 | -0.0155 | -0.3022 | 0.0951 | 0.0185 | 0.0320 | 0.0276 |
| 693 | 0 | 0.700 | 1.200 | 6.960 | -0.0252 | -0.2909 | 0.0969 | 0.0191 | 0.0317 | 0.0269 |
| 694 | 0 | 0.700 | 1.200 | 6.960 | -0.0238 | -0.2969 | 0.0927 | 0.0186 | 0.0325 | 0.0256 |
| 695 | 0 | 0.700 | 2.125 | 6.950 | -0.1925 | -0.9621 | 0.7247 | 0.0947 | 0.2127 | 0.1790 |
| 696 | 0 | 0.700 | 2.125 | 6.950 | -0.2095 | -0.9554 | 0.7239 | 0.0962 | 0.2192 | 0.1794 |
| 697 | 0 | 0.700 | 2.125 | 6.950 | -0.2130 | -0.9576 | 0.7222 | 0.0947 | 0.2184 | 0.1791 |
| 698 | 0 | 0.700 | 2.125 | 6.950 | -0.2254 | -0.9689 | 0.7388 | 0.0905 | 0.2138 | 0.1841 |
| 699 | 0 | 0.700 | 2.125 | 6.950 | -0.2221 | -0.9713 | 0.7254 | 0.0951 | 0.2231 | 0.1817 |
| 700 | 0 | 0.685 | 0.395 | 0.265 | -0.2320 | 0.0177 | -0.9624 | 0.0161 | 0.0213 | 0.0336 |
| 701 | 0 | 0.685 | 0.395 | 0.265 | -0.2347 | 0.0213 | -0.9544 | 0.0164 | 0.0228 | 0.0318 |
| 702 | 0 | 0.685 | 0.395 | 0.265 | -0.2290 | 0.0203 | -0.9355 | 0.0148 | 0.0210 | 0.0290 |
| 703 | 0 | 0.685 | 0.395 | 0.265 | -0.2086 | 0.0065 | -0.9192 | 0.0162 | 0.0231 | 0.0312 |
| 704 | 0 | 0.685 | 0.395 | 0.265 | -0.2092 | 0.0098 | -0.9134 | 0.0171 | 0.0209 | 0.0310 |

705 0 0.685 0.395 0.265 -0.2061 0.0023 -0.9087 0.0173 0.0223 0.0299
706 0 0.685 0.395 0.265 -0.2049 -0.0149 -0.9169 0.0173 0.0214 0.0319
707 0 0.685 0.395 0.265 -0.2122 0.0031 -0.9075 0.0176 0.0225 0.0326
708 0 0.685 0.395 0.265 -0.2077 -0.0015 -0.8991 0.0173 0.0233 0.0282
709 0 0.685 0.395 0.265 -0.2222 0.0058 -0.9460 0.0195 0.0244 0.0316
710 0 0.685 0.395 0.265 -0.2232 0.0121 -0.9372 0.0170 0.0212 0.0292
711 0 0.685 0.395 0.265 -0.2132 0.0164 -0.9110 0.0164 0.0233 0.0269
712 0 0.685 0.395 0.265 -0.2268 0.0169 -0.9304 0.0171 0.0228 0.0297
713 0 0.685 0.395 0.265 -0.2284 0.0217 -0.9526 0.0161 0.0234 0.0259
714 0 0.685 0.395 0.265 -0.2248 0.0146 -0.9343 0.0152 0.0235 0.0269
715 0 0.685 0.395 0.265 -0.2222 0.0386 -0.9725 0.0141 0.0234 0.0280
716 0 0.685 0.395 0.265 -0.2108 0.0296 -0.9614 0.0168 0.0262 0.0287
717 0 0.685 0.395 0.265 -0.2175 0.0334 -0.9808 0.0152 0.0253 0.0279
718 0 0.685 0.395 0.265 -0.2160 0.0145 -0.9284 0.0170 0.0240 0.0278
719 0 0.685 0.395 0.265 -0.2013 0.0029 -0.9394 0.0164 0.0243 0.0288
720 0 0.685 0.395 0.265 -0.1953 -0.0081 -0.9538 0.0166 0.0253 0.0268
721 0 0.685 0.395 0.265 -0.1974 -0.0059 -0.9647 0.0182 0.0262 0.0257
722 0 0.685 0.395 0.265 -0.2232 0.0122 -0.9522 0.0180 0.0227 0.0281
723 0 0.685 0.395 0.265 -0.2037 0.0103 -0.9614 0.0171 0.0257 0.0274
724 0 0.685 0.395 0.265 -0.2040 0.0027 -0.9639 0.0170 0.0267 0.0278
725 0 0.685 0.395 0.265 -0.2250 0.0207 -0.9752 0.0171 0.0243 0.0286
726 0 0.685 0.395 0.265 -0.2175 0.0190 -0.9724 0.0166 0.0244 0.0305
727 0 0.685 0.395 0.265 -0.2004 0.0057 -0.9796 0.0177 0.0264 0.0270
728 0 0.685 0.395 0.265 -0.2063 -0.0074 -0.9133 0.0175 0.0266 0.0257
729 0 0.685 0.395 0.265 -0.2009 -0.0021 -0.9255 0.0173 0.0257 0.0252
730 0 0.685 0.395 0.265 -0.2032 -0.0127 -0.9610 0.0193 0.0288 0.0263
731 0 0.685 0.395 0.265 -0.1974 -0.0243 -0.9342 0.0179 0.0261 0.0280
732 0 0.685 0.395 0.265 -0.2112 -0.0093 -0.9366 0.0181 0.0256 0.0279
733 0 0.685 0.395 0.265 -0.2118 -0.0057 -0.9262 0.0183 0.0262 0.0313
734 0 0.685 0.395 0.265 -0.2224 0.0074 -0.9192 0.0162 0.0234 0.0280
735 0 0.685 0.395 0.265 -0.2188 0.0119 -0.9153 0.0174 0.0241 0.0286
736 0 0.685 0.395 0.265 -0.2196 0.0154 -0.9116 0.0165 0.0225 0.0264
737 0 0.685 0.395 0.265 -0.2166 0.0072 -0.9247 0.0177 0.0255 0.0273
738 0 0.685 0.395 0.265 -0.2162 -0.0013 -0.9163 0.0176 0.0255 0.0267
739 0 0.685 0.395 0.265 -0.2008 -0.0042 -0.9258 0.0173 0.0260 0.0263
740 0 0.685 0.395 0.265 -0.2059 -0.0028 -0.9501 0.0176 0.0279 0.0264
741 0 0.685 0.395 0.265 -0.2041 -0.0073 -0.9614 0.0176 0.0292 0.0287
742 0 0.685 0.395 0.265 -0.1880 -0.0150 -0.9637 0.0184 0.0296 0.0266
743 0 0.685 0.395 0.265 -0.1848 -0.0117 -0.9685 0.0183 0.0284 0.0278
744 0 0.685 0.395 0.265 -0.1862 -0.0122 -0.9729 0.0198 0.0301 0.0288
745 0 0.685 0.395 0.265 -0.1906 -0.0111 -0.9598 0.0197 0.0283 0.0273
746 0 0.685 0.395 0.265 -0.1867 -0.0120 -0.9683 0.0190 0.0294 0.0306
747 0 0.685 0.395 0.265 -0.1855 -0.0216 -0.9611 0.0208 0.0304 0.0280
748 0 0.685 0.395 0.265 -0.1872 -0.0157 -0.9738 0.0192 0.0307 0.0319
749 0 0.685 0.395 0.265 -0.1799 -0.0219 -0.9699 0.0199 0.0307 0.0327

Experimental data summary file for fully loaded model load space

800 0 0.700 2.050 0.460 0.1083 -0.2962 1.0762 0.0651 0.1882 0.3198
801 0 0.700 2.050 0.460 0.1128 -0.3133 1.0962 0.0659 0.1921 0.3361
802 0 0.700 2.050 0.460 0.1026 -0.3160 1.1355 0.0672 0.2008 0.3424
803 0 0.700 2.190 2.260 -0.1915 -0.8047 0.6129 0.1725 0.1785 0.2626
804 0 0.700 2.190 2.260 -0.2273 -0.8261 0.6783 0.1617 0.1850 0.2595

| | | | | | | | | | | |
|-----|---|-------|-------|-------|---------|---------|---------|--------|--------|--------|
| 805 | 0 | 0.700 | 2.190 | 2.260 | -0.2222 | -0.7856 | 0.6565 | 0.1646 | 0.1725 | 0.2581 |
| 806 | 0 | 0.700 | 2.180 | 4.465 | 0.0712 | -0.9846 | 0.4755 | 0.0934 | 0.1199 | 0.1437 |
| 807 | 0 | 0.700 | 2.180 | 4.465 | 0.0261 | -0.9956 | 0.5335 | 0.0935 | 0.1178 | 0.1505 |
| 808 | 0 | 0.700 | 2.180 | 4.465 | 0.0890 | -0.9631 | 0.4982 | 0.1027 | 0.1238 | 0.1449 |
| 809 | 0 | 0.700 | 2.125 | 6.950 | 0.3564 | -0.3788 | 0.0692 | 0.0331 | 0.1102 | 0.0853 |
| 810 | 0 | 0.700 | 2.125 | 6.950 | 0.3600 | -0.4194 | 0.0719 | 0.0317 | 0.0925 | 0.0894 |
| 811 | 0 | 0.700 | 2.125 | 6.950 | 0.3527 | -0.4111 | 0.0507 | 0.0319 | 0.1036 | 0.0898 |
| 812 | 0 | 0.700 | 1.200 | 6.960 | -0.2297 | 0.0587 | -0.0654 | 0.0124 | 0.0194 | 0.0149 |
| 813 | 0 | 0.700 | 1.200 | 6.960 | -0.2164 | 0.0782 | -0.0557 | 0.0107 | 0.0202 | 0.0139 |
| 814 | 0 | 0.700 | 1.200 | 6.960 | -0.2208 | 0.0613 | -0.0513 | 0.0117 | 0.0230 | 0.0138 |
| 815 | 0 | 0.700 | 0.395 | 6.960 | -0.0807 | 0.0944 | -0.1043 | 0.0075 | 0.0092 | 0.0106 |
| 816 | 0 | 0.700 | 0.395 | 6.960 | -0.0859 | 0.0762 | -0.0957 | 0.0078 | 0.0108 | 0.0115 |
| 817 | 0 | 0.700 | 0.395 | 6.960 | -0.0699 | 0.0901 | -0.0872 | 0.0072 | 0.0105 | 0.0105 |
| 818 | 0 | 0.780 | 0.600 | 2.045 | 0.1270 | -0.0043 | -0.8769 | 0.0094 | 0.0039 | 0.0062 |
| 819 | 0 | 0.780 | 0.600 | 2.045 | 0.1413 | -0.0168 | -0.8717 | 0.0087 | 0.0041 | 0.0054 |
| 820 | 0 | 0.780 | 0.600 | 2.045 | 0.1435 | -0.0194 | -0.8700 | 0.0089 | 0.0042 | 0.0054 |
| 821 | 0 | 0.780 | 0.600 | 2.045 | 0.0615 | -0.0138 | -0.8247 | 0.0070 | 0.0034 | 0.0042 |
| 822 | 0 | 0.780 | 0.600 | 2.045 | 0.0616 | -0.0248 | -0.8010 | 0.0072 | 0.0043 | 0.0049 |
| 823 | 0 | 0.780 | 0.600 | 2.045 | 0.0700 | -0.0377 | -0.7784 | 0.0065 | 0.0040 | 0.0043 |
| 824 | 0 | 0.780 | 1.300 | 2.045 | 0.0395 | -0.0080 | -0.5128 | 0.0073 | 0.0065 | 0.0191 |
| 825 | 0 | 0.780 | 1.300 | 2.045 | 0.0353 | 0.0059 | -0.5075 | 0.0071 | 0.0066 | 0.0179 |
| 826 | 0 | 0.780 | 1.300 | 2.045 | 0.0358 | -0.0008 | -0.4997 | 0.0075 | 0.0070 | 0.0193 |
| 827 | 0 | 0.790 | 1.300 | 2.045 | 0.0269 | 0.0024 | -0.5174 | 0.0070 | 0.0075 | 0.0217 |
| 828 | 0 | 0.790 | 1.300 | 2.045 | 0.0311 | -0.0352 | -0.5150 | 0.0072 | 0.0080 | 0.0191 |
| 829 | 0 | 0.790 | 1.300 | 2.045 | 0.0244 | -0.0362 | -0.5095 | 0.0073 | 0.0084 | 0.0200 |
| 830 | 0 | 0.790 | 1.300 | 2.045 | 0.0148 | -0.0201 | -0.5157 | 0.0077 | 0.0080 | 0.0207 |
| 831 | 0 | 0.790 | 1.300 | 2.045 | 0.0138 | -0.0178 | -0.5286 | 0.0075 | 0.0080 | 0.0202 |
| 832 | 0 | 0.790 | 1.300 | 2.045 | 0.0062 | -0.0092 | -0.5206 | 0.0077 | 0.0079 | 0.0211 |
| 833 | 0 | 0.780 | 0.600 | 0.220 | 0.0414 | -0.3081 | -1.3221 | 0.0091 | 0.0073 | 0.0078 |
| 834 | 0 | 0.780 | 0.600 | 0.220 | 0.0536 | -0.3036 | -1.3126 | 0.0090 | 0.0071 | 0.0081 |
| 835 | 0 | 0.780 | 0.600 | 0.220 | 0.0753 | -0.2748 | -1.2951 | 0.0096 | 0.0069 | 0.0082 |
| 836 | 0 | 0.780 | 0.600 | 0.220 | 0.1556 | -0.2488 | -1.2579 | 0.0057 | 0.0065 | 0.0055 |
| 837 | 0 | 0.780 | 0.600 | 0.220 | 0.1776 | -0.2438 | -1.2481 | 0.0056 | 0.0058 | 0.0054 |
| 838 | 0 | 0.780 | 0.600 | 0.220 | 0.1862 | -0.2487 | -1.2553 | 0.0054 | 0.0058 | 0.0053 |
| 839 | 0 | 0.780 | 0.600 | 0.220 | 0.1729 | -0.2288 | -1.2451 | 0.0056 | 0.0056 | 0.0053 |
| 840 | 0 | 0.780 | 0.600 | 0.220 | 0.1720 | -0.2369 | -1.2641 | 0.0060 | 0.0057 | 0.0055 |
| 841 | 0 | 0.780 | 0.600 | 0.220 | 0.1651 | -0.2338 | -1.2555 | 0.0061 | 0.0057 | 0.0053 |
| 842 | 0 | 0.780 | 0.600 | 0.220 | 0.1611 | -0.2453 | -1.2681 | 0.0059 | 0.0059 | 0.0052 |
| 843 | 0 | 0.780 | 0.600 | 0.220 | 0.1451 | -0.2491 | -1.2425 | 0.0059 | 0.0058 | 0.0052 |
| 844 | 0 | 0.780 | 0.600 | 0.220 | 0.1356 | -0.2506 | -1.2408 | 0.0057 | 0.0058 | 0.0053 |
| 845 | 0 | 0.780 | 0.600 | 0.220 | 0.1369 | -0.2463 | -1.2364 | 0.0058 | 0.0057 | 0.0053 |
| 846 | 0 | 0.780 | 0.600 | 0.220 | 0.1271 | -0.2473 | -1.2290 | 0.0055 | 0.0057 | 0.0049 |
| 847 | 0 | 0.780 | 0.600 | 0.220 | 0.1177 | -0.2485 | -1.2234 | 0.0056 | 0.0060 | 0.0050 |
| 848 | 0 | 0.780 | 0.600 | 0.220 | 0.1260 | -0.2479 | -1.2291 | 0.0054 | 0.0057 | 0.0050 |
| 849 | 0 | 0.780 | 0.600 | 0.220 | 0.1150 | -0.2501 | -1.2213 | 0.0055 | 0.0057 | 0.0049 |
| 850 | 0 | 0.780 | 0.600 | 0.220 | 0.1122 | -0.2545 | -1.2209 | 0.0056 | 0.0058 | 0.0050 |
| 851 | 0 | 0.780 | 0.600 | 0.220 | 0.1327 | -0.2474 | -1.2336 | 0.0053 | 0.0057 | 0.0049 |
| 852 | 0 | 0.780 | 0.600 | 0.220 | 0.1092 | -0.2454 | -1.2174 | 0.0052 | 0.0055 | 0.0048 |
| 853 | 0 | 0.780 | 0.600 | 0.220 | 0.1037 | -0.2467 | -1.2039 | 0.0052 | 0.0057 | 0.0048 |
| 854 | 0 | 0.780 | 0.600 | 0.220 | 0.1352 | -0.1829 | -1.1400 | 0.0057 | 0.0061 | 0.0056 |
| 855 | 0 | 0.780 | 0.600 | 0.220 | 0.1235 | -0.2070 | -1.1723 | 0.0056 | 0.0061 | 0.0054 |
| 856 | 0 | 0.780 | 0.600 | 0.220 | 0.1189 | -0.2183 | -1.2000 | 0.0055 | 0.0063 | 0.0051 |
| 857 | 0 | 0.780 | 0.600 | 0.220 | 0.1303 | -0.2189 | -1.1951 | 0.0057 | 0.0064 | 0.0053 |

| | | | | | | | | | | |
|-----|---|-------|-------|-------|---------|---------|---------|---------------------|--------|--------|
| 858 | 0 | 0.780 | 0.600 | 0.220 | 0.1337 | -0.2375 | -1.2155 | 0.0061 | 0.0069 | 0.0057 |
| 859 | 0 | 0.780 | 0.600 | 0.220 | 0.1386 | -0.2416 | -1.2220 | 0.0058 | 0.0070 | 0.0055 |
| 860 | 0 | 0.780 | 1.300 | 0.240 | 0.1209 | -0.0072 | -0.2199 | 0.0055 | 0.0027 | 0.0112 |
| 861 | 0 | 0.780 | 1.300 | 0.240 | 0.1302 | -0.0020 | -0.2436 | 0.0049 | 0.0026 | 0.0109 |
| 862 | 0 | 0.780 | 1.300 | 0.240 | 0.1327 | -0.0039 | -0.2496 | 0.0054 | 0.0027 | 0.0113 |
| 863 | 0 | 0.780 | 1.300 | 0.240 | 0.1381 | 0.0039 | -0.2618 | 0.0055 | 0.0032 | 0.0119 |
| 864 | 0 | 0.780 | 1.300 | 0.240 | 0.1395 | 0.0047 | -0.2609 | 0.0060 | 0.0031 | 0.0121 |
| 865 | 0 | 0.780 | 1.300 | 0.240 | 0.1428 | -0.0008 | -0.2737 | 0.0056 | 0.0033 | 0.0120 |
| 866 | 0 | 0.780 | 0.600 | 4.275 | 0.0391 | -0.0549 | -0.5124 | 0.0044 | 0.0019 | 0.0036 |
| 867 | 0 | 0.780 | 0.600 | 4.275 | 0.0370 | -0.0426 | -0.4641 | 0.0038 | 0.0017 | 0.0033 |
| 868 | 0 | 0.780 | 0.600 | 4.275 | 0.0145 | -0.0257 | -0.4481 | 0.0034 | 0.0015 | 0.0031 |
| 869 | 0 | 0.780 | 1.300 | 4.275 | -0.0638 | -0.4049 | -0.1678 | variance data error | | |
| 870 | 0 | 0.780 | 1.300 | 4.275 | 0.0088 | -0.0392 | -0.1982 | 0.0051 | 0.0049 | 0.0107 |
| 871 | 0 | 0.780 | 1.300 | 4.275 | -0.0031 | -0.0628 | -0.2277 | variance data error | | |
| 872 | 0 | 1.210 | 1.300 | 2.000 | -0.0073 | -0.1594 | -0.2337 | 0.0117 | 0.0230 | 0.0213 |
| 873 | 0 | 1.210 | 1.300 | 2.000 | 0.0053 | -0.1647 | -0.2343 | 0.0119 | 0.0226 | 0.0227 |
| 874 | 0 | 1.210 | 1.300 | 2.000 | 0.0327 | -0.1731 | -0.2446 | 0.0137 | 0.0252 | 0.0284 |

For each of these runs the original data is stored in compressed format, native to the ultrasonic anemometer, in a DOS file named R###.CMP where ### corresponds to the run number. These files were also expanded to ASCII text format and named R###.TXT. These ASCII files were then combined with the position and orientation data to standardise the output component directions before analysis. The summary output files from this initial GENSTAT analysis were:

EXPT.### - position, mean and variance of each run. ### being the final run in the file.

DEXPT.### - position, mean and variance of half run. Thus each run number appears twice, associated with the first and second halves of each run which have been treated separately. ### again corresponds to the final run number in the file.

R###.MAG - standardised u,v,w component time series with magnitude time series. This file is then processed by a spectral analysis program to derive the spectrum, cross-spectrum and Reynolds stress spectra for each run.

R###.ACR - autocorrelation function for run ##.

R###.CCR - cross-correlation function for run ## with a predefined reference time series.

LSCALE.### - position, integral length scale and positive length scale derived from the autocorrelation functions. ### being the final run number in the file.

SHEAR.### - position and mean shear stress components for each run. ### being the final run in the file.

Subsequent GENSTAT routines combined the autocorrelation and cross-correlation results for individual runs which repeated the same position.

appendix 3 CFD methodology

In this section a brief overview of the numerical procedures behind CFD will be given. The material presented here is available in many texts on the subject of CFD and its methodologies [Abbot and Basco (1989), Chow (1979), Patankar (1980)], which are themselves a topic of much current research [Leschziner (1989), UMIST (1995)]. For simplicity a general finite volume technique with standard k- ϵ turbulence model will be outlined.

The Navier-Stokes equations

$$\frac{\partial \rho}{\partial t} + \frac{\partial(\rho U_i)}{\partial x_i} = 0 \quad (1)$$

$$\frac{\partial(\rho U_i)}{\partial t} + \frac{\partial(\rho U_i U_j)}{\partial x_j} = -\frac{\partial P}{\partial x_i} + \frac{\partial}{\partial x_j} \left(\mu \left(\frac{\partial U_i}{\partial x_j} + \frac{\partial U_j}{\partial x_i} \right) \right) + \rho g_i \quad (2)$$

where

ρ is the fluid density

μ is the fluid viscosity

P is the fluid pressure

U_i is the fluid velocity in the x_i direction

t is the time

and g is the gravitational force vector

represent the amalgamation of the conservation laws for mass and momentum in the three cartesian axes to give a continuity equation (1) and the momentum transport equations (2). These equations are not directly soluble, except in simplified cases in which dimensional analysis allows certain terms to be neglected [Acheson (1990)]. Therefore a numerical solution approach is taken in realistic situations. Taking the incompressible gas form of (1) and (2) for simplicity

$$\frac{\partial U_i}{\partial x_i} = 0 \quad (3)$$

$$\frac{\partial U_i}{\partial t} + U_j \frac{\partial U_i}{\partial x_j} = -\frac{1}{\rho} \frac{\partial P}{\partial x_i} + \nu \frac{\partial^2 U_i}{\partial x_j^2} + g_i \quad (4)$$

where

$\nu = \mu/\rho$ the kinematic viscosity.

The first step is to consider the variables U_i and P as consisting of separable mean and fluctuating components. This process, called Reynolds averaging, is assumed in order that the control volumes, or cells, used to discretise the problem-solution space or domain, can be larger than the Kolmogorov scale. Each variable is therefore separated into a time averaged and fluctuating part, say

$$U_i = \bar{U}_i + u_i \quad (5)$$

where the bar represents the time averaged term, then note that

$$\bar{u}_i = 0 \quad (6)$$

by definition.

Substituting (5) into (3) and time averaging the whole equation implies

$$\overline{\frac{\partial}{\partial x_i}(\bar{U}_i + u_i)} = \frac{\partial}{\partial x_i}(\overline{\bar{U}_i + u_i}) = \frac{\partial \bar{U}_i}{\partial x_i} = 0 \quad (7)$$

Similarly substituting into (4) and time averaging gives

$$\frac{\partial \bar{U}_i}{\partial t} + \bar{U}_j \frac{\partial \bar{U}_i}{\partial x_j} + \frac{\partial}{\partial x_j}(\overline{u_i u_j}) = -\frac{1}{\rho} \frac{\partial \bar{P}}{\partial x_i} + \nu \frac{\partial^2 \bar{U}_i}{\partial x_j^2} + \bar{g}_i \quad (8)$$

Notice that this process has given rise to an extra term involving the correlation of fluctuating components which does not vanish under time averaging. This Reynolds stress term expresses the increased mixing due to turbulent processes within the flow. The presence of this term means, however, that the equation set is no longer closed, there are 10 unknowns (three mean velocity components, six Reynolds stresses and the pressure) with only 4 equations in (7) and (8). In order to resolve this situation it is possible either to extend the number of equations, including transport equations for the Reynolds stresses for example, or to model the unknown terms as expressions of the other variables. The former approach, called second moment closure, is obviously more physically and mathematically appropriate but suffers from practical difficulties, not least of which is that each new equation introduced also contains further unknowns to be evaluated. The latter, modelling, approach is currently the most widely used with a number of possible models suggested [UMIST 1995, 1996, Gould 1996]

The most widely used model at present is the k - ϵ turbulence model of Launder and Spalding (1974). This is an 'eddy-viscosity' model, so called because the Reynolds stress term (which expresses turbulent mixing or diffusion) is modelled as a diffusion like term with a variable viscosity called the eddy (or turbulent) viscosity μ_t , (9).

$$-\overline{\rho u_i u_j} = \mu_t \left(\frac{\partial \bar{U}_i}{\partial x_j} + \frac{\partial \bar{U}_j}{\partial x_i} \right) - \frac{2}{3} \rho k \delta_{ij} \quad (9)$$

where $k = \frac{1}{2}(\overline{u_i u_i})$ is the specific turbulent kinetic energy.

This reduces the number of unknowns from the 10 to 6 because the 6 Reynolds stresses can now be expressed as functions of k and μ_t . Also the number of equations can be increased by deriving a transport equation for k (10) from the Navier-Stokes equations (3,4)

$$\frac{\partial k}{\partial t} + \bar{U}_j \frac{\partial k}{\partial x_j} = - \frac{\partial}{\partial x_j} \left(\frac{1}{2} \overline{u_j u_i u_i} + \frac{1}{\rho} \overline{\rho u_j} \right) + \nu \frac{\partial^2 k}{\partial x_j^2} - \overline{u_i u_j} \frac{\partial \bar{U}_i}{\partial x_j} - \nu \frac{\partial u_i}{\partial x_k} \frac{\partial u_i}{\partial x_k} \quad (10)$$

However this new equation contains three terms which include second and third order correlations which must be modelled.

The eddy viscosity hypothesis (9) allows the first of these terms, the production term for k (P_k) to be rewritten as

$$P_k = - \overline{\rho u_i u_j} \frac{\partial \bar{U}_i}{\partial x_j} = \mu_t \left(\frac{\partial \bar{U}_i}{\partial x_j} + \frac{\partial \bar{U}_j}{\partial x_i} \right) \frac{\partial \bar{U}_i}{\partial x_j} \quad (11)$$

The next term requiring modelling, the transport term, is expressed as

$$- \left(\frac{1}{2} \overline{u_j u_i u_i} + \frac{1}{\rho} \overline{\rho u_j} \right) = \frac{\mu_t}{\rho \sigma_k} \frac{\partial k}{\partial x_j} \quad (12)$$

where σ_k is an empirical constant

by means of the generalised gradient diffusion hypothesis. Finally the dissipation rate of k is given the term ϵ and defined as

$$\epsilon = \nu \frac{\partial u_i}{\partial x_k} \frac{\partial u_i}{\partial x_k} \quad (13)$$

Thus the k equation (10) can be written in its modelled form

$$\frac{\partial k}{\partial t} + \bar{U}_j \frac{\partial k}{\partial x_j} = \frac{\partial}{\partial x_j} \left(\frac{\mu_t}{\rho \sigma_k} \frac{\partial k}{\partial x_j} \right) + \nu \frac{\partial^2 k}{\partial x_j^2} + \frac{\mu_t}{\rho} \left(\frac{\partial \bar{U}_i}{\partial x_j} + \frac{\partial \bar{U}_j}{\partial x_i} \right) \frac{\partial \bar{U}_i}{\partial x_j} - \epsilon \quad (14)$$

Consider now the characteristic velocity (V_c) and length scale (L_c) of the turbulent flow. Dimensional analysis shows that

$$V_c = \sqrt{k} \quad L_c = \frac{k^{3/2}}{\epsilon} \quad (15)$$

This suggests that the eddy viscosity

$$\mu_t \propto \rho V_c L_c \Rightarrow \mu_t = \rho C_\mu \frac{k^2}{\epsilon} \quad (16)$$

where C_μ is an empirical constant of proportionality.

This maintains the number of equations (five) and the number of unknowns (six) but expresses the turbulent parameters in terms of k and ϵ rather than k and μ_t .

One further equation is required to close the equation set. In this case a transport equation for ϵ defined in a similar way to that for k .

$$\frac{\partial \epsilon}{\partial t} + \bar{U}_j \frac{\partial \epsilon}{\partial x_j} = \frac{\partial}{\partial x_j} \left(\frac{\mu_t}{\rho \sigma_\epsilon} \frac{\partial \epsilon}{\partial x_j} \right) + \nu \frac{\partial^2 \epsilon}{\partial x_j^2} + \frac{\epsilon}{\rho k} (C_{\epsilon 1} P_k - C_{\epsilon 2} \rho \epsilon) \quad (17)$$

where σ_ϵ , $C_{\epsilon 1}$ and $C_{\epsilon 2}$ are empirical constants.

This now gives six equations in six unknowns and allows progress on the evaluation of specific problems. The remaining empirical constants are determined from experimental data of simple flows or by computer optimisation. The values normally taken are (Launder and Spalding 1974):

| C_μ | $C_{\epsilon 1}$ | $C_{\epsilon 2}$ | σ_k | σ_ϵ |
|---------|------------------|------------------|------------|-------------------|
| 0.09 | 1.44 | 1.92 | 1.00 | 1.30 |

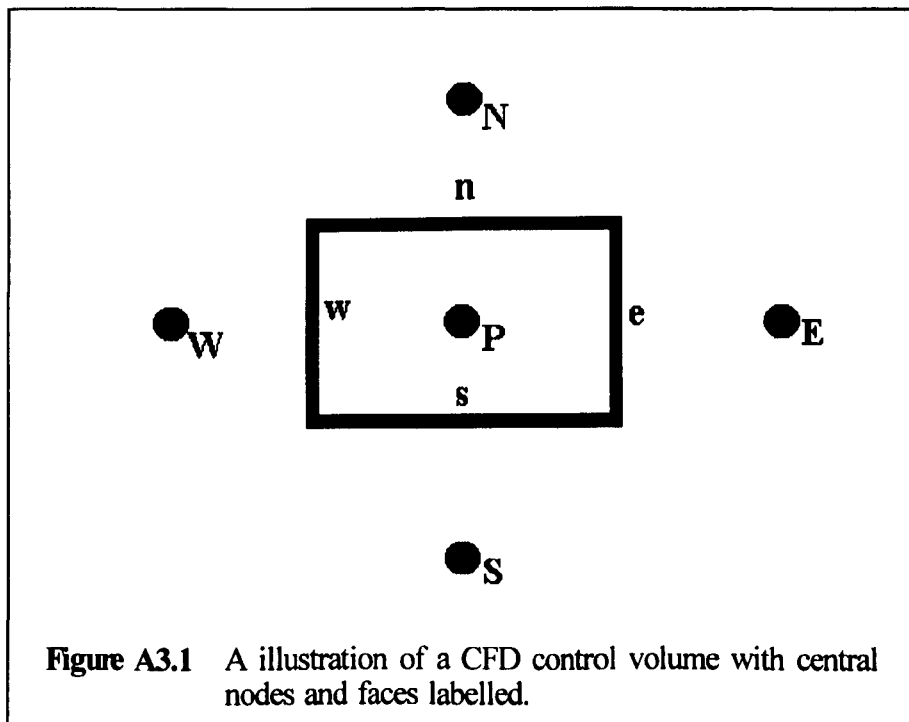
One particular feature to notice about these six equations (7,8 substituting 9,14 and 17) is the similarity of form which the modelling has provided. All these equations can be expressed in a form directly comparable to the

original equations and therefore a standard solution procedure can be adopted.

The next objective is to replace these differential transport equations with a set of algebraic equations which can provide the values of all the variables at discrete locations throughout the problem-solution space. In order to do this the space is divided into control volumes and the transport equations are integrated over each volume. Consider, for example, a simple steady two-dimensional flow. The transport equations are all of the form

$$\frac{\partial(\rho U\Phi)}{\partial x} + \frac{\partial(\rho V\Phi)}{\partial y} = \frac{\partial}{\partial x}\left(\Gamma\frac{\partial\Phi}{\partial x}\right) + \frac{\partial}{\partial y}\left(\Gamma\frac{\partial\Phi}{\partial y}\right) + S_{\Phi} \quad (18)$$

where Γ is the diffusivity of variable Φ



Integration over the control volume (figure A3.1) gives

$$\begin{aligned}
 & (\rho U \Phi \Delta A)_w - (\rho U \Phi \Delta A)_e \\
 & + (\rho V \Phi \Delta A)_s - (\rho V \Phi \Delta A)_n \\
 & = \left(\Gamma \Delta A \frac{\partial \Phi}{\partial x} \right)_w - \left(\Gamma \Delta A \frac{\partial \Phi}{\partial x} \right)_e \\
 & + \left(\Gamma \Delta A \frac{\partial \Phi}{\partial y} \right)_s - \left(\Gamma \Delta A \frac{\partial \Phi}{\partial y} \right)_n \\
 & + S_\Phi \cdot \text{Volume of cell}
 \end{aligned} \tag{19}$$

where ΔA is the area of the appropriate side of the control volume

Now the practical difficulty occurs in evaluating U , V , Φ and $\frac{\partial \Phi}{\partial x}$ at the appropriate cell faces. In PHOENICS the velocity component information is stored for the cell faces and therefore evaluation is explicit. For the other variables whose values correspond to cell centres (**P**, **N**, **S**, **E** and **W** in figure A3.1) some form of interpolation is necessary. Various forms exist, from simple central differencing e.g.

$$\left(\frac{\partial \Phi}{\partial x} \right)_e = \frac{\Phi_E - \Phi_P}{\Delta x} \tag{20}$$

to higher order upwind differencing schemes which take into account a number of points upstream of the face in question in order to give a more physically realistic value at the face. In PHOENICS the system used is called the hybrid system, a combination of central differencing (20), and first order upwind differencing, where the value at the cell face is taken to be equal to the value at the upstream cell centre.

Having chosen appropriate discretisation schemes for the variables one can write algebraic equations for each control volume relating the value of Φ at node **P** to the values at **N**, **S**, **E** and **W**, and others as appropriate to the differencing scheme. This gives an expression of the form

$$A_P \Phi_P = A_W \Phi_W + A_E \Phi_E + A_N \Phi_N + A_S \Phi_S + S_\Phi \cdot \text{Volume of cell} \tag{21}$$

$$\text{where } A_E = \left(\frac{\Gamma \Delta A}{\Delta x} \right)_e + \max(-\rho \Delta A U, 0)_e \tag{22}$$

if first order upwind differencing is used

$$\text{and} \quad A_p = A_w + A_e + A_n + A_s \quad (23)$$

Now the unknown variables can be evaluated by an iterative procedure which seeks to satisfy this relationship between each cell and its neighbours. The procedure used in PHOENICS is based on the SIMPLE algorithm (Patankar and Spalding 1972) which begins with an initial user supplied flow field approximation and within each iteration performs the following steps.

1. Update the mean flow field through solution of the mean momentum equations, using the turbulence and effective viscosity fields from the previous iteration.
2. Update the pressure field through solution of the continuity equation using the new velocity field.
3. Update the turbulence parameter fields using the new mean velocity and pressure fields.
4. Calculate the new effective viscosity field.

These steps are repeated as often as required and convergence is monitored by consideration of the discrepancies in the algebraic equations over the whole field of solution *i.e.* the total absolute deviation (residual) from the conservation of Φ over the domain. Once a suitably small value of this residual has been obtained for each variable the solution can be considered as reasonable in a numerical sense. However, the problems of grid independence, physical realism *etc* must then be addressed.

appendix 4 CFD model instruction summary

This section contains edited instruction files which create the load space model simulation. The first of these covers the isothermal cases, the second contains the changes necessary for the heated load cases.

PHOENICS Q1 input file summary

```
*****
*
* GROUP 1. Run identifiers and other preliminaries.
*
TEXT(CTV Simulation Version 2.5
*
* Grid multiplier H for grid sensitivity studies
INTEGER(H);H=1
* Separate H parameters for each cart direction
* these can be used directly or set =H in general
INTEGER(HX);HX=H
INTEGER(HY);HY=H
INTEGER(HZ);HZ=H
*
* Roof inlet velocity divisor
REAL(RVD);RVD=1
* Mass flow geometry correction factor
REAL(MFAC);MFAC=0.132
*
* Define tke and ep levels for initial/inlet b.c.
REAL(KI);KI=0.01
REAL(E);E=1
*
* Specify loading case in SLD
* 0=NO LOAD
* 1=FRONT LOAD
* 3=FULL LOAD
* N.B. for side load use other grid
INTEGER(SLD);SLD=0
*
* Angle to vertical of forward jets
REAL(AGL);AGL=60
*
* Define pi for ease of use
REAL(PI);PI=3.14159265
* Calc sin and cos of this angle
REAL(CN);CN=(AGL*PI/180)
CN=COS(CN)
REAL(SN);SN=(AGL*PI/180)
SN=SIN(SN)
*
* Elliptic Simulation
PARAB=F
*
*****
```

```

*
* GROUP 2. Time-dependence and related parameters.
*
* Steady-state simulation
STEADY=T
*
*****
*
* GROUP 6. Body-fitting and other grid distortions.
*
BFC=T
NONORT=T
STORE(UCRT,VCRT,WCRT)
*
* Grid instructions not included
*
*****
*
* GROUP 7. Variables (including porosities) named,
*       stored & solved.
*
* Solve for U1 (the VELOCITY_IN_THE_X_DIRECTION)
SOLVE(U1)
* Solve for V1 (the VELOCITY_IN_THE_Y_DIRECTION)
SOLVE(V1)
* Solve for W1 (the VELOCITY_IN_THE_Z_DIRECTION)
SOLVE(W1)
* Solve for P1 by whole-field method
* The PRESSURE
SOLVE(P1)
SOLUTN(P1,Y,Y,Y,N,N,N)
* Store ENUT (the EFFECTIVE_VISCOSITY)
STORE(ENUT)
*
*****
*
* GROUP 8. Terms (in differential equations) and devices.
*
*
*****
*
* GROUP 9. Properties of the medium (or media).
*
* Reference pressure (N/m^2)
PRESS0=1.0000E+05
* CONSTANT density formulation
* Density (kg/m^3)
REAL(RREF1)
RHO1=1.1610E+00;RREF1=RHO1
* Laminar kinematic viscosity (m^2/s)
ENUL=1.5890E-05
* Turbulence treatment K-E
* Active built-in K-E model

```

```

TURMOD(KEMODL)
  * Reference kinematic viscosity
REAL(ENLREF);ENLREF=1.5890E-05
  *
  *****
  *
  * GROUP 10. Interphase-transfer processes and properties.
  *
  *
  *****
  *
  * GROUP 11. Initialization of fields of variables,
  *           porosities, etc.
  *
  *
  * Define partition wall load space/p chamber
CONPOR(PART1,0,CELL,-1,-18*HX,-1,-2*HY,-(3*HZ+1),-4*HZ)
CONPOR(PART2,0,CELL,-1,-3*HX,-(2*HY+1),-5*HY,-(3*HZ+1),-4*HZ)
CONPOR(PART3,0,CELL,-(16*HX+1),-18*HX,-(2*HY+1),-5*HY,-(3*HZ+1),-4*$
HZ)
CONPOR(PART4,0,CELL,-1,-18*HX,-(5*HY+1),-17*HY,-(3*HZ+1),-4*HZ)
  *
  * Initialize field values of KE
FIINIT(KE)=KI
  * Initialize field values of EP
FIINIT(EP)=E
  *
  * Define load slq=1 = front load ; slq=3 = full load
IF ((SLD.EQ.1).OR.(SLD.EQ.3)) THEN
  * blockage patches for stacks
CONPOR(BX12F1,0.007,SOUTH,-(1*HX+1),-8*HX,1*HY+1,1*HY+1,10*HZ+1,13*$
HZ)
CONPOR(BX12TP,0.0816,NORTH,1*HX+1,8*HX,4*HY,4*HY,10*HZ+1,13*HZ)
CONPOR(BX12SE,0.147,EAST,8*HX,8*HX,1*HY+1,4*HY,10*HZ+1,13*HZ)
CONPOR(BX12SW,0.147,WEST,1*HX+1,1*HX+1,1*HY+1,4*HY,10*HZ+1,13*HZ)
CONPOR(BX12SH,0.147,HIGH,1*HX+1,8*HX,1*HY+1,4*HY,13*HZ,13*HZ)
CONPOR(BX12SL,0.147,LOW,1*HX+1,8*HX,1*HY+1,4*HY,10*HZ+1,10*HZ+1)
CONPOR(BX12IX,0.11,HIGH,1*HX+1,8*HX,1*HY+1,4*HY,12*HZ,12*HZ)
CONPOR(BX12IZ,0.11,EAST,5*HX,5*HX,1*HY+1,4*HY,10*HZ+1,13*HZ)
  *
  * plus others covering the other boxes
ENDIF
IF (SLD.EQ.3) THEN
  * further blockages exactly as above
ENDIF
  *
  *
  *****
  *
  * GROUP 12. Convection and diffusion adjustments
  *
  *
  *****

```

```

*
* GROUP 13. Boundary conditions and special sources
*
* form drag patches
IF (SLD.EQ.1) THEN
PATCH(FDTP1,NORTH,1*HX+1,8*HX,4*HY,4*HY,10*HZ+1,20*HZ,#1,#1)
COVAL(FDTP1,V1,-(RHO1*(1-0.0816)),0)

PATCH(FDSD1,EAST,1*HX,1*HX,1*HY+1,4*HY,10*HZ+1,20*HZ,#1,#1)
COVAL(FDSD1,U1,-(RHO1*(1-0.147)),0)

PATCH(FDLN1,HIGH,1*HX+1,8*HX,1*HY+1,4*HY,10*HZ,20*HZ,#1,#1)
COVAL(FDLN1,W1,-(RHO1*(1-0.147)),0)
* plus others covering the other boxes
ENDIF

IF (SLD.EQ.3) THEN
* alternative form drag patches as above
ENDIF
*
* INLET boundary conditions
INLET(BFCIN1,NORTH,1,1*HX,17*HY,17*HY,4*HZ+1,7*HZ,#1,#NREGT)
VALUE(BFCIN1,U1,GRND1)
VALUE(BFCIN1,V1,GRND1)
VALUE(BFCIN1,W1,GRND1)
VALUE(BFCIN1,UCRT,0)
VALUE(BFCIN1,VCRT,-7.64/RVD)
VALUE(BFCIN1,WCRT,1.35/RVD)
COVAL(BFCIN1,KE,ONLYMS,KI)
COVAL(BFCIN1,EP,ONLYMS,E)
VALUE(BFCIN1,P1,MFAC*7.64*RREF1)
* plus other bfc inlets 2 ... 5
INLET(IN6,NORTH,1,1*HX,17*HY,17*HY,7*HZ+1,11*HZ,#1,#NREGT)
COVAL(IN6,U1,ONLYMS,0)
COVAL(IN6,V1,ONLYMS,-8.50/RVD)
COVAL(IN6,W1,ONLYMS,1.50/RVD)
COVAL(IN6,KE,ONLYMS,KI)
COVAL(IN6,EP,ONLYMS,E)
VALUE(IN6,P1,MFAC*8.50*RREF1)
* plus other inlets in6a ... in12
*
* OUTLET boundary condition, name OUT
PATCH(OUT,LOW,7*HX+1,18*HX,8*HY+1,10*HY,1,1,#1,#NREGT)
COVAL(OUT,P1,1000,-2.5)
* WALL FUNCTION ROUGHNESS LENGTH
WALLA=5.0E-04
* WALL boundary condition, name SIDE
PATCH(SIDE,WWALL,1,1,#1,#NREGY,#1,#NREGZ,#1,#NREGT)
COVAL(SIDE,V1,GRND2,0.0)
COVAL(SIDE,W1,GRND2,0.0)
COVAL(SIDE,KE,GRND2,GRND2)
COVAL(SIDE,EP,GRND2,GRND2)
* WALL boundary condition, name END

```

```

PATCH(END,HWALL,#1,#NREGX,#1,#NREGY,29*HZ,29*HZ,#1,#1)
COVAL(END,U1,GRND2,0.0)
COVAL(END,V1,GRND2,0.0)
COVAL(END,KE,GRND2,GRND2)
COVAL(END,EP,GRND2,GRND2)
  * WALL boundary condition, name FRONT
PATCH(FRONT,LWALL,#1,#NREGX,1,8*HY,1,1,#1,#NREGT)
COVAL(FRONT,U1,GRND2,0.0)
COVAL(FRONT,V1,GRND2,0.0)
COVAL(FRONT,KE,GRND2,GRND2)
COVAL(FRONT,EP,GRND2,GRND2)
  * WALL boundary condition, name F2
PATCH(F2,LWALL,1,7*HX,8*HY+1,10*HY,1,1,#1,#NREGT)
COVAL(F2,U1,GRND2,0.0)
COVAL(F2,V1,GRND2,0.0)
COVAL(F2,KE,GRND2,GRND2)
COVAL(F2,EP,GRND2,GRND2)
  * WALL boundary condition, name F3
PATCH(F3,LWALL,#1,#NREGX,10*HY+1,#NREGY,1,1,#1,#NREGT)
COVAL(F3,U1,GRND2,0.0)
COVAL(F3,V1,GRND2,0.0)
COVAL(F3,KE,GRND2,GRND2)
COVAL(F3,EP,GRND2,GRND2)
  * WALL B.C. FLOOR
PATCH(FLOOR,SWALL,#1,#NREGX,1,1,#1,#NREGZ,#1,#NREGT)
COVAL(FLOOR,U1,GRND2,0)
COVAL(FLOOR,W1,GRND2,0)
COVAL(FLOOR,KE,GRND2,GRND2)
COVAL(FLOOR,EP,GRND2,GRND2)
  *
  *****
  *
  * GROUP 15. Termination criteria for sweeps and
  *       outer iterations.
  *
  * Number of sweeps
LSWEEP=5000
  *
  *****
  *
  * GROUP 16. Termination criteria for inner iterations.
  *
SELREF=F
  *
  *****
  *
  * GROUP 17. Under-relaxation and related devices.
  *
RELAX(P1,LINRLX,0.2)
RELAX(U1,FALSDT,0.1)
RELAX(V1,FALSDT,0.1)
RELAX(W1,FALSDT,0.1)
RELAX(KE,FALSDT,0.01)

```

```

RELAX(EP,FALSDT,0.01)
*
*****
*
* GROUP 19. Data communicated by SATELLITE to GROUND
*
RSG13=1.161
*
*****
*
* GROUP 20. Control of preliminary printout
*
ECHO=T
*
*****
*
* GROUP 21. Frequency and extent of field printout.
*
OUTPUT(P1,N,N,N,Y,Y,Y)
OUTPUT(U1,N,N,N,Y,Y,Y)
OUTPUT(V1,N,N,N,Y,Y,Y)
OUTPUT(W1,N,N,N,Y,Y,Y)
OUTPUT(KE,Y,N,N,Y,Y,Y)
OUTPUT(EP,N,N,N,Y,Y,Y)
OUTPUT(UCRT,Y,N,N,N,N,N)
OUTPUT(VCRT,Y,N,N,N,N,N)
OUTPUT(WCRT,Y,N,N,N,N,N)
OUTPUT(ENUT,N,N,N,N,N,N)
*
*****
*
* GROUP 22. Location of spot-value & frequency of
*           residual printout.
*
* Assign cell-indicies of spot-point monitoring location
IXMON=5*HX
IYMON=6*HY
IZMON=20*HZ
TSTSWP=1000
*
*****
*
* GROUP 23. Variable-by-variable field printout and plot
*           and/or tabulation of spot-values and residuals.
*
* Control tabulation & plotting of spot-values/residuals
* Tables and plots
ITABL=1
* Set the frequency of tabulation and plotting
NPLT=1
*
IZPRF=4*HZ+1
NXPRIN=1

```

NYPRIN=1

NZPRIN=1

*

STOP

Heated model modifications

```
*****
*
* GROUP 9. Properties of the medium (or media).
*
* Heat flow data
* Specific heat J per Kg per K
CP1=1007
* Reference enthalpy
REAL(HREF1);HREF1=0
* Volume expansivity 1/K
REAL(VEXP1);VEXP1=3.33E-03
* Prandtl number
PRNDTL(H1)=0.736
* Turbulent Prandtl number
PRT(H1)=1
* Temperature tmp1=tmp1a+H1*tmp1b
* so tmp1a=reference temp, tmp1b=1/cp1
TMP1A=22
TMP1B=1/CP1
TMP1=GRND2
*
*****
*
* GROUP 11. Initialization of fields of variables,
* porosities, etc.
*
* Initialize field values of H1
FIINIT(H1)=0
*****
*
* GROUP 13. Boundary conditions and special sources
*
* GRAVITY field
PATCH(BUOYANCY,PHASEM,#1,#NREGX,#1,#NREGY,#1,#NREGZ,#1,#NREGT)
COVAL(BUOYANCY,U1,FIXFLU,GRND3)
COVAL(BUOYANCY,V1,FIXFLU,GRND3)
COVAL(BUOYANCY,W1,FIXFLU,GRND3)
* gravity resolutes
RSG8=0;RSG9=-9.80665;RSG10=0
* set constants for BOUSSINESQ approximation
RSG2=-VEXP1/CP1;RSG1=-RSG2*HREF1
*
* HEAT SOURCE patches
IF (SLD.EQ.1) THEN
PATCH(HS12,VOLUME,1*HX+1,8*HX,1*HY+1,4*HY,10*HZ+1,13*HZ,#1,#1)
COVAL(HS12,H1,FIXFLU,1067)
* plus others to cover other boxes
ENDIF

IF (SLD.EQ.3) THEN
* other heat sources as above
ENDIF
```

```

*
* OUTLET boundary condition, name OUT
PATCH(VENT1,SOUTH,7,8,1,1,5,#NREGZ,#1,#NREGT)
COVAL(VENT1,P1,1000,0)
PATCH(VENT2,SOUTH,16,18,1,1,5,#NREGZ,#1,#NREGT)
COVAL(VENT2,P1,1000,0)

* WALL boundary condition, name SIDE
COVAL(SIDE,H1,0.4/PRNDTL(H1),0)
* plus others for other wall areas
* WALL B.C. FLOOR
PATCH(FLOOR1,SWALL,1,6,1,1,5,#NREGZ,#1,#NREGT)
COVAL(FLOOR1,U1,GRND2,0)
COVAL(FLOOR1,W1,GRND2,0)
COVAL(FLOOR1,KE,GRND2,GRND2)
COVAL(FLOOR1,EP,GRND2,GRND2)
COVAL(FLOOR1,H1,0.4/PRNDTL(H1),0)
* plus others to cover other floor areas
*****

*
* GROUP 17. Under-relaxation and related devices.
*
RELAX(H1,FALSDT,0.01)
*
*****

*
* GROUP 21. Frequency and extent of field printout.
*
OUTPUT(H1,N,N,N,Y,Y)
OUTPUT(TMP1,Y,N,N,N,N)

```

appendix 5 Ventilation rate calculation results

This section contains the detailed ventilation rate calculation results for all the simulation cases. Results are presented as: (ventilation rate [m^3s^{-1}]) & (continuity error [m^3s^{-1}])

The ventilation rate is calculated from the mean velocity field accounting for the area porosity associated with each face of the chick box and is actually the ventilation rate for a pair of chick boxes side by side on a trolley. This is very similar because of the orientation of the mean flow for back to front of the load space. Having calculated the flow through each face of the box the sign associated with each flow rate indicates whether inflow or outflow is taking place. The ventilation rate is then either the total inflow or outflow value. However, being a numerical calculation these values are often different, therefore the value presented here is the mean of the net inflow and outflow values. The continuity error is then the difference between the net inflow and outflow values and for comparison half that value is given here.

For each simulation the results are presented as box slabs, broken into trolley shelves, which are cross-sections along the length of the model load space. Thus the pair of figures associated with the topmost box on the middle shelf of the trolley at the front of the load space and next to the wall (remembering the symmetry condition) is given in box slab 1 (nearest the wall), on the left hand side (the front of the load space), in the middle group of three figures (the boxes on the middle shelf) and is the topmost pair (the topmost box). This position is highlighted below on the data for the basic empty model load space simulation.

Empty model load space, EFF grid and 100% inlet jet speed
 VENTILATION RATE (M3/SEC) CALCULATED FROM CFD DATA FOR BOX PAIRS

XZ PLANES

BOX SLAB 1 MEAN & ERROR

| | | | | | |
|----------------------------|------------------|------------------|------------------|------------------|------------------|
| 0.0994 & 0.0187 | 0.0699 & 0.0349 | 0.0992 & 0.0335 | 0.0911 & 0.0349 | 0.0485 & 0.0327 | 0.1331 & 0.0287 |
| 0.0610 & 0.0272 | 0.0809 & 0.0324 | 0.0548 & 0.0326 | 0.0687 & 0.0294 | 0.0931 & 0.0220 | 0.1688 & 0.0185 |
| 0.0609 & 0.0286 | 0.1526 & 0.0319 | 0.1307 & 0.0294 | 0.1259 & 0.0211 | 0.1247 & 0.0151 | 0.1895 & 0.0118 |
| 0.1792 & 0.0226 | 0.2609 & 0.0196 | 0.2342 & 0.0172 | 0.1887 & 0.0119 | 0.1592 & 0.0070 | 0.2211 & 0.0016 |
| 0.2320 & 0.0189 | 0.2923 & 0.0128 | 0.2621 & 0.0118 | 0.2069 & 0.0093 | 0.1668 & 0.0047 | 0.2234 & -0.0010 |
| 0.2815 & 0.0138 | 0.3097 & 0.0062 | 0.2771 & 0.0067 | 0.2191 & 0.0069 | 0.1700 & 0.0026 | 0.2175 & -0.0021 |
| 0.3468 & -0.0122 | 0.3220 & -0.0146 | 0.2780 & -0.0113 | 0.2208 & -0.0058 | 0.1699 & -0.0049 | 0.1939 & -0.0041 |
| 0.2805 & -0.0245 | 0.2862 & -0.0252 | 0.2512 & -0.0220 | 0.2083 & -0.0162 | 0.1590 & -0.0121 | 0.1888 & -0.0167 |
| 0.1833 & -0.0338 | 0.2177 & -0.0339 | 0.1912 & -0.0305 | 0.1627 & -0.0246 | 0.1260 & -0.0179 | 0.1481 & -0.0262 |

BOX SLAB 2 MEAN & ERROR

| | | | | | |
|------------------|------------------|------------------|------------------|------------------|------------------|
| 0.2709 & -0.0129 | 0.1762 & -0.0274 | 0.1010 & -0.0161 | 0.0700 & -0.0178 | 0.1117 & -0.0252 | 0.1382 & -0.0199 |
| 0.3157 & -0.0040 | 0.1237 & -0.0424 | 0.0500 & -0.0159 | 0.1089 & -0.0157 | 0.1720 & -0.0217 | 0.0619 & -0.0297 |
| 0.3256 & 0.0010 | 0.0864 & -0.0421 | 0.0741 & -0.0171 | 0.1376 & -0.0211 | 0.2141 & -0.0153 | 0.0711 & -0.0218 |
| 0.2847 & 0.0035 | 0.2249 & -0.0188 | 0.1452 & -0.0169 | 0.1963 & -0.0115 | 0.2617 & -0.0063 | 0.1645 & -0.0036 |
| 0.2586 & 0.0034 | 0.2516 & -0.0115 | 0.1765 & -0.0128 | 0.2131 & -0.0082 | 0.2703 & -0.0033 | 0.1861 & 0.0005 |
| 0.2308 & 0.0027 | 0.2648 & -0.0054 | 0.1994 & -0.0082 | 0.2220 & -0.0052 | 0.2703 & -0.0007 | 0.1931 & 0.0025 |
| 0.2011 & 0.0056 | 0.2817 & 0.0141 | 0.2265 & 0.0114 | 0.2103 & 0.0086 | 0.2433 & 0.0104 | 0.1726 & 0.0030 |
| 0.2335 & 0.0195 | 0.2554 & 0.0256 | 0.2145 & 0.0237 | 0.1950 & 0.0200 | 0.2149 & 0.0192 | 0.1710 & 0.0154 |
| 0.2154 & 0.0313 | 0.1969 & 0.0365 | 0.1659 & 0.0344 | 0.1487 & 0.0305 | 0.1619 & 0.0287 | 0.1337 & 0.0235 |

The **highlighted** value corresponds to the topmost box on the middle shelf of the trolley at the front and next to the wall of the empty model load space.

Empty model load space, EFF grid and 66% inlet jet speed
 VENTILATION RATE (M3/SEC) CALCULATED FROM CFD DATA FOR BOX PAIRS

XZ PLANES

BOX SLAB 1 MEAN & ERROR

| | | | | | |
|-----------------|-----------------|-----------------|-----------------|-----------------|-----------------|
| 0.0818 & 0.0142 | 0.0627 & 0.0206 | 0.1228 & 0.0252 | 0.1119 & 0.0301 | 0.0591 & 0.0293 | 0.0797 & 0.0268 |
| 0.0567 & 0.0168 | 0.0316 & 0.0229 | 0.0760 & 0.0234 | 0.0551 & 0.0274 | 0.0669 & 0.0200 | 0.1216 & 0.0203 |
| 0.0312 & 0.0216 | 0.0738 & 0.0242 | 0.0449 & 0.0233 | 0.0775 & 0.0206 | 0.0973 & 0.0141 | 0.1438 & 0.0125 |

| | | | | | |
|-----------------|-----------------|-----------------|-----------------|-----------------|------------------|
| 0.1201 & 0.0220 | 0.1733 & 0.0221 | 0.1431 & 0.0183 | 0.1397 & 0.0106 | 0.1335 & 0.0066 | 0.1726 & 0.0048 |
| 0.1737 & 0.0187 | 0.2124 & 0.0163 | 0.1761 & 0.0135 | 0.1552 & 0.0076 | 0.1411 & 0.0035 | 0.1837 & 0.0006 |
| 0.2251 & 0.0136 | 0.2370 & 0.0093 | 0.1962 & 0.0086 | 0.1640 & 0.0052 | 0.1437 & 0.0009 | 0.1866 & -0.0023 |

| | | | | | |
|------------------|------------------|------------------|------------------|------------------|------------------|
| 0.2921 & -0.0098 | 0.2585 & -0.0103 | 0.2026 & -0.0066 | 0.1624 & -0.0041 | 0.1412 & -0.0051 | 0.1677 & -0.0043 |
| 0.2314 & -0.0196 | 0.2337 & -0.0194 | 0.1871 & -0.0153 | 0.1529 & -0.0113 | 0.1293 & -0.0106 | 0.1588 & -0.0118 |
| 0.1465 & -0.0264 | 0.1808 & -0.0268 | 0.1446 & -0.0221 | 0.1204 & -0.0173 | 0.1016 & -0.0149 | 0.1294 & -0.0202 |

BOX SLAB 2 MEAN & ERROR

| | | | | | |
|------------------|------------------|------------------|------------------|------------------|------------------|
| 0.1662 & -0.0140 | 0.2273 & -0.0116 | 0.1219 & -0.0129 | 0.0511 & -0.0169 | 0.0771 & -0.0230 | 0.2048 & -0.0066 |
| 0.1956 & -0.0134 | 0.1892 & -0.0255 | 0.0874 & -0.0115 | 0.0816 & -0.0102 | 0.1192 & -0.0204 | 0.1527 & -0.0145 |
| 0.2332 & -0.0081 | 0.1438 & -0.0353 | 0.0578 & -0.0107 | 0.1023 & -0.0137 | 0.1580 & -0.0140 | 0.0882 & -0.0226 |

| | | | | | |
|-----------------|------------------|------------------|------------------|------------------|------------------|
| 0.2408 & 0.0002 | 0.1073 & -0.0270 | 0.0606 & -0.0151 | 0.1362 & -0.0118 | 0.2007 & -0.0062 | 0.0655 & -0.0136 |
| 0.2196 & 0.0012 | 0.1570 & -0.0174 | 0.0894 & -0.0151 | 0.1552 & -0.0081 | 0.2103 & -0.0029 | 0.1095 & -0.0052 |
| 0.1942 & 0.0011 | 0.1811 & -0.0109 | 0.1158 & -0.0110 | 0.1666 & -0.0050 | 0.2124 & -0.0001 | 0.1348 & 0.0000 |

| | | | | | |
|-----------------|-----------------|-----------------|-----------------|-----------------|-----------------|
| 0.1682 & 0.0034 | 0.2119 & 0.0080 | 0.1479 & 0.0051 | 0.1599 & 0.0059 | 0.1966 & 0.0093 | 0.1372 & 0.0039 |
| 0.2048 & 0.0159 | 0.1994 & 0.0179 | 0.1490 & 0.0151 | 0.1482 & 0.0141 | 0.1724 & 0.0158 | 0.1321 & 0.0109 |
| 0.1935 & 0.0262 | 0.1587 & 0.0270 | 0.1207 & 0.0235 | 0.1146 & 0.0221 | 0.1296 & 0.0222 | 0.1071 & 0.0185 |

Empty model load space, EFF grid and 50% inlet jet speed
 VENTILATION RATE (M3/SEC) CALCULATED FROM CFD DATA FOR BOX PAIRS

XZ PLANES

BOX SLAB 1 MEAN & ERROR

| | | | | | |
|-----------------|-----------------|-----------------|-----------------|-----------------|-----------------|
| 0.0544 & 0.0116 | 0.0621 & 0.0160 | 0.1276 & 0.0217 | 0.1500 & 0.0247 | 0.0914 & 0.0290 | 0.0399 & 0.0243 |
| 0.0346 & 0.0126 | 0.0363 & 0.0165 | 0.0862 & 0.0175 | 0.0993 & 0.0213 | 0.0354 & 0.0198 | 0.0601 & 0.0208 |
| 0.0150 & 0.0144 | 0.0448 & 0.0149 | 0.0521 & 0.0128 | 0.0598 & 0.0193 | 0.0610 & 0.0135 | 0.0925 & 0.0164 |

| | | | | | |
|-----------------|-----------------|-----------------|-----------------|-----------------|------------------|
| 0.0845 & 0.0167 | 0.0959 & 0.0120 | 0.0550 & 0.0122 | 0.0720 & 0.0143 | 0.0998 & 0.0069 | 0.1254 & 0.0058 |
| 0.1284 & 0.0162 | 0.1207 & 0.0126 | 0.0801 & 0.0139 | 0.0971 & 0.0108 | 0.1100 & 0.0043 | 0.1323 & 0.0031 |
| 0.1779 & 0.0140 | 0.1458 & 0.0119 | 0.1073 & 0.0131 | 0.1129 & 0.0073 | 0.1146 & 0.0016 | 0.1383 & -0.0004 |

| | | | | | |
|------------------|------------------|------------------|------------------|------------------|------------------|
| 0.2515 & -0.0062 | 0.1834 & -0.0038 | 0.1342 & -0.0003 | 0.1116 & -0.0022 | 0.1169 & -0.0042 | 0.1307 & -0.0042 |
| 0.2014 & -0.0153 | 0.1753 & -0.0124 | 0.1336 & -0.0082 | 0.1050 & -0.0070 | 0.1076 & -0.0085 | 0.1207 & -0.0072 |
| 0.1278 & -0.0215 | 0.1400 & -0.0184 | 0.1097 & -0.0143 | 0.0831 & -0.0109 | 0.0860 & -0.0121 | 0.1040 & -0.0138 |

BOX SLAB 2 MEAN & ERROR

| | | | | | |
|------------------|------------------|------------------|------------------|------------------|------------------|
| 0.1034 & -0.0146 | 0.2183 & -0.0048 | 0.1555 & -0.0115 | 0.0830 & -0.0182 | 0.0886 & -0.0184 | 0.2186 & -0.0070 |
| 0.1287 & -0.0121 | 0.1944 & -0.0151 | 0.1224 & -0.0079 | 0.0388 & -0.0142 | 0.0526 & -0.0202 | 0.1999 & -0.0083 |
| 0.1523 & -0.0068 | 0.1583 & -0.0213 | 0.0986 & -0.0050 | 0.0703 & -0.0067 | 0.0908 & -0.0163 | 0.1637 & -0.0085 |

| | | | | | |
|------------------|------------------|------------------|------------------|------------------|------------------|
| 0.1727 & -0.0065 | 0.0744 & -0.0231 | 0.0740 & -0.0071 | 0.0874 & -0.0067 | 0.1456 & -0.0073 | 0.0603 & -0.0163 |
| 0.1762 & -0.0045 | 0.0344 & -0.0266 | 0.0568 & -0.0085 | 0.0913 & -0.0089 | 0.1568 & -0.0045 | 0.0179 & -0.0141 |
| 0.1677 & -0.0025 | 0.0976 & -0.0205 | 0.0518 & -0.0096 | 0.0919 & -0.0084 | 0.1625 & -0.0014 | 0.0566 & -0.0068 |

| | | | | | |
|-----------------|-----------------|------------------|-----------------|-----------------|-----------------|
| 0.1464 & 0.0005 | 0.1572 & 0.0020 | 0.0809 & -0.0030 | 0.1027 & 0.0017 | 0.1572 & 0.0074 | 0.1013 & 0.0024 |
| 0.1885 & 0.0128 | 0.1581 & 0.0115 | 0.0912 & 0.0057 | 0.1022 & 0.0077 | 0.1390 & 0.0127 | 0.1004 & 0.0060 |
| 0.1826 & 0.0231 | 0.1316 & 0.0197 | 0.0828 & 0.0129 | 0.0841 & 0.0137 | 0.1050 & 0.0174 | 0.0894 & 0.0139 |

Empty model load space, ES grid and 100% inlet jet speed
 VENTILATION RATE (M3/SEC) CALCULATED FROM CFD DATA FOR BOX PAIRS

XZ PLANES

BOX SLAB 1 MEAN & ERROR

| | | | | | |
|-----------------|-----------------|-----------------|-----------------|-----------------|-----------------|
| 0.0283 & 0.0222 | 0.1272 & 0.0298 | 0.1223 & 0.0322 | 0.0752 & 0.0340 | 0.0799 & 0.0279 | 0.1103 & 0.0207 |
| 0.0590 & 0.0254 | 0.0713 & 0.0319 | 0.0608 & 0.0323 | 0.0745 & 0.0246 | 0.1101 & 0.0183 | 0.1568 & 0.0170 |
| 0.1225 & 0.0338 | 0.0836 & 0.0335 | 0.1031 & 0.0276 | 0.1180 & 0.0181 | 0.1414 & 0.0140 | 0.1872 & 0.0144 |

| | | | | | |
|-----------------|-----------------|-----------------|-----------------|-----------------|-----------------|
| 0.2643 & 0.0292 | 0.2196 & 0.0241 | 0.1952 & 0.0151 | 0.1690 & 0.0102 | 0.1855 & 0.0087 | 0.2234 & 0.0087 |
| 0.3178 & 0.0207 | 0.2608 & 0.0146 | 0.2221 & 0.0103 | 0.1834 & 0.0072 | 0.1980 & 0.0056 | 0.2307 & 0.0045 |
| 0.3529 & 0.0120 | 0.2813 & 0.0064 | 0.2385 & 0.0058 | 0.1911 & 0.0043 | 0.2080 & 0.0023 | 0.2302 & 0.0007 |

| | | | | | |
|------------------|------------------|------------------|------------------|------------------|------------------|
| 0.3872 & -0.0128 | 0.2849 & -0.0136 | 0.2435 & -0.0095 | 0.1880 & -0.0063 | 0.2079 & -0.0101 | 0.2128 & -0.0090 |
| 0.3505 & -0.0267 | 0.2550 & -0.0235 | 0.2254 & -0.0197 | 0.1740 & -0.0136 | 0.1851 & -0.0174 | 0.1947 & -0.0170 |
| 0.2738 & -0.0401 | 0.1942 & -0.0311 | 0.1750 & -0.0280 | 0.1372 & -0.0199 | 0.1417 & -0.0231 | 0.1502 & -0.0226 |

BOX SLAB 2 MEAN & ERROR

| | | | | | |
|------------------|------------------|------------------|------------------|------------------|------------------|
| 0.1111 & -0.0202 | 0.1792 & -0.0102 | 0.0583 & -0.0173 | 0.1097 & -0.0185 | 0.0567 & -0.0229 | 0.2420 & 0.0033 |
| 0.0729 & -0.0400 | 0.1545 & -0.0148 | 0.0957 & -0.0086 | 0.1575 & -0.0214 | 0.1104 & -0.0203 | 0.2338 & -0.0000 |
| 0.1075 & -0.0461 | 0.1151 & -0.0193 | 0.1174 & -0.0031 | 0.1885 & -0.0173 | 0.1618 & -0.0157 | 0.2002 & -0.0013 |

| | | | | | |
|------------------|------------------|------------------|------------------|------------------|------------------|
| 0.2612 & -0.0200 | 0.1103 & -0.0264 | 0.1441 & -0.0144 | 0.2393 & -0.0083 | 0.2218 & -0.0094 | 0.1072 & -0.0122 |
| 0.2780 & -0.0117 | 0.1642 & -0.0201 | 0.1681 & -0.0114 | 0.2495 & -0.0050 | 0.2352 & -0.0052 | 0.0628 & -0.0136 |
| 0.2802 & -0.0047 | 0.2016 & -0.0125 | 0.1851 & -0.0079 | 0.2517 & -0.0017 | 0.2401 & -0.0009 | 0.0187 & -0.0123 |

| | | | | | |
|-----------------|-----------------|-----------------|-----------------|-----------------|------------------|
| 0.2820 & 0.0151 | 0.2468 & 0.0112 | 0.1978 & 0.0077 | 0.2292 & 0.0107 | 0.2315 & 0.0129 | 0.0911 & -0.0014 |
| 0.2580 & 0.0272 | 0.2361 & 0.0244 | 0.1881 & 0.0188 | 0.2044 & 0.0199 | 0.2046 & 0.0209 | 0.1147 & 0.0112 |
| 0.2007 & 0.0375 | 0.1868 & 0.0371 | 0.1470 & 0.0288 | 0.1540 & 0.0300 | 0.1546 & 0.0280 | 0.1047 & 0.0227 |

Empty model load space, ES grid and 50% inlet jet speed
 VENTILATION RATE (M3/SEC) CALCULATED FROM CFD DATA FOR BOX PAIRS

XZ PLANES

BOX SLAB 1 MEAN & ERROR

| | | | | | |
|-----------------|-----------------|-----------------|-----------------|-----------------|-----------------|
| 0.0179 & 0.0133 | 0.1152 & 0.0188 | 0.1485 & 0.0192 | 0.1260 & 0.0259 | 0.0533 & 0.0291 | 0.0818 & 0.0136 |
| 0.0470 & 0.0138 | 0.0806 & 0.0166 | 0.1128 & 0.0163 | 0.0702 & 0.0229 | 0.0685 & 0.0234 | 0.0427 & 0.0163 |
| 0.0797 & 0.0142 | 0.0493 & 0.0122 | 0.0867 & 0.0156 | 0.0308 & 0.0194 | 0.0930 & 0.0147 | 0.0335 & 0.0150 |

| | | | | | |
|-----------------|-----------------|-----------------|-----------------|-----------------|-----------------|
| 0.1404 & 0.0128 | 0.0637 & 0.0085 | 0.0453 & 0.0147 | 0.0870 & 0.0093 | 0.1248 & 0.0041 | 0.0801 & 0.0096 |
| 0.1689 & 0.0125 | 0.0806 & 0.0086 | 0.0714 & 0.0124 | 0.1001 & 0.0065 | 0.1313 & 0.0032 | 0.0911 & 0.0075 |
| 0.1959 & 0.0116 | 0.0978 & 0.0092 | 0.0922 & 0.0097 | 0.1078 & 0.0041 | 0.1356 & 0.0029 | 0.0968 & 0.0058 |

| | | | | | |
|------------------|------------------|------------------|------------------|------------------|------------------|
| 0.2363 & -0.0033 | 0.1211 & -0.0001 | 0.1093 & -0.0015 | 0.1095 & -0.0041 | 0.1461 & -0.0042 | 0.0911 & -0.0024 |
| 0.2247 & -0.0140 | 0.1238 & -0.0078 | 0.1082 & -0.0076 | 0.0996 & -0.0081 | 0.1386 & -0.0100 | 0.0807 & -0.0062 |
| 0.1814 & -0.0230 | 0.1028 & -0.0134 | 0.0881 & -0.0123 | 0.0782 & -0.0108 | 0.1130 & -0.0154 | 0.0590 & -0.0085 |

BOX SLAB 2 MEAN & ERROR

| | | | | | |
|------------------|------------------|------------------|------------------|------------------|------------------|
| 0.1385 & -0.0091 | 0.1951 & -0.0070 | 0.1110 & -0.0152 | 0.0939 & -0.0202 | 0.1756 & -0.0102 | 0.1886 & -0.0037 |
| 0.0927 & -0.0195 | 0.1737 & -0.0071 | 0.0688 & -0.0112 | 0.0550 & -0.0194 | 0.1406 & -0.0106 | 0.1894 & -0.0044 |
| 0.0499 & -0.0197 | 0.1466 & -0.0049 | 0.0400 & -0.0131 | 0.0849 & -0.0125 | 0.0895 & -0.0129 | 0.1822 & -0.0039 |

| | | | | | |
|------------------|------------------|------------------|------------------|------------------|------------------|
| 0.0614 & -0.0156 | 0.1005 & -0.0054 | 0.0783 & -0.0056 | 0.1217 & -0.0099 | 0.0276 & -0.0106 | 0.1504 & -0.0028 |
| 0.0996 & -0.0149 | 0.0844 & -0.0079 | 0.0905 & -0.0019 | 0.1353 & -0.0066 | 0.0594 & -0.0093 | 0.1256 & -0.0022 |
| 0.1338 & -0.0137 | 0.0646 & -0.0117 | 0.0869 & -0.0002 | 0.1463 & -0.0037 | 0.0843 & -0.0082 | 0.0990 & -0.0015 |

| | | | | | |
|-----------------|------------------|------------------|-----------------|-----------------|------------------|
| 0.1790 & 0.0035 | 0.0857 & -0.0057 | 0.0803 & -0.0012 | 0.1448 & 0.0064 | 0.1239 & 0.0033 | 0.0294 & -0.0043 |
| 0.1803 & 0.0144 | 0.0999 & 0.0041 | 0.0844 & 0.0048 | 0.1306 & 0.0116 | 0.1223 & 0.0105 | 0.0098 & -0.0007 |
| 0.1497 & 0.0237 | 0.0923 & 0.0123 | 0.0740 & 0.0102 | 0.1008 & 0.0166 | 0.0994 & 0.0167 | 0.0249 & 0.0033 |

Front half loaded model load space, standard load model and 100% inlet jet speed
 VENTILATION RATE (M3/SEC) CALCULATED FROM CFD DATA FOR BOX PAIRS

XZ PLANES

BOX SLAB 1 MEAN & ERROR

| | | | | | |
|-----------------|-----------------|------------------|------------------|-----------------|-----------------|
| 0.0293 & 0.0221 | 0.0018 & 0.0007 | 0.0022 & 0.0006 | 0.0023 & 0.0004 | 0.0819 & 0.0269 | 0.0939 & 0.0272 |
| 0.0677 & 0.0206 | 0.0007 & 0.0001 | 0.0012 & -0.0004 | 0.0013 & -0.0006 | 0.0335 & 0.0198 | 0.1249 & 0.0170 |
| 0.1035 & 0.0191 | 0.0010 & 0.0004 | 0.0014 & -0.0004 | 0.0015 & -0.0005 | 0.0737 & 0.0145 | 0.1437 & 0.0121 |

| | | | | | |
|-----------------|-----------------|------------------|------------------|-----------------|-----------------|
| 0.1943 & 0.0169 | 0.0048 & 0.0025 | 0.0053 & 0.0015 | 0.0042 & 0.0015 | 0.1117 & 0.0085 | 0.1737 & 0.0053 |
| 0.2222 & 0.0103 | 0.0020 & 0.0005 | 0.0027 & -0.0007 | 0.0017 & -0.0006 | 0.1315 & 0.0071 | 0.1826 & 0.0046 |
| 0.2443 & 0.0053 | 0.0019 & 0.0005 | 0.0026 & -0.0008 | 0.0018 & -0.0007 | 0.1502 & 0.0051 | 0.1903 & 0.0045 |

| | | | | | |
|------------------|-----------------|------------------|------------------|------------------|------------------|
| 0.3153 & -0.0093 | 0.0029 & 0.0018 | 0.0036 & 0.0005 | 0.0032 & 0.0007 | 0.1420 & -0.0038 | 0.2023 & -0.0085 |
| 0.2507 & -0.0261 | 0.0016 & 0.0009 | 0.0025 & -0.0004 | 0.0020 & -0.0003 | 0.1394 & -0.0092 | 0.1852 & -0.0176 |
| 0.1490 & -0.0386 | 0.0017 & 0.0007 | 0.0024 & -0.0004 | 0.0020 & -0.0004 | 0.1188 & -0.0142 | 0.1422 & -0.0247 |

BOX SLAB 2 MEAN & ERROR

| | | | | | |
|------------------|-----------------|-----------------|------------------|------------------|------------------|
| 0.0960 & -0.0089 | 0.0032 & 0.0021 | 0.0020 & 0.0003 | 0.0022 & 0.0006 | 0.1480 & -0.0189 | 0.0995 & -0.0244 |
| 0.1163 & -0.0132 | 0.0015 & 0.0012 | 0.0021 & 0.0001 | 0.0018 & 0.0000 | 0.1829 & -0.0152 | 0.0478 & -0.0296 |
| 0.1402 & -0.0100 | 0.0014 & 0.0012 | 0.0023 & 0.0000 | 0.0019 & -0.0001 | 0.1959 & -0.0103 | 0.1075 & -0.0189 |

| | | | | | |
|------------------|-----------------|------------------|------------------|------------------|------------------|
| 0.1008 & -0.0094 | 0.0019 & 0.0012 | 0.0032 & -0.0001 | 0.0028 & -0.0006 | 0.2181 & -0.0039 | 0.1771 & -0.0066 |
| 0.0968 & -0.0127 | 0.0017 & 0.0013 | 0.0029 & -0.0004 | 0.0022 & -0.0001 | 0.2050 & -0.0027 | 0.1912 & -0.0045 |
| 0.1083 & -0.0081 | 0.0018 & 0.0012 | 0.0029 & -0.0004 | 0.0022 & -0.0001 | 0.1856 & -0.0015 | 0.1917 & -0.0046 |

| | | | | | |
|------------------|-----------------|------------------|------------------|-----------------|-----------------|
| 0.0898 & -0.0115 | 0.0019 & 0.0013 | 0.0033 & -0.0002 | 0.0030 & -0.0007 | 0.1761 & 0.0062 | 0.1925 & 0.0107 |
| 0.1649 & -0.0035 | 0.0018 & 0.0012 | 0.0028 & -0.0003 | 0.0024 & -0.0001 | 0.1428 & 0.0111 | 0.1749 & 0.0187 |
| 0.2168 & 0.0106 | 0.0019 & 0.0011 | 0.0028 & -0.0003 | 0.0024 & -0.0000 | 0.0974 & 0.0165 | 0.1355 & 0.0257 |

Front half loaded model load space, reduced porosity load model and 100% inlet jet speed
 VENTILATION RATE (M3/SEC) CALCULATED FROM CFD DATA FOR BOX PAIRS

XZ PLANES

BOX SLAB 1 MEAN & ERROR

| | | | | | |
|-----------------|-----------------|------------------|------------------|-----------------|-----------------|
| 0.0331 & 0.0237 | 0.0024 & 0.0010 | 0.0027 & 0.0008 | 0.0028 & 0.0006 | 0.0821 & 0.0270 | 0.0985 & 0.0273 |
| 0.0760 & 0.0224 | 0.0006 & 0.0003 | 0.0010 & -0.0004 | 0.0012 & -0.0006 | 0.0344 & 0.0193 | 0.1295 & 0.0169 |
| 0.1182 & 0.0225 | 0.0008 & 0.0007 | 0.0012 & -0.0003 | 0.0014 & -0.0005 | 0.0736 & 0.0136 | 0.1479 & 0.0118 |

| | | | | | |
|-----------------|-----------------|------------------|------------------|-----------------|-----------------|
| 0.2316 & 0.0211 | 0.0039 & 0.0022 | 0.0043 & 0.0008 | 0.0031 & 0.0004 | 0.1039 & 0.0077 | 0.1754 & 0.0047 |
| 0.2706 & 0.0146 | 0.0016 & 0.0007 | 0.0023 & -0.0005 | 0.0019 & -0.0004 | 0.1231 & 0.0065 | 0.1835 & 0.0039 |
| 0.3035 & 0.0091 | 0.0016 & 0.0008 | 0.0023 & -0.0005 | 0.0020 & -0.0004 | 0.1425 & 0.0048 | 0.1889 & 0.0041 |

| | | | | | |
|------------------|-----------------|------------------|------------------|------------------|------------------|
| 0.3900 & -0.0086 | 0.0029 & 0.0013 | 0.0031 & -0.0001 | 0.0027 & -0.0001 | 0.1342 & -0.0035 | 0.1994 & -0.0078 |
| 0.3277 & -0.0264 | 0.0018 & 0.0006 | 0.0023 & -0.0004 | 0.0020 & -0.0005 | 0.1336 & -0.0088 | 0.1840 & -0.0173 |
| 0.2230 & -0.0425 | 0.0023 & 0.0004 | 0.0025 & -0.0004 | 0.0023 & -0.0005 | 0.1152 & -0.0138 | 0.1418 & -0.0246 |

BOX SLAB 2 MEAN & ERROR

| | | | | | |
|------------------|-----------------|------------------|------------------|------------------|------------------|
| 0.1402 & -0.0126 | 0.0032 & 0.0022 | 0.0019 & 0.0007 | 0.0024 & 0.0011 | 0.1440 & -0.0196 | 0.1019 & -0.0239 |
| 0.1677 & -0.0156 | 0.0012 & 0.0009 | 0.0016 & 0.0000 | 0.0016 & 0.0000 | 0.1814 & -0.0160 | 0.0440 & -0.0294 |
| 0.1961 & -0.0128 | 0.0013 & 0.0010 | 0.0018 & -0.0001 | 0.0018 & -0.0001 | 0.1963 & -0.0112 | 0.1025 & -0.0189 |

| | | | | | |
|------------------|-----------------|------------------|------------------|------------------|------------------|
| 0.1862 & -0.0210 | 0.0025 & 0.0020 | 0.0036 & -0.0000 | 0.0035 & -0.0008 | 0.2251 & -0.0047 | 0.1731 & -0.0062 |
| 0.2038 & -0.0234 | 0.0018 & 0.0014 | 0.0031 & -0.0004 | 0.0026 & 0.0000 | 0.2132 & -0.0034 | 0.1872 & -0.0041 |
| 0.2325 & -0.0125 | 0.0021 & 0.0012 | 0.0030 & -0.0004 | 0.0025 & 0.0001 | 0.1948 & -0.0021 | 0.1904 & -0.0044 |

| | | | | | |
|------------------|-----------------|------------------|------------------|-----------------|-----------------|
| 0.1919 & -0.0090 | 0.0020 & 0.0020 | 0.0039 & -0.0008 | 0.0037 & -0.0014 | 0.1864 & 0.0063 | 0.1906 & 0.0095 |
| 0.2661 & 0.0111 | 0.0022 & 0.0017 | 0.0032 & -0.0003 | 0.0025 & -0.0001 | 0.1525 & 0.0117 | 0.1754 & 0.0181 |
| 0.2833 & 0.0361 | 0.0029 & 0.0012 | 0.0032 & -0.0002 | 0.0025 & 0.0001 | 0.1059 & 0.0180 | 0.1365 & 0.0254 |

Front half loaded model load space, standard load model and 50% inlet jet speed
 VENTILATION RATE (M3/SEC) CALCULATED FROM CFD DATA FOR BOX PAIRS

XZ PLANES

BOX SLAB 1 MEAN & ERROR

| | | | | | |
|------------------|-----------------|------------------|------------------|------------------|------------------|
| 0.0592 & 0.0121 | 0.0013 & 0.0006 | 0.0014 & 0.0003 | 0.0014 & 0.0001 | 0.0930 & 0.0200 | 0.0315 & 0.0223 |
| 0.0851 & 0.0102 | 0.0005 & 0.0003 | 0.0008 & -0.0003 | 0.0008 & -0.0004 | 0.0394 & 0.0143 | 0.0565 & 0.0183 |
| 0.1088 & 0.0098 | 0.0007 & 0.0005 | 0.0010 & -0.0003 | 0.0009 & -0.0003 | 0.0188 & 0.0110 | 0.0778 & 0.0122 |
| 0.1722 & 0.0069 | 0.0029 & 0.0016 | 0.0036 & 0.0008 | 0.0026 & 0.0007 | 0.0458 & 0.0069 | 0.1071 & 0.0057 |
| 0.1873 & 0.0016 | 0.0014 & 0.0005 | 0.0021 & -0.0005 | 0.0013 & -0.0004 | 0.0601 & 0.0055 | 0.1152 & 0.0031 |
| 0.1995 & -0.0007 | 0.0014 & 0.0005 | 0.0021 & -0.0005 | 0.0013 & -0.0004 | 0.0734 & 0.0035 | 0.1234 & 0.0005 |
| 0.2391 & -0.0142 | 0.0022 & 0.0016 | 0.0029 & 0.0003 | 0.0023 & 0.0003 | 0.0672 & -0.0014 | 0.1226 & -0.0021 |
| 0.1574 & -0.0236 | 0.0013 & 0.0008 | 0.0021 & -0.0003 | 0.0016 & -0.0002 | 0.0697 & -0.0046 | 0.1203 & -0.0088 |
| 0.0582 & -0.0244 | 0.0014 & 0.0007 | 0.0021 & -0.0003 | 0.0016 & -0.0003 | 0.0640 & -0.0072 | 0.0981 & -0.0146 |

BOX SLAB 2 MEAN & ERROR

| | | | | | |
|------------------|-----------------|------------------|------------------|------------------|------------------|
| 0.0173 & -0.0039 | 0.0025 & 0.0016 | 0.0022 & 0.0007 | 0.0019 & 0.0008 | 0.0640 & -0.0162 | 0.1899 & -0.0059 |
| 0.0158 & -0.0062 | 0.0013 & 0.0010 | 0.0017 & 0.0001 | 0.0013 & 0.0001 | 0.1012 & -0.0128 | 0.1594 & -0.0084 |
| 0.0178 & -0.0067 | 0.0011 & 0.0010 | 0.0017 & 0.0000 | 0.0013 & -0.0000 | 0.1245 & -0.0093 | 0.1036 & -0.0129 |
| 0.0429 & -0.0063 | 0.0014 & 0.0009 | 0.0026 & -0.0000 | 0.0019 & -0.0003 | 0.1504 & -0.0047 | 0.0187 & -0.0152 |
| 0.0408 & -0.0083 | 0.0013 & 0.0010 | 0.0023 & -0.0003 | 0.0017 & -0.0001 | 0.1441 & -0.0031 | 0.0512 & -0.0086 |
| 0.0420 & -0.0060 | 0.0013 & 0.0009 | 0.0023 & -0.0003 | 0.0017 & -0.0001 | 0.1309 & -0.0016 | 0.0782 & -0.0031 |
| 0.0641 & -0.0102 | 0.0017 & 0.0012 | 0.0028 & -0.0000 | 0.0021 & -0.0003 | 0.1239 & 0.0032 | 0.0938 & 0.0016 |
| 0.0704 & -0.0058 | 0.0014 & 0.0009 | 0.0024 & -0.0003 | 0.0019 & -0.0002 | 0.0967 & 0.0061 | 0.0948 & 0.0075 |
| 0.1224 & 0.0010 | 0.0015 & 0.0008 | 0.0023 & -0.0003 | 0.0019 & -0.0001 | 0.0617 & 0.0085 | 0.0788 & 0.0131 |

Front half loaded model load space, reduced porosity load model and 50% inlet jet speed
 VENTILATION RATE (M3/SEC) CALCULATED FROM CFD DATA FOR BOX PAIRS

XZ PLANES

BOX SLAB 1 MEAN & ERROR

| | | | | | |
|------------------|-----------------|------------------|------------------|------------------|------------------|
| 0.0542 & 0.0129 | 0.0017 & 0.0009 | 0.0018 & 0.0006 | 0.0017 & 0.0004 | 0.0649 & 0.0179 | 0.0629 & 0.0191 |
| 0.0806 & 0.0108 | 0.0007 & 0.0005 | 0.0008 & -0.0003 | 0.0007 & -0.0003 | 0.0184 & 0.0125 | 0.0880 & 0.0125 |
| 0.1052 & 0.0112 | 0.0008 & 0.0007 | 0.0009 & -0.0002 | 0.0009 & -0.0003 | 0.0332 & 0.0093 | 0.1012 & 0.0076 |
| 0.1744 & 0.0094 | 0.0026 & 0.0018 | 0.0032 & 0.0007 | 0.0022 & 0.0003 | 0.0482 & 0.0058 | 0.1168 & 0.0024 |
| 0.1966 & 0.0054 | 0.0011 & 0.0007 | 0.0018 & -0.0003 | 0.0014 & -0.0003 | 0.0602 & 0.0049 | 0.1220 & 0.0004 |
| 0.2185 & 0.0039 | 0.0012 & 0.0006 | 0.0019 & -0.0004 | 0.0015 & -0.0003 | 0.0725 & 0.0034 | 0.1214 & -0.0005 |
| 0.2799 & -0.0102 | 0.0030 & 0.0022 | 0.0028 & 0.0002 | 0.0020 & -0.0002 | 0.0619 & -0.0015 | 0.1136 & -0.0040 |
| 0.2160 & -0.0212 | 0.0015 & 0.0008 | 0.0020 & -0.0003 | 0.0016 & -0.0004 | 0.0632 & -0.0040 | 0.1063 & -0.0096 |
| 0.1300 & -0.0274 | 0.0018 & 0.0004 | 0.0020 & -0.0003 | 0.0017 & -0.0003 | 0.0576 & -0.0061 | 0.0827 & -0.0138 |

BOX SLAB 2 MEAN & ERROR

| | | | | | |
|------------------|-----------------|------------------|------------------|------------------|------------------|
| 0.0199 & -0.0060 | 0.0023 & 0.0016 | 0.0019 & 0.0007 | 0.0019 & 0.0008 | 0.0761 & -0.0135 | 0.1410 & -0.0053 |
| 0.0332 & -0.0083 | 0.0010 & 0.0008 | 0.0014 & 0.0000 | 0.0012 & 0.0000 | 0.1120 & -0.0106 | 0.0963 & -0.0109 |
| 0.0466 & -0.0078 | 0.0009 & 0.0008 | 0.0015 & -0.0001 | 0.0013 & -0.0001 | 0.1252 & -0.0082 | 0.0562 & -0.0152 |
| 0.0355 & -0.0116 | 0.0017 & 0.0013 | 0.0029 & 0.0001 | 0.0024 & -0.0004 | 0.1505 & -0.0048 | 0.0457 & -0.0074 |
| 0.0432 & -0.0152 | 0.0013 & 0.0010 | 0.0024 & -0.0003 | 0.0019 & -0.0000 | 0.1429 & -0.0035 | 0.0750 & -0.0028 |
| 0.0623 & -0.0137 | 0.0015 & 0.0008 | 0.0024 & -0.0003 | 0.0019 & -0.0000 | 0.1288 & -0.0024 | 0.0882 & -0.0011 |
| 0.0805 & -0.0151 | 0.0025 & 0.0022 | 0.0028 & -0.0002 | 0.0026 & -0.0007 | 0.1230 & 0.0027 | 0.0938 & 0.0020 |
| 0.1691 & 0.0010 | 0.0016 & 0.0013 | 0.0025 & -0.0003 | 0.0020 & -0.0001 | 0.0962 & 0.0054 | 0.0914 & 0.0077 |
| 0.2055 & 0.0235 | 0.0021 & 0.0008 | 0.0025 & -0.0003 | 0.0020 & -0.0000 | 0.0624 & 0.0080 | 0.0748 & 0.0118 |

Front half loaded model load space, standard heated load model and 77% inlet jet speed
 VENTILATION RATE (M3/SEC) CALCULATED FROM CFD DATA FOR BOX PAIRS

XZ PLANES

BOX SLAB 1 MEAN & ERROR

| | | | | | |
|------------------|------------------|------------------|------------------|------------------|------------------|
| 0.0954 & 0.0249 | 0.0031 & -0.0001 | 0.0044 & 0.0006 | 0.0042 & 0.0005 | 0.0848 & 0.0233 | 0.1504 & 0.0272 |
| 0.0441 & 0.0216 | 0.0016 & -0.0008 | 0.0034 & 0.0000 | 0.0031 & 0.0000 | 0.0895 & 0.0170 | 0.2049 & 0.0206 |
| 0.0319 & 0.0182 | 0.0019 & -0.0004 | 0.0034 & 0.0001 | 0.0031 & 0.0001 | 0.0951 & 0.0133 | 0.2427 & 0.0149 |
| 0.0911 & 0.0126 | 0.0035 & 0.0017 | 0.0029 & 0.0012 | 0.0038 & 0.0011 | 0.1147 & 0.0086 | 0.3014 & 0.0057 |
| 0.1049 & 0.0058 | 0.0011 & -0.0000 | 0.0009 & -0.0004 | 0.0016 & -0.0004 | 0.1147 & 0.0064 | 0.3212 & 0.0019 |
| 0.1168 & -0.0003 | 0.0012 & 0.0001 | 0.0009 & -0.0003 | 0.0013 & -0.0002 | 0.1115 & 0.0044 | 0.3349 & -0.0013 |
| 0.1262 & -0.0151 | 0.0021 & -0.0007 | 0.0017 & -0.0009 | 0.0010 & -0.0001 | 0.1055 & 0.0000 | 0.3390 & -0.0097 |
| 0.0573 & -0.0234 | 0.0012 & 0.0003 | 0.0011 & -0.0003 | 0.0007 & -0.0002 | 0.1106 & -0.0010 | 0.3209 & -0.0132 |
| 0.1160 & -0.0258 | 0.0015 & 0.0002 | 0.0011 & -0.0001 | 0.0008 & -0.0001 | 0.1128 & 0.0031 | 0.2826 & -0.0110 |

BOX SLAB 2 MEAN & ERROR

| | | | | | |
|------------------|------------------|------------------|------------------|------------------|------------------|
| 0.2574 & -0.0124 | 0.0045 & 0.0021 | 0.0032 & 0.0009 | 0.0030 & 0.0005 | 0.1223 & -0.0179 | 0.3148 & -0.0001 |
| 0.2824 & -0.0127 | 0.0016 & 0.0002 | 0.0022 & 0.0007 | 0.0021 & 0.0006 | 0.0680 & -0.0193 | 0.2955 & -0.0037 |
| 0.3037 & -0.0080 | 0.0013 & 0.0002 | 0.0018 & 0.0007 | 0.0016 & 0.0006 | 0.0970 & -0.0120 | 0.2579 & -0.0051 |
| 0.2835 & -0.0056 | 0.0019 & 0.0005 | 0.0021 & -0.0007 | 0.0013 & -0.0007 | 0.1237 & -0.0029 | 0.1629 & -0.0057 |
| 0.2825 & -0.0045 | 0.0012 & 0.0010 | 0.0016 & -0.0002 | 0.0009 & -0.0001 | 0.1191 & -0.0007 | 0.1437 & -0.0074 |
| 0.2868 & 0.0012 | 0.0015 & 0.0009 | 0.0017 & -0.0001 | 0.0011 & 0.0000 | 0.1047 & 0.0005 | 0.1253 & -0.0051 |
| 0.2197 & 0.0036 | 0.0025 & -0.0003 | 0.0024 & -0.0008 | 0.0015 & -0.0000 | 0.0762 & 0.0036 | 0.1106 & 0.0060 |
| 0.2305 & 0.0074 | 0.0012 & 0.0008 | 0.0017 & -0.0002 | 0.0015 & -0.0001 | 0.0507 & 0.0043 | 0.1271 & 0.0088 |
| 0.2266 & 0.0175 | 0.0014 & 0.0008 | 0.0017 & -0.0001 | 0.0016 & -0.0001 | 0.1049 & 0.0018 | 0.1512 & 0.0057 |

Side half loaded model load space, standard load model and 50% inlet jet speed
 VENTILATION RATE (M3/SEC) CALCULATED FROM CFD DATA FOR BOX PAIRS

XZ PLANES

BOX SLAB 1 MEAN & ERROR

| | | | | | |
|------------------|------------------|------------------|------------------|------------------|------------------|
| 0.0021 & 0.0000 | 0.0015 & 0.0001 | 0.0018 & -0.0000 | 0.0020 & 0.0003 | 0.0020 & 0.0005 | 0.0012 & 0.0005 |
| 0.0011 & -0.0004 | 0.0009 & -0.0003 | 0.0014 & -0.0003 | 0.0015 & -0.0002 | 0.0013 & 0.0000 | 0.0010 & 0.0004 |
| 0.0011 & -0.0002 | 0.0010 & -0.0003 | 0.0015 & -0.0003 | 0.0015 & -0.0002 | 0.0013 & 0.0000 | 0.0010 & 0.0004 |
| 0.0045 & 0.0011 | 0.0027 & 0.0016 | 0.0033 & 0.0008 | 0.0036 & 0.0010 | 0.0033 & 0.0012 | 0.0021 & 0.0014 |
| 0.0022 & -0.0007 | 0.0010 & 0.0001 | 0.0018 & -0.0004 | 0.0016 & -0.0006 | 0.0013 & -0.0005 | 0.0005 & -0.0001 |
| 0.0021 & -0.0007 | 0.0010 & -0.0000 | 0.0017 & -0.0005 | 0.0016 & -0.0006 | 0.0012 & -0.0006 | 0.0005 & -0.0002 |
| 0.0031 & 0.0004 | 0.0015 & 0.0009 | 0.0024 & 0.0001 | 0.0022 & 0.0000 | 0.0017 & 0.0000 | 0.0010 & 0.0002 |
| 0.0023 & -0.0002 | 0.0010 & 0.0006 | 0.0022 & -0.0001 | 0.0016 & -0.0003 | 0.0012 & -0.0003 | 0.0006 & -0.0001 |
| 0.0023 & -0.0002 | 0.0009 & 0.0006 | 0.0021 & -0.0001 | 0.0016 & -0.0003 | 0.0012 & -0.0003 | 0.0007 & -0.0000 |

BOX SLAB 2 MEAN & ERROR

| | | | | | |
|------------------|------------------|------------------|------------------|------------------|------------------|
| 0.0495 & -0.0080 | 0.0605 & 0.0018 | 0.0186 & 0.0002 | 0.0812 & 0.0011 | 0.1216 & 0.0007 | 0.1242 & 0.0051 |
| 0.0232 & -0.0093 | 0.0489 & 0.0008 | 0.0081 & 0.0000 | 0.0662 & -0.0002 | 0.1118 & -0.0001 | 0.1322 & 0.0045 |
| 0.0350 & -0.0080 | 0.0585 & 0.0006 | 0.0146 & -0.0009 | 0.0583 & -0.0021 | 0.1019 & -0.0007 | 0.1392 & 0.0027 |
| 0.0567 & -0.0006 | 0.0697 & 0.0000 | 0.0299 & 0.0010 | 0.0700 & -0.0008 | 0.1016 & 0.0009 | 0.1383 & 0.0018 |
| 0.0558 & -0.0008 | 0.0698 & -0.0011 | 0.0357 & 0.0001 | 0.0691 & -0.0019 | 0.1015 & -0.0005 | 0.1323 & 0.0008 |
| 0.0554 & -0.0006 | 0.0674 & -0.0011 | 0.0396 & -0.0001 | 0.0667 & -0.0020 | 0.0982 & -0.0015 | 0.1235 & -0.0002 |
| 0.0580 & -0.0008 | 0.0637 & -0.0012 | 0.0500 & -0.0006 | 0.0633 & -0.0023 | 0.0780 & -0.0041 | 0.0863 & -0.0032 |
| 0.0555 & -0.0011 | 0.0591 & -0.0013 | 0.0495 & -0.0010 | 0.0566 & -0.0027 | 0.0634 & -0.0044 | 0.0657 & -0.0043 |
| 0.0613 & -0.0008 | 0.0548 & -0.0010 | 0.0480 & -0.0009 | 0.0487 & -0.0028 | 0.0477 & -0.0047 | 0.0435 & -0.0057 |

Side half loaded model load space, reduced porosity load model and 50% inlet jet speed
 VENTILATION RATE (M3/SEC) CALCULATED FROM CFD DATA FOR BOX PAIRS

XZ PLANES

BOX SLAB 1 MEAN & ERROR

| | | | | | |
|------------------|------------------|------------------|------------------|------------------|------------------|
| 0.0023 & 0.0001 | 0.0015 & 0.0002 | 0.0017 & 0.0000 | 0.0021 & 0.0004 | 0.0023 & 0.0006 | 0.0013 & 0.0005 |
| 0.0010 & -0.0004 | 0.0007 & -0.0002 | 0.0010 & -0.0003 | 0.0013 & -0.0002 | 0.0013 & -0.0001 | 0.0009 & 0.0003 |
| 0.0009 & -0.0002 | 0.0007 & -0.0002 | 0.0010 & -0.0002 | 0.0012 & -0.0003 | 0.0012 & -0.0001 | 0.0009 & 0.0003 |
| 0.0030 & 0.0003 | 0.0015 & 0.0010 | 0.0020 & 0.0002 | 0.0023 & 0.0003 | 0.0022 & 0.0004 | 0.0011 & 0.0007 |
| 0.0017 & -0.0004 | 0.0007 & 0.0003 | 0.0014 & -0.0002 | 0.0013 & -0.0004 | 0.0011 & -0.0004 | 0.0003 & -0.0001 |
| 0.0017 & -0.0003 | 0.0008 & 0.0002 | 0.0014 & -0.0002 | 0.0013 & -0.0004 | 0.0010 & -0.0004 | 0.0004 & -0.0001 |
| 0.0030 & 0.0003 | 0.0015 & 0.0008 | 0.0023 & -0.0000 | 0.0021 & -0.0001 | 0.0017 & -0.0001 | 0.0008 & 0.0001 |
| 0.0021 & -0.0004 | 0.0010 & 0.0004 | 0.0020 & -0.0002 | 0.0016 & -0.0004 | 0.0012 & -0.0004 | 0.0005 & -0.0001 |
| 0.0021 & -0.0004 | 0.0010 & 0.0003 | 0.0021 & -0.0002 | 0.0017 & -0.0005 | 0.0013 & -0.0004 | 0.0006 & -0.0000 |

BOX SLAB 2 MEAN & ERROR

| | | | | | |
|------------------|------------------|------------------|------------------|------------------|------------------|
| 0.0538 & -0.0075 | 0.0573 & 0.0032 | 0.0218 & 0.0012 | 0.0744 & 0.0009 | 0.1219 & 0.0008 | 0.1277 & 0.0051 |
| 0.0276 & -0.0083 | 0.0469 & 0.0021 | 0.0121 & 0.0013 | 0.0583 & 0.0005 | 0.1106 & 0.0006 | 0.1356 & 0.0047 |
| 0.0337 & -0.0061 | 0.0606 & 0.0014 | 0.0181 & 0.0005 | 0.0529 & -0.0009 | 0.1004 & 0.0006 | 0.1424 & 0.0034 |
| 0.0529 & -0.0024 | 0.0709 & -0.0012 | 0.0317 & -0.0003 | 0.0594 & -0.0026 | 0.0969 & -0.0002 | 0.1392 & 0.0011 |
| 0.0563 & -0.0018 | 0.0688 & -0.0019 | 0.0378 & -0.0005 | 0.0562 & -0.0030 | 0.0948 & -0.0014 | 0.1307 & 0.0002 |
| 0.0576 & -0.0013 | 0.0644 & -0.0017 | 0.0440 & -0.0003 | 0.0525 & -0.0024 | 0.0903 & -0.0023 | 0.1205 & -0.0007 |
| 0.0567 & -0.0014 | 0.0565 & -0.0013 | 0.0493 & -0.0005 | 0.0495 & -0.0020 | 0.0683 & -0.0042 | 0.0798 & -0.0032 |
| 0.0633 & -0.0012 | 0.0511 & -0.0011 | 0.0528 & -0.0005 | 0.0436 & -0.0020 | 0.0533 & -0.0041 | 0.0584 & -0.0040 |
| 0.0698 & -0.0001 | 0.0579 & -0.0000 | 0.0569 & 0.0003 | 0.0465 & -0.0011 | 0.0383 & -0.0035 | 0.0359 & -0.0048 |

Fully loaded model load space, reduced porosity load model and 100% inlet jet speed
 VENTILATION RATE (M3/SEC) CALCULATED FROM CFD DATA FOR BOX PAIRS

XZ PLANES

BOX SLAB 1 MEAN & ERROR

| | | | | | |
|------------------|------------------|------------------|------------------|------------------|------------------|
| 0.0022 & -0.0001 | 0.0008 & -0.0004 | 0.0020 & 0.0003 | 0.0023 & 0.0004 | 0.0024 & 0.0007 | 0.0031 & 0.0013 |
| 0.0011 & -0.0004 | 0.0006 & 0.0000 | 0.0008 & -0.0003 | 0.0010 & -0.0005 | 0.0009 & -0.0003 | 0.0013 & -0.0004 |
| 0.0012 & -0.0000 | 0.0007 & 0.0005 | 0.0009 & -0.0002 | 0.0011 & -0.0004 | 0.0010 & -0.0003 | 0.0014 & -0.0004 |
| 0.0039 & 0.0020 | 0.0032 & 0.0016 | 0.0039 & 0.0004 | 0.0033 & 0.0002 | 0.0025 & 0.0002 | 0.0025 & 0.0002 |
| 0.0015 & 0.0001 | 0.0016 & 0.0005 | 0.0025 & -0.0005 | 0.0020 & -0.0006 | 0.0013 & -0.0005 | 0.0015 & -0.0004 |
| 0.0015 & -0.0001 | 0.0016 & 0.0005 | 0.0025 & -0.0004 | 0.0020 & -0.0005 | 0.0013 & -0.0004 | 0.0014 & -0.0003 |
| 0.0068 & 0.0051 | 0.0032 & 0.0019 | 0.0036 & -0.0000 | 0.0027 & -0.0001 | 0.0018 & -0.0002 | 0.0017 & -0.0003 |
| 0.0025 & 0.0016 | 0.0020 & 0.0009 | 0.0029 & -0.0005 | 0.0020 & -0.0006 | 0.0012 & -0.0005 | 0.0015 & -0.0003 |
| 0.0024 & 0.0015 | 0.0020 & 0.0009 | 0.0029 & -0.0005 | 0.0020 & -0.0006 | 0.0014 & -0.0005 | 0.0019 & -0.0005 |

BOX SLAB 2 MEAN & ERROR

| | | | | | |
|------------------|-----------------|------------------|------------------|------------------|------------------|
| 0.0026 & -0.0013 | 0.0019 & 0.0006 | 0.0022 & -0.0002 | 0.0016 & 0.0002 | 0.0013 & 0.0007 | 0.0042 & 0.0016 |
| 0.0011 & 0.0007 | 0.0014 & 0.0011 | 0.0021 & 0.0001 | 0.0017 & -0.0001 | 0.0009 & -0.0001 | 0.0014 & -0.0001 |
| 0.0013 & 0.0008 | 0.0014 & 0.0010 | 0.0023 & -0.0000 | 0.0018 & -0.0001 | 0.0011 & -0.0002 | 0.0010 & -0.0002 |
| 0.0017 & 0.0011 | 0.0018 & 0.0013 | 0.0032 & -0.0003 | 0.0026 & -0.0002 | 0.0018 & -0.0003 | 0.0017 & -0.0004 |
| 0.0010 & 0.0004 | 0.0017 & 0.0012 | 0.0031 & -0.0003 | 0.0023 & -0.0004 | 0.0015 & -0.0004 | 0.0015 & -0.0002 |
| 0.0012 & 0.0004 | 0.0018 & 0.0011 | 0.0032 & -0.0003 | 0.0023 & -0.0004 | 0.0016 & -0.0004 | 0.0016 & -0.0002 |
| 0.0067 & 0.0052 | 0.0025 & 0.0017 | 0.0037 & -0.0004 | 0.0027 & -0.0004 | 0.0020 & -0.0007 | 0.0031 & -0.0011 |
| 0.0028 & 0.0018 | 0.0021 & 0.0014 | 0.0035 & -0.0004 | 0.0024 & -0.0005 | 0.0017 & -0.0004 | 0.0021 & 0.0001 |
| 0.0028 & 0.0017 | 0.0021 & 0.0014 | 0.0034 & -0.0003 | 0.0024 & -0.0004 | 0.0018 & -0.0002 | 0.0022 & 0.0003 |

Fully loaded model load space, reduced porosity load model and 50% inlet jet speed
 VENTILATION RATE (M3/SEC) CALCULATED FROM CFD DATA FOR BOX PAIRS

XZ PLANES

BOX SLAB 1 MEAN & ERROR

| | | | | | |
|------------------|-----------------|------------------|------------------|------------------|------------------|
| 0.0021 & 0.0007 | 0.0013 & 0.0008 | 0.0018 & 0.0010 | 0.0018 & 0.0009 | 0.0018 & 0.0010 | 0.0030 & 0.0014 |
| 0.0009 & -0.0002 | 0.0005 & 0.0000 | 0.0006 & -0.0002 | 0.0007 & -0.0003 | 0.0006 & -0.0001 | 0.0012 & -0.0001 |
| 0.0010 & -0.0002 | 0.0006 & 0.0000 | 0.0008 & -0.0003 | 0.0009 & -0.0004 | 0.0007 & -0.0003 | 0.0013 & -0.0003 |
| 0.0042 & 0.0029 | 0.0036 & 0.0025 | 0.0038 & 0.0012 | 0.0031 & 0.0008 | 0.0023 & 0.0006 | 0.0021 & 0.0004 |
| 0.0013 & 0.0002 | 0.0014 & 0.0006 | 0.0022 & -0.0003 | 0.0017 & -0.0005 | 0.0010 & -0.0004 | 0.0013 & -0.0003 |
| 0.0015 & -0.0003 | 0.0016 & 0.0003 | 0.0022 & -0.0006 | 0.0017 & -0.0006 | 0.0010 & -0.0004 | 0.0013 & -0.0003 |
| 0.0070 & 0.0053 | 0.0036 & 0.0023 | 0.0038 & 0.0003 | 0.0028 & 0.0002 | 0.0018 & -0.0000 | 0.0015 & -0.0003 |
| 0.0025 & 0.0016 | 0.0020 & 0.0009 | 0.0028 & -0.0004 | 0.0019 & -0.0005 | 0.0012 & -0.0004 | 0.0015 & -0.0002 |
| 0.0024 & 0.0014 | 0.0019 & 0.0008 | 0.0027 & -0.0005 | 0.0018 & -0.0005 | 0.0012 & -0.0004 | 0.0015 & -0.0002 |

BOX SLAB 2 MEAN & ERROR

| | | | | | |
|------------------|-----------------|------------------|------------------|------------------|------------------|
| 0.0007 & -0.0000 | 0.0015 & 0.0012 | 0.0019 & 0.0007 | 0.0018 & 0.0008 | 0.0015 & 0.0010 | 0.0036 & 0.0015 |
| 0.0005 & 0.0003 | 0.0008 & 0.0005 | 0.0012 & -0.0000 | 0.0010 & -0.0001 | 0.0004 & -0.0001 | 0.0013 & -0.0001 |
| 0.0007 & 0.0004 | 0.0007 & 0.0005 | 0.0014 & -0.0001 | 0.0010 & -0.0002 | 0.0006 & -0.0002 | 0.0010 & -0.0001 |
| 0.0023 & 0.0017 | 0.0023 & 0.0017 | 0.0033 & 0.0003 | 0.0026 & 0.0002 | 0.0019 & 0.0002 | 0.0015 & 0.0001 |
| 0.0010 & 0.0004 | 0.0015 & 0.0009 | 0.0026 & -0.0003 | 0.0018 & -0.0004 | 0.0011 & -0.0004 | 0.0013 & -0.0002 |
| 0.0011 & 0.0002 | 0.0016 & 0.0008 | 0.0027 & -0.0004 | 0.0018 & -0.0004 | 0.0011 & -0.0004 | 0.0014 & -0.0002 |
| 0.0070 & 0.0054 | 0.0029 & 0.0020 | 0.0037 & -0.0000 | 0.0028 & -0.0000 | 0.0019 & -0.0001 | 0.0020 & -0.0004 |
| 0.0028 & 0.0018 | 0.0020 & 0.0013 | 0.0031 & -0.0004 | 0.0021 & -0.0004 | 0.0014 & -0.0004 | 0.0017 & -0.0001 |
| 0.0027 & 0.0016 | 0.0020 & 0.0012 | 0.0031 & -0.0004 | 0.0021 & -0.0004 | 0.0014 & -0.0003 | 0.0016 & 0.0000 |

Fully loaded model load space, standard load model and 50% inlet jet speed
 VENTILATION RATE (M3/SEC) CALCULATED FROM CFD DATA FOR BOX PAIRS

XZ PLANES

BOX SLAB 1 MEAN & ERROR

| | | | | | |
|------------------|------------------|------------------|------------------|------------------|------------------|
| 0.0018 & 0.0004 | 0.0011 & 0.0003 | 0.0016 & 0.0007 | 0.0015 & 0.0006 | 0.0017 & 0.0008 | 0.0030 & 0.0012 |
| 0.0010 & -0.0003 | 0.0007 & -0.0002 | 0.0008 & -0.0002 | 0.0008 & -0.0003 | 0.0008 & -0.0002 | 0.0017 & -0.0001 |
| 0.0011 & -0.0002 | 0.0008 & -0.0002 | 0.0010 & -0.0004 | 0.0011 & -0.0005 | 0.0009 & -0.0003 | 0.0018 & -0.0003 |
| 0.0042 & 0.0030 | 0.0038 & 0.0027 | 0.0044 & 0.0016 | 0.0037 & 0.0013 | 0.0029 & 0.0012 | 0.0027 & 0.0011 |
| 0.0013 & 0.0003 | 0.0016 & 0.0006 | 0.0024 & -0.0004 | 0.0018 & -0.0005 | 0.0011 & -0.0005 | 0.0013 & -0.0002 |
| 0.0016 & -0.0001 | 0.0018 & 0.0003 | 0.0025 & -0.0006 | 0.0018 & -0.0007 | 0.0011 & -0.0006 | 0.0014 & -0.0004 |
| 0.0064 & 0.0047 | 0.0032 & 0.0023 | 0.0042 & 0.0005 | 0.0033 & 0.0004 | 0.0025 & 0.0003 | 0.0021 & 0.0001 |
| 0.0027 & 0.0017 | 0.0021 & 0.0012 | 0.0031 & -0.0004 | 0.0021 & -0.0004 | 0.0014 & -0.0004 | 0.0018 & -0.0001 |
| 0.0026 & 0.0016 | 0.0020 & 0.0011 | 0.0030 & -0.0005 | 0.0020 & -0.0005 | 0.0014 & -0.0004 | 0.0018 & -0.0000 |

BOX SLAB 2 MEAN & ERROR

| | | | | | |
|-----------------|-----------------|------------------|------------------|------------------|------------------|
| 0.0007 & 0.0001 | 0.0015 & 0.0011 | 0.0018 & 0.0008 | 0.0018 & 0.0009 | 0.0018 & 0.0012 | 0.0040 & 0.0017 |
| 0.0006 & 0.0004 | 0.0008 & 0.0006 | 0.0012 & 0.0000 | 0.0009 & -0.0000 | 0.0004 & 0.0001 | 0.0015 & 0.0001 |
| 0.0006 & 0.0004 | 0.0008 & 0.0005 | 0.0012 & -0.0000 | 0.0009 & -0.0001 | 0.0004 & -0.0001 | 0.0012 & 0.0000 |
| 0.0022 & 0.0017 | 0.0023 & 0.0017 | 0.0034 & 0.0005 | 0.0027 & 0.0005 | 0.0021 & 0.0006 | 0.0021 & 0.0006 |
| 0.0010 & 0.0004 | 0.0015 & 0.0009 | 0.0026 & -0.0003 | 0.0017 & -0.0004 | 0.0011 & -0.0003 | 0.0014 & -0.0002 |
| 0.0012 & 0.0004 | 0.0016 & 0.0009 | 0.0027 & -0.0004 | 0.0018 & -0.0005 | 0.0010 & -0.0004 | 0.0015 & -0.0003 |
| 0.0066 & 0.0049 | 0.0027 & 0.0019 | 0.0041 & 0.0001 | 0.0033 & 0.0002 | 0.0025 & 0.0002 | 0.0022 & 0.0000 |
| 0.0028 & 0.0019 | 0.0021 & 0.0014 | 0.0033 & -0.0004 | 0.0023 & -0.0005 | 0.0015 & -0.0004 | 0.0020 & -0.0001 |
| 0.0029 & 0.0018 | 0.0021 & 0.0013 | 0.0033 & -0.0004 | 0.0022 & -0.0005 | 0.0015 & -0.0004 | 0.0020 & -0.0001 |

Fully loaded model load space, standard load model and 50% inlet jet speed
 A repeat of the above simulation, using different initial conditions.
 VENTILATION RATE (M3/SEC) CALCULATED FROM CFD DATA FOR BOX PAIRS

XZ PLANES

BOX SLAB 1 MEAN & ERROR

| | | | | | |
|------------------|------------------|------------------|------------------|------------------|------------------|
| 0.0024 & 0.0006 | 0.0009 & 0.0003 | 0.0015 & 0.0006 | 0.0016 & 0.0006 | 0.0025 & 0.0015 | 0.0039 & 0.0020 |
| 0.0012 & -0.0003 | 0.0006 & -0.0001 | 0.0008 & -0.0002 | 0.0008 & -0.0003 | 0.0011 & -0.0003 | 0.0015 & -0.0002 |
| 0.0014 & -0.0001 | 0.0007 & -0.0001 | 0.0010 & -0.0003 | 0.0010 & -0.0004 | 0.0013 & -0.0004 | 0.0019 & -0.0005 |
| 0.0051 & 0.0035 | 0.0037 & 0.0024 | 0.0041 & 0.0013 | 0.0035 & 0.0014 | 0.0043 & 0.0021 | 0.0038 & 0.0017 |
| 0.0015 & 0.0002 | 0.0016 & 0.0005 | 0.0022 & -0.0004 | 0.0015 & -0.0005 | 0.0013 & -0.0004 | 0.0015 & -0.0004 |
| 0.0017 & -0.0003 | 0.0017 & 0.0003 | 0.0023 & -0.0006 | 0.0015 & -0.0007 | 0.0013 & -0.0006 | 0.0015 & -0.0005 |
| 0.0068 & 0.0049 | 0.0031 & 0.0021 | 0.0039 & 0.0005 | 0.0033 & 0.0006 | 0.0030 & 0.0009 | 0.0024 & 0.0005 |
| 0.0025 & 0.0016 | 0.0019 & 0.0010 | 0.0028 & -0.0004 | 0.0020 & -0.0004 | 0.0013 & -0.0003 | 0.0015 & -0.0001 |
| 0.0023 & 0.0014 | 0.0019 & 0.0009 | 0.0027 & -0.0004 | 0.0019 & -0.0004 | 0.0013 & -0.0003 | 0.0016 & -0.0001 |

BOX SLAB 2 MEAN & ERROR

| | | | | | |
|------------------|-----------------|------------------|------------------|------------------|------------------|
| 0.0008 & -0.0003 | 0.0018 & 0.0014 | 0.0017 & 0.0007 | 0.0018 & 0.0010 | 0.0028 & 0.0019 | 0.0047 & 0.0022 |
| 0.0008 & 0.0005 | 0.0009 & 0.0007 | 0.0011 & 0.0001 | 0.0007 & 0.0000 | 0.0003 & 0.0001 | 0.0015 & 0.0001 |
| 0.0011 & 0.0007 | 0.0008 & 0.0006 | 0.0012 & -0.0000 | 0.0007 & -0.0001 | 0.0004 & -0.0001 | 0.0011 & -0.0000 |
| 0.0025 & 0.0019 | 0.0023 & 0.0017 | 0.0033 & 0.0004 | 0.0028 & 0.0005 | 0.0025 & 0.0009 | 0.0023 & 0.0009 |
| 0.0011 & 0.0005 | 0.0015 & 0.0009 | 0.0025 & -0.0003 | 0.0017 & -0.0004 | 0.0011 & -0.0003 | 0.0013 & -0.0002 |
| 0.0013 & 0.0003 | 0.0016 & 0.0009 | 0.0026 & -0.0004 | 0.0017 & -0.0005 | 0.0010 & -0.0004 | 0.0014 & -0.0003 |
| 0.0075 & 0.0055 | 0.0026 & 0.0018 | 0.0039 & 0.0001 | 0.0031 & 0.0001 | 0.0019 & -0.0000 | 0.0017 & -0.0001 |
| 0.0032 & 0.0022 | 0.0020 & 0.0013 | 0.0031 & -0.0004 | 0.0023 & -0.0004 | 0.0015 & -0.0002 | 0.0017 & 0.0001 |
| 0.0032 & 0.0023 | 0.0020 & 0.0012 | 0.0031 & -0.0004 | 0.0022 & -0.0004 | 0.0015 & -0.0002 | 0.0017 & 0.0002 |

Fully loaded model load space, standard heated load model and 77% inlet jet speed
 VENTILATION RATE (M3/SEC) CALCULATED FROM CFD DATA FOR BOX PAIRS

XZ PLANES

BOX SLAB 1 MEAN & ERROR

| | | | | | |
|------------------|------------------|------------------|------------------|------------------|------------------|
| 0.0016 & -0.0006 | 0.0010 & -0.0010 | 0.0032 & 0.0006 | 0.0032 & 0.0007 | 0.0035 & 0.0013 | 0.0066 & 0.0027 |
| 0.0010 & -0.0005 | 0.0010 & -0.0005 | 0.0021 & -0.0002 | 0.0021 & -0.0003 | 0.0021 & -0.0000 | 0.0035 & -0.0001 |
| 0.0012 & 0.0000 | 0.0011 & 0.0000 | 0.0022 & -0.0001 | 0.0022 & -0.0003 | 0.0022 & -0.0001 | 0.0038 & -0.0004 |
| 0.0038 & 0.0016 | 0.0034 & 0.0016 | 0.0044 & 0.0019 | 0.0044 & 0.0022 | 0.0043 & 0.0024 | 0.0050 & 0.0027 |
| 0.0013 & -0.0002 | 0.0013 & -0.0001 | 0.0015 & -0.0005 | 0.0013 & -0.0006 | 0.0012 & -0.0005 | 0.0018 & -0.0002 |
| 0.0012 & -0.0001 | 0.0011 & -0.0001 | 0.0015 & -0.0007 | 0.0014 & -0.0009 | 0.0013 & -0.0007 | 0.0019 & -0.0004 |
| 0.0027 & 0.0019 | 0.0020 & 0.0013 | 0.0033 & 0.0013 | 0.0034 & 0.0017 | 0.0035 & 0.0017 | 0.0058 & 0.0017 |
| 0.0010 & 0.0006 | 0.0009 & 0.0004 | 0.0015 & -0.0003 | 0.0012 & -0.0003 | 0.0010 & -0.0004 | 0.0035 & -0.0003 |
| 0.0010 & 0.0006 | 0.0009 & 0.0003 | 0.0015 & -0.0004 | 0.0012 & -0.0005 | 0.0010 & -0.0005 | 0.0035 & -0.0004 |

BOX SLAB 2 MEAN & ERROR

| | | | | | |
|------------------|-----------------|------------------|------------------|------------------|------------------|
| 0.0037 & -0.0025 | 0.0017 & 0.0009 | 0.0019 & 0.0008 | 0.0032 & 0.0016 | 0.0039 & 0.0022 | 0.0084 & 0.0036 |
| 0.0015 & 0.0008 | 0.0012 & 0.0009 | 0.0009 & 0.0005 | 0.0010 & 0.0004 | 0.0012 & 0.0004 | 0.0034 & 0.0002 |
| 0.0020 & 0.0013 | 0.0014 & 0.0009 | 0.0009 & 0.0004 | 0.0005 & 0.0002 | 0.0006 & 0.0003 | 0.0029 & 0.0001 |
| 0.0016 & -0.0004 | 0.0013 & 0.0006 | 0.0022 & 0.0000 | 0.0021 & 0.0004 | 0.0015 & 0.0005 | 0.0028 & 0.0013 |
| 0.0007 & 0.0004 | 0.0010 & 0.0007 | 0.0019 & -0.0002 | 0.0013 & -0.0003 | 0.0006 & -0.0003 | 0.0008 & -0.0000 |
| 0.0007 & 0.0004 | 0.0010 & 0.0007 | 0.0019 & -0.0002 | 0.0012 & -0.0004 | 0.0008 & -0.0002 | 0.0006 & 0.0000 |
| 0.0024 & 0.0017 | 0.0011 & 0.0008 | 0.0025 & 0.0005 | 0.0026 & 0.0008 | 0.0030 & 0.0013 | 0.0050 & 0.0013 |
| 0.0012 & 0.0007 | 0.0009 & 0.0005 | 0.0016 & -0.0002 | 0.0012 & -0.0003 | 0.0010 & -0.0004 | 0.0034 & -0.0002 |
| 0.0013 & 0.0008 | 0.0008 & 0.0005 | 0.0016 & -0.0003 | 0.0011 & -0.0004 | 0.0011 & -0.0006 | 0.0035 & -0.0003 |

Fully loaded model load space, reduced porosity heated load model and 77% inlet jet speed
 VENTILATION RATE (M3/SEC) CALCULATED FROM CFD DATA FOR BOX PAIRS

XZ PLANES

BOX SLAB 1 MEAN & ERROR

| | | | | | |
|------------------|------------------|------------------|------------------|------------------|------------------|
| 0.0015 & -0.0006 | 0.0013 & -0.0012 | 0.0021 & 0.0001 | 0.0031 & 0.0005 | 0.0042 & 0.0017 | 0.0080 & 0.0036 |
| 0.0006 & -0.0003 | 0.0006 & 0.0001 | 0.0010 & 0.0000 | 0.0013 & -0.0002 | 0.0019 & -0.0000 | 0.0032 & -0.0001 |
| 0.0009 & 0.0003 | 0.0010 & 0.0007 | 0.0013 & 0.0004 | 0.0012 & 0.0001 | 0.0019 & -0.0001 | 0.0036 & -0.0006 |
| 0.0014 & -0.0003 | 0.0010 & -0.0003 | 0.0014 & -0.0002 | 0.0019 & 0.0002 | 0.0022 & 0.0006 | 0.0029 & 0.0009 |
| 0.0007 & 0.0000 | 0.0005 & 0.0002 | 0.0006 & -0.0002 | 0.0007 & -0.0003 | 0.0007 & -0.0002 | 0.0011 & -0.0002 |
| 0.0009 & 0.0004 | 0.0007 & 0.0007 | 0.0007 & 0.0002 | 0.0008 & -0.0001 | 0.0008 & -0.0001 | 0.0011 & -0.0001 |
| 0.0022 & 0.0013 | 0.0011 & -0.0004 | 0.0015 & -0.0001 | 0.0024 & 0.0005 | 0.0031 & 0.0010 | 0.0053 & 0.0008 |
| 0.0011 & 0.0007 | 0.0005 & 0.0002 | 0.0007 & -0.0003 | 0.0008 & -0.0005 | 0.0011 & -0.0005 | 0.0036 & -0.0007 |
| 0.0013 & 0.0005 | 0.0009 & 0.0002 | 0.0010 & -0.0003 | 0.0009 & -0.0004 | 0.0012 & -0.0005 | 0.0037 & -0.0007 |

BOX SLAB 2 MEAN & ERROR

| | | | | | |
|------------------|------------------|------------------|------------------|------------------|------------------|
| 0.0040 & -0.0023 | 0.0018 & 0.0002 | 0.0016 & 0.0002 | 0.0028 & 0.0011 | 0.0038 & 0.0021 | 0.0085 & 0.0033 |
| 0.0013 & 0.0007 | 0.0013 & 0.0010 | 0.0008 & 0.0004 | 0.0009 & 0.0001 | 0.0011 & 0.0003 | 0.0034 & -0.0001 |
| 0.0015 & 0.0010 | 0.0015 & 0.0010 | 0.0009 & 0.0004 | 0.0003 & 0.0000 | 0.0009 & -0.0000 | 0.0029 & -0.0002 |
| 0.0021 & -0.0009 | 0.0023 & -0.0001 | 0.0030 & -0.0009 | 0.0018 & -0.0003 | 0.0014 & 0.0002 | 0.0014 & 0.0004 |
| 0.0007 & 0.0003 | 0.0012 & 0.0009 | 0.0022 & -0.0001 | 0.0016 & -0.0002 | 0.0011 & -0.0002 | 0.0006 & -0.0001 |
| 0.0007 & 0.0005 | 0.0013 & 0.0010 | 0.0023 & -0.0000 | 0.0017 & -0.0002 | 0.0012 & -0.0002 | 0.0006 & -0.0001 |
| 0.0018 & 0.0012 | 0.0023 & -0.0005 | 0.0025 & -0.0008 | 0.0017 & -0.0001 | 0.0025 & 0.0005 | 0.0046 & 0.0006 |
| 0.0013 & 0.0009 | 0.0010 & 0.0006 | 0.0016 & -0.0002 | 0.0012 & -0.0004 | 0.0012 & -0.0006 | 0.0038 & -0.0005 |
| 0.0015 & 0.0010 | 0.0010 & 0.0007 | 0.0015 & -0.0001 | 0.0011 & -0.0004 | 0.0012 & -0.0007 | 0.0040 & -0.0007 |

appendix 6 Experimental - Numerical comparison results

The results presented here are the detailed output from the comparison methodology described in section 5. For each simulation there is a page of results comparing the experimental data and the corresponding cell values of the simulation results. Below is an explanation of the layout of each of these pages.

CINDeRS comparison of Expt data file C:\GENSTAT\TOTEXPT.DAT Experimental data file
and PHOENICS results file C:\CFD\EMPTY.RES Numerical results data file

with mirror image data. Using data reflected in the symmetry plane (see section 5.1)

| VARIABLE | | MINIMUM | MEAN | MAXIMUM | SD MEANS |
|-------------|-------------|---------|---------|---------|----------|
| X component | | | | | |
| | CFD data | -0.4601 | -0.0504 | 0.3979 | |
| | Expt data | -0.4863 | -0.0202 | 0.7269 | 0.0757 |
| | CFD Error | -0.6212 | -0.0302 | 0.3490 | |
| | Error (SDs) | 0.0773 | 1.8894 | 8.2084 | |

Total Abs Error
112% of Abs Total
=202 SDs of 181

Absolute error (% of measured total) is given in the left hand column for each variable.

The mean, range and experimental error for the first variable (the u-component). The minimum, mean and maximum are calculated separately for each row (i.e. the data and the errors) and therefore the maximum error \neq max CFD - max Experimental value.

This data is repeated for each variable considered.

| | |
|-------------|---------------------------------------|
| Y component | The v-component of velocity |
| Z component | The w-component of velocity |
| Turb KE/kg | The specific turbulent kinetic energy |
| Magnitude | The magnitude of velocity |

CFD Volume flow = 3747 m3/hr 99% of expt. Volume flow rate achieved by the simulation, also expressed as air changes per hour.
CFD Volume flow = 92 ach/hr

| Distribution of error | in SDs of | X comp. | Y comp. | Z comp. | TKE/kg | Magnitude |
|---------------------------|-----------|---------|---------|---------|--------|-----------|
| Error between 0 and 1 SDs | 31 % | 16 % | 26 % | 33 % | 26 % | |
| Error between 1 and 2 SDs | 32 % | 20 % | 22 % | 25 % | 21 % | |
| Error between 2 and 3 SDs | 17 % | 21 % | 23 % | 19 % | 20 % | |
| Error between 3 and 4 SDs | 11 % | 12 % | 12 % | 5 % | 10 % | |
| Error between 4 and 5 SDs | 6 % | 14 % | 10 % | 7 % | 9 % | |
| Error between 5 and 6 SDs | 1 % | 9 % | 4 % | 2 % | 4 % | |
| Error between 6 and 7 SDs | 2 % | 3 % | 1 % | 1 % | 7 % | |
| Error between 7 and 8 SDs | 0 % | 2 % | 1 % | 2 % | 0 % | |
| Errors greater than 8 SDs | 1 % | 3 % | 0 % | 7 % | 4 % | |

Distribution of the error in bands of 1 SDs for each variable (column) as a % of cells considered.

| | | | | | |
|-----------------------------|------|------|------|------|------|
| Cells within 3 SDs of expt | 79 % | 57 % | 72 % | 77 % | 66 % |
| Cells within 6 SDs of expt | 97 % | 93 % | 98 % | 90 % | 90 % |
| Cells outside 6 SDs of expt | 3 % | 7 % | 2 % | 10 % | 10 % |

The % of cells considered which pass the 3 SDs and 6 SDs acceptance levels, calculated from the distribution of error above.

Proportion of grid tested by expt 107 cells out of 8874 = 1 %

The number of cells considered (i.e. containing experimental data) in this comparison analysis also expressed as a % of the total number of cells in the simulation grid.

Empty load space case - simulation number 1

CINDERS comparison of Expt data file C:\GENSTAT\TOTEXPT.DAT
and PHOENICS results file C:\CFD\EMPTY.RES

with mirror image data.

| VARIABLE | | MINIMUM | MEAN | MAXIMUM | SD MEANS |
|-------------------|-------------|---------|---------|---------|----------|
| X component | CFD data | -0.4601 | -0.0504 | 0.3979 | |
| Total Abs Error | Expt data | -0.4863 | -0.0202 | 0.7269 | 0.0757 |
| 112% of Abs Total | CFD Error | -0.6212 | -0.0302 | 0.3490 | |
| =202 SDs of 181 | Error (SDs) | 0.0773 | 1.8894 | 8.2084 | |
| Y component | CFD data | -1.9790 | 0.0025 | 0.6229 | |
| Total Abs Error | Expt data | -0.9351 | 0.0130 | 0.6725 | 0.0980 |
| 143% of Abs Total | CFD Error | -1.3929 | -0.0105 | 0.6452 | |
| =329 SDs of 230 | Error (SDs) | 0.0207 | 3.0739 | 14.2110 | |
| Z component | CFD data | -0.7947 | -0.1711 | 0.9766 | |
| Total Abs Error | Expt data | -0.9351 | -0.0751 | 1.0221 | 0.1253 |
| 101% of Abs Total | CFD Error | -0.7094 | -0.0960 | 0.9362 | |
| =245 SDs of 242 | Error (SDs) | 0.0455 | 2.2873 | 7.4690 | |
| Turb KE/kg | CFD data | 0.0005 | 0.1238 | 1.1000 | |
| Total Abs Error | Expt data | 0.0188 | 0.1097 | 0.3297 | 0.0233 |
| 67% of Abs Total | CFD Error | -0.1875 | 0.0142 | 0.8868 | |
| =338 SDs of 504 | Error (SDs) | 0.0193 | 3.1607 | 38.0610 | |
| Magnitude | CFD data | 0.1720 | 0.5552 | 2.1083 | |
| Total Abs Error | Expt data | 0.0449 | 0.4352 | 1.3899 | 0.0850 |
| 54% of Abs Total | CFD Error | -0.5785 | 0.1200 | 1.2329 | |
| =295 SDs of 548 | Error (SDs) | 0.0624 | 2.7537 | 14.5095 | |

CFD Volume flow = 3747 m3/hr 99% of expt.
CFD Volume flow = 92 ach/hr

| Distribution of error | in SDs of | X comp. | Y comp. | Z comp. | TKE/kg | Magnitude |
|-----------------------------|-----------|---------|---------|---------|--------|-----------|
| Error between 0 and 1 SDs | | 31 % | 16 % | 26 % | 33 % | 26 % |
| Error between 1 and 2 SDs | | 32 % | 20 % | 22 % | 25 % | 21 % |
| Error between 2 and 3 SDs | | 17 % | 21 % | 23 % | 19 % | 20 % |
| Error between 3 and 4 SDs | | 11 % | 12 % | 12 % | 5 % | 10 % |
| Error between 4 and 5 SDs | | 6 % | 14 % | 10 % | 7 % | 9 % |
| Error between 5 and 6 SDs | | 1 % | 9 % | 4 % | 2 % | 4 % |
| Error between 6 and 7 SDs | | 2 % | 3 % | 1 % | 1 % | 7 % |
| Error between 7 and 8 SDs | | 0 % | 2 % | 1 % | 2 % | 0 % |
| Errors greater than 8 SDs | | 1 % | 3 % | 0 % | 7 % | 4 % |
| Cells within 3 SDs of expt | | 79 % | 57 % | 72 % | 77 % | 66 % |
| Cells within 6 SDs of expt | | 97 % | 93 % | 98 % | 90 % | 90 % |
| Cells outside 6 SDs of expt | | 3 % | 7 % | 2 % | 10 % | 10 % |

Proportion of grid tested by expt 107 cells out of 8874 = 1 %

Empty load space case - simulation number 2

CINDeRS comparison of Expt data file c:\user\adq\totexpt.dat
and PHOENICS results file c:\user\adq\rvd15.res

with mirror image data.

| VARIABLE | | MINIMUM | MEAN | MAXIMUM | SD MEANS |
|-------------------|-------------|---------|---------|---------|----------|
| X component | CFD data | -0.4052 | -0.0460 | 0.3188 | |
| Total Abs Error | Expt data | -0.4863 | -0.0202 | 0.7269 | 0.0757 |
| 93% of Abs Total | CFD Error | -0.6187 | -0.0258 | 0.2699 | |
| =169 SDs of 181 | Error (SDs) | 0.0081 | 1.5783 | 8.1753 | |
| Y component | CFD data | -1.7830 | 0.0011 | 0.5220 | |
| Total Abs Error | Expt data | -0.9351 | 0.0130 | 0.6725 | 0.0980 |
| 117% of Abs Total | CFD Error | -1.3319 | -0.0120 | 0.6232 | |
| =270 SDs of 230 | Error (SDs) | 0.0285 | 2.5249 | 13.5887 | |
| Z component | CFD data | -0.7953 | -0.1362 | 0.8516 | |
| Total Abs Error | Expt data | -0.9351 | -0.0751 | 1.0221 | 0.1253 |
| 83% of Abs Total | CFD Error | -0.6340 | -0.0611 | 0.6752 | |
| =202 SDs of 242 | Error (SDs) | 0.0096 | 1.8873 | 5.3868 | |
| Turb KE/kg | CFD data | 0.0001 | 0.0795 | 0.6023 | |
| Total Abs Error | Expt data | 0.0188 | 0.1097 | 0.3297 | 0.0233 |
| 59% of Abs Total | CFD Error | -0.1904 | -0.0301 | 0.3891 | |
| =295 SDs of 504 | Error (SDs) | 0.1485 | 2.7575 | 16.6988 | |
| Magnitude | CFD data | 0.1383 | 0.4660 | 1.9243 | |
| Total Abs Error | Expt data | 0.0449 | 0.4352 | 1.3899 | 0.0850 |
| 43% of Abs Total | CFD Error | -0.4191 | 0.0308 | 1.0678 | |
| =238 SDs of 548 | Error (SDs) | 0.0045 | 2.2248 | 12.5672 | |

CFD Volume flow = 3746 m3/hr 99% of expt.
CFD Volume flow = 92 ach/hr

| Distribution of error | | X comp. | Y comp. | Z comp. | TKE/kg | Magnitude |
|-----------------------------|------|---------|---------|---------|--------|-----------|
| in SDs of | | | | | | |
| Error between 0 and 1 SDs | 39 % | 21 % | 27 % | 23 % | 22 % | |
| Error between 1 and 2 SDs | 36 % | 25 % | 34 % | 26 % | 34 % | |
| Error between 2 and 3 SDs | 13 % | 21 % | 18 % | 21 % | 20 % | |
| Error between 3 and 4 SDs | 6 % | 11 % | 15 % | 12 % | 12 % | |
| Error between 4 and 5 SDs | 3 % | 15 % | 5 % | 4 % | 7 % | |
| Error between 5 and 6 SDs | 2 % | 3 % | 2 % | 5 % | 1 % | |
| Error between 6 and 7 SDs | 1 % | 2 % | 0 % | 0 % | 2 % | |
| Error between 7 and 8 SDs | 0 % | 0 % | 0 % | 3 % | 0 % | |
| Errors greater than 8 SDs | 1 % | 2 % | 0 % | 6 % | 2 % | |
| Cells within 3 SDs of expt | 88 % | 67 % | 79 % | 71 % | 76 % | |
| Cells within 6 SDs of expt | 98 % | 96 % | 100 % | 92 % | 96 % | |
| Cells outside 6 SDs of expt | 2 % | 4 % | 0 % | 8 % | 4 % | |

Proportion of grid tested by expt 107 cells out of 8874 = 1 %

Empty load space case - simulation number 3

CINDeRS comparison of Expt data file c:\user\adq\totexpt.dat
and PHOENICS results file c:\user\adq\emprvd20.res

with mirror image data.

| VARIABLE | | MINIMUM | MEAN | MAXIMUM | SD MEANS |
|-------------------|-------------|---------|---------|---------|----------|
| X component | CFD data | -0.3730 | -0.0360 | 0.2909 | |
| Total Abs Error | Expt data | -0.4863 | -0.0202 | 0.7269 | 0.0757 |
| 86% of Abs Total | CFD Error | -0.5822 | -0.0158 | 0.2260 | |
| =155 SDs of 181 | Error (SDs) | 0.0422 | 1.4509 | 7.6930 | |
| Y component | CFD data | -1.7700 | -0.0038 | 0.4586 | |
| Total Abs Error | Expt data | -0.9351 | 0.0130 | 0.6725 | 0.0980 |
| 107% of Abs Total | CFD Error | -1.3189 | -0.0169 | 0.6075 | |
| =248 SDs of 230 | Error (SDs) | 0.0017 | 2.3140 | 13.4560 | |
| Z component | CFD data | -0.8049 | -0.1225 | 1.1530 | |
| Total Abs Error | Expt data | -0.9351 | -0.0751 | 1.0221 | 0.1253 |
| 72% of Abs Total | CFD Error | -0.7476 | -0.0474 | 0.5767 | |
| =174 SDs of 242 | Error (SDs) | 0.0120 | 1.6298 | 5.9644 | |
| Turb KE/kg | CFD data | 0.0001 | 0.0554 | 0.3874 | |
| Total Abs Error | Expt data | 0.0188 | 0.1097 | 0.3297 | 0.0233 |
| 59% of Abs Total | CFD Error | -0.2223 | -0.0543 | 0.1339 | |
| =299 SDs of 504 | Error (SDs) | 0.0919 | 2.7898 | 9.5407 | |
| Magnitude | CFD data | 0.1125 | 0.4182 | 1.8465 | |
| Total Abs Error | Expt data | 0.0449 | 0.4352 | 1.3899 | 0.0850 |
| 42% of Abs Total | CFD Error | -0.5380 | -0.0170 | 0.9900 | |
| =230 SDs of 548 | Error (SDs) | 0.0126 | 2.1485 | 11.6515 | |

CFD Volume flow = 3746 m3/hr 99% of expt.
CFD Volume flow = 92 ach/hr

| Distribution of error | in SDs of | X comp. | Y comp. | Z comp. | TKE/kg | Magnitude |
|-----------------------------|-----------|---------|---------|---------|--------|-----------|
| Error between 0 and 1 SDs | | 45 % | 25 % | 37 % | 14 % | 26 % |
| Error between 1 and 2 SDs | | 26 % | 34 % | 33 % | 28 % | 27 % |
| Error between 2 and 3 SDs | | 21 % | 13 % | 16 % | 20 % | 26 % |
| Error between 3 and 4 SDs | | 5 % | 13 % | 12 % | 17 % | 8 % |
| Error between 4 and 5 SDs | | 3 % | 7 % | 1 % | 10 % | 7 % |
| Error between 5 and 6 SDs | | 0 % | 4 % | 1 % | 6 % | 0 % |
| Error between 6 and 7 SDs | | 0 % | 1 % | 0 % | 3 % | 3 % |
| Error between 7 and 8 SDs | | 1 % | 1 % | 0 % | 1 % | 1 % |
| Errors greater than 8 SDs | | 0 % | 2 % | 0 % | 2 % | 1 % |
| Cells within 3 SDs of expt | | 92 % | 72 % | 86 % | 62 % | 79 % |
| Cells within 6 SDs of expt | | 99 % | 96 % | 100 % | 94 % | 95 % |
| Cells outside 6 SDs of expt | | 1 % | 4 % | 0 % | 6 % | 5 % |

Proportion of grid tested by expt 107 cells out of 8874 = 1 %

Empty load space case - simulation number 4

CINDeRS comparison of Expt data file c:\user\adq\totexpt.dat
and PHOENICS results file c:\user\adq\eside2.res

with mirror image data.

| VARIABLE | | MINIMUM | MEAN | MAXIMUM | SD MEANS |
|-------------------|-------------|---------|---------|---------|----------|
| X component | CFD data | -0.4712 | -0.0495 | 0.4627 | |
| Total Abs Error | Expt data | -0.4863 | -0.0202 | 0.7269 | 0.0757 |
| 111% of Abs Total | CFD Error | -0.6538 | -0.0293 | 0.4138 | |
| =201 SDs of 181 | Error (SDs) | 0.0489 | 1.8773 | 8.6394 | |
| Y component | CFD data | -1.8580 | 0.0107 | 0.6425 | |
| Total Abs Error | Expt data | -0.9351 | 0.0130 | 0.6725 | 0.0980 |
| 136% of Abs Total | CFD Error | -1.4069 | -0.0024 | 0.6434 | |
| =314 SDs of 230 | Error (SDs) | 0.0082 | 2.9348 | 14.3538 | |
| Z component | CFD data | -0.8268 | -0.1617 | 0.9746 | |
| Total Abs Error | Expt data | -0.9351 | -0.0751 | 1.0221 | 0.1253 |
| 87% of Abs Total | CFD Error | -0.6349 | -0.0866 | 0.9342 | |
| =212 SDs of 242 | Error (SDs) | 0.0508 | 1.9806 | 7.4531 | |
| Turb KE/kg | CFD data | 0.0016 | 0.1346 | 1.1270 | |
| Total Abs Error | Expt data | 0.0188 | 0.1097 | 0.3297 | 0.0233 |
| 71% of Abs Total | CFD Error | -0.1879 | 0.0249 | 0.9137 | |
| =360 SDs of 504 | Error (SDs) | 0.0245 | 3.3648 | 39.2199 | |
| Magnitude | CFD data | 0.0543 | 0.5197 | 2.0994 | |
| Total Abs Error | Expt data | 0.0449 | 0.4352 | 1.3899 | 0.0850 |
| 46% of Abs Total | CFD Error | -0.3885 | 0.0845 | 1.2429 | |
| =251 SDs of 548 | Error (SDs) | 0.0510 | 2.3420 | 14.6278 | |

CFD Volume flow = 3747 m3/hr 99% of expt.

CFD Volume flow = 92 ach/hr

| Distribution of error | in SDs of | X comp. | Y comp. | Z comp. | TKE/kg | Magnitude |
|-----------------------------|-----------|---------|---------|---------|--------|-----------|
| Error between 0 and 1 SDs | 39 % | 21 % | 33 % | 34 % | 31 % | |
| Error between 1 and 2 SDs | 22 % | 15 % | 21 % | 21 % | 23 % | |
| Error between 2 and 3 SDs | 19 % | 21 % | 23 % | 19 % | 18 % | |
| Error between 3 and 4 SDs | 11 % | 13 % | 14 % | 7 % | 13 % | |
| Error between 4 and 5 SDs | 4 % | 14 % | 6 % | 5 % | 8 % | |
| Error between 5 and 6 SDs | 1 % | 10 % | 3 % | 5 % | 3 % | |
| Error between 6 and 7 SDs | 1 % | 3 % | 0 % | 2 % | 0 % | |
| Error between 7 and 8 SDs | 2 % | 0 % | 1 % | 1 % | 0 % | |
| Errors greater than 8 SDs | 1 % | 2 % | 0 % | 8 % | 4 % | |
| Cells within 3 SDs of expt | 80 % | 58 % | 77 % | 73 % | 72 % | |
| Cells within 6 SDs of expt | 96 % | 95 % | 99 % | 89 % | 96 % | |
| Cells outside 6 SDs of expt | 4 % | 5 % | 1 % | 11 % | 4 % | |

Proportion of grid tested by expt 107 cells out of 8874 = 1 %

Empty load space case - simulation number 5

CINDeRS comparison of Expt data file c:\user\adq\totexpt.dat
and PHOENICS results file c:\user\adq\esiderv2.res

with mirror image data.

| VARIABLE | | MINIMUM | MEAN | MAXIMUM | SD MEANS |
|-------------------|-------------|---------|---------|---------|----------|
| X component | CFD data | -0.3555 | -0.0287 | 0.2928 | |
| Total Abs Error | Expt data | -0.4863 | -0.0202 | 0.7269 | 0.0757 |
| 84% of Abs Total | CFD Error | -0.5476 | -0.0085 | 0.2365 | |
| =152 SDs of 181 | Error (SDs) | 0.0244 | 1.4163 | 7.2358 | |
| Y component | CFD data | -1.6840 | -0.0062 | 0.4375 | |
| Total Abs Error | Expt data | -0.9351 | 0.0130 | 0.6725 | 0.0980 |
| 105% of Abs Total | CFD Error | -1.2329 | -0.0193 | 0.5965 | |
| =241 SDs of 230 | Error (SDs) | 0.0458 | 2.2538 | 12.5786 | |
| Z component | CFD data | -0.8077 | -0.1175 | 1.2710 | |
| Total Abs Error | Expt data | -0.9351 | -0.0751 | 1.0221 | 0.1253 |
| 71% of Abs Total | CFD Error | -0.7808 | -0.0423 | 0.5906 | |
| =173 SDs of 242 | Error (SDs) | 0.0024 | 1.6175 | 6.2292 | |
| Turb KE/kg | CFD data | 0.0009 | 0.0603 | 0.3819 | |
| Total Abs Error | Expt data | 0.0188 | 0.1097 | 0.3297 | 0.0233 |
| 55% of Abs Total | CFD Error | -0.2569 | -0.0493 | 0.1413 | |
| =278 SDs of 504 | Error (SDs) | 0.0223 | 2.5997 | 11.0254 | |
| Magnitude | CFD data | 0.0905 | 0.4161 | 1.7613 | |
| Total Abs Error | Expt data | 0.0449 | 0.4352 | 1.3899 | 0.0850 |
| 41% of Abs Total | CFD Error | -0.5388 | -0.0191 | 0.9048 | |
| =225 SDs of 548 | Error (SDs) | 0.0199 | 2.1012 | 10.6487 | |

CFD Volume flow = 3747 m3/hr 99% of expt.
CFD Volume flow = 92 ach/hr

| Distribution of error in SDs of | X comp. | Y comp. | Z comp. | TKE/kg | Magnitude |
|------------------------------------|---------|---------|---------|--------|-----------|
| Error between 0 and 1 SDs | 44 % | 30 % | 37 % | 18 % | 28 % |
| Error between 1 and 2 SDs | 25 % | 26 % | 32 % | 27 % | 32 % |
| Error between 2 and 3 SDs | 22 % | 18 % | 15 % | 21 % | 16 % |
| Error between 3 and 4 SDs | 6 % | 13 % | 10 % | 13 % | 9 % |
| Error between 4 and 5 SDs | 2 % | 5 % | 5 % | 11 % | 7 % |
| Error between 5 and 6 SDs | 0 % | 4 % | 0 % | 5 % | 5 % |
| Error between 6 and 7 SDs | 0 % | 2 % | 1 % | 2 % | 1 % |
| Error between 7 and 8 SDs | 1 % | 1 % | 0 % | 1 % | 0 % |
| Errors greater than 8 SDs | 0 % | 2 % | 0 % | 2 % | 2 % |
| Cells within 3 SDs of expt | 92 % | 74 % | 84 % | 66 % | 76 % |
| Cells within 6 SDs of expt | 99 % | 95 % | 99 % | 95 % | 97 % |
| Cells outside 6 SDs of expt | 1 % | 5 % | 1 % | 5 % | 3 % |

Proportion of grid tested by expt 107 cells out of 8874 = 1 %

Empty load space case - simulation number 6

CINDeRS comparison of Expt data file c:\user\adq\totexpt.dat
and PHOENICS results file c:\user\adq\exd2.res

with mirror image data.

| VARIABLE | | MINIMUM | MEAN | MAXIMUM | SD MEANS |
|-------------------|-------------|---------|---------|---------|----------|
| X component | CFD data | -0.4147 | -0.0433 | 0.2863 | |
| Total Abs Error | Expt data | -0.4863 | -0.0226 | 0.7269 | 0.0752 |
| 86% of Abs Total | CFD Error | -0.7136 | -0.0207 | 0.2440 | |
| =161 SDs of 188 | Error (SDs) | 0.0142 | 1.4630 | 9.4898 | |
| Y component | CFD data | -1.5650 | 0.0341 | 0.4469 | |
| Total Abs Error | Expt data | -0.9351 | 0.0186 | 0.6725 | 0.0986 |
| 114% of Abs Total | CFD Error | -1.1139 | 0.0154 | 0.5826 | |
| =270 SDs of 237 | Error (SDs) | 0.0324 | 2.4570 | 11.2931 | |
| Z component | CFD data | -0.8071 | -0.1337 | 0.9807 | |
| Total Abs Error | Expt data | -0.9351 | -0.0765 | 1.0221 | 0.1171 |
| 75% of Abs Total | CFD Error | -0.7838 | -0.0572 | 0.6186 | |
| =203 SDs of 270 | Error (SDs) | 0.0006 | 1.8484 | 6.6922 | |
| Turb KE/kg | CFD data | 0.0002 | 0.0526 | 0.6029 | |
| Total Abs Error | Expt data | 0.0188 | 0.1105 | 0.3297 | 0.0236 |
| 65% of Abs Total | CFD Error | -0.2441 | -0.0578 | 0.3897 | |
| =337 SDs of 515 | Error (SDs) | 0.1753 | 3.0614 | 16.4974 | |
| Magnitude | CFD data | 0.0296 | 0.4120 | 1.6981 | |
| Total Abs Error | Expt data | 0.0449 | 0.4390 | 1.3899 | 0.0856 |
| 42% of Abs Total | CFD Error | -0.6984 | -0.0269 | 0.8417 | |
| =235 SDs of 564 | Error (SDs) | 0.0032 | 2.1319 | 9.8383 | |

CFD Volume flow = 3747 m3/hr 99% of expt.
CFD Volume flow = 92 ach/hr

| Distribution of error | | X comp. | Y comp. | Z comp. | TKE/kg | Magnitude |
|-----------------------------|------|---------|---------|---------|--------|-----------|
| in SDs of | | | | | | |
| Error between 0 and 1 SDs | 43 % | 27 % | 33 % | 13 % | 30 % | |
| Error between 1 and 2 SDs | 35 % | 22 % | 27 % | 26 % | 28 % | |
| Error between 2 and 3 SDs | 9 % | 15 % | 19 % | 18 % | 17 % | |
| Error between 3 and 4 SDs | 8 % | 15 % | 15 % | 17 % | 11 % | |
| Error between 4 and 5 SDs | 2 % | 14 % | 2 % | 13 % | 7 % | |
| Error between 5 and 6 SDs | 1 % | 4 % | 3 % | 4 % | 4 % | |
| Error between 6 and 7 SDs | 1 % | 0 % | 1 % | 5 % | 0 % | |
| Error between 7 and 8 SDs | 0 % | 3 % | 0 % | 1 % | 1 % | |
| Errors greater than 8 SDs | 1 % | 1 % | 0 % | 4 % | 2 % | |
| Cells within 3 SDs of expt | 87 % | 64 % | 79 % | 57 % | 75 % | |
| Cells within 6 SDs of expt | 98 % | 96 % | 99 % | 91 % | 97 % | |
| Cells outside 6 SDs of expt | 2 % | 4 % | 1 % | 9 % | 3 % | |

Proportion of grid tested by expt 110 cells out of 17748 = 1 %

Empty load space case - simulation number 7

CINDeRS comparison of Expt data file c:\user\adq\totexpt.dat
and PHOENICS results file c:\user\adq\eyd2.res

with mirror image data.

| VARIABLE | | MINIMUM | MEAN | MAXIMUM | SD MEANS |
|-------------------|-------------|---------|---------|---------|----------|
| X component | CFD data | -0.3272 | -0.0123 | 0.4893 | |
| Total Abs Error | Expt data | -0.4863 | -0.0206 | 0.7269 | 0.0754 |
| 104% of Abs Total | CFD Error | -0.4175 | 0.0083 | 0.3104 | |
| =190 SDs of 183 | Error (SDs) | 0.0518 | 1.7633 | 5.5404 | |
| Y component | CFD data | -1.5740 | 0.0065 | 0.4534 | |
| Total Abs Error | Expt data | -0.9351 | 0.0116 | 0.6725 | 0.0981 |
| 105% of Abs Total | CFD Error | -0.8193 | -0.0051 | 0.6776 | |
| =244 SDs of 232 | Error (SDs) | 0.0520 | 2.2549 | 8.3556 | |
| Z component | CFD data | -0.7658 | -0.1341 | 0.7990 | |
| Total Abs Error | Expt data | -0.9351 | -0.0716 | 1.0221 | 0.1253 |
| 92% of Abs Total | CFD Error | -0.8655 | -0.0624 | 0.5989 | |
| =225 SDs of 245 | Error (SDs) | 0.0438 | 2.0822 | 6.9050 | |
| Turb KE/kg | CFD data | 0.0002 | 0.0378 | 0.2034 | |
| Total Abs Error | Expt data | 0.0188 | 0.1102 | 0.3297 | 0.0233 |
| 66% of Abs Total | CFD Error | -0.2652 | -0.0724 | 0.0253 | |
| =338 SDs of 510 | Error (SDs) | 0.1217 | 3.1273 | 11.3606 | |
| Magnitude | CFD data | 0.0734 | 0.3530 | 1.6465 | |
| Total Abs Error | Expt data | 0.0449 | 0.4344 | 1.3899 | 0.0850 |
| 45% of Abs Total | CFD Error | -0.9860 | -0.0814 | 0.7678 | |
| =247 SDs of 552 | Error (SDs) | 0.0168 | 2.2841 | 11.6054 | |

CFD Volume flow = 3747 m3/hr 99% of expt.

CFD Volume flow = 92 ach/hr

Distribution of error

| | in SDs of | X comp. | Y comp. | Z comp. | TKE/kg | Magnitude |
|-----------------------------|-----------|---------|---------|---------|--------|-----------|
| Error between 0 and 1 SDs | 38 % | 28 % | 29 % | 19 % | 19 % | 28 % |
| Error between 1 and 2 SDs | 26 % | 26 % | 19 % | 21 % | 21 % | 23 % |
| Error between 2 and 3 SDs | 14 % | 21 % | 25 % | 18 % | 18 % | 21 % |
| Error between 3 and 4 SDs | 16 % | 8 % | 19 % | 11 % | 14 % | 14 % |
| Error between 4 and 5 SDs | 5 % | 6 % | 8 % | 9 % | 6 % | 6 % |
| Error between 5 and 6 SDs | 2 % | 6 % | 0 % | 7 % | 6 % | 6 % |
| Error between 6 and 7 SDs | 0 % | 3 % | 1 % | 6 % | 1 % | 1 % |
| Error between 7 and 8 SDs | 0 % | 1 % | 0 % | 4 % | 0 % | 0 % |
| Errors greater than 8 SDs | 0 % | 1 % | 0 % | 5 % | 2 % | 2 % |
| Cells within 3 SDs of expt | 78 % | 75 % | 72 % | 58 % | 72 % | 72 % |
| Cells within 6 SDs of expt | 100 % | 95 % | 99 % | 86 % | 97 % | 97 % |
| Cells outside 6 SDs of expt | 0 % | 5 % | 1 % | 14 % | 3 % | 3 % |

Proportion of grid tested by expt 108 cells out of 17748 = 1 %

Empty load space case - simulation number 8

CINDERS comparison of Expt data file c:\user\adq\totexpt.dat
and PHOENICS results file c:\user\adq\ezd2.res

with mirror image data.

| VARIABLE | | MINIMUM | MEAN | MAXIMUM | SD MEANS |
|-------------------|-------------|---------|---------|---------|----------|
| X component | CFD data | -0.3996 | -0.0263 | 0.2972 | |
| Total Abs Error | Expt data | -0.4863 | -0.0210 | 0.7269 | 0.0761 |
| 88% of Abs Total | CFD Error | -0.6913 | -0.0053 | 0.2416 | |
| =162 SDs of 183 | Error (SDs) | 0.0038 | 1.4693 | 9.0830 | |
| Y component | CFD data | -1.8750 | 0.0114 | 0.4355 | |
| Total Abs Error | Expt data | -0.9351 | 0.0111 | 0.6725 | 0.0944 |
| 117% of Abs Total | CFD Error | -1.4239 | 0.0003 | 0.5498 | |
| =285 SDs of 243 | Error (SDs) | 0.0291 | 2.5868 | 15.0854 | |
| Z component | CFD data | -0.8086 | -0.1367 | 0.9792 | |
| Total Abs Error | Expt data | -0.9351 | -0.0734 | 1.0221 | 0.1261 |
| 81% of Abs Total | CFD Error | -0.6986 | -0.0633 | 0.5748 | |
| =199 SDs of 246 | Error (SDs) | 0.0008 | 1.8121 | 5.5396 | |
| Turb KE/kg | CFD data | 0.0007 | 0.0550 | 0.3540 | |
| Total Abs Error | Expt data | 0.0188 | 0.1105 | 0.3297 | 0.0231 |
| 60% of Abs Total | CFD Error | -0.2133 | -0.0555 | 0.1561 | |
| =316 SDs of 526 | Error (SDs) | 0.0372 | 2.8690 | 9.2316 | |
| Magnitude | CFD data | 0.0852 | 0.3969 | 1.9610 | |
| Total Abs Error | Expt data | 0.0449 | 0.4309 | 1.3899 | 0.0852 |
| 44% of Abs Total | CFD Error | -0.5581 | -0.0340 | 1.1046 | |
| =242 SDs of 557 | Error (SDs) | 0.0349 | 2.2013 | 12.9700 | |

CFD Volume flow = 3747 m3/hr 99% of expt.

CFD Volume flow = 92 ach/hr

Distribution of error

| | in SDs of | X comp. | Y comp. | Z comp. | TKE/kg | Magnitude |
|-----------------------------|-----------|---------|---------|---------|--------|-----------|
| Error between 0 and 1 SDs | 46 % | 27 % | 35 % | 18 % | 31 % | |
| Error between 1 and 2 SDs | 23 % | 23 % | 24 % | 27 % | 24 % | |
| Error between 2 and 3 SDs | 22 % | 14 % | 24 % | 13 % | 20 % | |
| Error between 3 and 4 SDs | 6 % | 15 % | 10 % | 16 % | 11 % | |
| Error between 4 and 5 SDs | 2 % | 10 % | 7 % | 11 % | 8 % | |
| Error between 5 and 6 SDs | 0 % | 8 % | 1 % | 6 % | 3 % | |
| Error between 6 and 7 SDs | 0 % | 1 % | 0 % | 3 % | 2 % | |
| Error between 7 and 8 SDs | 0 % | 0 % | 0 % | 2 % | 0 % | |
| Errors greater than 8 SDs | 1 % | 3 % | 0 % | 4 % | 2 % | |
| Cells within 3 SDs of expt | 91 % | 64 % | 82 % | 58 % | 75 % | |
| Cells within 6 SDs of expt | 99 % | 96 % | 100 % | 92 % | 96 % | |
| Cells outside 6 SDs of expt | 1 % | 4 % | 0 % | 8 % | 4 % | |

Proportion of grid tested by expt 110 cells out of 17748 = 1 %

Front half loaded load space case - simulation number 1

CINDeRS comparison of Expt data file c:\user\adq\totfexpt.dat
and PHOENICS results file c:\user\adq\front2.res

with mirror image data.

| VARIABLE | | MINIMUM | MEAN | MAXIMUM | SD MEANS |
|-------------------|-------------|---------|---------|---------|----------|
| X component | CFD data | -0.2516 | 0.0127 | 0.3824 | |
| Total Abs Error | Expt data | -0.3864 | 0.0231 | 0.4497 | 0.1292 |
| 114% of Abs Total | CFD Error | -0.5227 | -0.0104 | 0.5631 | |
| =88 SDs of 77 | Error (SDs) | 0.0181 | 0.8888 | 4.3589 | |
| Y component | CFD data | -1.8830 | -0.1078 | 0.5285 | |
| Total Abs Error | Expt data | -0.8981 | -0.0109 | 0.7412 | 0.1150 |
| 112% of Abs Total | CFD Error | -1.0366 | -0.0970 | 0.4483 | |
| =188 SDs of 168 | Error (SDs) | 0.0078 | 1.8976 | 9.0105 | |
| Z component | CFD data | -0.7051 | -0.2231 | 0.8926 | |
| Total Abs Error | Expt data | -0.9472 | -0.2470 | 1.2555 | 0.1270 |
| 52% of Abs Total | CFD Error | -0.5455 | 0.0239 | 0.5928 | |
| =130 SDs of 252 | Error (SDs) | 0.0362 | 1.3174 | 4.6679 | |
| Turb KE/kg | CFD data | 0.0006 | 0.1793 | 1.2180 | |
| Total Abs Error | Expt data | 0.0020 | 0.0523 | 0.2701 | 0.0107 |
| 277% of Abs Total | CFD Error | -0.1445 | 0.1269 | 0.9479 | |
| =1336 SDs of 482 | Error (SDs) | 0.0675 | 13.4925 | 88.2910 | |
| Magnitude | CFD data | 0.0093 | 0.4799 | 1.9756 | |
| Total Abs Error | Expt data | 0.0935 | 0.4560 | 1.2568 | 0.1023 |
| 37% of Abs Total | CFD Error | -0.4783 | 0.0238 | 1.1530 | |
| =165 SDs of 441 | Error (SDs) | 0.0267 | 1.6620 | 11.2755 | |

CFD Volume flow = 3747 m³/hr 99% of expt.
CFD Volume flow = 92 ach/hr

| Distribution of error | in SDs of | X comp. | Y comp. | Z comp. | TKE/kg | Magnitude |
|-----------------------------|-----------|---------|---------|---------|--------|-----------|
| Error between 0 and 1 SDs | | 67 % | 37 % | 45 % | 10 % | 39 % |
| Error between 1 and 2 SDs | | 21 % | 23 % | 34 % | 10 % | 32 % |
| Error between 2 and 3 SDs | | 9 % | 16 % | 15 % | 6 % | 15 % |
| Error between 3 and 4 SDs | | 1 % | 16 % | 2 % | 10 % | 6 % |
| Error between 4 and 5 SDs | | 2 % | 3 % | 3 % | 7 % | 5 % |
| Error between 5 and 6 SDs | | 0 % | 2 % | 0 % | 1 % | 0 % |
| Error between 6 and 7 SDs | | 0 % | 0 % | 0 % | 4 % | 0 % |
| Error between 7 and 8 SDs | | 0 % | 0 % | 0 % | 3 % | 1 % |
| Errors greater than 8 SDs | | 0 % | 2 % | 0 % | 48 % | 1 % |
| Cells within 3 SDs of expt | | 97 % | 77 % | 95 % | 26 % | 87 % |
| Cells within 6 SDs of expt | | 100 % | 98 % | 100 % | 44 % | 98 % |
| Cells outside 6 SDs of expt | | 0 % | 2 % | 0 % | 56 % | 2 % |

Proportion of grid tested by expt 99 cells out of 8874 = 1 %

Front half loaded load space case - simulation number 2

CINDeRS comparison of Expt data file c:\user\adq\totfexpt.dat
and PHOENICS results file c:\user\adq\front4.res

with mirror image data.

| VARIABLE | | MINIMUM | MEAN | MAXIMUM | SD MEANS |
|-------------------|-------------|---------|---------|---------|----------|
| X component | CFD data | -0.3267 | -0.0033 | 0.3789 | |
| Total Abs Error | Expt data | -0.3864 | 0.0231 | 0.4497 | 0.1292 |
| 123% of Abs Total | CFD Error | -0.5398 | -0.0264 | 0.5609 | |
| =95 SDs of 77 | Error (SDs) | 0.0008 | 0.9579 | 4.3419 | |
| Y component | CFD data | -1.8940 | -0.0556 | 0.6068 | |
| Total Abs Error | Expt data | -0.8981 | -0.0109 | 0.7412 | 0.1150 |
| 105% of Abs Total | CFD Error | -1.0526 | -0.0447 | 0.7515 | |
| =176 SDs of 168 | Error (SDs) | 0.0052 | 1.7824 | 9.1495 | |
| Z component | CFD data | -0.8178 | -0.2617 | 0.7180 | |
| Total Abs Error | Expt data | -0.9472 | -0.2470 | 1.2555 | 0.1270 |
| 55% of Abs Total | CFD Error | -0.9290 | -0.0147 | 0.5865 | |
| =137 SDs of 252 | Error (SDs) | 0.0409 | 1.3870 | 7.3150 | |
| Turb KE/kg | CFD data | 0.0006 | 0.1575 | 1.1910 | |
| Total Abs Error | Expt data | 0.0020 | 0.0523 | 0.2701 | 0.0107 |
| 236% of Abs Total | CFD Error | -0.1445 | 0.1052 | 0.9210 | |
| =1139 SDs of 482 | Error (SDs) | 0.1327 | 11.5019 | 85.7762 | |
| Magnitude | CFD data | 0.0962 | 0.5074 | 2.0055 | |
| Total Abs Error | Expt data | 0.0935 | 0.4560 | 1.2568 | 0.1023 |
| 40% of Abs Total | CFD Error | -0.9289 | 0.0513 | 1.1757 | |
| =177 SDs of 441 | Error (SDs) | 0.0522 | 1.7863 | 11.4974 | |

CFD Volume flow = 3747 m³/hr 99% of expt.
CFD Volume flow = 92 ach/hr

| Distribution of error | in SDs of | X comp. | Y comp. | Z comp. | TKE/kg | Magnitude |
|-----------------------------|-----------|---------|---------|---------|--------|-----------|
| Error between 0 and 1 SDs | | 63 % | 43 % | 42 % | 13 % | 34 % |
| Error between 1 and 2 SDs | | 23 % | 24 % | 39 % | 8 % | 40 % |
| Error between 2 and 3 SDs | | 10 % | 11 % | 11 % | 10 % | 9 % |
| Error between 3 and 4 SDs | | 2 % | 10 % | 3 % | 7 % | 7 % |
| Error between 4 and 5 SDs | | 2 % | 4 % | 3 % | 5 % | 5 % |
| Error between 5 and 6 SDs | | 0 % | 3 % | 0 % | 1 % | 1 % |
| Error between 6 and 7 SDs | | 0 % | 2 % | 0 % | 6 % | 0 % |
| Error between 7 and 8 SDs | | 0 % | 0 % | 1 % | 3 % | 0 % |
| Errors greater than 8 SDs | | 0 % | 2 % | 0 % | 46 % | 3 % |
| Cells within 3 SDs of expt | | 96 % | 79 % | 93 % | 31 % | 84 % |
| Cells within 6 SDs of expt | | 100 % | 96 % | 99 % | 44 % | 97 % |
| Cells outside 6 SDs of expt | | 0 % | 4 % | 1 % | 56 % | 3 % |

Proportion of grid tested by expt 99 cells out of 8874 = 1 %

Front half loaded load space case - simulation number 3

CINDeRS comparison of Expt data file C:\GENSTAT\TOTFEEXPT.DAT
and PHOENICS results file C:\CFD\FRONT5.RES

with mirror image data.

| VARIABLE | | MINIMUM | MEAN | MAXIMUM | SD MEANS |
|-------------------|-------------|---------|---------|---------|----------|
| X component | CFD data | -0.2130 | -0.0022 | 0.1711 | |
| Total Abs Error | Expt data | -0.3864 | 0.0231 | 0.4497 | 0.1292 |
| 103% of Abs Total | CFD Error | -0.4739 | -0.0252 | 0.3737 | |
| =79 SDs of 77 | Error (SDs) | 0.0021 | 0.8012 | 3.6685 | |
| Y component | CFD data | -1.6720 | -0.0971 | 0.3947 | |
| Total Abs Error | Expt data | -0.8981 | -0.0109 | 0.7412 | 0.1150 |
| 87% of Abs Total | CFD Error | -0.9106 | -0.0862 | 0.4365 | |
| =146 SDs of 168 | Error (SDs) | 0.0174 | 1.4789 | 7.9152 | |
| Z component | CFD data | -0.5745 | -0.1788 | 0.9345 | |
| Total Abs Error | Expt data | -0.9472 | -0.2470 | 1.2555 | 0.1270 |
| 50% of Abs Total | CFD Error | -0.4044 | 0.0682 | 0.6190 | |
| =126 SDs of 252 | Error (SDs) | 0.0112 | 1.2742 | 4.8738 | |
| Turb KE/kg | CFD data | 0.0001 | 0.1020 | 0.4814 | |
| Total Abs Error | Expt data | 0.0020 | 0.0523 | 0.2701 | 0.0107 |
| 150% of Abs Total | CFD Error | -0.1441 | 0.0497 | 0.2852 | |
| =723 SDs of 482 | Error (SDs) | 0.0512 | 7.3059 | 26.5632 | |
| Magnitude | CFD data | 0.0627 | 0.3574 | 1.7362 | |
| Total Abs Error | Expt data | 0.0935 | 0.4560 | 1.2568 | 0.1023 |
| 40% of Abs Total | CFD Error | -0.5675 | -0.0986 | 0.9590 | |
| =176 SDs of 441 | Error (SDs) | 0.0085 | 1.7762 | 9.3776 | |

CFD Volume flow = 3746 m3/hr 99% of expt.

CFD Volume flow = 92 ach/hr

| Distribution of error | in SDs of | X comp. | Y comp. | Z comp. | TKE/kg | Magnitude |
|-----------------------------|-----------|---------|---------|---------|--------|-----------|
| Error between 0 and 1 SDs | | 71 % | 38 % | 44 % | 14 % | 26 % |
| Error between 1 and 2 SDs | | 23 % | 37 % | 37 % | 12 % | 39 % |
| Error between 2 and 3 SDs | | 5 % | 12 % | 13 % | 14 % | 20 % |
| Error between 3 and 4 SDs | | 1 % | 9 % | 4 % | 8 % | 7 % |
| Error between 4 and 5 SDs | | 0 % | 0 % | 1 % | 4 % | 5 % |
| Error between 5 and 6 SDs | | 0 % | 1 % | 0 % | 2 % | 1 % |
| Error between 6 and 7 SDs | | 0 % | 1 % | 0 % | 4 % | 0 % |
| Error between 7 and 8 SDs | | 0 % | 1 % | 0 % | 4 % | 0 % |
| Errors greater than 8 SDs | | 0 % | 0 % | 0 % | 37 % | 1 % |
| Cells within 3 SDs of expt | | 99 % | 88 % | 95 % | 40 % | 86 % |
| Cells within 6 SDs of expt | | 100 % | 98 % | 100 % | 55 % | 99 % |
| Cells outside 6 SDs of expt | | 0 % | 2 % | 0 % | 45 % | 1 % |

Proportion of grid tested by expt 99 cells out of 8874 = 1 %

Front half loaded load space case - simulation number 4

CINDeRS comparison of Expt data file C:\GENSTAT\TOTFEXPT.DAT
and PHOENICS results file C:\CFD\RESULTS\FRONT8.RES

with mirror image data.

| VARIABLE | | MINIMUM | MEAN | MAXIMUM | SD MEANS |
|-------------------|-------------|---------|---------|---------|----------|
| X component | CFD data | -0.1745 | -0.0084 | 0.1913 | |
| Total Abs Error | Expt data | -0.3864 | 0.0231 | 0.4497 | 0.1292 |
| 103% of Abs Total | CFD Error | -0.4793 | -0.0315 | 0.3341 | |
| =79 SDs of 77 | Error (SDs) | 0.0174 | 0.8002 | 3.7101 | |
| Y component | CFD data | -1.5600 | -0.0730 | 0.3526 | |
| Total Abs Error | Expt data | -0.8981 | -0.0109 | 0.7412 | 0.1150 |
| 81% of Abs Total | CFD Error | -0.7686 | -0.0621 | 0.4020 | |
| =136 SDs of 168 | Error (SDs) | 0.0000 | 1.3774 | 6.6810 | |
| Z component | CFD data | -0.6817 | -0.2044 | 0.6636 | |
| Total Abs Error | Expt data | -0.9472 | -0.2470 | 1.2555 | 0.1270 |
| 49% of Abs Total | CFD Error | -0.5919 | 0.0427 | 0.6134 | |
| =124 SDs of 252 | Error (SDs) | 0.0165 | 1.2499 | 4.8300 | |
| Turb KE/kg | CFD data | 0.0001 | 0.0981 | 0.5034 | |
| Total Abs Error | Expt data | 0.0020 | 0.0523 | 0.2701 | 0.0107 |
| 134% of Abs Total | CFD Error | -0.1454 | 0.0458 | 0.3245 | |
| =648 SDs of 482 | Error (SDs) | 0.0261 | 6.5474 | 30.2189 | |
| Magnitude | CFD data | 0.0595 | 0.3685 | 1.6097 | |
| Total Abs Error | Expt data | 0.0935 | 0.4560 | 1.2568 | 0.1023 |
| 36% of Abs Total | CFD Error | -0.5743 | -0.0875 | 0.8325 | |
| =160 SDs of 441 | Error (SDs) | 0.0130 | 1.6186 | 8.1407 | |

CFD Volume flow = 3748 m3/hr 99% of expt.
CFD Volume flow = 92 ach/hr

| Distribution of error | | X comp. | Y comp. | Z comp. | TKE/kg | Magnitude |
|-----------------------------|-------|---------|---------|---------|--------|-----------|
| in SDs of | | | | | | |
| Error between 0 and 1 SDs | 69 % | 48 % | 44 % | 16 % | 36 % | |
| Error between 1 and 2 SDs | 26 % | 28 % | 37 % | 12 % | 36 % | |
| Error between 2 and 3 SDs | 4 % | 11 % | 14 % | 11 % | 16 % | |
| Error between 3 and 4 SDs | 1 % | 7 % | 2 % | 9 % | 4 % | |
| Error between 4 and 5 SDs | 0 % | 3 % | 2 % | 9 % | 5 % | |
| Error between 5 and 6 SDs | 0 % | 1 % | 0 % | 2 % | 1 % | |
| Error between 6 and 7 SDs | 0 % | 1 % | 0 % | 8 % | 0 % | |
| Error between 7 and 8 SDs | 0 % | 0 % | 0 % | 3 % | 0 % | |
| Errors greater than 8 SDs | 0 % | 0 % | 0 % | 29 % | 1 % | |
| Cells within 3 SDs of expt | 99 % | 88 % | 96 % | 39 % | 89 % | |
| Cells within 6 SDs of expt | 100 % | 99 % | 100 % | 60 % | 99 % | |
| Cells outside 6 SDs of expt | 0 % | 1 % | 0 % | 40 % | 1 % | |

Proportion of grid tested by expt 99 cells out of 8874 = 1 %

Side half loaded load space case - simulation number 1

CINDERS comparison of Expt data file c:\user\adq\totsexpt.dat
and PHOENICS results file c:\user\adq\side3.res

with mirror image data.

| VARIABLE | | MINIMUM | MEAN | MAXIMUM | SD MEANS |
|-------------------|-------------|---------|---------|---------|----------|
| X component | CFD data | -0.2687 | -0.0080 | 0.1440 | |
| Total Abs Error | Expt data | -0.3823 | -0.0134 | 0.2803 | 0.0397 |
| 77% of Abs Total | CFD Error | -0.1848 | 0.0053 | 0.2516 | |
| =136 SDs of 177 | Error (SDs) | 0.0127 | 1.7843 | 6.3423 | |
| Y component | CFD data | -1.7630 | -0.0876 | 0.3715 | |
| Total Abs Error | Expt data | -0.9631 | 0.0236 | 0.7342 | 0.0685 |
| 100% of Abs Total | CFD Error | -1.1305 | -0.1111 | 0.7993 | |
| =226 SDs of 226 | Error (SDs) | 0.0015 | 2.9683 | 16.4919 | |
| Z component | CFD data | -0.6953 | -0.1747 | 0.5999 | |
| Total Abs Error | Expt data | -1.1687 | -0.1884 | 1.0764 | 0.0901 |
| 52% of Abs Total | CFD Error | -0.7713 | 0.0137 | 0.4914 | |
| =176 SDs of 339 | Error (SDs) | 0.0533 | 2.3223 | 8.5593 | |
| Turb KE/kg | CFD data | 0.0010 | 0.1297 | 0.5968 | |
| Total Abs Error | Expt data | 0.0065 | 0.0638 | 0.2462 | 0.0072 |
| 131% of Abs Total | CFD Error | -0.1365 | 0.0659 | 0.5773 | |
| =883 SDs of 672 | Error (SDs) | 0.2576 | 11.6237 | 79.9491 | |
| Magnitude | CFD data | 0.0168 | 0.3721 | 1.8678 | |
| Total Abs Error | Expt data | 0.0486 | 0.5109 | 1.2252 | 0.0755 |
| 44% of Abs Total | CFD Error | -0.9939 | -0.1389 | 1.1136 | |
| =226 SDs of 515 | Error (SDs) | 0.1270 | 2.9799 | 14.7583 | |

CFD Volume flow = 3747 m3/hr 99% of expt.
CFD Volume flow = 92 ach/hr

Distribution of error

| | in SDs of | X comp. | Y comp. | Z comp. | TKE/kg | Magnitude |
|-----------------------------|-----------|---------|---------|---------|--------|-----------|
| Error between 0 and 1 SDs | 38 % | 28 % | 24 % | 7 % | 25 % | |
| Error between 1 and 2 SDs | 28 % | 20 % | 26 % | 8 % | 21 % | |
| Error between 2 and 3 SDs | 14 % | 14 % | 26 % | 9 % | 16 % | |
| Error between 3 and 4 SDs | 11 % | 12 % | 11 % | 8 % | 17 % | |
| Error between 4 and 5 SDs | 7 % | 4 % | 5 % | 8 % | 8 % | |
| Error between 5 and 6 SDs | 1 % | 11 % | 4 % | 7 % | 1 % | |
| Error between 6 and 7 SDs | 1 % | 5 % | 0 % | 11 % | 5 % | |
| Error between 7 and 8 SDs | 0 % | 3 % | 1 % | 5 % | 0 % | |
| Errors greater than 8 SDs | 0 % | 4 % | 3 % | 38 % | 7 % | |
| Cells within 3 SDs of expt | 80 % | 62 % | 76 % | 24 % | 62 % | |
| Cells within 6 SDs of expt | 99 % | 88 % | 96 % | 46 % | 88 % | |
| Cells outside 6 SDs of expt | 1 % | 12 % | 4 % | 54 % | 12 % | |

Proportion of grid tested by expt 76 cells out of 8874 = 1 %

Side half loaded load space case - simulation number 2

CINDERS comparison of Expt data file c:\user\adq\totsexpt.dat
and PHOENICS results file c:\user\adq\side5.res

with mirror image data.

| VARIABLE | | MINIMUM | MEAN | MAXIMUM | SD MEANS |
|------------------|-------------|---------|---------|---------|----------|
| X component | CFD data | -0.2504 | -0.0117 | 0.1359 | |
| Total Abs Error | Expt data | -0.3823 | -0.0134 | 0.2803 | 0.0397 |
| 79% of Abs Total | CFD Error | -0.1679 | 0.0017 | 0.2620 | |
| =139 SDs of 177 | Error (SDs) | 0.0627 | 1.8339 | 6.6052 | |
| Y component | CFD data | -1.7730 | -0.0395 | 0.3542 | |
| Total Abs Error | Expt data | -0.9631 | 0.0236 | 0.7342 | 0.0685 |
| 78% of Abs Total | CFD Error | -1.1405 | -0.0630 | 0.7965 | |
| =175 SDs of 226 | Error (SDs) | 0.0219 | 2.3080 | 16.6378 | |
| Z component | CFD data | -0.7119 | -0.1844 | 0.5923 | |
| Total Abs Error | Expt data | -1.1687 | -0.1884 | 1.0764 | 0.0901 |
| 51% of Abs Total | CFD Error | -0.7892 | 0.0040 | 0.4568 | |
| =174 SDs of 339 | Error (SDs) | 0.0017 | 2.2886 | 8.7580 | |
| Turb KE/kg | CFD data | 0.0010 | 0.0980 | 0.3805 | |
| Total Abs Error | Expt data | 0.0065 | 0.0638 | 0.2462 | 0.0072 |
| 86% of Abs Total | CFD Error | -0.1377 | 0.0342 | 0.2073 | |
| =576 SDs of 672 | Error (SDs) | 0.1018 | 7.5732 | 28.7064 | |
| Magnitude | CFD data | 0.0294 | 0.3565 | 1.8738 | |
| Total Abs Error | Expt data | 0.0486 | 0.5109 | 1.2252 | 0.0755 |
| 45% of Abs Total | CFD Error | -0.9924 | -0.1544 | 1.1196 | |
| =231 SDs of 515 | Error (SDs) | 0.0136 | 3.0350 | 14.8386 | |

CFD Volume flow = 3746 m3/hr 99% of expt.
CFD Volume flow = 92 ach/hr

Distribution of error

| | in SDs of | X comp. | Y comp. | Z comp. | TKE/kg | Magnitude |
|-----------------------------|-----------|---------|---------|---------|--------|-----------|
| Error between 0 and 1 SDs | 30 % | 33 % | 20 % | 8 % | 21 % | |
| Error between 1 and 2 SDs | 39 % | 29 % | 32 % | 8 % | 25 % | |
| Error between 2 and 3 SDs | 11 % | 18 % | 25 % | 12 % | 14 % | |
| Error between 3 and 4 SDs | 12 % | 5 % | 12 % | 8 % | 16 % | |
| Error between 4 and 5 SDs | 5 % | 3 % | 5 % | 9 % | 8 % | |
| Error between 5 and 6 SDs | 1 % | 5 % | 3 % | 8 % | 5 % | |
| Error between 6 and 7 SDs | 1 % | 1 % | 0 % | 11 % | 4 % | |
| Error between 7 and 8 SDs | 0 % | 1 % | 1 % | 4 % | 0 % | |
| Errors greater than 8 SDs | 0 % | 4 % | 3 % | 33 % | 7 % | |
| Cells within 3 SDs of expt | 80 % | 80 % | 76 % | 28 % | 61 % | |
| Cells within 6 SDs of expt | 99 % | 93 % | 96 % | 53 % | 89 % | |
| Cells outside 6 SDs of expt | 1 % | 7 % | 4 % | 47 % | 11 % | |

Proportion of grid tested by expt 76 cells out of 8874 = 1 %

Fully loaded load space case - simulation number 1

CINDERS comparison of Expt data file c:\user\adq\fullexpt.dat
and PHOENICS results file c:\user\adq\full12.res

with mirror image data.

| VARIABLE | | MINIMUM | MEAN | MAXIMUM | SD MEANS |
|-------------------|-------------|---------|----------|----------|----------|
| X component | CFD data | -0.1088 | 0.0182 | 0.1492 | |
| Total Abs Error | Expt data | -0.2223 | 0.0315 | 0.3564 | 0.0207 |
| 94% of Abs Total | CFD Error | -0.4652 | -0.0133 | 0.2713 | |
| =68 SDs of 72 | Error (SDs) | 0.3762 | 5.2045 | 22.5165 | |
| Y component | CFD data | -1.4950 | -0.3539 | -0.0037 | |
| Total Abs Error | Expt data | -0.9811 | -0.2199 | 0.0869 | 0.0148 |
| 84% of Abs Total | CFD Error | -0.6895 | -0.1340 | 0.2348 | |
| =180 SDs of 214 | Error (SDs) | 1.0613 | 13.8476 | 46.5193 | |
| Z component | CFD data | -0.8747 | -0.1308 | 0.5192 | |
| Total Abs Error | Expt data | -1.2358 | -0.1220 | 1.1026 | 0.0249 |
| 45% of Abs Total | CFD Error | -1.1180 | -0.0087 | 0.4541 | |
| =113 SDs of 250 | Error (SDs) | 0.6760 | 8.6937 | 44.9839 | |
| Turb KE/kg | CFD data | 0.0003 | 0.5037 | 3.2290 | |
| Total Abs Error | Expt data | 0.0045 | 0.0784 | 0.3025 | 0.0034 |
| 588% of Abs Total | CFD Error | -0.1101 | 0.4253 | 3.2202 | |
| =1746 SDs of 297 | Error (SDs) | 4.0642 | 134.3360 | 937.9082 | |
| Magnitude | CFD data | 0.1671 | 0.5851 | 1.5623 | |
| Total Abs Error | Expt data | 0.1514 | 0.6248 | 1.2665 | 0.0258 |
| 38% of Abs Total | CFD Error | -0.9829 | -0.0397 | 0.5059 | |
| =119 SDs of 315 | Error (SDs) | 0.1383 | 9.1511 | 38.1587 | |

CFD Volume flow = 3746 m3/hr 99% of expt.
CFD Volume flow = 92 ach/hr

Distribution of error

| | in SDs of | X comp. | Y comp. | Z comp. | TKE/kg | Magnitude |
|-----------------------------|-----------|---------|---------|---------|--------|-----------|
| Error between 0 and 1 SDs | 15 % | 0 % | 15 % | 0 % | 15 % | |
| Error between 1 and 2 SDs | 31 % | 8 % | 23 % | 0 % | 0 % | |
| Error between 2 and 3 SDs | 8 % | 23 % | 8 % | 0 % | 23 % | |
| Error between 3 and 4 SDs | 15 % | 0 % | 8 % | 0 % | 0 % | |
| Error between 4 and 5 SDs | 0 % | 8 % | 0 % | 8 % | 15 % | |
| Error between 5 and 6 SDs | 0 % | 8 % | 0 % | 0 % | 0 % | |
| Error between 6 and 7 SDs | 8 % | 0 % | 0 % | 8 % | 0 % | |
| Error between 7 and 8 SDs | 0 % | 0 % | 0 % | 0 % | 8 % | |
| Errors greater than 8 SDs | 23 % | 54 % | 46 % | 85 % | 38 % | |
| Cells within 3 SDs of expt | 54 % | 31 % | 46 % | 0 % | 38 % | |
| Cells within 6 SDs of expt | 69 % | 46 % | 54 % | 8 % | 54 % | |
| Cells outside 6 SDs of expt | 31 % | 54 % | 46 % | 92 % | 46 % | |

Proportion of grid tested by expt 13 cells out of 8874 = 0 %

Fully loaded load space case - simulation number 2

CINDERS comparison of Expt data file c:\user\adq\fullexpt.dat
and PHOENICS results file c:\user\adq\full110.res

with mirror image data.

| VARIABLE | | MINIMUM | MEAN | MAXIMUM | SD MEANS |
|-------------------|-------------|---------|----------|----------|----------|
| X component | CFD data | -0.1794 | 0.0048 | 0.2279 | |
| Total Abs Error | Expt data | -0.2223 | 0.0315 | 0.3564 | 0.0207 |
| 109% of Abs Total | CFD Error | -0.5358 | -0.0267 | 0.3003 | |
| =79 SDs of 72 | Error (SDs) | 0.3621 | 6.0462 | 25.9340 | |
| Y component | CFD data | -1.8860 | -0.3708 | 0.0003 | |
| Total Abs Error | Expt data | -0.9811 | -0.2199 | 0.0869 | 0.0148 |
| 105% of Abs Total | CFD Error | -1.0805 | -0.1509 | 0.2934 | |
| =224 SDs of 214 | Error (SDs) | 0.0596 | 17.2116 | 72.8981 | |
| Z component | CFD data | -0.7816 | -0.1554 | 0.7069 | |
| Total Abs Error | Expt data | -1.2358 | -0.1220 | 1.1026 | 0.0249 |
| 52% of Abs Total | CFD Error | -1.2011 | -0.0333 | 0.5869 | |
| =131 SDs of 250 | Error (SDs) | 0.0456 | 10.0567 | 48.3289 | |
| Turb KE/kg | CFD data | 0.0002 | 0.5994 | 2.9410 | |
| Total Abs Error | Expt data | 0.0045 | 0.0784 | 0.3025 | 0.0034 |
| 693% of Abs Total | CFD Error | -0.1100 | 0.5209 | 2.9322 | |
| =2058 SDs of 297 | Error (SDs) | 4.1097 | 158.2739 | 854.0253 | |
| Magnitude | CFD data | 0.1904 | 0.7131 | 1.9961 | |
| Total Abs Error | Expt data | 0.1514 | 0.6248 | 1.2665 | 0.0258 |
| 51% of Abs Total | CFD Error | -0.9013 | 0.0882 | 0.9398 | |
| =160 SDs of 315 | Error (SDs) | 0.2220 | 12.2967 | 36.4818 | |

CFD Volume flow = 3747 m3/hr 99% of expt.
CFD Volume flow = 92 ach/hr

| Distribution of error | in SDs of | X comp. | Y comp. | Z comp. | TKE/kg | Magnitude |
|-----------------------------|-----------|---------|---------|---------|--------|-----------|
| Error between 0 and 1 SDs | | 23 % | 15 % | 15 % | 0 % | 15 % |
| Error between 1 and 2 SDs | | 8 % | 15 % | 23 % | 0 % | 8 % |
| Error between 2 and 3 SDs | | 15 % | 8 % | 0 % | 0 % | 0 % |
| Error between 3 and 4 SDs | | 0 % | 0 % | 0 % | 0 % | 8 % |
| Error between 4 and 5 SDs | | 8 % | 0 % | 8 % | 8 % | 0 % |
| Error between 5 and 6 SDs | | 8 % | 0 % | 8 % | 0 % | 23 % |
| Error between 6 and 7 SDs | | 15 % | 0 % | 0 % | 8 % | 8 % |
| Error between 7 and 8 SDs | | 8 % | 15 % | 8 % | 0 % | 0 % |
| Errors greater than 8 SDs | | 15 % | 46 % | 38 % | 85 % | 38 % |
| Cells within 3 SDs of expt | | 46 % | 38 % | 38 % | 0 % | 23 % |
| Cells within 6 SDs of expt | | 62 % | 38 % | 54 % | 8 % | 54 % |
| Cells outside 6 SDs of expt | | 38 % | 62 % | 46 % | 92 % | 46 % |

Proportion of grid tested by expt 13 cells out of 8874 = 0 %

Fully loaded load space case - simulation number 3

CINDeRS comparison of Expt data file c:\user\adq\fullexpt.dat
and PHOENICS results file c:\user\adq\full11.res

with mirror image data.

| VARIABLE | | MINIMUM | MEAN | MAXIMUM | SD MEANS |
|-------------------|-------------|---------|----------|----------|----------|
| X component | CFD data | -0.1101 | 0.0059 | 0.1500 | |
| Total Abs Error | Expt data | -0.2223 | 0.0315 | 0.3564 | 0.0207 |
| 97% of Abs Total | CFD Error | -0.4665 | -0.0255 | 0.2684 | |
| =70 SDs of 72 | Error (SDs) | 0.1554 | 5.3631 | 22.5795 | |
| Y component | CFD data | -1.5000 | -0.3295 | 0.0000 | |
| Total Abs Error | Expt data | -0.9811 | -0.2199 | 0.0869 | 0.0148 |
| 75% of Abs Total | CFD Error | -0.6945 | -0.1095 | 0.2320 | |
| =161 SDs of 214 | Error (SDs) | 0.0596 | 12.3658 | 46.8566 | |
| Z component | CFD data | -0.7425 | -0.1317 | 0.5013 | |
| Total Abs Error | Expt data | -1.2358 | -0.1220 | 1.1026 | 0.0249 |
| 46% of Abs Total | CFD Error | -1.1028 | -0.0096 | 0.4933 | |
| =116 SDs of 250 | Error (SDs) | 0.0443 | 8.8856 | 44.3734 | |
| Turb KE/kg | CFD data | 0.0002 | 0.4600 | 2.9640 | |
| Total Abs Error | Expt data | 0.0045 | 0.0784 | 0.3025 | 0.0034 |
| 535% of Abs Total | CFD Error | -0.1102 | 0.3816 | 2.9552 | |
| =1588 SDs of 297 | Error (SDs) | 4.0964 | 122.1285 | 860.7243 | |
| Magnitude | CFD data | 0.1684 | 0.5765 | 1.5647 | |
| Total Abs Error | Expt data | 0.1514 | 0.6248 | 1.2665 | 0.0258 |
| 38% of Abs Total | CFD Error | -0.9817 | -0.0484 | 0.5083 | |
| =121 SDs of 315 | Error (SDs) | 0.3630 | 9.3077 | 38.1092 | |

CFD Volume flow = 3746 m³/hr 99% of expt.
CFD Volume flow = 92 ach/hr

| Distribution of error | in SDs of | | | | | |
|-----------------------------|-----------|---------|---------|--------|-----------|--|
| | X comp. | Y comp. | Z comp. | TKE/kg | Magnitude | |
| Error between 0 and 1 SDs | 15 % | 15 % | 31 % | 0 % | 15 % | |
| Error between 1 and 2 SDs | 23 % | 23 % | 8 % | 0 % | 8 % | |
| Error between 2 and 3 SDs | 15 % | 8 % | 8 % | 0 % | 23 % | |
| Error between 3 and 4 SDs | 8 % | 0 % | 0 % | 0 % | 0 % | |
| Error between 4 and 5 SDs | 0 % | 0 % | 8 % | 8 % | 8 % | |
| Error between 5 and 6 SDs | 0 % | 0 % | 0 % | 0 % | 0 % | |
| Error between 6 and 7 SDs | 15 % | 0 % | 8 % | 8 % | 8 % | |
| Error between 7 and 8 SDs | 0 % | 8 % | 0 % | 0 % | 0 % | |
| Errors greater than 8 SDs | 23 % | 46 % | 38 % | 85 % | 38 % | |
| Cells within 3 SDs of expt | 54 % | 46 % | 46 % | 0 % | 46 % | |
| Cells within 6 SDs of expt | 62 % | 46 % | 54 % | 8 % | 54 % | |
| Cells outside 6 SDs of expt | 38 % | 54 % | 46 % | 92 % | 46 % | |

Proportion of grid tested by expt 13 cells out of 8874 = 0 %